National Library of Canada
Bibliothèque nationale du Canada

Acquisitions and Bibliographic Services Branch
Direction des acquisitions et des services bibliographiques

395 Wellington Street
Ottawa, Ontario
K1A 0N4

395, rue Wellington
Ottawa (Ontario)
K1A 0N4

Your file Votre référence

Our file Notre référence

NOTICE

The quality of this microform is heavily dependent upon the quality of the original thesis submitted for microfilming. Every effort has been made to ensure the highest quality of reproduction possible.

If pages are missing, contact the university which granted the degree.

Some pages may have indistinct print especially if the original pages were typed with a poor typewriter ribbon or if the university sent us an inferior photocopy.

Reproduction in full or in part of this microform is governed by the Canadian Copyright Act, R.S.C. 1970, c. C-30, and subsequent amendments.

AVIS

La qualité de cette microforme dépend grandement de la qualité de la thèse soumise au microfilmage. Nous avons tout fait pour assurer une qualité supérieure de reproduction.

S'il manque des pages, veuillez communiquer avec l'université qui a conféré le grade.

La qualité d'impression de certaines pages peut laisser à désirer, surtout si les pages originales ont été dactylographiées à l'aide d'un ruban usé ou si l'université nous a fait parvenir une photocopie de qualité inférieure.

La reproduction, même partielle, de cette microforme est soumise à la Loi canadienne sur le droit d'auteur, SRC 1970, c. C-30, et ses amendements subséquents.

Canada

Stress Memory Measurement

using

the Kaiser Effect of Acoustic Emission

by

Mohammed Momayezzadeh, B.Sc., M.Sc.

A thesis submitted to the faculty of Graduate Studies and Research
in partial fulfillment of the requirements for the
Degree of Doctor of Philosophy

Department of Mining and Metallurgical Engineering
McGill University
Montreal, Canada
January, 1993

© Mohammed Momayezzadeh, 1993

National Library of Canada
Bibliothèque nationale du Canada

Acquisitions and Bibliographic Services Branch
Direction des acquisitions et des services bibliographiques

395 Wellington Street
Ottawa, Ontario
K1A 0N4

395, rue Wellington
Ottawa (Ontario)
K1A 0N4

Your file Votre référence

Our file Notre référence

The author has granted an irrevocable non-exclusive licence allowing the National Library of Canada to reproduce, loan, distribute or sell copies of his/her thesis by any means and in any form or format, making this thesis available to interested persons.

L'auteur a accordé une licence irrévocable et non exclusive permettant à la Bibliothèque nationale du Canada de reproduire, prêter, distribuer ou vendre des copies de sa thèse de quelque manière et sous quelque forme que ce soit pour mettre des exemplaires de cette thèse à la disposition des personnes intéressées.

The author retains ownership of the copyright in his/her thesis. Neither the thesis nor substantial extracts from it may be printed or otherwise reproduced without his/her permission.

L'auteur conserve la propriété du droit d'auteur qui protège sa thèse. Ni la thèse ni des extraits substantiels de celle-ci ne doivent être imprimés ou autrement reproduits sans son autorisation.

ISBN 0-315-87942-4

Canada

Abstract

This thesis investigates in detail the stress memory of hard rocks under uniaxial compressive conditions as a time-saving and inexpensive alternative to traditional in-situ stress measurement techniques. Extensive laboratory experiments are carried out to assess the influence of parameters such as transducer/amplifier frequency response, signal definition parameters, stress rate, strain rate, specimen size, stress level, delay time, temperature, water content, confining pressure, and directional loading on the Kaiser Effect of Stanstead granite and other rock types. Based on these findings and a new data processing technique developed for estimating the previous stress level, a testing procedure is suggested and used to determine in-situ stresses from core samples with respect to their drilling orientations. In two case studies, the estimated stresses using the Kaiser Effect phenomenon are in good agreement with values obtained from conventional techniques while in the third study, no stress value was obtained due to the inability of the rock type to generate acoustic emissions. The results of this investigation show that the Kaiser Effect could become an economical method of stress measurement in hard and isotropic rock types.

Résumé

Cette thèse examine en détail la mémoire de contrainte qu'ont les roches dures en les soumettant à une charge compressive uniaxiale. Cette alternative peu coûteuse permet de réduire le temps d'acquisition des données comparativement aux méthodes conventionnelles de mesures de contraintes. Des tests approfondis ont été effectués en laboratoire afin d'evaluer l'influence de paramètres tels que la réponse en fréquence des capteurs et amplificateurs, les paramètres d'identification du signal, le taux de chargement, le taux de déformation, la grandeur de l'échantillon, la charge, le délai, la température, l'humidité et enfin la pression latérale et le chargement dirigé, sur l'Effet Kaiser du granite Stanstead et d'autres types de roches. En se basant sur les résultats obtenus et une nouvelle technique de traitement des données, une procédure est développée et utilisée pour mesurer, à partir de carottes, les contraintes dans les massifs rocheux en tenant compte de l'orientation du trou de forage. Parmi trois études de cas, se basant sur l'Effet Kaiser pour l'estimation de la contrainte in-situ, les deux premiers ont produits des résultats en accord avec ceux obtenus par des méthodes conventionnelles. Cependant, dans le dernier cas, aucune mesure n'a pu être obtenue à cause d'une insuffisance d'émissions acoustiques provenant de la roche. Les résultats de ces recherches montrent que l'Effet Kaiser pourrait s'avérer une méthode économique pour mesurer les contraintes dans les roches dures et isotropiques.

Acknowledgments

The author gratefully acknowledges the support and assistance of his thesis supervisor, Dr. F.P. Hassani, and wishes to thank him for the opportunity to work on this research project.

This project was funded under grant #661-133/88 by Natural Sciences and Engineering Research Council of Canada. The author acknowledges the financial contributions made by Noranda Technology Center and wishes to express his gratitude to Dr. Jacques Nantel, Dr. Yves Potvin and Mr. Harold Kanduth of Noranda Technology Center for their assistance in various matters related to this project.

The efforts of the rock mechanics laboratory technicians, Messrs. F. Azad and M. Girard for preparing more than 1000 different rock specimens tested during this work is especially appreciated. The author wishes to acknowledge the assistance of Messrs. Dave Woodcock of Atomic Energy of Canada and Sam Spearing of Anglo-American Corporation of South Africa for providing the cores and related data for the in-situ stress measurement programme.

The author wishes to acknowledge particularly the special support and assistance of his contemporaries: Mr. V. Mlakar for many interesting and enlightening discussions on the subject of fracture mechanics, Mr. A. Sadri for collecting and analyzing the fractographic data and Mr. S. Ameri for performing many experiments during the last stage of this work.

Finally, the author wishes to express his deepest affection and gratitude to his parents and sister for their undivided care, support, interest and encouragement over the years.

Table of Contents

Abstract i

Résumé ii

Acknowledgements iii

Table of Contents iv

List of Figures ix

List of Tables xiii

CHAPTER 1
Introduction 1-1

CHAPTER 2
Standard Stress Measurement Techniques 2-1
2.1) Introduction 2-1
2.2) Stress Measurement Techniques 2-2
2.2.1) Borehole Deformation (overcoring) Method 2-3
2.2.2) Flatjack Method 2-5
2.2.3) Hydraulic Fracturing 2-7
2.2.4) Propagation Velocity Method 2-9
2.2.5) Core Discing 2-10
2.2.6) Other Methods of Determining Stress in Rocks 2-10
2.3) Conclusions 2-13

CHAPTER 3
Acoustic Emission Method 3-1
3.1) Introduction 3-1
3.2) Historical Background 3-1
3.3) Properties of Microseismic Events 3-5
3.4) Microseismic Equipment 3-10

3.4.1) Sensors 3-10
3.4.1.1) Velocity Gages 3-10
3.4.1.2) Accelerometers 3-11
3.4.2) Wave Guides 3-11
3.4.3) Couplants 3-11
3.4.4) Preamplifiers 3-12
3.4.5) Cables 3-12
3.4.6) Data Processor 3-13

CHAPTER 4
Kaiser Effect Stress Measurement Method 4-1
4.1) Introduction 4-1
4.2) Data Processing 4-2
4.3) Kaiser Effect in Rock Materials 4-6
4.3.1) Physical Changes 4-6
4.3.2) Uniaxial Cyclic Loading 4-8
4.3.3) Directional Loading 4-9
4.3.4) Confining Pressure 4-10
4.3.5) Retention Time 4-13
4.4) Kaiser Effect in Soil Materials 4-15
4.5) Kaiser Effect in Concrete 4-16
4.6) Kaiser Effect in Ice and Snow 4-17

CHAPTER 5
Mechanisms of Brittle Failure in Rocks 5-1
5.1) Introduction 5-1
5.2) Observation Techniques 5-1
5.3) Initial Microstructure 5-2
5.4) Basic Principles of Fracture Mechanics 5-3
5.5) Mechanisms of Fracture Development Based on Stress-Strain Relationship 5-6
5.6) Crack Propagation Studies Based on Fractographic Technique 5-9

CHAPTER 6
Test Setup & Equipment 6-1
6.1) Introduction 6-1

6.2) Servo-Controlled Hydraulic Stiff Testing Machine 6-1
6.2.1) Straining Frame 6-2
6.2.2) Hydraulic Power Pack 6-4
6.2.3) System 2000 Analog Control Console 6-4
6.2.3.1) The SL 2000 Command Module 6-4
6.2.3.2) System Amplification and Control Modules 6-6
6.2.3.3) System Programming and Data Monitoring Units 6-8
6.2.4) Apple II Micro-Computer System 6-13
6.3) Acoustic Emission Monitoring System 6-16
6.3.1) Acoustic Emission Transducers 6-17
6.3.2) Pre-amplifiers 6-17
6.3.3) Cables 6-17
6.3.4) Signal Processor Unit 6-18
6.3.5) Ring-Down Counter/Event Duration Module 6-18
6.3.6) Amplitude/Rise Time Module 6-19
6.3.7) Time Difference Module 6-19
6.3.8) Parametric Input Module 6-19
6.3.9) Intelligent Graphics Terminal (IGT) 6-19
6.3.10) Software 6-20
6.4) Sample Preparation 6-21
6.5) Reduction of Spurious Noise 6-21

CHAPTER 7

Maximum Curvature Method 7-1
7.1) Introduction 7-1
7.2) Method of Tangents 7-1
7.3) Maximum Curvature Method 7-4
7.3.1) Measuring the Maximum Curvature of the Exponential Function. 7-6
7.3.2) Application of the Maximum Curvature Method to Long Length Acoustic Emission Data 7-10
7.3.3) Application of Maximum Curvature Method to Short Length Acoustic Emission Data 7-16
7.3.4) Maximum Curvature Method Algorithm 7-23
7.4) Conclusions 7-25

CHAPTER 8
Mechanical & Petrographic Study of Stanstead Granite 8-1
8.1) Introduction 8-1
8.2) Mechanical Properties of Stanstead Granite 8-1
8.3) Fracture Study in Relation to Acoustic Emission 8-4
8.3.1) Testing Programme 8-4
8.3.2) Petrographic Analysis 8-5
8.3.3) Porosity 8-5
8.3.4) Fractography 8-8
8.4) Discussion 8-12

CHAPTER 9
Laboratory Programme: Factors Affecting Stress Memory 9-1
9.1) Introduction 9-1
9.2) Selection of Transducer/Amplifier Frequency Response 9-1
9.3) Signal Definition Parameters 9-3
9.4) Effect of Loading Mode 9-6
9.4.1) Effect of Load Rate 9-6
9.4.2) Effect of Displacement Rate 9-10
9.4.3) Discussion 9-18
9.5) Effect of Specimen Size 9-18
9.6) Effect of Stress Level 9-19
9.7) Effect of Delay Time 9-23
9.8) Effect of Physical Changes 9-24
9.8.1) Effect of Water Disturbance 9-24
9.8.2) Effect of Temperature Disturbance 9-28
9.8.3) Discussion 9-29
9.9) Effect of Confining Pressure 9-29
9.10) Effect of Directional Loading 9-35
9.11) Remarks 9-36
9.12) Suggested Testing Method 9-39

CHAPTER 10
Laboratory Programme: Stress Memory of Various Rocks 10-1
10.1) Introduction 10-1
10.2) Description of Rock Types 10-1

10.2.1) Gabbro 10-1
10.2.2) Charnokite 10-1
10.2.3) Gneiss 10-1
10.2.4) Limestone 10-2
10.2.5) Darlye Dale Sandstone 10-2
10.3) Test Results 10-2
10.4) Discussion 10-13

CHAPTER 11
Field Programme: In-situ Stress Determination 11-1
11.1) Introduction 11-1
11.2) AECL Underground Research Laboratory 11-1
11.2.1) Geology 11-2
11.2.2) Mechanical Properties 11-5
11.2.3) Testing Program 11-5
11.2.4) Test Site 11-5
11.2.5) URL Test Results 11-8
11.2.6) Kaiser Effect Testing Program 11-8
11.2.7) Data Analysis 11-10
11.3) President Gold Mine 11-11
11.4) Conclusions 11-17

CHAPTER 12
General Conclusions & Recommendations 12-1
12.1) Introduction 12-1
12.2) Maximum Curvature Method 12-1
12.3) Fracture Mechanics and Kaiser Effect 12-2
12.4) Factors Affecting Stress Memory 12-3
12.5) Stress Memory of Hard Rocks 12-5
12.6) In-situ Stress Determination 12-6
12.7) Kaiser Effect Appraisal 12-7
12.7.1) Noranda's Copper Mine 12-8
12.7.2) Rock Types Exhibiting the Kaiser Effect 12-10
12.8) Recommendations for Future Work 12-11

References R-1

List of Figures

Figure 2-1: Borehole Deformation (overcoring) Method. 2-4
Figure 2-2: Absolute Stress Determination by the Flatjack Method. 2-6
Figure 2-3: Diagram of the Pressurized Section. 2-8
Figure 2-4: Schematic of the Photoelastic Borehole Stressmeter. 2-12

Figure 3-1: Fundamental Parameters Describing an Event. 3-7
Figure 3-2: Frequency Range for Seismic and Microseismic Monitoring. 3-8
Figure 3-3: Effect of Increased Travel Distance on the Frequency of Rock Noise. 3-9

Figure 4-1: Example of Estimation of Geo-Stress by Kaiser Effect. 4-3
Figure 4-2: Difference Method Based on AE Counts. 4-4
Figure 4-3: Difference Method Based on the Sum of AE Rate. 4-5
Figure 4-4: Existence of Kaiser Effect at Low Confining Pressure. 4-12
Figure 4-5: Relationship Between Initial Estimated Stress from Kaiser Effect and Number of Elapsed Days. 4-14

Figure 5-1: Schematic Figure Illustrating Three Modes of Fracture. 5-5
Figure 5-2: Four Types of Microcrack Nucleation Mechanism. 5-8
Figure 5-3: Schematic Illustration of Two Types of Crack Interactions Between Overlapping Cracks. 5-12

Figure 6-1: Hydraulic Stiff Testing Press. 6-3
Figure 6-2: Schematic Representation of System 2000 Analogue Console. 6-5
Figure 6-3: Waveform Output of SL 2253 Ramp Generator. 6-10
Figure 6-4: Generated Waveforms of SL 2253 Ramp Generator. 6-11
Figure 6-5: Waveform Output of Creep Test Routine. 6-14
Figure 6-6: Waveform Output of Cyclic Test Routine. 6-15
Figure 6-7: Coring Machine. 6-22
Figure 6-8: Grinding Machine 6-23

Figure 7-1: Simplified Algorithm Implementing the Method of Tangents.....7-3
Figure 7-2: Estimation of Kaiser Effect Using the Method of Tangents for Sample GE501.....7-5
Figure 7-3: Curvature of Function f(t) is the Rate θ Changes as a Function of Time.....7-7
Figure 7-4: Graph of Exponential Function and its Associated Curvatures.....7-9
Figure 7-5: Kaiser Effect Curve and Related Curvature using Raw Data for Sample GE501.....7-11
Figure 7-6: Kaiser Effect Curve and Related Curvature using Smoothed Data for Sample GE501.....7-13
Figure 7-7: Previous Load Estimates using MCM and Method of Tangents.....7-15
Figure 7-8: Kaiser Effect Curve and Related Curvature using Smoothed Data as a Function of Time.....7-17
Figure 7-9: Application of MCM to Short but Well-Defined Data from a Limestone Sample.....7-18
Figure 7-10: Kaiser Effect Curve and Related Curvature for Short Length Series Before Scaling.....7-20
Figure 7-11: Kaiser Effect Curve and Related Curvature for Short Length Series After Scaling.....7-21
Figure 7-12: Effect of Scaling on Curvature for Short Length Series.....7-22
Figure 7-13: Simplified Algorithm Implementing the Maximum Curvature Method.....7-24

Figure 8-1: Stress-Strain Relationship for Stanstead Granite.....8-2
Figure 8-2: Changes in Porosity as a Function of Load.....8-7
Figure 8-3: Increase in Total Number of Events as a Function of Stress.....8-9
Figure 8-4: State of Fractures in Stanstead Granite During Initial Stages of Loading.....8-10
Figure 8-5: State of Fractures in Stanstead Granite During Intermediate Stages of Loading.....8-11
Figure 8-6: State of Fractures in Stanstead Granite During Final Stages of Loading.....8-13
Figure 8-7: Number of Fractures Parallel to Stress Direction vs Stress Level.....8-15
Figure 8-8: Number of Fractures Perpendicular to Stress Direction vs Stress Level.....8-16

Figure 8-9: Opening of Twinings at 30% of Failure. 8-17
Figure 8-10: Opening of Twinings at 80% of Failure. 8-18

Figure 9-1: Energy Distribution for 5 Different Samples During the Second Load Cycle. 9-5
Figure 9-2: Effect of Loading Rate on Kaiser Effect for Samples Tested under Load Control. 9-8
Figure 9-3: Standard Deviation for Estimated Loads Shown in Figure 9-2. 9-9
Figure 9-4: Result of Kaiser Effect Test under Load Control Using the Very Fast Rate. 9-11
Figure 9-5: Result of Kaiser Effect Test under Load Control Using the Very Slow Rate. 9-12
Figure 9-6: Effect of Loading Rate for Samples Tested under Displacement Control. 9-14
Figure 9-7: Standard Deviation for Estimated Loads Shown in Figure 9-6. 9-15
Figure 9-8: Result of Kaiser Effect Test under Displacement Control Using the Very Slow Rate. 9-16
Figure 9-9: Result of Kaiser Effect Test under Displacement Control Using the Very Fast Rate. 9-17
Figure 9-10: Effect of Load Level on Stress Memory. 9-21
Figure 9-11: Errors in Estimated Load as a Function of Load Level. 9-22
Figure 9-12: Estimated Loads as a Function of Elapsed Hours 9-25
Figure 9-13: Estimated Loads as a Function of Elapsed Days 9-26
Figure 9-14: Standard Deviation for Estimated Loads in Figure 9-13 9-27
Figure 9-15: Kaiser Effect Curve and its Associated Curvature for a Confining Pressure of 7 MPa. 9-32
Figure 9-16: Kaiser Effect Curve and its Associated Curvature for a Confining Pressure of 14 MPa. 9-33
Figure 9-17: Relationship Between Confining Pressure and Estimated Axial Stress. 9-34
Figure 9-18: Schematic of Granite Block Stressed and Cored in Three Different Directions. 9-37

Figure 10-1: Effect of Time on Stress Memory of Gabbro. 10-3
Figure 10-2: Kaiser Effect and Associated Curvature for Gabbro. 10-4
Figure 10-3: Effect of Time on Stress Memory of Charnokite 10-5

Figure 10-4: Kaiser Effect and Associated Curvature for Charnokite..... 10-6
Figure 10-5: Effect of Time on Stress Memory of Gneiss..... 10-7
Figure 10-6: Kaiser Effect and Associated Curvature for Gneiss..... 10-8
Figure 10-7: Effect of Time on Stress Memory of Limestone..... 10-9
Figure 10-8: Kaiser Effect and Associated Curvature for Limestone..... 10-10
Figure 10-9: Effect of Time on Stress Memory of Sandstone..... 10-11
Figure 10-10: Kaiser Effect and Associated Curvature for Sandstone..... 10-12

Figure 11-1: Location of the Underground Research Laboratory..... 11-3
Figure 11-2: Simplified Block Diagram of the URL Site Geology..... 11-4
Figure 11-3: Plan View of the 240 and 420 Levels Showing Sample Borehole Locations..... 11-6
Figure 11-4: Section Showing the Relative Locations of the Sampled Boreholes..... 11-7
Figure 11-5: Cumulative AE and its Associated Curvature from Borehole 404-016-SM4..... 11-9
Figure 11-6: Plan View of Vertical Borehole Location..... 11-12
Figure 11-7: Section Showing the Dike and Borehole Location..... 11-13
Figure 11-8: Variation of the Ratio of Average Horizontal to Vertical Stress with Depth..... 11-15
Figure 11-9: (a) Variation of Vertical Stress. (b) Variation of Horizontal Stress with Depth..... 11-16

Figure 12-1: Cumulative AE and its Associated Curvature from Sample GP25.... 12-10

List of Tables

Table 7-1: Results of Estimating Kaiser Effect using MCM and the Method of Tangents.....7-14

Table 8-1: Mechanical and Physical Properties of Stanstead Granite.....8-3
Table 8-2: Petrographic Analysis of Stanstead Granite. 8-6

Table 9-1: List of Transducers Utilized. 9-2
Table 9-2: List of Amplifiers Utilized.....9-2
Table 9-3: Load Rates for the First and Second Load Cycles under Load Control Mode. 9-7
Table 9-4: Load Rates for the First and Second Load Cycles under Displacement Control Mode.....9-13
Table 9-5: Effect of Diameter on Stress Memory Determination. 9-20
Table 9-6: Effect of Length to Diameter Ratio on Stress Memory Determination. 9-20
Table 9-7: Effect of Water Disturbance on Estimated Load from Stanstead Granite Samples. 9-30
Table 9-8: Effect of Temperature Treatment on Estimated Load from Stanstead Granite Samples. 9-30

CHAPTER 1

Introduction

The stability of underground excavations not only contributes to improve production but also insures the safety of the personnel. Irrespective of the size of the mining operation, a scientific analysis and design of underground rock excavations profits vastly from the knowledge and understanding of existing stresses within the rock mass. In practice, parameters such as the magnitude of the stress and the strength of the structure are estimated rather conservatively, to provide an acceptable margin of safety. More reliable data regarding the stresses acting on a structure and more accurate estimates of its residual strength (potential for carrying more load) would result in increased production and structural stability.

Stress is defined as force per unit area and according to the first law of motion, force is defined as the product of mass times acceleration. In the International System of Units, stress is defined in Pascal (Pa), area in meter squared (m^2), force in Newton (N), mass in kilogram (kg) and the acceleration in meter per second squared (m/s^2). From the rock mechanics point of view, one Newton or one Pascal is a relatively small force and stress respectively. Because of the magnitude of stresses one must deal with in mining engineering practice, this quantity is generally expressed in mega Pascal (MPa) which is equivalent to 10^6 Pa. Similarly, force is expressed in kilo Newton (kN) or 10^3 N.

Stresses found in rock masses can be grouped according to their origin into natural stresses and induced stresses. The former are the stresses found in rock before excavation and the latter are the result of stress changes due to manmade excavations. Natural stresses are comprised of gravitational stresses, tectonic stresses, residual stresses and thermal stresses and are examined in detail elsewhere [86].

Theoretical evaluations of the state of in-situ stress are often just estimates that cannot take into account all contributing elements and conditions because the stress-strain equations developed for this purpose are all based on the assumption

that the rock mass is linear-elastic, homogeneous and isotropic, which is not always applicable. The in-situ stress determination is not an easy task. A number of techniques and equipment have and are being developed to measure this parameter with certain limitations. The main disadvantage of the established rock stress measuring methods such as overcoring, flatjack, stress-meter and hydrofracturing, which hinders their extensive use is the cost and time restrictions associated with each measurement. For example, the expenditures related to one overcoring test is about $8,000 CDN, neglecting the cost of drilling, transportation and man-power.

To aid the situation, this thesis represents the initial part of a research project undertaken by the Department of Mining and Metallurgical Engineering to investigate in detail the feasibility of determining in-situ stresses in hard rocks using the Kaiser Effect phenomenon. To do so, core samples extracted from a given mine environment will be tested with reference to drilling orientation. The main advantage of this method is that the Kaiser Effect is only dependent on the level of applied stress, i.e., no strain measurements are necessary. In turn, no constitutive model of the rock mass would be required to estimate stresses at a given point. In addition, the Kaiser Effect tests can be conducted at a very low cost and shorter time for the mining engineer.

The Kaiser Effect phenomenon was first discovered by Dr. Joseph Kaiser of Munich in 1953. He observed that when the stress on a metal under tension is relaxed from a level of historic high, and stressed again, there is little or no acoustic emission activity measured before the previous maximum is reached. Once the level of historic high is exceeded, there is a significant outburst in the rate of acoustic emissions.

The Kaiser Effect phenomenon can also be observed in geological materials. In 1976, Kanagawa et al. [37] made the first attempt at estimating in-situ stresses using the memory of the maximum stress level locked in the rock samples recovered from an underground excavation. Since then only a handful of researchers have attempted to use the Kaiser Effect to estimate paleo-stress in geological materials. As described in the previous paragraph, the stress memory reveals itself by an outburst in the number of acoustic emission events when a rock specimen is loaded beyond the level of previous maximum stress. Acoustic

emission events (referred to as microseismic events in geological materials) are generated when the material under load responds by making small-scale displacement adjustments to reach a state of equilibrium. These small-scale displacement adjustments could be the result of intergranular re-arrangements, twinning and fracture initiation and/or propagation between and/or through the rock's mineral constituents.

The main objective of this research project is to contribute to detailed understanding of the Kaiser Effect phenomenon in hard rocks under uniaxial compressive testing conditions. This topic has received limited attention in the past and has stirred considerable controversy in its use and application. It is hoped that the results of this work would provide an easy and inexpensive technique to determine stresses for the mining engineer and to increase the use of stress measurement in the design and planning of mining excavations.

The first part of this research programme conducts a fundamental study to examine in detail the major parameters which are likely to affect the stress memory of rocks. Based on the knowledge and experience gained from the laboratory programme, the second part aims at conducting a comparative study between stress values estimated in the laboratory with the results obtained in the field using traditional methods. By performing a large number of laboratory experiments on different rock types, it would be possible to evaluate how efficient, accurate, and economical the Kaiser Effect method is compared to other stress measurement techniques. The work carried out in this thesis is organized in twelve chapters as follows:

Chapter 1, the current chapter, introduces the topic of stress measurement in rocks, the Kaiser Effect phenomenon in materials, the need for more efficient and accurate stress measurement techniques and the extent of research carried out in this work.

Chapter 2 presents an overview of the most common methods used today to measure in-situ stresses in the field of mining engineering.

Chapter 3 reviews the acoustic emission method in geological materials from its conception to its acceptance in the world as a practical engineering tool.

Chapter 4 is a state-of-the-art report on the advances made in the field of stress memory measurement in geological materials using the Kaiser Effect phenomenon.

Chapter 5 describes the mechanisms of brittle failure in rocks and discusses the techniques that are available today to sight direct evidence of stress induced features.

Chapter 6 elaborates on the important aspects of the testing equipment available to carry out this investigation. In addition, details regarding sample preparation and the approach used to reduce the level of spurious noise generated by the testing equipment are also discussed.

Chapter 7 presents a new method called the Maximum Curvature Method (MCM) for determining the previous stress level. This method is an important contribution to the field of the Kaiser Effect in the sense that it represents the first truly objective method proposed to identify the Kaiser Effect from acoustic emission data. Details concerning the implementation of the algorithm are given. In addition, the results of a study comparing the performance of the MCM with the other objective technique that has been used in the past, the Method of Tangents, are discussed.

Chapter 8 describes the mechanical and petrographic properties of the main rock type (Stanstead granite) used in this investigation. To understand the mechanisms responsible for triggering stress memory, a detailed study was carried out to identify the type of fractures that generate acoustic emissions in Stanstead granite at different stress levels.

Chapter 9 presents the most comprehensive investigation of its kind into various factors affecting the stress memory of rocks, in particular Stanstead granite. This work is unique in the sense that it studies all the elements that could influence the Kaiser Effect under uniaxial compressive conditions by testing a very large number of samples using the same rock type, test procedure and equipment. The Maximum Curvature Method is applied to acoustic emission data to measure the recollection of previous stress level. This means that every attempt is made to use

a common denominator such that the data from all experiments could be analyzed and compared independently of each other. A testing procedure for the Kaiser Effect experiments is proposed at the end of this chapter.

Chapter 10 investigates the effect of time on stress memory of five different rock types. The tests were carried out over periods of time ranging from 1 week to 21 weeks, using the testing procedure developed in Chapter 9. The data for estimating the Kaiser Effect are analyzed by applying the Maximum Curvature Method.

Chapter 11 presents the results of the field component of this research programme. Cores from two different underground locations in Canada and one gold mine in South Africa were tested and the estimated stresses were compared with in-situ values determined by theoretical and conventional methods. Details regarding the methods and equations used to derive the magnitude of the major and minor principle stresses are given along with a discussion about the importance of obtaining high resolution acoustic emission data from rock specimens.

Chapter 12 summarizes the research findings and discusses the applicability of the Kaiser Effect to measure in-situ stresses in certain types of hard rocks. Recommendations are also made to further the existing body of knowledge on the subject of stress memory and in-situ stress measurement using the Kaiser Effect phenomenon.

References lists over 90 articles, reports and books cited in this thesis. It is a comprehensive and up-to-date bibliography on the subject of stress memory measurement in geological materials.

CHAPTER 2

Standard Stress Measurement Techniques

2.1) Introduction

Designing or evaluating the stability of structures in rock masses requires a knowledge of the state of stress. The structure may be a mine, tunnel, underground power station, hardened military installation or a storage reservoir for oil and natural gas.

For design purposes, it is desirable to estimate the state of stress at the proposed site before underground access is made possible. Where the geology is well-suited, the sub-surface stress may be estimated from the weight of the overlying rock mass. In this situation, the vertical component of stress is determined at the desired point, using the following equation:

$$\sigma = \rho \cdot g \cdot h \qquad (2\text{-}1)$$

where σ = the stress (MPa).
ρ = the density of the rock (t/m^3).
h = the depth of measurement (m).
g = the gravitational acceleration (9.81 m/s^2).

This approach has produced excellent results compared with underground measurements, although exceptions have been encountered in the proximity of large mechanical defects in the rock mass such as faults [1]. The horizontal component of stress has also been calculated by assuming that the subsurface rock mass is homogeneous, isotropic, linear-elastic, laterally constrained, that no tectonic forces are in action and by assuming in addition that the vertical stress is known. However, actual in-situ measurements have shown unambiguously that horizontal stresses many times the magnitude calculated using the above approach may be present [1].

It is clear that the estimation of the stress field cannot be made on a rational basis only. Many investigators have studied this problem and a number of techniques and instruments have been developed for determining the state of stress in a rock mass. The following sections will present an overview of various procedures that have been used over the years for this purpose.

2.2) Stress Measurement Techniques

No device or procedure has been developed to date that will measure stress directly. This quantity must therefore be determined indirectly, by measuring displacements or deformation. Most techniques for measuring stress from displacement rely on the theory of elasticity i.e. they can be applied if the rock medium is linear-elastic or nearly so.

The complete stress tensor in a homogeneous, isotropic and linear-elastic medium can be determined from six strain component measurements. The governing equations are:

$$\sigma_x = \lambda e + 2G\varepsilon_x \quad , \quad \tau_{xy} = G\gamma_{xy} \tag{2-2a}$$

$$\sigma_y = \lambda e + 2G\varepsilon_y \quad , \quad \tau_{yz} = G\gamma_{yz} \tag{2-2b}$$

$$\sigma_z = \lambda e + 2G\varepsilon_z \quad , \quad \tau_{zx} = G\gamma_{zx} \tag{2-2c}$$

where σ_x, σ_y, σ_z, are the normal components of stress,
τ_{xy}, τ_{yz}, τ_{zx} are the shear components of stress,
ε_x, ε_y, ε_z are the normal components of strain.
γ_{xy}, γ_{yz}, γ_{zx} are the shear components of strain.
e is the volumetric strain.
G is the modulus of rigidity.
λ is Lame's constant.

None of the instruments designed to measure displacements can provide the six components of strain simultaneously. In general, these instruments measure only a part of these strain components. For example, the strain rosette provides three strain measurements from a free surface which are used to calculate the principal stresses parallel to that surface.

2.2.1) Borehole Deformation (overcoring) Method

The method of overcoring was developed by the United States Bureau of Mines [2]. The general procedure of measuring in-situ stress using the overcoring method is illustrated in Figure 2-1. The essential features of this procedure are as follows [3]: first, a large diameter hole, typically 100 mm (NQ size) or 150 mm is drilled into the rock surface to about 200 mm of the desired location for stress measurement. A small diameter hole, 38 mm (EX size) and about 600 mm in length, concentric with the larger hole is then drilled through the test position. The borehole deformation gage is inserted in this hole, radially oriented in an area free of fractures and joints. Next, the section of the core containing the gage is concentrically overcored with a larger diameter bit, thus stress relieving the core containing the gage.

The corresponding changes in the strain or deformation are monitored during overcoring using the gauge connected to a digital strain indicator. The stress is evaluated from the measured changes in the strain. The modulus of deformation required in the calculation of stress is determined by testing the overcored rock sample in a biaxial chamber after recovery from the hole.

Typically, during the in-situ stress measurement cycle, the gage is moved to a point farther in the hole, oriented at 60 degrees from the original position and the overcoring process is repeated. This cycle is continued for the 60 degrees rosette positions until the desired range of depths has been investigated. Where tests are carried out in three holes, the holes should be oriented at 45 to 60 degrees to each other to allow statistical analysis to be used to determine the complete stress tensor.

The overcoring method for determining the absolute stress or the change in stress in rock is satisfactory for use in rock that is relatively isotropic and linear-elastic. If a rock is anisotropic, has a non-linear stress-strain curve or has a large area within the stress-strain curve, the accuracy of stress determination is decreased in proportion to the extent of these deviations [1]. Although rocks may exhibit these unfavorable characteristics, some information can be obtained by this procedure regarding the direction or the ratio of the secondary principal stresses.

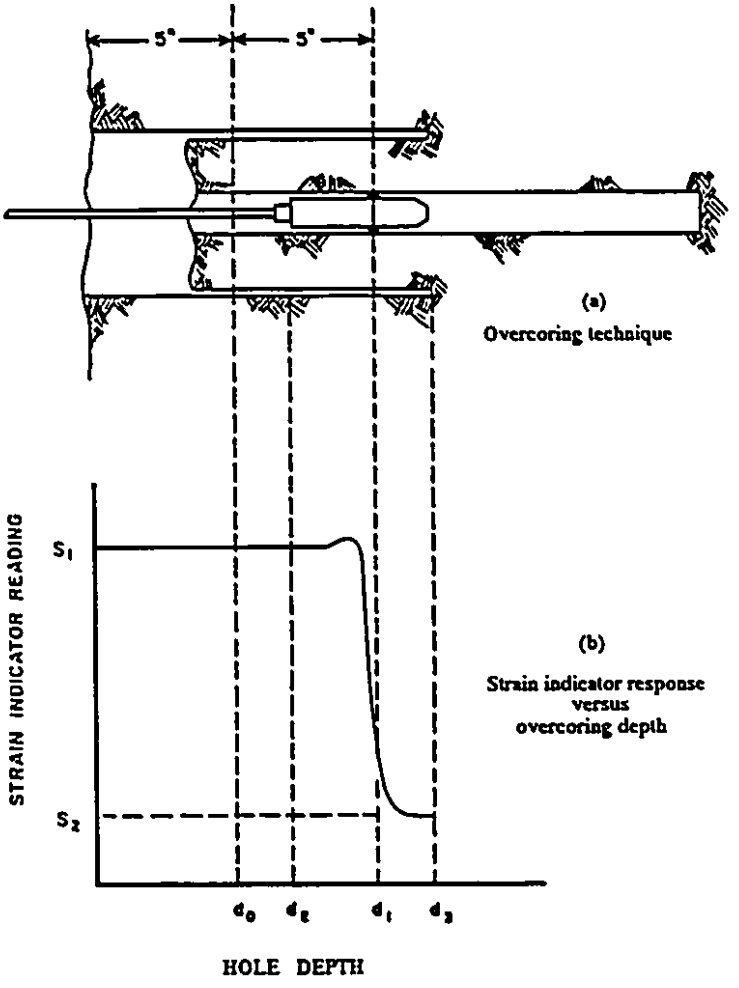

Figure 2-1: Borehole Deformation (overcoring) Method.

There are several gauges available to carry out overcoring tests. The most widely used gauges are the doorstopper cell from South Africa (CSIR gage), Lulea triaxial gage from Sweden, the USBM deformation gage and the CSIRO hollow inclusion cell [3]. For example, tests using the USBM deformation gage are relatively simple and two tests can be generally carried out each day. The instrument is rugged and reliable and a success rate of 30% can be expected [3]. Installing the CSIRO cell is much more complex compared with the USBM gage because it has to be glued in place. The full curing time of the glue is 12 to 16 hours. This implies that a maximum of one test a day can be undertaken. Problems associated with the use of this gage are significant. For instance, if there is a slight flow of water or gas at the end of the hole, it is possible that the glue will be washed out before setting, leaving bubbles around the gage. The success rate using these cells are significantly lower, the gages are not reusable and they are expensive. In contrast to the USBM gage, the disposition of the strain gages allows the determination of the three dimensional stress field around a single borehole. It is a good practice to conduct CSIRO tests in a second borehole of different orientation to confirm the results of the measurements [3].

2.2.2) Flatjack Method

Developed by Habib and Marchand [4], the flatjack method measures the absolute stress in a rock mass. As shown in Figure 2-2 two vibrating wire strain gages are mounted on a rock surface oriented in such a way as to measure in the line of the intended stress determination, in order to take an initial strain reading. A slot is then cut between the strain gages of sufficient area to produce a partial strain relief and a flatjack is grouted therein. Allowing enough time for the grout to cure, the flatjack is pressurized to a value such that the strain gauges indicate the initial value. The exerted pressure is assumed to be equal to the stress normal to the plane of the flatjack that existed in the rock before the slot was cut.

This procedure was later modified by Panek and Stock [5] by replacing the surface mounted strain gauges with copper foil jacketed resistance gauges grouted in slots cut above and below the intended flatjack slot. These gages are placed directly above and below the center of the flatjack and oriented so that they will measure the strain in the direction normal to the flatjack. This modification

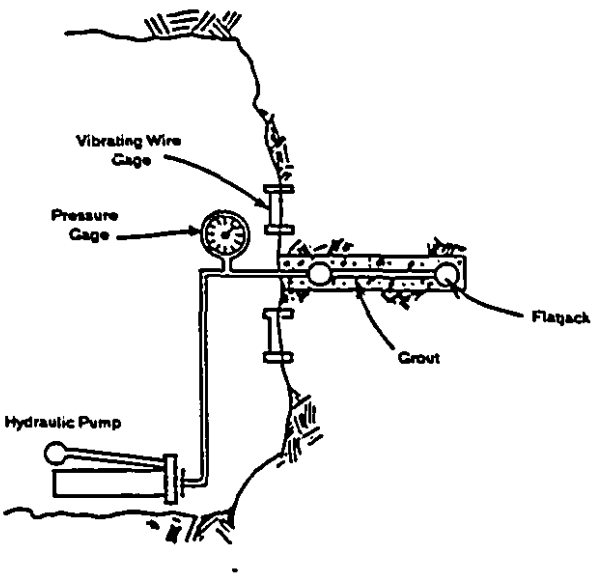

Figure 2-2: Absolute Stress Determination by the Flatjack Method.

improved the sensitivity and accuracy of stress determination. The procedure was further modified to replace the strain gauges by small hydraulic cells grouted in drill holes. The sensitivity of the hydraulic cells was found to be comparable to that of strain gauges.

The flatjack method does not require any knowledge of the elastic constants of the rock. Because of the difficulty in cutting deep flatjack slots, the method is limited to near surface measurements. The method is especially useful for measuring stress in inelastic rock [1]. Because of the stability of the flatjack and the hydraulic sensing device, the method is suitable for measuring stress changes over long periods of time. The method can therefore be used to monitor changes of stress produced by continued underground excavation. However, because of the averaging effect due to the comparatively large area of the flatjack, it is less sensitive to local variations in the rock stress.

2.2.3) Hydraulic Fracturing

The general concept of determining the triaxial state of in-situ stress using the hydro-fracturing method has been outlined by Hubbert and Willis [6] and Haimson and Fairhurst [7] and many subsequent authors. In general, the method assumes that the borehole is parallel to one of the principle stress axes. Except in areas of extreme relief, the vertical stress is assumed to be the principal stress. The other two principal stresses are therefore horizontal, plain strain conditions are applicable and the analysis may be considered in two dimensions [3].

Hydraulic fracturing is also used in the petroleum industry to enhance well production [1]. A section of the well is sealed off with packers as shown in Figure 2-3 and then the fluid pressure in this section is increased until surrounding rock is fractured. From a consideration of the stresses produced by the fluid pressure on the walls of the section, Kehle [8] has shown that inferences can be made regarding the stress field in the proximity of the well.

Test zones are selected in fracture free areas with minimal inherent fabric and where potential planes of weakness are absent. Borehole length must be in

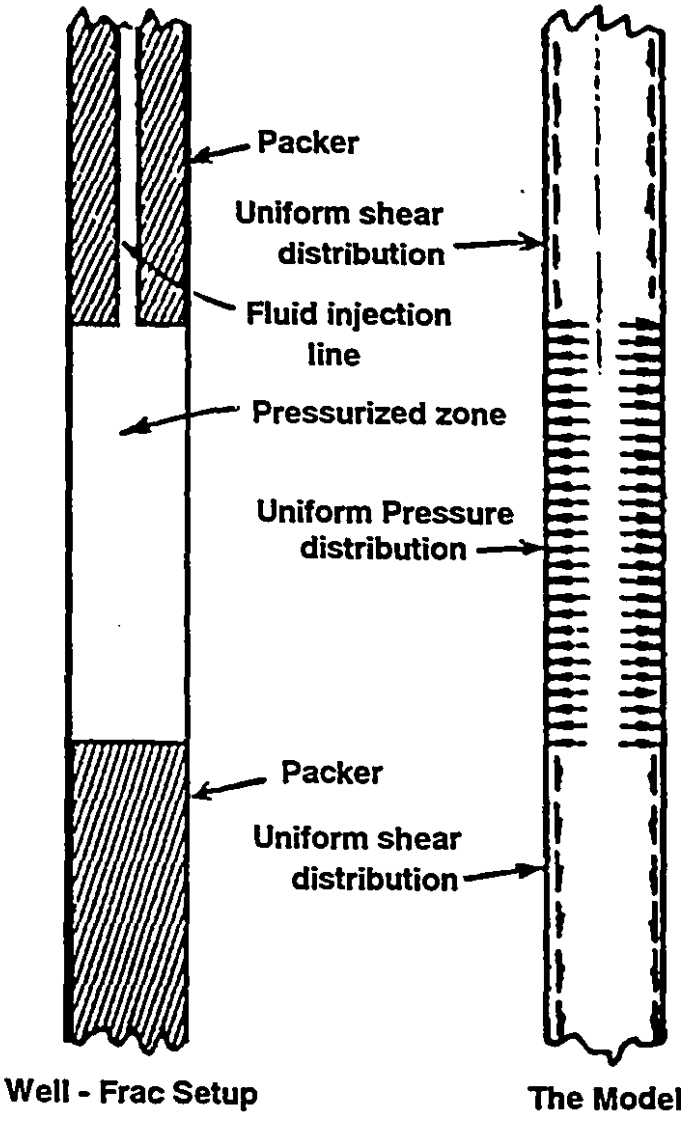

Figure 2-3: Diagram of the Pressurized Section.

excess of 1 meter and the diameter similar to that used for overcoring. The hydro-fracturing testing procedure comprises the following sequences [3]:

a) first cycle during which the pressure in the test zone is increased until new fractures develop (sudden drop in pressure and increase in flow rate) or until the maximum attainable pressure is reached. In order to avoid fluid penetration in the rock, the breakdown should be achieved in less than two minutes from the start of pumping. At this point, the pump is turned off and the pressure decay is monitored and recorded. Enough time must be allowed for the pore water pressure to dissipate.
b) second cycle (same as first cycle).
c) third cycle (same as first cycle).
d) last cycle or stepwise re-fracture where the injection flow rate is kept at a constant value so that stable pressure is obtained. This procedure is repeated several times at various pressure levels. The flow is monitored as number of pump strokes over a period of time.

Once the hydro-fracturing test is completed, it is important to determine the direction of fractures. An impression packer is lowered into the hole and inflated to about 5 MPa. This pressure is held for 30 minutes so that the fracture trace makes its impression on the uncured rubber wrap. The impressions on the wrap are then sketched and photographed for later analysis.

Thus, hydraulic fracturing provides a means of obtaining information regarding the state of minimum principle stress in boreholes without any knowledge of the elastic constants of the rock mass. In order to obtain estimates of the maximum principle stress, significant assumptions regarding pore water pressure, tensile strength of the rock mass and elasticity must be made. Because the maximum principal stress is the most important component in underground excavation design, the indirectness of the method in determining this parameter makes the method of hydraulic fracturing questionable [1].

2.2.4) Propagation Velocity Method

The velocity of a longitudinal wave passing through a rock mass is a function of the density, modulus of elasticity and Poisson's ratio of the medium and the

acceleration of gravity. For a number of rock types, the modulus of elasticity and Poisson's ratio depend on the stress [9]. In order to determine this stress, the propagation velocity is measured between two points in the rock mass. The rock is sampled by coring, and a velocity versus stress measurement is established by laboratory testing. The master curve thus obtained will serve as the basis for estimating the in-situ stress from in-situ propagation velocity measurements.

At first glance, this procedure is simple in principle, however, a number of difficulties arise in practice. For example, the velocity-stress relationship for some rocks is constant at medium to high stress levels. Therefore, for these rocks, the method is not applicable. Another problem concerns the fact that for rocks that exhibit significant velocity changes as a function of stress, there may be a large specimen-to-specimen deviation in the velocity at a particular stress level. If these deviations are similar in magnitude to the change in velocity with stress, the precision of the results is questionable. In addition, where the rock mass is fractured or jointed, the reproducibility of the in-situ measurements may be poor.

2.2.5) Core Discing

Exploratory drill cores may provide information about the subsurface state of stress. Obert and Stephenson [10] first reported that core disking will occur in a triaxially loaded body when the radial stress applied to the body is greater than the axial compressive stress plus the value of the radial stress needed to produce discing at zero axial stress.

2.2.6) Other Methods of Determining Stress in Rocks

A number of additional techniques and instruments are available for determining the state of stress in a rock mass. Instruments such as rigid deformeters for surface or axial borehole require no special procedural instructions to place them in service.

Surveying equipment such as levels, theodolites and tachymeters have been used to measure lateral and vertical movement in surface and underground mines.

For example, surface displacements have been converted into strains in order to calculate the stress in large structural members such as roof lamina [1].

Where safety considerations prohibit the presence of an observer in the measurement area, fluid levels and tilt meters are used to provide an accurate and comparatively inexpensive means of measuring both large and small vertical displacements such as floor heave or roof sag. These instruments are subject to errors due to differences in the atmospheric pressure and temperature at both ends of the tube.

Photo elastic strain and stress meters operate on the principle that the stress-dependent fringe pattern developed in the model is produced by the transmission of polarized light through a birefringent model material. Zandman and Wood [11], Roberts [12] and Barron [13] have described various devices of this kind. These instruments are only suitable for measuring stress changes. Figure 2-4 shows the operation of one such device as described by Roberts [12]. A glass cylinder about 11/2 in length and a diameter just less than the size of the drill hole is placed and cemented in the drill hole. If the hole is subjected to load, the glass is strained and displays an isochromatic fringe pattern when observed under a circular polarized light. The light is provided by a lamp and a polarized filter placed on the opposite end of the glass from the observer. Changes in the secondary principle stress ratio produce corresponding changes in the fringe pattern which are characteristics of the applied state of stress.

The stress-strain behavior of some rocks, especially salt, has been proposed as the basis for in-situ stress determinations. If the process is stopped at σ_1 and the load removed, the strain will not be recovered completely but rather will return to some point e. If the rock specimen is loaded again, the strain will follow a new loading path from e to c and then continue along the characteristic curve from c to d. If a rock mass were loaded by the weight of the superincumbent rock to some point b and the stress relieved, it should return to point e. If the same rock were then reloaded it would follow the curve ecd. The pre-existing state of stress in the rock could be estimated from the position of the knee at point b, corresponding to the stress σ_1. Laboratory studies by various investigators have indicated that the knee of the reloading curve is often not well defined, and hence the accuracy of the determination may be poor.

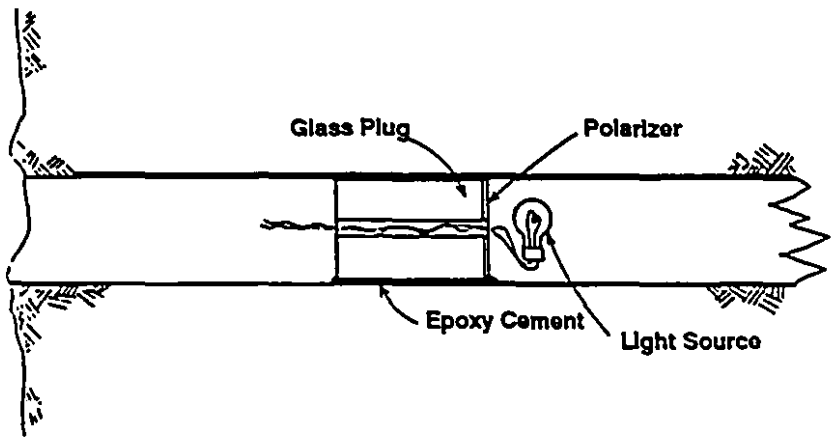

Figure 2-4: Schematic of the Photoelastic Borehole Stressmeter.

Hult [14] and Hult et al. [15] proposed methods of determining rock stress based on a knowledge of the time-dependent deformation characteristics of rock. For example, if a hydraulic cell is placed in a borehole in close contact with a viscous rock, after a long period of time, the pressure in the hydraulic cell should be equal to that in the rock. Of course this test would not be practical. However, if the time-dependent characteristics of the rock were known from laboratory creep tests, it would not be necessary to continue the test for a very long time. Rather the stress could be estimated from creep measurements made over shorter periods of time.

Hult et al. [15] suggested that the time-dependent behavior of rock might be estimated from rheological models (spring-dashpot models) such as the Maxwell, Voigt or Burger models. However, most static creep tests indicate that the time-dependent behavior of rock does not conform to that expressed by any of these models, or at least not by models with four or fewer spring-dashpot elements.

2.3) Conclusions

Due to the large number of existing instruments and procedures for measuring the in-situ stress, there is no accepted uniformity or standardization among researchers or in the industry. ASTM has made a number of suggestions and recommendations regarding the specification and calibration of commercially available equipment. The specifications concern the design and fabrication of the instrument, sensitivity, magnification, range and length of deformation and strain gauges. In addition, the basis for relating the measured strain quantity to in-situ stress must be explicitly explained as well as monitoring the time-stability of the instrument if measurements are to be made over extended periods of time or in adverse underground conditions.

CHAPTER 3

Acoustic Emission Method

3.1) Introduction

ASTM E610-82 [16] defines acoustic emission (AE) as "the class of phenomenon whereby transient elastic waves are generated by the rapid release of energy from localized sources within a material, or the transient elastic waves so generated. Acoustic Emission is the recommended term for general use. Other terms that have been used in AE literature include (1) stress wave emission, (2) microseismic activity and (3) emission or acoustic emission with other qualifying modifiers".

Dr. H.R. Hardy of Pennsylvania State University suggested the use of the term microseismic activity to describe the phenomenon of acoustic emission in geological materials. In this document, the terms microseismic and acoustic emission will be used interchangeably, both referring to Hardy's definition. Therefore, given the scope of the present research, no references will be made to studies carried out using other materials. One must however recognize the fact that today, the bulk of acoustic emission publications in the world deals with the study and application of this phenomenon in metals, synthetic and composite materials.

3.2) Historical Background

The microseismic method was born in 1938 when the U.S. Bureau of Mines began a research program to determine whether a relationship could be established between seismic velocity and pillar load. Two geophones were placed in a pillar at a predetermined separation. A seismic pulse was sent along the pillar and from the time it took this pulse to travel between the two geophones, a seismic velocity was calculated. Subsequent experiments revealed that higher than normal seismic velocities were associated with pillar loads. It was also noticed that spurious seismic signals at a rate of 4 or 5 a minute were generated within the pillar. It was

concluded that these naturally occurring seismic signals were the result of high stress conditions in the pillar [17].

Obert [18] conducted similar tests in a deep copper mine where the same self-generating seismic signals were observed. During the test, the ground that had been quiet became seismically active and the level of rock noise increased continuously for 15 minutes before terminating with a rock burst some 50 feet from the test site. These findings prompted the U.S. Bureau of Mines to conduct a series of laboratory and field tests to learn about the occurrence of these self-generated seismic signals. Laboratory experiments showed that rock specimens loaded in a testing machine produced sub-audible rock noise and the number of emissions increased as failure approached.

The first microseismic listening device was quite simple. It consisted of a geophone to detect seismic signals, an amplifier to boost the level of the signals and a head set for listening to the amplified signals. Field applications of the microseismic method consisted of listening to suspected unstable rock structures. A microseismic rate was calculated by counting the number of emissions detected per minute. Standards were developed based on the emission rate in order to monitor the stability of the structure. For example, a low steady rate of less than a few emissions per minute was indicative of a stable background noise. Emission rates greater than 10 per minute reflected potentially unstable conditions. A sudden increase in microseismic activity (10 to 20 fold) was interpreted as imminent failure (rock burst) in a nearby rock structure.

In early forties, the U.S. Bureau of Mines [19] and the Canadian Federal Department of Mines [20] initiated a series of programs towards the prediction of rock burst in underground mines. Based on previous experience, it was expected that all rock bursting would be preceded by a dramatic and easily detectable increase in seismic activity. However, the microseismic monitoring of Ahmeek mine in Northern Michigan failed to produce the desired results. It should be noted that the "predictions" were made after the rock burst occurred based on detailed analysis of the data. Among the fourteen predictions that would have been made over the 40 day monitoring period, only 9 predictions would have been followed by rock bursts, five predictions would not have been followed by rock burst and 2 would not have been predicted at all. Based on this and subsequent

works, it was concluded in the U.S. and Canada that the microseismic method is not suited for routine prediction of rock burst.

In the early days, the success of most microseismic monitoring was directly related to the listener's experience, knowledge and enthusiasm. An operator for example, could distinguish rock noise from mine and cultural noise. Some operators were even able to tell whether the signals they were hearing came from a pillar or from the surrounding rock. Monitoring mine activity was usually conducted between shifts or during lunch or dinner breaks when the mine activity was stopped or at a minimum. While the microseismic monitoring showed real potential, determining true rock noise and locating its source was fraught with uncertainty [21].

The microseismic method became popular after the publication of the initial U.S. Bureau of Mines report. The method was applied throughout the world in hard and soft rock mines as well as in civil engineering excavations. At this point single channel monitoring was replaced by multi-channel monitoring and for the first time the output of the sensors were recorded on slow-speed chart paper. This improvement allowed the possibility of monitoring larger areas and enabled the analyst to make a judgment about the origin and relative size of individual events. For instance, it was presumed that when an event was detected by more than one geophone, the channel reflecting the greatest amplitude was nearest the source. In addition, recording data during desired time periods could be programmed on timers, thus eliminating the need for manned monitoring [21].

In late 1950's, nearly 20 years after its conception, the microseismic method was regarded as more of a novelty than an engineering tool. The reason for this lack of confidence was that the method was too subjective and qualitative to be reliably used for delineating areas of high stress and potential failure. Despite considerable usage and continued research by the U.S. Bureau of Mines [20], it had not advanced beyond its initial and early successes.

During the same period, the same phenomenon was independently discovered in metals (e.g. Dr. Joseph Kaiser of Munich) and referred to as acoustic emissions. Acoustic emission research in metals rapidly expanded and encompassed other applications such as leak detection in steel reservoirs and

fatigue testing of spare parts, enjoying greater success than that achieved with geological materials.

In the early 1960's the progresses made in the field of solid-state electronics allowed acoustic emission techniques to become more sophisticated. Widespread use of multi-channel monitoring systems equipped with magnetic tapes to store data from a number of geophones prompted researchers to attempt determining the source of rock noises by triangulation [21]. In South Africa, Cook used an array of 14 velocity type geophones to locate the source of large seismic events and rock bursts accompanying deep mining [22]. Source location was performed by combining first arrival data from each geophone with their respective spatial coordinates and used a string model to calculate the source position. He concluded that most of the seismic activity originated in the solid rock immediately ahead of the working face.

The U.S. Bureau of Mines revived microseismic research in mid 1960's mainly due to increased interest showed by mining and construction companies. Blake and Duvall [23] developed a broad-band microseismic system for determining the source of microseismic events in the field. Using this new equipment and new data analysis techniques Blake and Leighton [24,25] located the source of every event in a deep mine. Delineating areas of high stress and recognizing some characteristic patterns that would lead to rock bursts became possible. Because of the potential of this technique as a promising tool for deep mining, the U.S. Bureau of Mines developed two new monitoring systems for use in research and investigations.

During the same period, traditional single channel microseismic monitoring systems continued to be used in underground and surface mines. This method proved to be effective in evaluating the stability of land slides or cut slopes in a number of cases, the most interesting being the work carried out by the California Highway Department to assess slide zones [26]. Here, it was reported that high microseismic rates were indicative of a moving or unstable slope. In some cases road closures through landslide areas were based on the results of this monitoring.

By the end of 1960's, the microseismic method was being used successfully in mining and civil engineering applications in underground and surface excavations.

Furthermore, laboratory studies provided much needed data to understand the behavior of these materials under various loading conditions. The microseismic method had finally become of age as a practical engineering tool.

The decade of 1970's can be remembered as a period when the microseismic method found a wide variety of applications and reached a new level of sophistication. Poland, Czechoslovakia and West Germany made important progress in improving ground control and reducing hazard from coal bumps [27,28,29]. Monitoring the stability of underground storage cavities and locating any potential failure zone [30], monitoring earth dams and embankments [31,32] are few examples of research and field studies carried out during this period.

In late 1970's and most of the 1980's the acoustic emission studies proved to be very useful in studying the mechanisms of rock failure, soil behavior and their evolution under stress [33,34]. Moreover, interests in field studies in the low frequency range of 10-10,000 Hz shifted to much higher frequencies. Monitoring in the 35 kHz range and higher were successfully used for field studies whereas laboratory experiments concentrated mainly around 30-200 kHz range. The Japanese became more active in the area of laboratory testing, especially in the 1980's with most of their research being conducted in areas such as failure mechanism, stress measurement and creep behavior in various rock types.

3.3) Properties of Microseismic Events

The microseismic activity is characterized by a number of parameters associated with the occurrence of a simple microseismic event or a group of events. Commonly used parameters are:

1) Total Events or Accumulated Activity: the total number of events detected during a specified time interval.
2) Microseismic Rate or Rock Noise Rate: the number of events detected per unit time.
3) Microseismic Peak Amplitude: the maximum amplitude of a recorded event in arbitrary units.
4) Microseismic Energy: a measure of the magnitude of a detected event as determined by any of a number of methods.

5) Total Energy or Accumulated Energy: the sum of the energy released by all events detected during a specific time interval.
6) Energy Release Rate or Energy Rate: the sum of the energy released by all events detected per unit time.
7) Energy per Event: the total energy divided by the total events detected during a specific time interval.

Figure 3-1 illustrates the fundamental parameters derived from the waveform of a microseismic event. The threshold level is arbitrary, normally set equal to two or three times the background noise level.

The frequency content of microseismic events depend in great part on the type of mechanism responsible for their generation, the volume of rock involved and the location of sensors. For instance, events that are associated with the formation of microcracks have frequencies in the higher end of the spectrum, generally between 150 to 160 Hz. Rockbursts on the other hand are made up of frequencies in the 120 to 130 Hz range. Furthermore, because the earth acts as a lowpass filter, higher frequency components of any event are attenuated as the distance between the source and receiver is increased. Figure 3-2 [35] shows the frequency spectra over which seismic and microseismic studies are most commonly conducted. Figure 3-3 [36] shows how increased travel time or distance filters out high frequency components of an event detected at two geophones separated a few hundred feet.

The duration of microseismic events vary from microseconds for small high frequency events up to tens of seconds for large rock bursts. The magnitude and energy level of events depend on the volume and properties of the stressed rock mass. The release of strain energy may be due to the formation of macrocracks in which case the measured energy would be in the 106 ft.lb range. Major rock bursts detected to date have been as large as 5 on the Richter scale. In general the larger the event, the lower the frequency content and for most of the observed events the energy is concentrated in the lower frequency components.

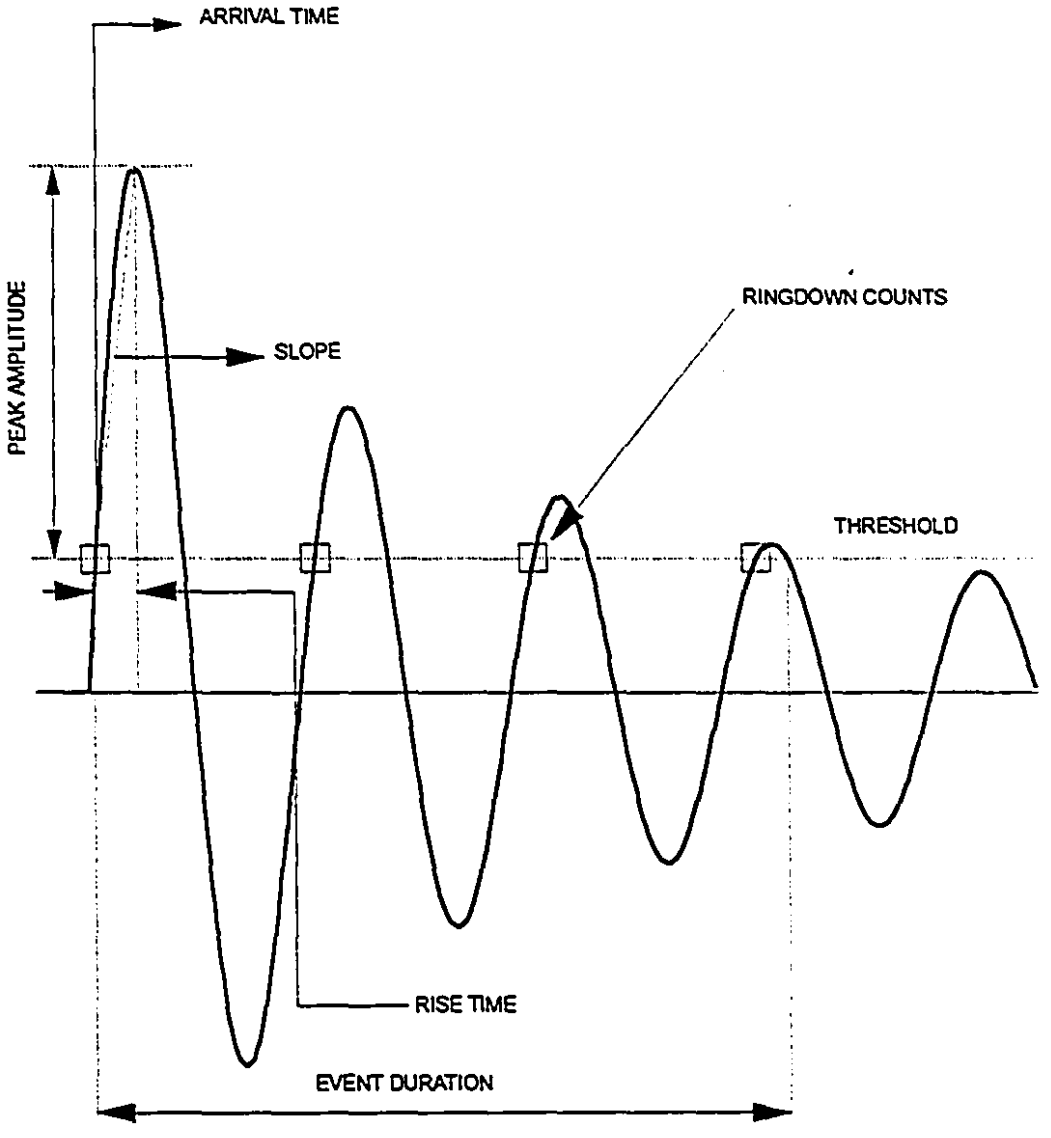

Figure 3-1: Fundamental Parameters Describing an Event.

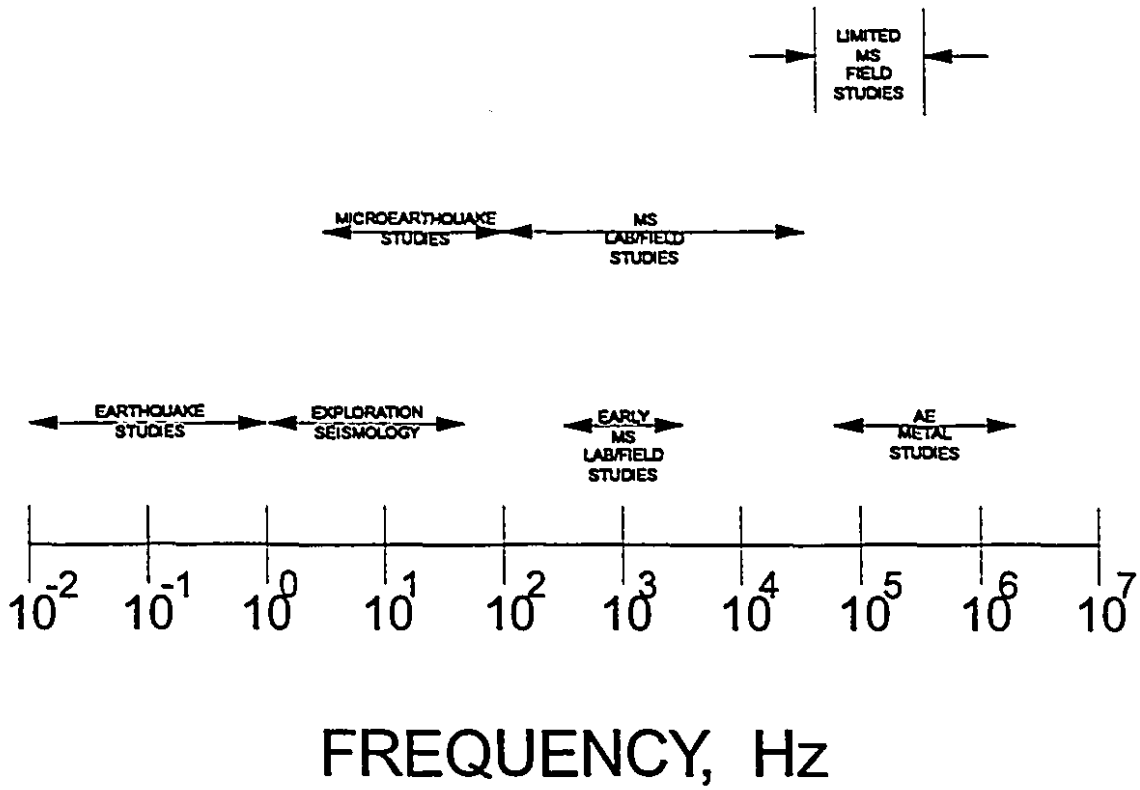

Figure 3-2: Frequency Range for Seismic and Microseismic Monitoring.

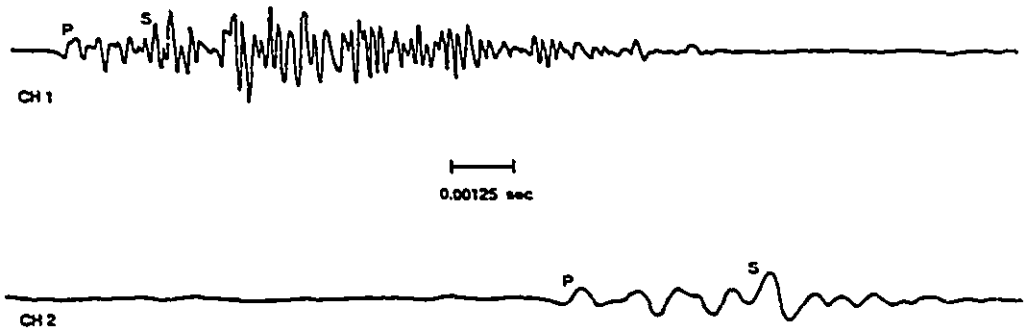

Figure 3-3: Effect of Increased Travel Distance on the Frequency of Rock Noise.

3.4) Microseismic Equipment

An ideal microseismic monitoring equipment, whether it is designed for field or laboratory studies must have enough dynamic range to detect all events from microcracking to rock bursting and should be sufficiently broad-band to respond to all frequencies. Because of technical and economical restrictions one can not build a system suitable for all applications. Therefore, the selection of a monitoring system for a given application must be done on the basis of the frequency range, magnitude range, attenuation characteristics and propagation velocities of the events one requires to detect. The basic components of a typical acoustic emission/microseismic system are presented in the following sections.

3.4.1) Sensors

Ground motions and surface displacements can be measured with respect to particle displacement, velocity and acceleration as a function of time. Two types of sensors are used in acoustic emission studies namely velocity gages and accelerometers.

Field studies generally make use of velocity gages and laboratory testing of materials is carried out with accelerometers. A wide selection of sensitivity and frequency responses are available for this type of transducers.

3.4.1.1) Velocity Gages

A velocity gage consists essentially of a case containing a fixed magnet bar inside a suspended coil. Ground movements cause the magnet to move with respect to the coil in a way that generates a voltage proportional to the particle velocity. Velocity gages are constructed to respond to vertical and horizontal vibrations, therefore the gage orientation must correspond to the direction of motion to be detected.

The sensitivity, natural frequency, coil resistance and the frequency response of a typical velocity gage may be 1.0 V/in/sec, 8 Hz, 870 ohms and 10-2500 Hz

respectively. The low output impedance of a velocity gage allows it to be readily matched with most amplifiers and recording equipment.

3.4.1.2) Accelerometers

Accelerometers usually consist of a piezoelectric material attached to a suspended mass such that the motion between the case and the mass generates a voltage in the piezoelectric element that is proportional to rock particle acceleration. The accelerometer has a very high impedance output in the kilo-ohms range and the frequency response covers the 10 kHz to 1 MHz range.

3.4.2) Wave Guides

As discussed previously in this chapter, signals are attenuated significantly as they pass through the earth. Wave guides (steel rods) have been found to be very useful in conducting AE signals from within the material to the receiving sensors. They may also provide a firm mounting surface for the sensor.

3.4.3) Couplants

Couplants are used to achieve an efficient signal transmission interface between the sensor and the medium to be monitored. The importance of using a couplant in an experiment becomes obvious by considering an acoustic wave being transmitted between two surfaces in contact. On the microscopic scale, these surfaces are quite rough and only a few spots are actually in contact. Consequently, the actual area transmitting a force is very small. However, if the microscopic gaps are filled with a fluid, the pressure will be uniformly transferred between these two surfaces. Water, petroleum jelly, lubricants and many other types of petroleum derived products are commonly used as couplant.

3.4.4) Preamplifiers

In all microseismic installations, the acoustic emission signals are amplified at the sensor. Where velocity gages are used, signal amplification is necessary because the gage output is very low level and it might be lost in extraneous noise picked up by the transducer cable and associated connections. For accelerometers the situation is worse, because of its high impedance. Without pre-amplification any appreciable cable length will attenuate its output below usable levels.

The impedance between the transducers and the preamplifiers must be matched to prevent both power loss and noise generation. Velocity gages which have a low impedance output can be connected to either a bipolar or field effect transistor (FET) type amplifiers. Accelerometers, however, because of their high impedance output, should only be connected to FET or charge amplifiers. In order to accommodate either a velocity gage or accelerometers a high input impedance FET voltage preamplifier is normally used.

In general, the preamplifier should have a fixed gain in the 40-60 dB range, a noise level in the 2.0 μvolt range (referred to shorted input), a flat or uniform frequency response over the frequency range of interest and low output impedance to transmit signals over long cable lengths without loss.

3.4.5) Cables

Virtually in all situations, the sensor is placed at some distance from the processing system. Metallic electrical cables are the most reliable, economical and widely used. However, a long transmission line acts as a lowpass filter, with amplitude loss. The resistance of the cable also causes an overall reduction in signal amplitude. These combined effects limit the frequency response that can be transmitted by a given type and length of cable. The larger the wire, the less resistance and usually less capacitance. When running long lengths, one should select a cable with as low a capacitance and resistance per foot as economically possible, considering size, weight and installation factors.

Cables must be properly shielded and grounded to prevent electrical field interference and should have a water proof jacket. For single-ended preamplifiers, 3-conductor shielded cable is normally used since the additional conductor permits transmission of power back to the preamplifier. For differential amplifiers, 4-conductor shielded cable is used so that the transducer signal common ground is isolated from the earth ground. The sensor high and low signal lines are tied to the differential inputs of the amplifier, thereby floating the transducer.

3.4.6) Data Processor

Events that are detected by a transducer are converted into electrical signals, pre-amplified and transmitted to a data processor unit. The processor may be very simple, consisting of only a post amplifier and an output stage for a single-channel portable system. On the other hand the data processor in a rock burst monitoring system is usually very sophisticated. It may contain a signal conditioner, a timing and control unit, an energy unit, a waveform analyzer, a computing and an output component.

Signal conditioning refers to the filtering and/or post-amplification of signals. Most often, electrical and mechanical noise at the measurement site must be filtered out because they mask the signal. Usually filtering will cutoff unwanted high or low frequencies, with notch filters to eliminate particular frequencies such as 60 Hz are common in field applications. Post-amplification is necessary if the level of pre-amplified signals is still too low for detection by the processing or recording equipment. Post-amplifiers have low internal circuit noise, broad frequency response, and usually provide a gain of 80 dB in 2 to 6 dB steps.

The timing and control unit of a data processor are usually a combination of hardware and software to provide:

1) a trigger to start a time window when a detected signal exceeds a preset threshold voltage.
2) a timing of subsequent first arrivals at other sensors as thresholds are exceeded.
3) a signal to an integrating or a waveform analysis circuit to operate on the incoming waveform.

4) a determination of the number of sensors hit during the time window to identify a real event.
5) time of arrival for every detected event.

The computing section of a data processor receives data from the timing and control section to determine:

1) X,Y,Z source location coordinates of each event.
2) emission rate, total number of events.
3) amplitude, energy and frequency distribution.
4) energy release rates and total energy.
5) statistical manipulation of the above data.

CHAPTER 4

The Kaiser Effect Stress Measurement Method

4.1) Introduction

The microseismic method (AE in geological materials) is based on the fact that the material under load responds by making small-scale displacement adjustments to reach a state of equilibrium. If equilibrium can not be reached, these adjustments become more frequent and are characterized by the release of seismic and acoustic energy: audible rock noise. In addition to these audible noises, a much larger amount of sub-audible rock noise is produced that can be detected only with sensitive electronic equipment [21].

ASTM E610-82 defines Kaiser Effect as "the absence of detectable acoustic emission at a fixed sensitivity level, until previously applied stress levels are exceeded".

This phenomenon was first discovered by Dr. Joseph Kaiser of Munich in 1953. He observed that when the stress on a metal under tension is relaxed from a level of historic high, and stressed again, there is little or no acoustic emission activity measured before the previous maximum is reached. Once the level of historic high is exceeded, there is a significant outburst in the rate of acoustic emissions. This phenomenon, now accepted as Kaiser Effect was first used to estimate stresses in rocks by Kanagawa et al. [37]. Different materials such as metals, ceramics, plastics, composites, glass, soils, concrete and ice have also been reported in the literature to exhibit this phenomenon.

Due to limited research carried out in the past on Kaiser Effect in geological materials, considerable controversy exists regarding its use and application. The following is a review of research conducted on Kaiser Effect in geological materials such as rocks, soils, concrete and ice.

4.2) Data Processing

In order to obtain the previous stress level in a sample under load, it is customary to plot time or load readings versus the cumulative number of AE events recorded during a test. The inflection point in the curve is usually used to estimated stresses using the Kaiser Effect method.

This technique was first used by Kanagawa et al. [37] to estimate stresses in rocks. Figure 4-1 shows their attempt to determine the geo-stress in an underground power plant in Japan, using tuff samples. The in-situ stresses estimated by the AE method were then compared with the values obtained from the overcoring method.

There are some cases where the Kaiser Effect can not be observed clearly by plotting the data using the previously described method. Yoshikawa and Mogi [38] presented a new method to remedy this situation. Their difference method consist of loading the sample once and plot the data as load or stress versus cumulative AE counts. If one reloads the sample after unloading, it can be seen that the AE activity for the second loading is very different from the first loading.

Figure 4-2 shows the difference in the AE count rate between the first and the second loading. Since the difference begins to increase markedly at the known previous maximum, they estimated the stress from this difference.

Hayashi [39] suggested a difference method based on the sum of AE rate and the sum of AE rate squared. This technique was employed to successfully determine the anisotropic stress state in a deep excavation near a nuclear power plant in Japan. This technique requires one load cycle and a knowledge of the acoustic emission rate for the sample tested. Figure 4-3 illustrates this technique.

Recently, Hughson and Crawford [54] used the felicity factor (well-known among AE researchers in metals and composite materials) to improve the estimates of stress using the Kaiser Effect method. The felicity factor is defined as the ratio of estimated stress using acoustic emissions over the known previous maximum stress. By determining the felicity factor for a given material at different stress levels, a felicity ratio profile is generated by joining the points plotted on a

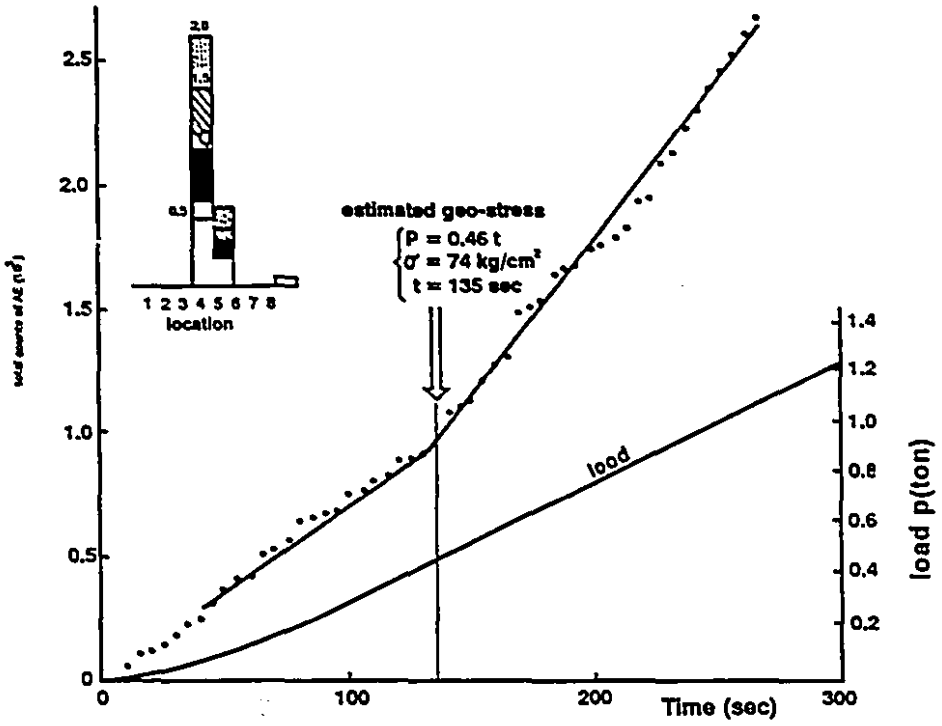

Figure 4-1: Example of Estimation of Geo-Stress by Kaiser Effect.

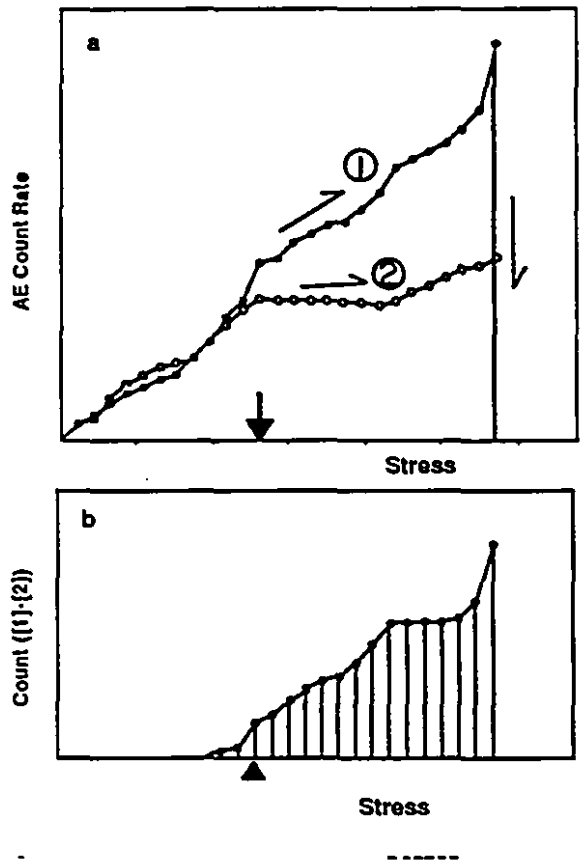

Figure 4-2: Difference Method Based on AE Counts.

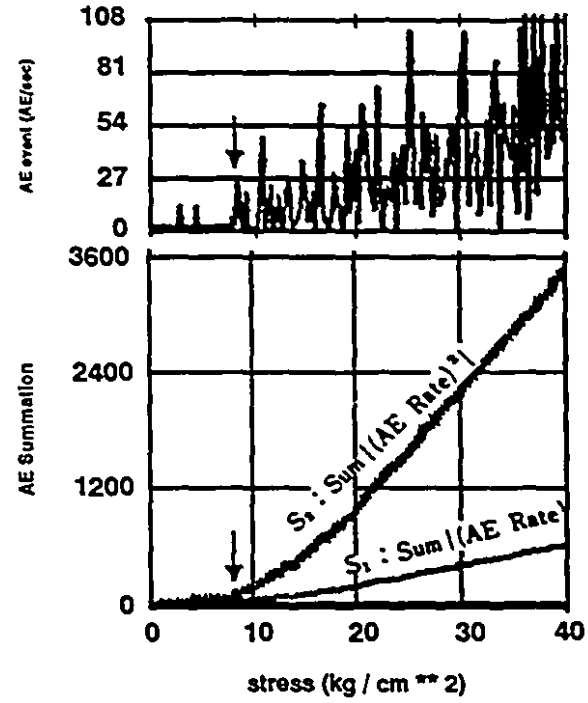

Figure 4-3: Difference Method Based on the Sum of AE Rate.

graph of recalled stress versus felicity factor. This profile may then be used to adjust a Kaiser Effect point determined by testing into an estimated previous maximum stress through a series of iterations.

4.3) Kaiser Effect in Rock Materials

Rocks have been the subject of more research than other geological materials in the past because of the need to measure in-situ stresses in underground excavations rapidly and economically. Several factors affecting the Kaiser Effect hysteresis have been investigated by various researchers. They have reported encouraging results from their experiments. The following sub-sections discuss research findings on factors that influence stress memory recollection of rocks under uniaxial and triaxial conditions.

4.3.1) Physical Changes

Environmental processes may greatly affect the recovery process of acoustic emission as well as the stress-strain relation in rock deformation. Studies carried out by many researchers has not lead to a conclusive evidence favoring a given hypothesis. It is however possible that various rock types may respond differently when the water content and temperature are altered.

Kurita and Fujii [40] demonstrated that the water content may be one of the most important factors in the Kaiser Effect hysteresis. These authors have shown that when a granite core was soaked in a water bath for one day, considerable AE was obtained, in the elastic region, at stresses far below the previous maximum. For the sample tested, the existence of Kaiser Effect is clearly indicated for the dry condition in the elastic stages of loading cycle as reported by these authors. When the sample was soaked in water for one day and reloaded again in the water bath, acoustic emissions begin to appear at a stress level far below the previous maximum. They confer that this behavior is consistent with the stress corrosion hypothesis, which argues that the presence of water causes weakening in the sample. Therefore, as it is not possible to know the exact physical conditions in the field, comparison between field and laboratory experiments may be difficult.

Yoshikawa and Mogi [43] studied the effect of water and temperature disturbances on Shinkomatsu andesite core samples obtained from deep bore holes in Manazuru, Japan, by applying their difference method. To investigate the influence of water the following experiments were set up:

a) samples that were previously stressed in dry condition were tested in dry condition.
b) samples that were previously stressed in dry condition were tested in wet condition.
c) samples that were previously stressed in dry condition were tested in dry condition after some time interval in a wet condition.
d) samples that were previously stressed in wet condition were tested in wet condition.
e) samples that were previously stressed in wet condition were tested in dry condition.
f) samples that were previously stressed in wet condition were tested in wet condition after some time interval in a dry condition.

The influence of temperature disturbance was also studied using a similar approach by stressing the sample that has been tested in a dry condition after being heated in an oven at 150 degrees Celsius. Identical experiments were carried out in a wet condition. These authors conclude that no remarkable influence of water and temperature on the stress history of the AE activity has been observed. It should be noted that when the reloading is applied in a wet condition or a sample is thermally disturbed, the so-called Kaiser Effect is sometimes unclear, when the data is processed using the conventional procedure. However, the stress history effect of the AE activity is always observed using the difference method.

Boyce [55] conducted similar studies by placing dolomite, shale, mica schist and mica gneiss samples in an oven at 115 degrees Celsius for two days. Upon the subsequent reloading of the samples, he reports that the effectiveness of the AE prediction method had dropped a little.

An interesting study on the thermal memory of rocks has been carried out by Montoto et al. [96]. Slow thermal cyclic tests on cubic specimens of intact Westerly granite, granodiorite, epidiorite and serpentinite in the range 20° to 500° C were performed. In the first cycle, the rock samples were heated to a pre-

determined temperature. It was then allowed to cool until the rock specimen was stabilized at the maximum temperature and the acoustic emission activity appears to have ceased. In the next cycle, the same rock specimen was heated to a maximum temperature 100° C higher than the previous test and cooled as described previously. This study corroborated the existence of a thermal Kaiser Effect, that is a substantial acoustic emission activity at a specific temperature, in a formerly heated rock, only occurs if that temperature is above the previous maximum temperature to which the rock has been subjected.

4.3.2) Uniaxial Cyclic Loading

Kaiser Effect studies on uniaxially compressed samples in laboratory have been carried out by a number of researchers on various rock types. Kanagawa et al. [37] may be the first to have made a serious effort to determine previous stress in geological materials using Kaiser Effect. They demonstrated that the Effect exists in tuff samples from boreholes. The cores were cut in various directions and loaded cyclically. According to these authors, their values are compatible with those obtained by the overcoring method and accurate enough for their engineering problem.

Hayashi et al. [41] have successfully determined spatial anisotropic geo-stresses, and hypothesize that the method might be useful in detecting tectonic stresses at great depths near seismically active faults. They have also verified their values with the results of overcoring tests and found small differences in magnitude, which can be used to investigate the over-consolidation rate or the tectonic stress rate relative to existing in-situ stress.

Sondergeld and Estey [42] however, have seriously questioned "the significance and existence of the Kaiser Effect in uniaxial stressing of rock". Their results show that during subsequent loading of the Westerly granite sample, an overwhelming number of AE events was detected at stress levels well below the level of historic high. This could be attributed however, to equipment malfunction or the small size of the sample tested (1.73 x 1.73 x 5.86 cm).

Vance [44] used cubic potash samples to investigate the existence of Kaiser Effect in rock salts by loading the samples to a level below the yield strength of the specimen. During the second reloading considerable number of events were detected as the stress level rose above the previous maximum. The Kaiser Effect point was determined when the change in the event count behavior was observed.

Murayama et al. [46] have studied the Kaiser Effect phenomenon in cubic (15 x 15 x 15 cm) Ikoma and Inada granite samples under unsaturated and saturated state of strain. In the first instance 10 cycles of loading were applied and acoustic emissions appeared at a point considerably lower than the previous maximum. In the case of saturated state of strain, 50 load cycles were applied and the previous stress level was estimated within 2 to 3% of the applied load. In a similar study, Michihiro et al. [91] investigated the strain dependence of the Kaiser Effect in various rock types. Their experiments show that the accuracy depends more the state of residual strain (whether the rock specimen has reached a state of saturated stress or not) than on the level of applied stress.

Holcomb and Martin [48] also performed uniaxial tests under strain controlled conditions on tuff samples. The objective was to determine peak stress induced by explosions as a function of distance at the Nevada Test Site. The results of this investigation did not produce a clear-cut answer to the problem at hand, however, the Kaiser Effect phenomenon was observed in control samples within few MPa of the applied stress.

Hughson and Crawford [51] report the existence of Kaiser Effect under uniaxial testing condition for such materials as amphibolite, andesite, gneiss, granite, limestone, diabase, quartz, rhyolite and sandstone. They caution that the Kaiser Effect does not occur abruptly for all the rock types tested, but rather within a transitional zone and that the transitional zone becomes wider and indistinct if the previous stress levels were maintained for a brief period of time.

4.3.3) Directional Loading

Directional loading tests are performed on laboratory samples and in-situ conditions in order to determine whether the Kaiser Effect is affected by stresses

from different directions. The rational for this approach is that the rock in the field is subjected to the three principle stresses for a long time and is therefore in a saturated state of strain. The saturated state of strain is defined as the state in which no further strain can be measured at a certain stress level. Two methods for creating a saturated state of strain in a specimen can be employed. One way is to apply load repeatedly until there is no further increase in residual strain. The second method consists of applying a constant stress by creep in order to achieve the desired results.

Michihiro et al. [50] have studied the influence of principal stresses in different directions on Kaiser Effect. The three principal stresses which differed in strength, were repeatedly applied to a cubic specimen measuring 15 x 15 x 15 cm to obtain a saturated state of strain in the three directions. Subsequently a cylindrical specimen (3 x 6 cm) was cored from each of the three principal directions of stress. Their studies show that in general Kaiser Effect in one direction was not affected by the stress from other directions and that the previous stress of a rock specimen in a saturated state of strain can be obtained within an error of 2% by utilizing the Kaiser Effect method.

The tests carried out by Watters and Soltani [49] in the field are not as conclusive as the laboratory experiments conducted by Michihiro et al. [50]. They were successful in obtaining acoustic emission response from the rock mass by loading the borehole in two different directions, using a jack. Two wave guides were grouted in holes on both sides of the bore hole. The jack was pressurized in increments of 3.45, 6.90 and 13.80 MPa. The pressure was maintained for 3 to 5 minutes at each pressure increment and acoustic emissions were recorded. The data showed Mogi and modified Mogi type behavior. In testing a granite boulder of dimensions 1 x 2 x 2 m, they observed directional behavior suggesting different AE levels in response to a stress field. Similar field trials in limestone did not produce the expected results.

4.3.4) Confining Pressure

Holcomb [45] has conducted a thorough study on the determination of Kaiser Effect in a Westerly granite specimen under triaxial conditions. As shown in

Figure 4-4, Kaiser Effect exists when low confining pressures are applied. Two cycles of a triaxial test at a confining pressure of 5 MPa were performed and the stress history and acoustic emission rate were plotted as a function of time. During the first cycle, an accelerating AE rate was observed as the stress level was raised. The rate dropped to zero during unloading of the specimen. During the second cycle no AE rate was detected below the previous peak stress. Then the AE rate abruptly increased as the stress rose above the historic high providing a marker for the Kaiser Effect phenomenon. The author, however, raises the question of non-uniqueness of paleo-stress estimation, because "the stress state that produces acoustic emissions is a strong function of the three principal stresses". He shows that as the confining pressure increases, the load required for the Kaiser Effect to be observed also increases. According to his data, the relationship between confining pressure and the required load is nearly linear for the Westerly granite and amounts to 3.38. In other words, for every 1 MPa increase in the pressure, the differential stress necessary to cause acoustic emission increases by about 3.4 MPa. Based on these findings, he argues that the initial state of stress can not be uniquely identified from uniaxial experiments such as those done by Kanagawa et al. [37].

In-situ stress determination tests in a borehole are also carried out by McElroy et al. [47]. In this case they have measured AE activity in a borehole by loading the side walls, using an Acoustic Emission Jack. They report that in one of the experiments, the previously applied stress could be reliably detected by the Kaiser Effect. The remaining tests (four altogether), revealed no dramatic anomalies in stress vs deformation data. Sudden increases in AE rate was however observed, in narrow stress ranges. These authors attribute this anomalous behavior to some form of in-situ stress.

Hughson and Crawford [52] have studied the influence of confining pressure on the Kaiser Effect response of Berea sandstone. The objective of the project was to find out whether a consistent relationship between the recalled stress and the triaxial stress state of the environment can be established. Core samples were subjected to different combinations of axial and confining stresses. Incremental steps of axial and confining pressure increase and decrease were kept to within 2 MPa. A given stress combination was held for a period of two hours to achieve stability as indicated by a substantial decay of residual AE during dwell. Each sample was then sub-cored to produce seven specimens parallel to the major axis

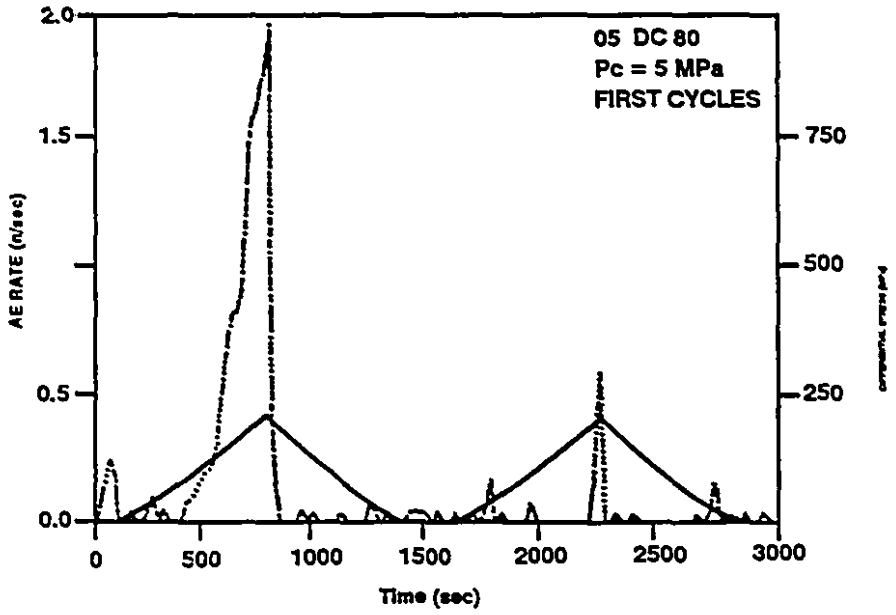

Figure 4-4: Existence of Kaiser Effect at Low Confining Pressure.

and four samples from each of the two directions in the plane of the confining pressure. The specimens were then tested under uniaxial stress conditions to look for the occurrence of the Kaiser Effect phenomenon. A graph similar to that of Holcomb [45] was then obtained by plotting the recalled axial stress versus deviatoric pre-stress. In this case the relationship is 1:1 for the Berea sandstone as opposed to 1:3.4 for Holcomb's Westerly granite.

The presence of the Kaiser Effect under sliding friction / stick slip condition has been studied by Dunning et al. [97]. These authors conclude that based on the fact that the Kaiser Effect was observed during frictional deformation, it would be interesting to draw analogies between the acoustic emission activity in small samples and seismic activity on a larger scale for faults or stressed lithosphere.

4.3.5) Retention Time

The Kaiser Effect retention time is a subject open for debate. A small number of researchers have addressed this important question, because if a bore hole is drilled into a rock mass, it must determined how long one can wait before reloading the rock sample in order to obtain an effective AE prediction. For instance Goodman [56] has reported recovery of Kaiser Effect for two sandstones and quartz diorite within several hours. Yoshikawa and Mogi [43] were able to see Kaiser Effect from one to five days. In a later study, the same authors [98], determined the Kaiser Effect load in a Shinkomatsu andesite with 20-40% accuracy after a three year period. These authors also note that in particular, the higher the initial stress level, the lower the estimated stress value and that the stress value determined using the Kaiser Effect gets smaller as time elapses.

Boyce [55] was also able to detect the previous stress level after 3 days. Kurita and Fujii [40] on the other hand have claimed that they were able to observe Kaiser Effect after a period of one month. Michihiro et al. [53] have shown that the estimate of initial stress existing in a rock mass by means of Kaiser Effect tends to decrease with time after coring as illustrated in Figure 4-5.

A study carried out by Friedel et al. [99] at the US Bureau of Mines on six different rock types showed that the pre-stress memory was retained in the rock for periods of up to at least five months. These authors state that the Kaiser Effect

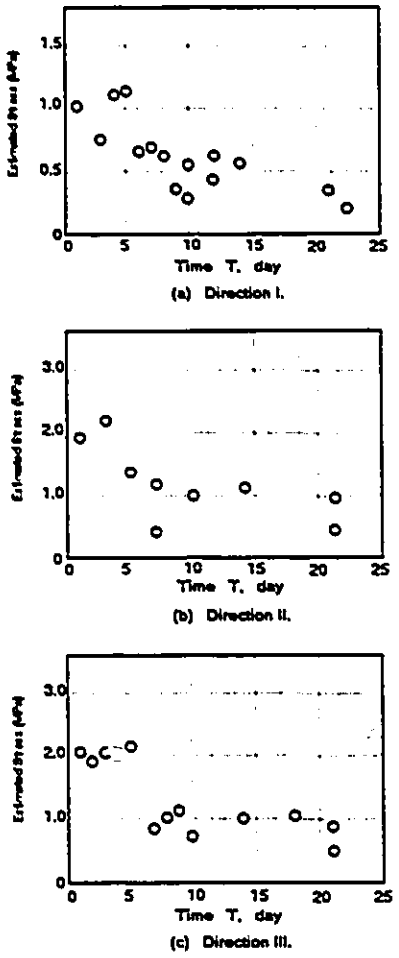

Figure 4-5: Relationship Between Initial Estimated Stress from Kaiser Effect and Number of Elapsed Days.

technique holds promise for providing a comparatively inexpensive and less complex method for examining stress history in rocks.

4.4) Kaiser Effect in Soil Materials

The main incentive in applying the Kaiser Effect method in soil materials is the determination of pre-consolidation pressure. This is important because a comparison to existing pressures allows for an instantaneous assessment of the likelihood of appreciable settlements. This goal is difficult to achieve because most field tests currently available have insufficient sensitivity for this purpose. For this reason, it is customary to determine the pre-consolidation pressure in fine-grained soil by bringing samples to the laboratory and then obtaining the value by traditional consolidation techniques [58]. Few researchers have attempted to estimate this value using the acoustic emission methods and report that satisfactory and faster results were obtained compared to conventional methods.

Tanimoto et al. [57] have reaffirmed the existence of Kaiser Effect phenomenon in various soil samples tested in laboratory under triaxial testing conditions. They also applied this method to determine the magnitude of in-situ horizontal stresses in a soil mass. Special pressure-meters were developed for monitoring acoustic emissions in the field. Pressure-meter tests carried out in a granite, crushed sandstone and mudstone fill showed that stress states determined by both methods were nearly identical.

Determination of pre-stress in granular soil has been addressed by Koerner et al. [58] using both acoustic emission method and the standard consolidation technique. By loading remolded granular soils in a consolidometer, the pre-stress load was first released and then re-applied in an incremental manner. Eighty tests were performed on five different granular soils, at four different saturation levels and for four different pre-stress conditions. The results of the experiments showed that deformation and acoustic emission methods predicted the originally applied pre-consolidation pressure to within 5% error. These authors conclude that AE is a viable method to predict pre-stress in granular soils.

Field tests to determine pre-consolidation pressures in cohesive soils have also been conducted by Koerner et al. [59]. Using a similar procedure as in the study of granular soil, these authors found that the average error between the known and the estimated values of stress varied from +2.5% to -4.4% in the case of direct deformation monitoring and from +5.5% to -7.0% in the case of acoustic emission monitoring. They believe that although the results of the deformation tests are more accurate, AE data are well within engineering accuracy for such determination. The strength of the acoustic emission method lies, according to these authors, in the fact that downhole deformation or volume measurements in the field can be readily carried out with an acoustic pressure-meter.

Deutsch et al. [60] developed an acoustic pressure-meter for use in the field. The instrument was tested in six sites where the soil material was fine-grained, derived from weathering of the parent bedrock. The value of horizontal pressure obtained by the acoustic emission method compared reasonably well with the horizontal component determined in laboratory. They infer from these results that the acoustic pressure-meter is capable of defining a new and additional parameter, i.e. Pc above those obtained from standard pressure-meter work in pre-drilled bore holes.

4.5) Kaiser Effect in Concrete

The study of Kaiser Effect in concrete has been limited to the recognition of its existence as reported by Mlakar [61], Cheng [62] and Hughson and Crawford [51]. Watters and Soltani [49] investigated the AE behavior mainly for the condition of no lateral constraint in the field. Two east-west and one north-south loading cycles were used to enable the AE response to directional loading to be observed. Very high acoustic emission activity was recorded during the initial loadings, thereafter dropping off at subsequent loadings, and then increasing dramatically until rupture. These authors interpret this activity as first the matrix failing and then the aggregate/mix. Muravin and Gur'ev [63] report that the existence of Kaiser Effect in concrete is closely related to the structural state of the material. They used 7 x 7 x 28 cm prisms of concrete with an initial water-cement ratio of 0.6. The concrete samples were 3.5 years old and were heat and moisture treated. They observed that under loads less than the limit of cracking, the

phenomenon can only be detected after a short period of time owing to the recovery of the structural integrity of cells. At the stage of non-linear creep, however, Kaiser Effect was violated due to the general expansion of the concrete and the occurrence of a large number of cracks. The phenomenon was not observed during the period of unstable crack growth.

4.6) Kaiser Effect in Ice and Snow

Bradley and St. Lawrence [64] observed the existence of Kaiser Effect in snow. Mityaev and Tokmagambetov [65] studied the generation of sound in cubic ice samples measuring 10 x 10 x 10 cm and 30 x 30 x 30 cm subjected to load. These authors speculate that Kaiser Effect can be used to predict the shifting activity of glaciers.

CHAPTER 5

Mechanisms of Brittle Failure in Rocks

5.1) Introduction

To understand different mechanisms of brittle failure in rock and to sight direct evidence of stress induced features, microscopic observations are performed. Various techniques are available to conduct this type of study. The methods utilized are limited to the degree of magnification required. The degree of heterogeneity may restrict the study initially under lower magnification in order to isolate localized cracking. The following sections will cover the technique of microscopic observations and the types of structures observed in pre-stressed and stressed materials under uniaxial testing conditions.

5.2) Observation Techniques

The most frequently used method to observe micro structure is optical microscopy. Thick, thin and polished sections are used to observe cracks and micro structure under various magnification ranges. Problems arise when attempts are made to distinguish original cracks from those induced by sample preparation. Thicker sections can sometimes be useful in determining distinctly artificially produced structures from real structures by observing the structure within the sample [66, 67].

Many authors have utilized decorative techniques in order to exaggerate the crack features. This is done by introducing fluorescent dyes and etching the sample [68]. These techniques are useful for larger intra and inter granular structures. With electron microscopy, crack characteristics and other micro structure can be studied with greater detail. Various electron microscopic techniques and modes can be applied to observe micro structure.

5.3) Initial Microstructure

Initial micro structure in rock is an important factor to be studied. According to several authors [67,69,70] initial micro structures are potential sites for the development of fractures. The features frequently considered include grain and twin boundaries, the contrast between different types, size, orientation of grains and micro cavities.

Among micro cavities, it is useful to distinguish between pores and micro cracks [67]. Pores are equidimensional spaces existing in inter and intra granular regions of a rock or along grain boundaries and fluid inclusions. Pore space can be further categorized on the basis of size, shape and relation to other pores: inter granular, connective and micro pores. Inter granular pores are large, irregularly shaped to equidimensional. Connective pores are smaller and narrower than inter granular pores. Finally, micro pores are defined as pores with dimensions equal to or smaller than a few microns. Pores are mainly responsible for the permeability in rocks. It has been noted that [71] crystalline evaporites contain intra granular void space referred to as fluid inclusions, and vacuoles.

Micro cracks that are part of the original system of the rock are developed in post deformational stages of the rock, due to tectonic, and structural activity. Micro crack features include cleavages, fractures and partings at original intact grains. These are usually narrow relative to their length and may be the main source of porosity and permeability in rocks with low permeability. Micro cracks have also been categorized and analyzed along several lines. Cracks can be typically divided into HARCs and LARCs [70]. Other studies into crack phenomena have been performed in terms of their density distributions in the rock and their orientation [72]. Others [70, 71, 73, 74, 75] have attached importance to length, aspect ratio, connectivity and spacing.

Micro cracks can prevail in all sizes, and they are the principle feature responsible for the development of behavior of brittle rock under stress. Anisotropic properties in the mechanical behavior of the rocks can also be due to the micro crack distribution. Using Scan Electron Microscope (S.E.M.) various features can be observed which may not be apparent by optical microscopy [69]. Fonseka [67] noted that cracks studied optically may in several aspects be artifacts

due to sample preparation, although genetically related to the initial micro crack and indirectly representing the initial structure.

In terms of identifying the features a summary of the most pertinent morphological features has been reported:

1) Long narrow sharp ended cracks are rare. These cracks vary in size and aspect ratio, the maximum not being more than 100 [66,69].
2) Elongated cavities or pores are commonly located along grain boundaries. Crack like cavities are rare, and more apparent in minerals with a good cleavage.
3) The ends of elongated cavities are rounded and appear to be formed by bridging of a longer cavity [71].
4) Equant cavities along inter granular and intra granular regions are present. They may possibly consist of vacuoles or fluid inclusions.

5.4) Basic Principles of Fracture Mechanics

In this section the common principles concerning fracture mechanics are examined. It is necessary to examine and understand the fracture process and criteria involved when stressing a rock sample. Krantz [70] among others, has summarized the important aspects of fracture propagation.

Cracks in a structure develop due to application of loads. There are three basic theories that govern the direction in which a crack will propagate. A knowledge of these theories, enables one to predict crack growth and fracture.

The first theory articulates that a crack tends to propagate in a direction perpendicular to the maximum tensile stress along the region surrounding the crack tip. Secondly, a crack will propagate in a direction which enhances the subsequent energy release rate. Finally, a crack will propagate in a direction along which the strain energy density is the lowest. Normally, in terms of fracture mechanic principles the first rule is defined by the Stress Intensity Factor (K), the second by the Crack Extension Force (G) and the third by the Strain Energy Density (S).

From the first theory four principles can be derived [70]. The first states, "Looking out from the crack tip of a propagating crack, further propagation will

generally be directed toward the local maximum principle stress and perpendicular to the local minimum principle stress". From this, three modes of crack development can occur. Mode I (or Extension Mode), whereby displacement is perpendicular to the crack plane, Mode II (or Sliding Mode), whereby displacement is in the plane of the crack and, Mode III (Tearing Mode), whereby the displacements are in the plane of the crack and parallel to the leading edge of the crack. The three Modes of crack propagation are illustrated in Figure 5-1. The general case of crack development involves the superposition of all three modes. The stresses associated with the crack field can be subdivided into Mode I, II and III components and each mode has associated with it, a stress tensor. A criterion for the propagation of crack growth is demonstrated by the Griffith Crack theory. This theory is related to the propagation of cracks originating from flaws, cracks or foreign matter [76].

The second principle states that "if a crack is not aligned with the principle stress, it will be subjected to a combination of stresses (i.e. Modes I, II and III). Thus the propagation of the fracture corresponds to the tensor sum of the stresses involved. "Such a combined mechanism can produce a complex fracture. For example, if a crack is subjected to Modes II and III stresses the imposed shear deflects the crack away from planar propagation into a direction where shear is minimized. In this sense, the shear stresses may be seen as playing a corrective role restoring deviant cracks to a stable path of orthogonal to the greatest principle tensile stress in the applied field" [77].

The third principle states that "a crack will propagate in its own plane unless subjected to a shear stress" [70].

The final principle states that "the zone of influence around a pore or cavity will change the extent and/or the orientation if the stresses applied to the cavity are changed". If a crack propagates in this zone of influence of cavities, the crack may be prone to changes in the local stress field and thus change its own zone of influence and deviate from its the propagation direction.

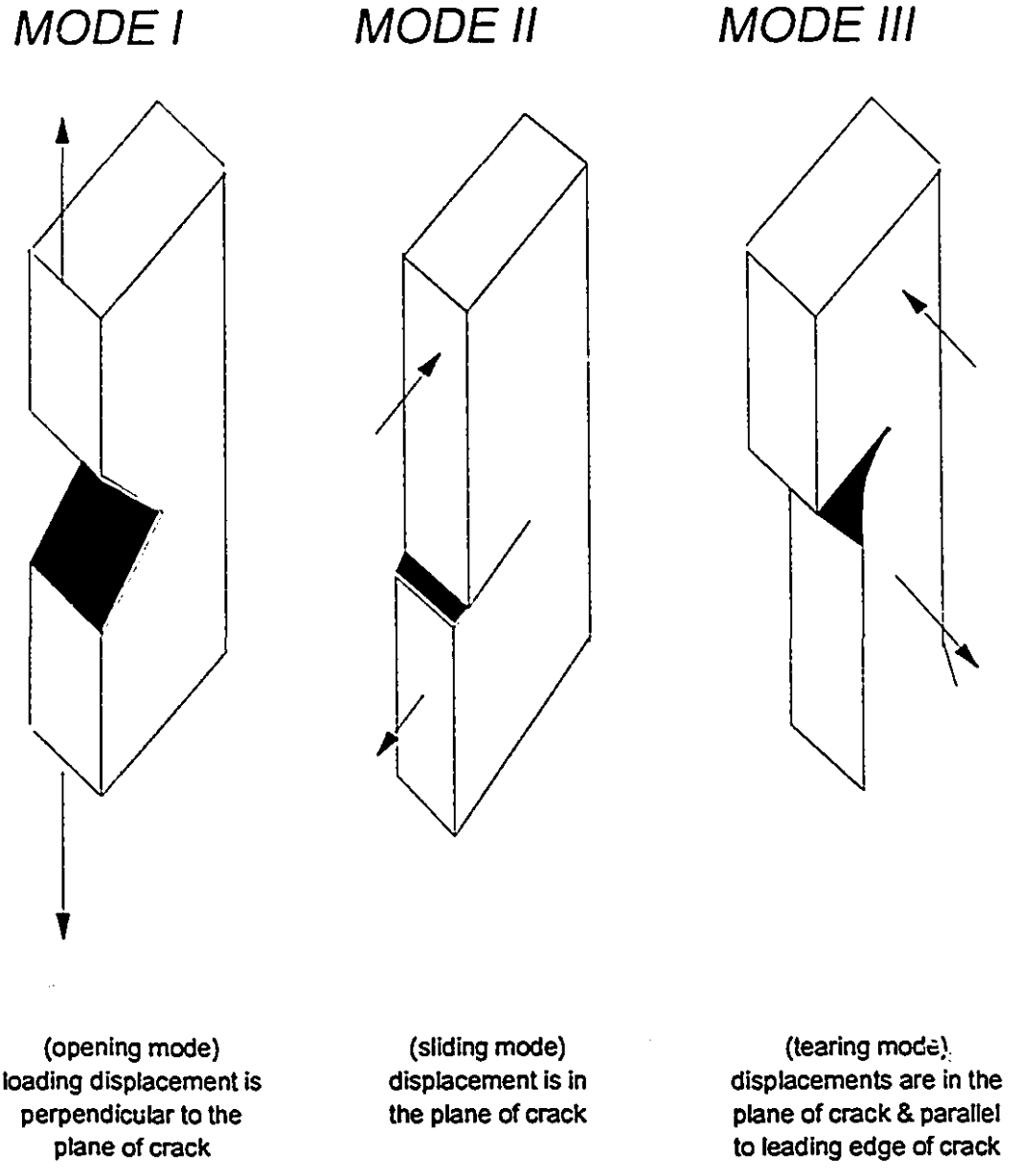

Figure 5-1: Schematic Figure Illustrating Three Modes of Fracture.

5.5) Mechanisms of Fracture Development Based on Stress-Strain Relationship

A majority of workers have related the development of fractures in rocks to corresponding stages of stress. Materials tested range from Sandstones to Granites, Marbles and Evaporites. In the majority of studies, the authors have discovered that there can be a breakdown of 4 regions of crack development with respect to the stress-strain curve. These include closing of pre-existing cracks, elastic deformation, stable and unstable fracture propagation. In many materials, cracks are generated due to pre-existing cracks, characterized by void space, grain boundary and other micro structure [78].

Sarfaraz and Ghosh [79] elaborate on three possibilities in which fractures can propagate in polycrystalline material, due to initial flaws. Micro cracks can be initiated intragranularly and propagate transgranularly, by intersecting slip bands or blockage of slip bands by a second particle. Secondly, micro cracks can also develop along grain boundaries due to second phase embrittlement or in the presence of voids. In the former case, the abundance of the second phase can influence the degree of cracking. When the phases possess cleavage characteristics, the energy required for crack nucleation decreases as the second phase increases, and thus the second phase assists in the cracking process.

If cleavage planes are favorably oriented with respect to the second phase, the cracks cross the particle matrix more easily. Finally, micro cracks can develop at grain boundaries due to disorientation.

Initial crack closure takes place in the rock, during the first portion of the loading cycle [73, 75]. This is characterized by an initial curvi-linear stress-strain curve. After crack closure, the stress-strain curve is linear, thus displaying a constant modulus of elasticity. According to Bienianski [75] some sliding takes places between adjacent faces of cracks. This results in the development of short tensile cracks formed along the length of the crack due to frictional phenomena. The application of Stroh's Model can explain the mechanism of the development of these cracks. In this model cracks nucleate from a wedge crack due to a pile up of dislocation or slip planes [75].

According to Bieniawski [75], where the glide lamellae are blocked by obstacles to glide a fracture can develop. The obstacles are usually grain boundary regions. The stress along the lamellae of the grains are relieved by two possible scenarios. In the first case, the stress ahead of the lamellae tip is resolved on to a glide plane. Secondly, if the stress is not large enough for the slip to occur, the minimum stress may nucleate a crack. Figure 5-2 shows an explanatory diagram of the possible situations.

Due to the irregularity of the surface of the crack faces, frictional shear resistance is produced. Points of contact do not move until they are sheared off. The distance between these interlocked points acts as Griffith Cracks openings. Fracture initiation progresses as the crack's tip grow. Fonseka [67] concluded that en-echelon and en-passant crack interactions occur in intra granular locations, grow in a manner typical of Griffith cracks, propagating under compressive shear. The initial cracks form at small angles to maximum compressive stress, eventually becoming stabilized. This results from shear movements of the crack faces. At this stage, the stress-strain curve is characterized by an increase in volumetric strain, the departure from linearity from the stress-strain curve, and a drastic increase in AE activity. From within this stage, short vertical cracks are developed, due to the irregularities of the crack surface and when it is overcome by shear movement of one crack face relative to another. Continual shear movement of the crack faces results in stable extension of the cracks located near the tip of the initial crack. At this point there is a departure from linearity on the stress-strain curve. Chains of small cracks along the grain boundary are reported by Fonseka [67] in Micro granodiorite, for samples loaded to 75% the failure stress.

The next stage comprises the region of stable fracture propagation characterized by cracks that develop in a direction parallel to the direction of maximum stress. A uniform distribution of cracks can not be observed due to the anisotropic nature of the rock. Also, various interactions of cracks can develop due to favorably oriented array of pre-stressed crack openings.

In this stage various crack interactions occur. With increasing stress, all cracks eventually coalesce, with different crack arrays joining but the principal failure mode is still parallel to the direction of maximum stress [73]. A change takes place in the pattern of cracks, such that there is a shattering of grains. The

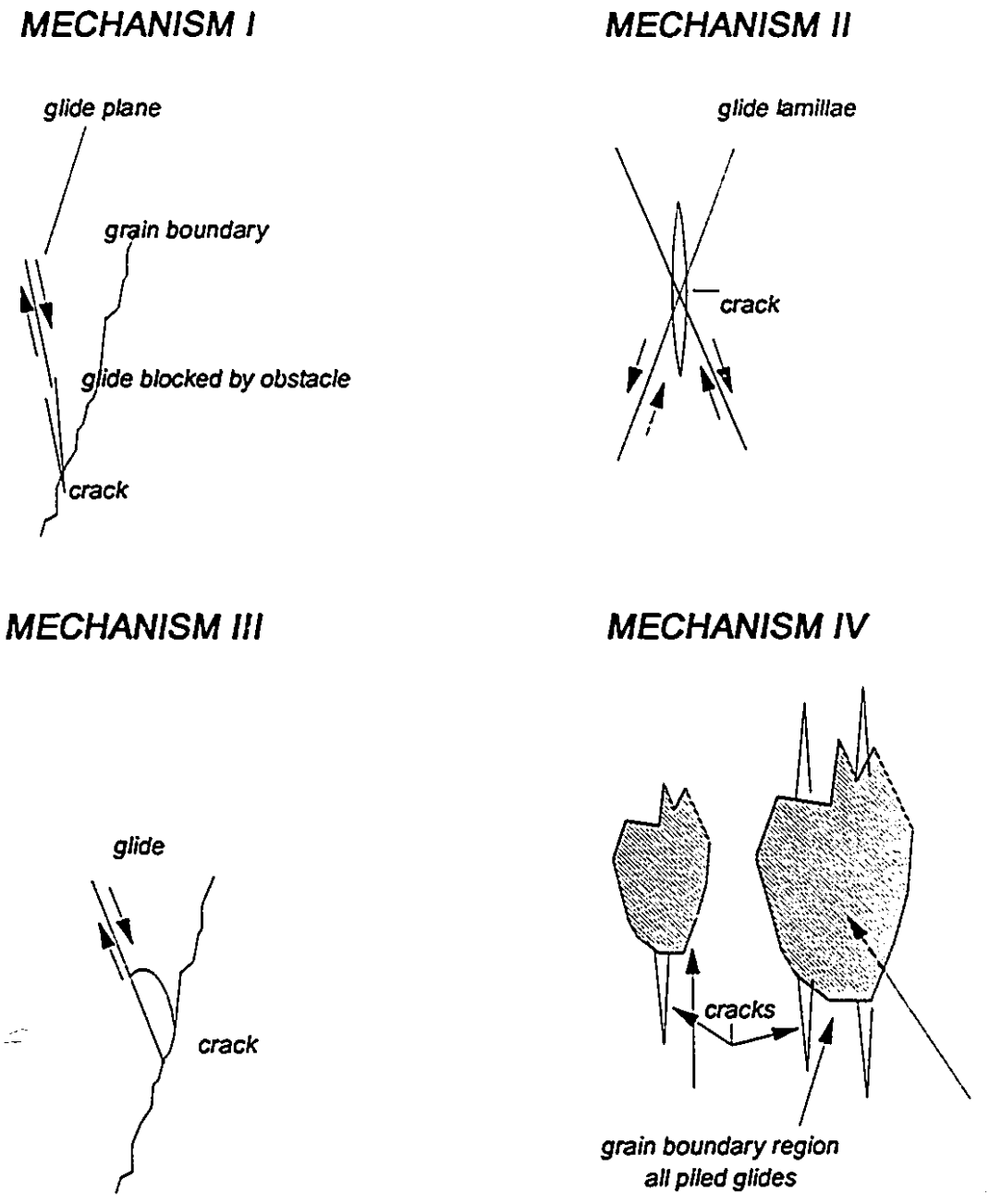

Figure 5-2: Four Types of Microcrack Nucleation Mechanism.

Critical Energy Release reaches a crucial value. The onset of unstable fracture propagation begins at this point. From this point on unstable fracture propagation predominates the deformation of the rock, characterized by a high velocity of fracture propagation. The increase is asymptotic as defined by the generation of acoustic emission. This is also referred to as the terminal velocity [75].

At the maximum strength of the rock, the terminal velocity is achieved. Beyond this point, there is macroscopic fracturing, characterized by forking and coalescing of cracks, leading to specimen rupture.

5.6) Crack Propagation Studies Based on Fractographic Technique

Prior to 1970, reports concerning fractography were thin, with much speculation and models of crack propagation had been postulated on the basis of analogous studies of homogeneous materials [73, 80]. Since late 1970's studies on deformed specimens have been carried out along two avenues, the first consisting of fractographic technique on specimens loaded to a pre-determined stress level and secondly, via S.E.M. studies at higher resolutions. For the latter, surfaces of sections were etched in order to remove superficial features [67]. Studies have been conducted in a variety of load configurations and material types. The scope of this study will cover only those considered to have contributed pertinent observations of identifying, characterizing and interpreting micro fracture phenomena.

A majority of the studies indicate that cracks are of intra and inter granular in nature. As mentioned previously, cracks develop from the growth of pre-existing void openings [70, 78]. Supportive evidence is reported by Tapponier and Brace [73], Sprunt and Brace [71]. The studies are based on samples of Granite loaded to a pre-determined level of load.

Several common observations were reported. It was found that an increase in the amount of grain boundary cracking both through rupturing of bridges in original elongated cavities and the development of new cavities.

Fonseka [67] and Kowallis [81] found that cracks originated along tectonically annealed cracks. Newly formed cleavage cracks occurred in Feldspars of Granite. This was apparent at the onset of dilatancy. At higher stresses, transgranularly axial cracks began to proliferate, starting at pores and at transverse grain boundaries. Also transgranular cracks were apparent through pre-existing elongated cavities and axial cracks originating at shear cracks. It was noted in all cases that newly formed cracks develop sharp ends with constant widths.

Similarly Kranz [70] also observed the formation of micro cracks and macro cracks derived from the intersection and coalescing of micro cavities. Two basic types of linkages were observed. These were termed en-echelon and en-passant. The former develops as a result of large shear stress concentrations between the crack tips in an arranged array. Figures 5-3a and 5-3b illustrate two modes of linking. Linkages are in a vertical direction as branch cracks grow towards maximum stress. When the cracks approach some small angle to the applied stress, shear linkages are observed. The latter occurs when two cracks approach each other from different planes. This results from two interacting stress fields approaching the crack tips.

Kranz [70] also concluded that crack propagation directions can be deflected from their preferred path due to the influence of nearby pore or void space. Cleavage cracks are not susceptible to zones of influence of voids. They occur on planes which have low tensile strength and would require Mode II and III stress to deviate the crack from the plane. Cleavage steps occur when cleavage cracks pass through a region containing dislocation with a screw component as a twist boundary. In this instance, both en-echelon and en-passant interactions occur together.

Cleavage cracks are easily formed in specimens that are loaded with high strain rates and low temperatures. Cleavage fractures can be categorically grouped and microscopically identified 4 ways.

The first occurs when cleavage cracks grow in parallel sets which are overlapped by secondary cleavage sets or aligned in the shear plane. This produces an en-echelon interaction. The second occurs when cleavage cracks are oriented in perpendicular planes or cleavage steps by screw dislocation. The third type forms

when the step is parallel to the crack propagation direction and perpendicular to the crack plane in which a twist boundary is present at an angle. Merging of cleavage steps typical of the third type can dictate the direction of local crack propagation. The fourth variety are referred to as cleavage tongues. These are easily developed during sample preparation. The grains involved are twinned. In these cases the twins first form due to a high deformation rate in the form of an advancing crack. The crack will migrate along the twin then return to the original crack plane.

Similarly Fonseka [67] followed the example of Kranz [70] but categorically distinguished two types of cracks, these being grain boundary cracks and intra granular cracks. The former consists of chains of small cracks lying along the grain boundary, the nature of them similar as observed by Tapponier and Brace [73] called LARCs, and Wawersik and Brace [78]. The latter have been broken down into en-passant and en-echelon cracks interactions. Both result from crack propagation out of the plane with initial repulsion upon overlapping (see Figure 5-3d). Kranz [70], Fonseka et al. [67] and Montoto [82] have also conducted AE testing but have only indirectly associated it to the micro fracture development in the rock. Also details on the fractures are inconsistent in associating them with the rock types tested. In this study Micro granodiorite, Dolomite and Marble have been observed, but the portion of the study conducted for fractography is inconsistent with one sole rock type, rather combining the observations into one group. According to several workers, the deformational features of rocks showing dissimilar structural characteristics may be similar but their dominance may vary as it may be controlled by the rocks texture, structure and most of all mineral characteristics. A rock possessing mineral components with strong cleavage characteristics will deform differently than those that do not. Also, rocks showing different grain sizes may possess a different stress field thus resulting in different types of transgranular relationships.

In a polycrystalline system of a rock consisting of cubic mineral phases, cracks meet at grain boundaries will contain a stress field which extends into adjacent grains. Due to the change in the crystallographic orientation of adjacent grains, there are some active slip systems with respect to the crack in neighboring grains. These slip systems will operate and relax stresses at the tip of the propagating crack. The crack can also deflect to propagate into adjacent grains due

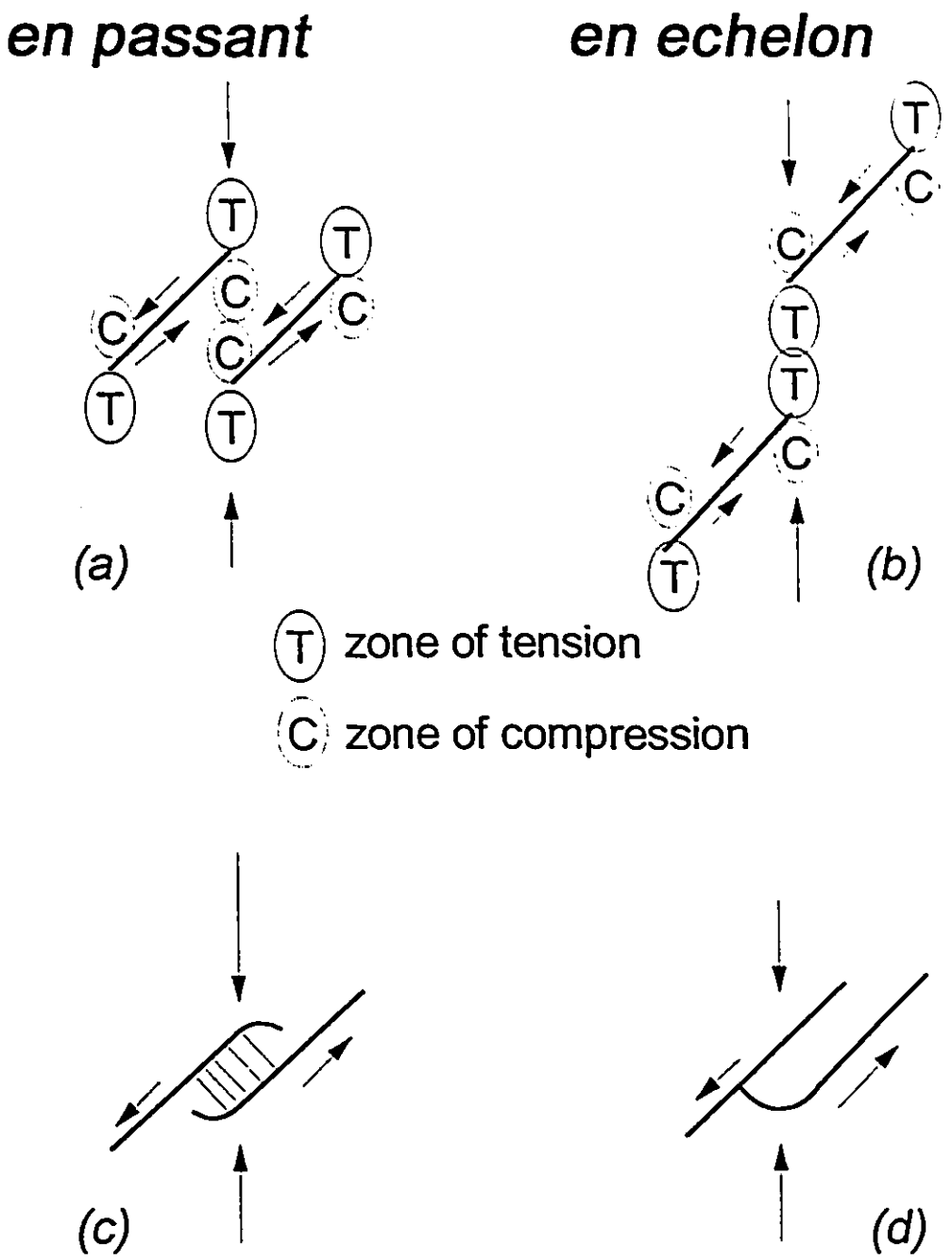

Figure 5-3: Schematic Illustration of Two Types of Crack Interactions Between Overlapping Cracks.

to favorable cleavage orientation. Micro crack nucleation and propagation activated by such systems have been reported by Olssen and Peng [83] for Marble loaded in triaxial compression configuration.

Four types of micro crack nucleation mechanisms have been identified, in which the glide is activated by an obstacle. Types I and II operate at the intersection of glide lamellae with grain boundaries.

Micro cracks developing resulting from type III mechanism forms at the intersection of the lamellae. Type IV is caused by a wedging action from a combination of strong and weak grains. Mechanisms I, III and IV were reported to lead to micro cracks oriented parallel to the direction of maximum compression. Mechanism II produces cracks lying in a plane of high shear stress. Faults are composed of en-echelon arrays of sub-axial cracks connected by packets of inclined twinned lamellae. According to the report, types I and IV were most frequently observed just beyond maximum stress.

Taponnier and Brace [73] observed micro cracks development in Westerly Granite loaded in a triaxial load configuration. Cracks were distinguished from pre-loading cracks as being long straight and narrow with sharp ends, in contrast to natural cavities which were round bridged and with blunt ends. The cracks were grouped into two categories. The first having a transgranular nature, was termed type 'B', and those associated with pre-existing arrays of grain boundary LARCs, (low aspect ratio cavities, cleavage planes or healed cracks) termed type 'A'.

The former variety were further subdivided into three groups. Those located in intra granular pores, those starting at high angle grain boundaries of different minerals and those starting along grain boundary LARCs inclined from 20 to 60 degrees to the load direction of compression. At loads up to 75% the failure strength, new cracks appeared at grain boundaries for dissimilar mineral grains at high angles to maximum stress and healed transgranular cracks forming due to shear.

Houpart [87] noted that more brittle rocks display a lower density of micro cracking, possibly due to a higher degree of homogeneity. The extreme result was

proven by tests conducted on fine grained Basalt, where the failure occurred along a shear plane transversely cutting the sample.

According to Sangha et al. [S4] micro cracks in Sandstone loaded under uniaxial compression were not controlled by local sample structural heterogeneity. Due to the lack of uniformity in the rock, variations in fracture modes were not apparent with respect to the axis of symmetry. It was observed that failure throughout the entirety of the sample occurred along the cement matrix rather than along the grain at all loading rates and stress levels. Failure was associated with an increase in the number of uniformly spaced short cracks rather than increasing propagating cracks. Samples displaying a high degree of bedding due to grain size variation showed no change in the form of crack propagation, but noted a slight irregular distribution of similar cracks.

CHAPTER 6

Test Setup & Equipment

6.1) Introduction

This research programme has been designed to study all the factors that could affect in a significant way the recollection of the Kaiser Effect phenomenon. Given the number of variables to investigate and the special requirements for some of the experiments such as the existence of Kaiser Effect during various stages of the loading cycle, a flexible and sophisticated testing equipment was needed to carry out this research.

Mechanical testing of materials has been performed in the Department of Mining and Metallurgical Engineering, McGill University, on a servo-controlled hydraulic stiff testing machine with a maximum capacity of 2500 kN. This press is interfaced with a micro-computer for the purpose of programming and monitoring experiments under various control modes such as load, displacement and strain. Acoustic emission response of specimens subject to stress are monitored using state-of-the-art AE equipment capable of recording AE signals over six channels at an average rate of 1200 hits per second over a wide range of frequencies. The system can also be used to carry out linear, planar and three dimensional source location experiments making it an outstanding monitoring tool for laboratory and field studies.

This chapter describes in detail the sample preparation equipment, the procedure used to eliminate spurious noise generated by the equipment and the philosophy behind the design of the servo-controlled hydraulic stiff testing machine and the AET 5500 Acoustic Emission Properties Analyzer System.

6.2) Servo-Controlled Hydraulic Stiff Testing Machine

Designed primarily as a testing equipment to enable research into the post-failure characteristics of various geological materials, the R.D.P. Howden 2500 kN

servo-controlled hydraulic stiff testing machine is a fully automated and micro-processor based system. Inherent in the design philosophy of the system is the fact that laboratory studies of rock characteristics require the facilities for loading a specimen under the desired test conditions and monitor these conditions together with the resulting mechanical behavior of the test specimen. Shown in Figure 6-1 are the system's main units:

a) four column straining frame with adjustable cross-head incorporating a double acting servo-controlled actuator.
b) hydraulic power pack.
c) System 2000 analog control console.
d) Apple II micro-computer system.

6.2.1) Straining Frame

The straining frame comprises four steel columns mounted on a base and fitted with a cross-head which can be positioned over the entire column length. Twin electrically driven screws are used to move and position the cross-head. When power is applied to the system the cross-head is automatically clamped hydraulically to the columns. This configuration offers greater flexibility when conducting test programs as various rock specimen sizes and variable scale model structures can be accommodated.

A fatigue rated, double acting, equal area hydraulic actuator is mounted on the cross-head. The actuator piston is reciprocated by the flow of pressurized hydraulic oil. The actuator has been designed to apply a maximum load of 2500 kN in compression and 1250 kN in tension over a total working stroke of 100 mm. The applied load is measured by a pressure transducer giving the differential pressure across the double acting piston. The incorporation of pressure transducers increase the overall machine stiffness and make the system less susceptible to off-center loading [85].

When testing very weak materials, the resolution of the load channel may be increased by the incorporation of a subsidiary load cell of 250 kN maximum capacity. The feedback signal used to control and monitor the overall movement of the actuator is provided by a linear voltage displacement transducer of ±50 mm

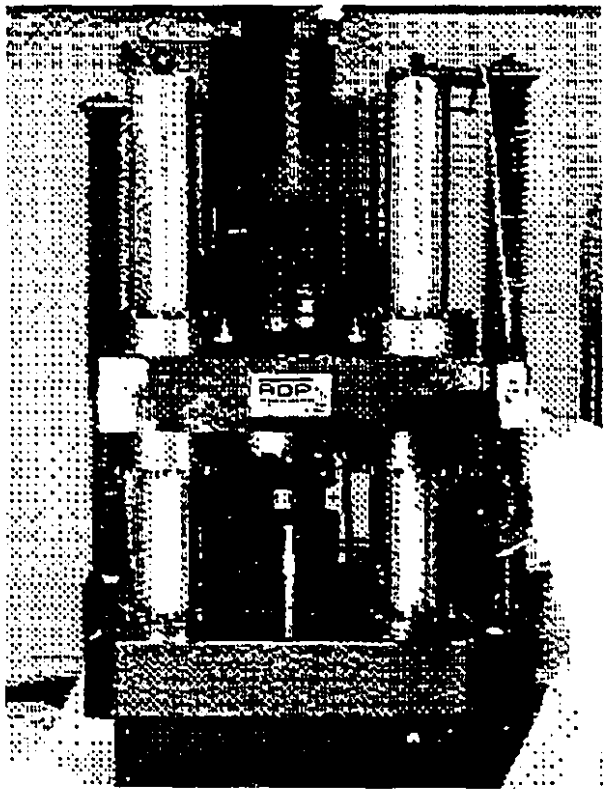

Figure 6-1: Hydraulic Stiff Testing Press.

stroke. The complete straining unit was designed to achieve a minimum stiff rating of greater than 2500 kN/mm.

6.2.2) Hydraulic Power Pack

The hydraulic power pack comprises a free standing, totally enclosed unit providing a fixed oil flow of 9 l/min at a constant 300 bar pressure. This will maintain a maximum continuous actuator velocity of 150 mm/sec. Pressurized hydraulic oil is generated by an electric motor driving a gear pump. The flow of oil to the servo-valve is controlled by solenoid operated pressure relief valves and high pressure accumulators. A secondary motor/pump unit, complete with control valves is incorporated to provide a low pressure first stage flow to the servo-valve enabling the system to be started and stopped without applying shock loads to the specimen.

High pressure steel filters are incorporated to screen the servo-valve and pump unit from contamination. The cooling system is based on circulating tap water. Multiple safety circuits are incorporated in the unit to protect the system against such malfunctioning conditions as high oil temperature, low oil level, blocked filters, loss of oil pressure, overload on pump motor and mains failure.

6.2.3) System 2000 Analog Control Console

The system 2000 analogue control console consists of a free standing cabinet which houses all the control and monitoring units necessary to operate the system under closed-loop control. A schematic representation of the system is given in Figure 6-2. The control system is divided into three part: the SL 2000 command module, the system amplification and control modules and the system programming and data monitoring units.

6.2.3.1) The SL 2000 Command Module

All front panel controls necessary to operate the electro-hydraulic servo-system under closed-loop control are built in the SL 2000 command module. The

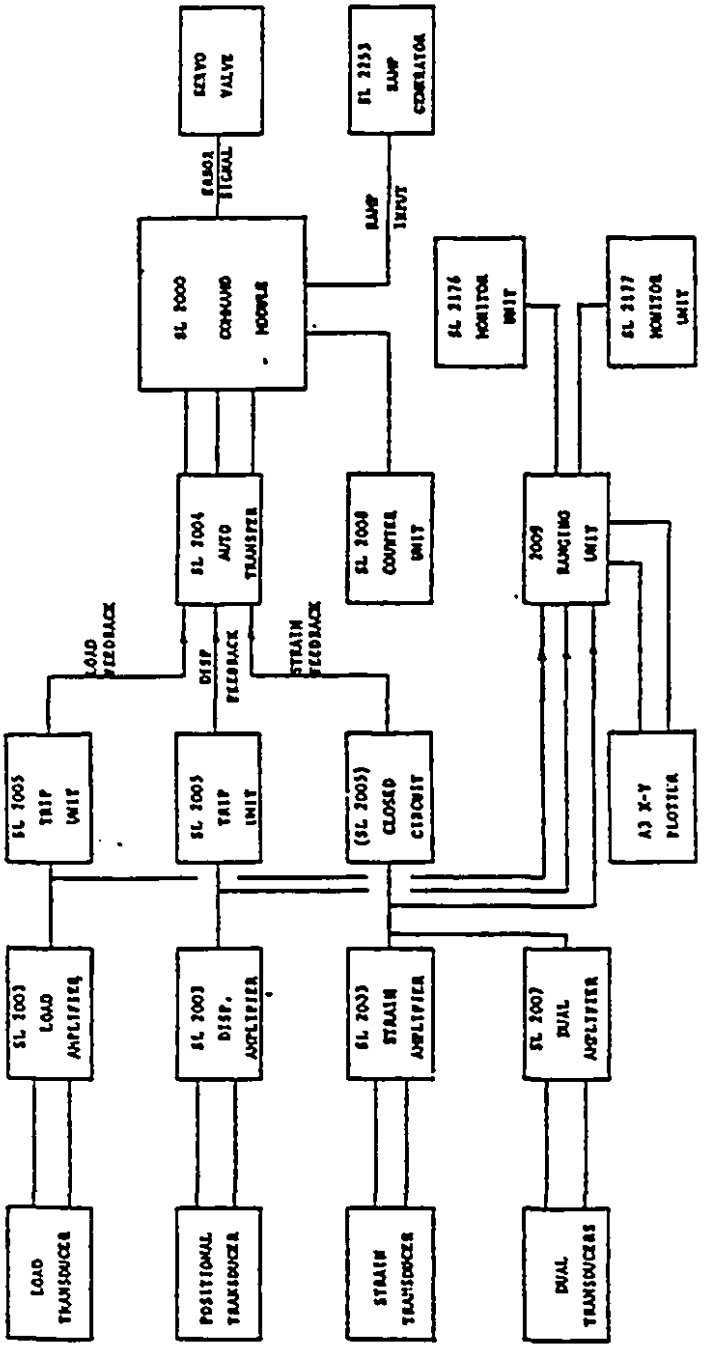

Figure 6-2: Schematic Representation of System 2000 Analogue Console.

system will operate using any one of the three designated control modes, namely load, displacement and strain.

A programmed logic controller ensures that the correct sequence of operation is executed. Any deviation from the correct sequence is prohibited and a system status is illuminated to inform the operator. The logic controller also contains programmed watchdog routines that continuously search for system faults or safety trip signals. In the event of a fault or trip condition, the controller will either shut down the power pack or hold the actuator in position at the trip level. The action of the logic controller will depend on what fault or trip signal is generated and from which unit. Appropriate system status is illuminated to inform the operator.

Each control circuit incorporates a static control device which provides manual control over the selected control parameter for static positioning. Built in the command module is an auto-balance board which continuously and automatically adjusts static control levels thus permitting a change in control mode to be achieved during a test, without imparting shock loads. Two input circuits designed for the feed of the system signals allow a generated test program signal to be entered either from the digital ramp generator incorporated in the system 2000 console or an external computer interfaced with the command module.

A key switch connects the mains supply to the SL 2012 power supply unit, mounted in the system 2000 sub-chassis. This unit provides stabilized operating d.c. supply of ±10 volts to the command module and all system units.

6.2.3.2) System Amplification and Control Modules

The R.D.P. Howden System 2000 is of modular design and suitable for operation in static, dynamic or through zero test requirements. All the amplification and control modules plug into a pre-wired sub-chassis and operate on a ±10 volt d.c. signal level. The modules incorporated in the present system include:

SL 2002 servo-valve drive amplifier which compares the feedback control signal of either load, displacement or strain with the static command signal which is fed to

the unit via the command module. The error signal produced is then converted into an error current signal which drives the electro-hydraulic servo-valve in closed-loop control. A front panel control is provided for the adjustment of overall system gain and it is complimented by feedback mode gain trimpots which are used to optimize the system response for each individual control mode.

SL 2003 carrier amplifiers are responsible for processing load, displacement and single strain channel feedback control signals. Each amplifier has an input sensitivity range of 1 mV to 30 volts r.m.s. allowing a wide range of system transducers including Linear Voltage Displacement Transducers (LVDT) of varying range, strain gauged load cells and pressure transducers to be used. Each amplifier allows the operator to set the gain, zero and quadrature balance for calibrating the transducers at the required performance level.

SL 2004 auto-transfer module used to monitor the load, displacement and strain feedback signals and automatically perform a change in the control mode from a selected primary mode to a selected secondary mode. Control mode changes occur when (a) the primary signal reaches a pre-determined level or (b) the primary and secondary signals deviate by a pre-determined amount.

SL 2005 dual trip units to monitor the output of the SL 2003 load and displacement carrier amplifiers. These modules are used for safeguarding experimental equipment which surrounds a specimen during a test. Each unit enables the operator to pre-select either a trip or hold level which instructs the logic controller to either shut down the system or hold the actuator at the static trip level.

SL 2007 twin channel carrier amplifier responsible for simultaneous signal conditioning for two transducers. As with the SL 2003 modules, the input voltage level is 1 mV to 30 volts r.m.s. and front panel gain, zero and quadrature controls are provided for separate calibration of each channel. This unit produces four output signals which can be used as the feedback control signal. The output signals are:

(a) output of transducer A.
(b) output of transducer B.
(c) output of (A+B)/2.

(d) output of A - B.

A separate output to the SL 2176 and SL 2177 monitoring units, which is essential in the setting up of system transducers, is provided by a second front panel switch designated "monitor". All strain channels are monitored and available for control.

SL 2008 monitors the total number of cycles programmed by the operator and the duration of the test. When the predetermined count or time is reached, the system is automatically shut down. The unit provides the range of pre-determined cycles from 1 to 999999 x 100 with a maximum predetermined test duration of 999999 seconds or 11.5 days.

SL 2016 displacement ranging unit conditions the sensitivity and resolution of the feedback control signal from the LVDT controlling and monitoring the actuator displacement. This module is a d.c. amplifier operating in the displacement feedback loop, being connected between the output of the displacement transducer amplifier and the command module. A variable gain setting can be selected in five fixed ranges of 1/2, 1, 2, 5 and 10 allowing control and monitoring of the actuator displacement over the ranges of ±100, 50, 25, 10 and 5 mm. The module provides the operator with a zero offset control which will apply the ranged displacement to a datum of top, center or bottom of the actuator stoke. The system can therefore be set up to apply purely compressive or tensile loads over the ranges of 5 to 100 mm displacement.

Provisions have been made for the inclusion of feedback signals generated by external subsidiary units, if required, thus expanding and improving the flexibility of the system and enhancing its overall testing capabilities.

6.2.3.3) System Programming and Data Monitoring Units

The units incorporated in the system 2000 control console for the generation of test ramps and monitoring of test signals are interfaced to the appropriate system transducers and amplifier circuits via the command module.

The generation of test programs is achieved using an SL 2253 programmable ramp generator. This waveform generator uses digital technology to produce a pre-programmed output with four accurately controlled independently variable time zones as shown in Figure 6-3. Each one of the time zones is selected on thumb-wheel switches in conjunction with the two ramp periods and the other for the two dwell periods. This allows the generation of trapezoidal waveform outputs where the time periods T1 and T4 are variable between 0 and 999999 seconds.

The operating output level, to which the ramp and dwell times are applied, is pre-selected on a ten turn potentiometer. The potentiometer is pre-calibrated so that 100% output is equivalent to the maximum operating ranges of the three control modes of load, displacement and strain. The ramp and dwell time periods are applied relative to the pre-selected output level of the potentiometer. The selection of the test control mode determines whether the load, displacement or strain is used as the test ramp input. Crystal timed digital circuitry controls a digital to analogue converter that produces a ramp staircase output of 4,096 steps each of approximately 2.5 mV to achieve the output level of 10 volts.

The output of the ramp generator can be uni-polar, having all four time periods in one polarity (compression or tension), or bipolar where the four time zones are produced in one polarity, then repeated in the opposite polarity. The operator can select whether to run either a single cycle of the programmed waveform or run the waveform continuously. When running a continuous cyclic program the duration and number of cycles is pre-determined by the SL 2008 counter module. Therefore, as shown in Figure 6-4, a number of different waveforms can be generated.

The monitoring and display of test variables is an important requirement of any testing facility. In this system, the monitoring of test variables is achieved through the incorporation of the SL 2009 ranging unit. This unit is designed to provide calibrated measurement ranges of the three feedback control channels and to supply these signals to monitoring and data logging equipment. The unit is interposed between the transducer amplifier outputs and data monitoring equipment. There are three virtually identical sections of displacement, load, and strain, the only difference being that the load section provides automatic decimal

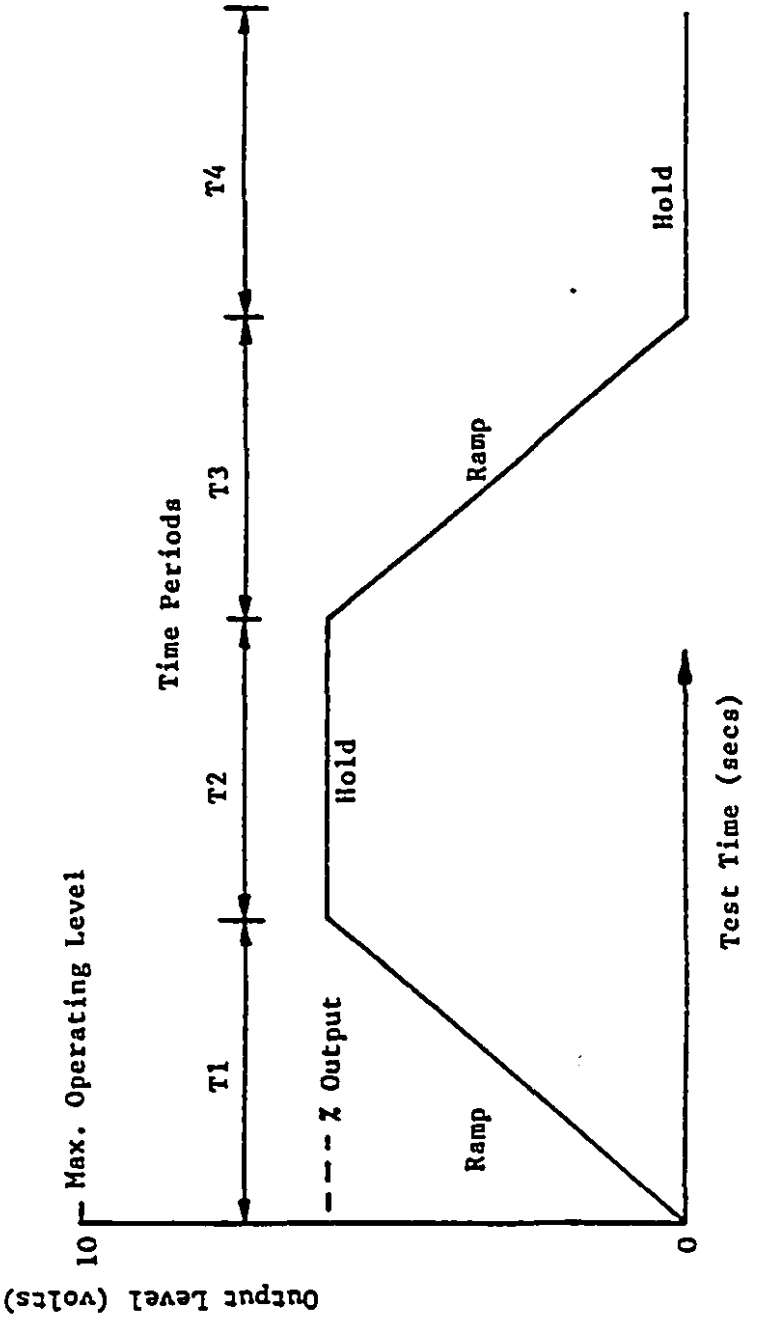

Figure 6-3: Waveform Output of SL 2253 Ramp Generator.

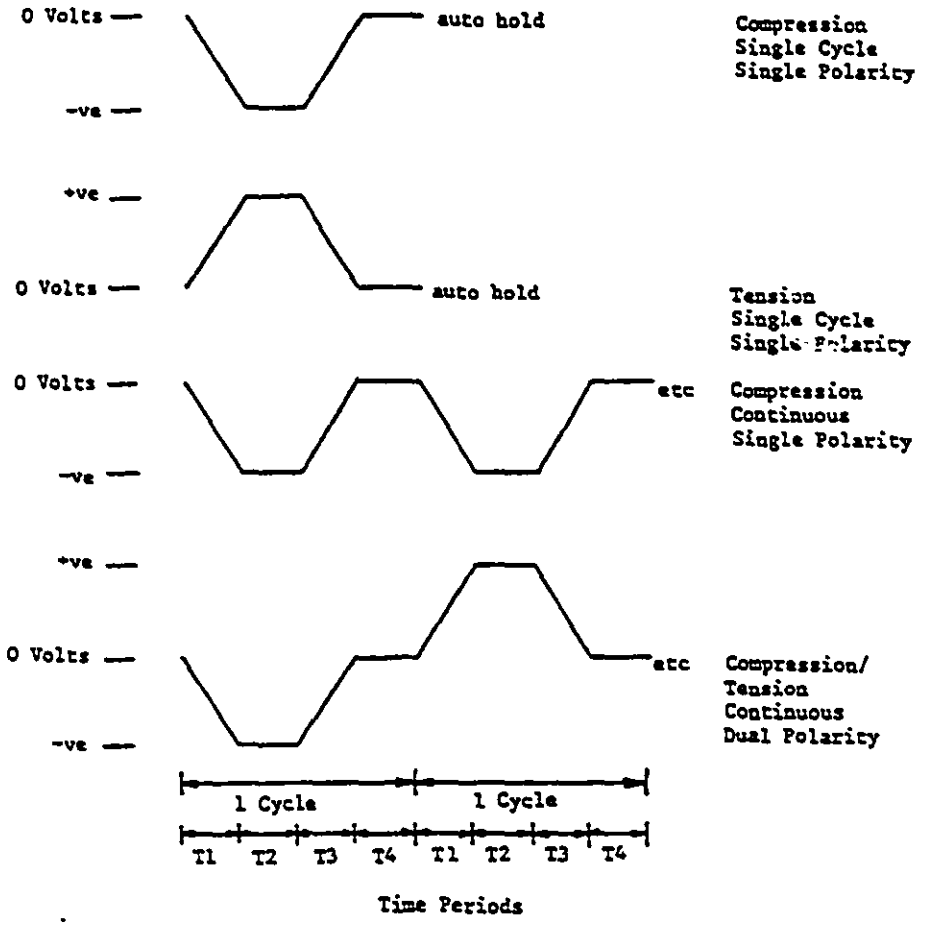

Figure 6-4: Generated Waveforms of SL 2253 Ramp Generator.

point selection for up to three different load transducers. Each section has four push button ranges, used in the calibration of transducers, and a calibrated zero suppression dial which can be used for either positive or negative suppression. The selected ranged output of the parameters are then used to provide signals for the SL 2176 and SL 2177 monitoring modules and data logging system and to drive an X-Y plotter.

The SL 2009 ranging unit can be calibrated to individual requirements. Each section contains ranged outputs of either ±100%, 50%, 25% or 10% of full scale output. The displacement channel is calibrated to an accuracy of 1% of output range with the ranged outputs calibrated to ±50, 25, 10 and 5 mm. The load channel is calibrated to British Standard 1610 grade A for both the pressure transducer and the shear force subsidiary load cell. Ranged outputs are obtained equivalent to ±2,500, 1000, 500 and 250 kN for the pressure transducer and ±250, 100, 50 and 25 kN for the load cell. For the strain channel, the ranged output will be equivalent to the percentage of the calibrated transducer range. Therefore, a transducer calibrated for 1 mm displacement could be used with the ranged outputs of ±1, 0.5, 0.2 and 0.1 mm.

The ranged outputs from the SL 2009 are supplied to the SL 2176 monitoring unit which provides digital display of the displacement, load and strain feedback control signals. Three displays indicate the static (continuous), maximum and minimum values. The channel required for display is selected via front-panel illuminated push buttons. The unit incorporates the provision for a fourth input channel as an auxiliary input. The SL 2177 monitor unit is incorporated to complement the SL 2176 unit. The SL 2177 unit is connected directly to the transducer amplifier outputs and has no provision for ranging. It provides a digital display of various signals selected on a five position front panel switch. The parameters that can be displayed are:

a) the displacement feedback level.
b) the load feedback level.
c) the strain feedback level.
d) the strain feedback signal from the SL 2007.
e) the strain feedback signal from an external input system.

Incorporated in the monitoring equipment is a Gould Series 6000 X-Y plotter for obtaining graphical outputs. The plotter is automatically ranged and driven from the ranged output signals of the Sl 2009 ranging unit.

6.2.4) Apple II Micro-Computer System

In order to complete the testing facility, an Apple II micro-computer is interfaced with the command module of the R.D.P. Howden press for the purpose of data logging and analysis. A sixteen channel analogue input signal interface (analogue to digital converter) takes the feedback signals into the computer. Six channels are interfaced at the command module for data retrieval. A seventh channel is used for the logging of the test duration. Nine channels are spare for future interfacing. A two channel analogue output interface card (digital to analogue converter) is incorporated for the generation of command signals sent over one channel, leaving the second one spare for future expansion of the system. A 32 channel digital input/output card communicates the digital control signals between the SL 2000 logic controller and the computer. In addition, a twin floppy disk unit is used for the purpose of storing various test parameters and data obtained during a test.

The current version of the software is quite straightforward. It contains two separate routines which enable the operator to perform tests under closed-loop control utilizing anyone of the three designated control modes, i.e. load, displacement and strain. The two waveform generating routines are designated as (a) CREEP testing routine and (b) CYCLIC testing routine. Both routines are conceptually modelled upon the SL 2253 ramp generator. Figures 6-5 and 6-6 show some of the typical waveform shapes that can be derived from the creep and cyclic routines respectively. As shown, the software allows the operator to enter more than one set of ramp and hold time periods of either compressive and tensile form. The present version of the program allows a maximum of 25 individual blocks to be entered for any given test. The time periods T1 and T2 for the creep test and T1 and T4 for the cyclic routine are individually variable from 0 to 10,000,000 seconds. This provides the system with the ability to reproduce tests undercomplex command signals with more variables than possible using the SL 2253 ramp generator.

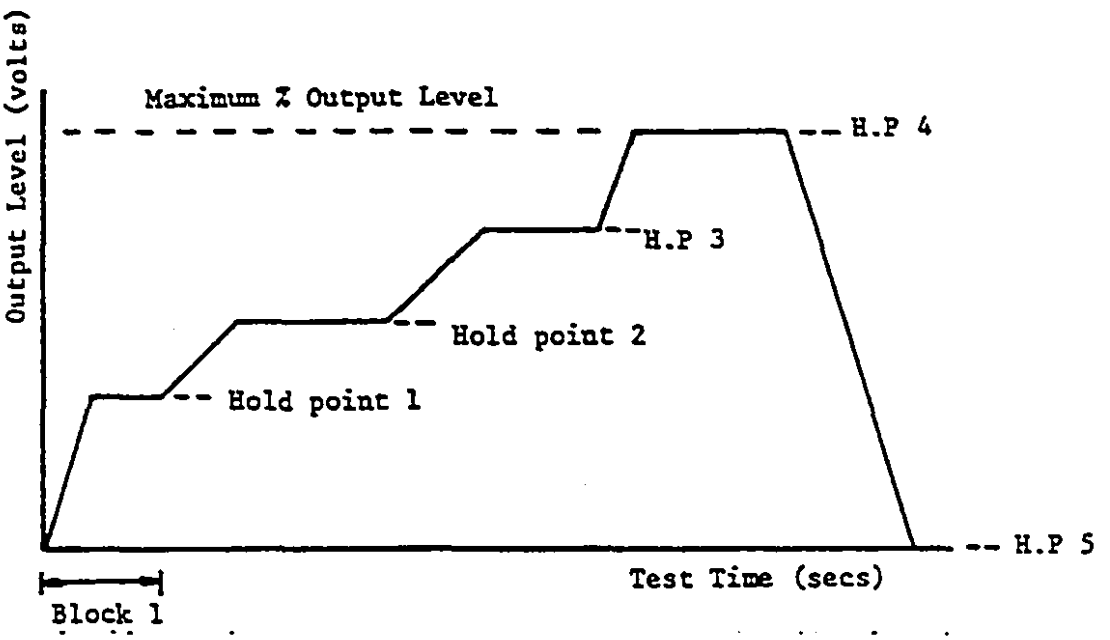

Figure 6-5: Waveform Output of Creep Test Routine.

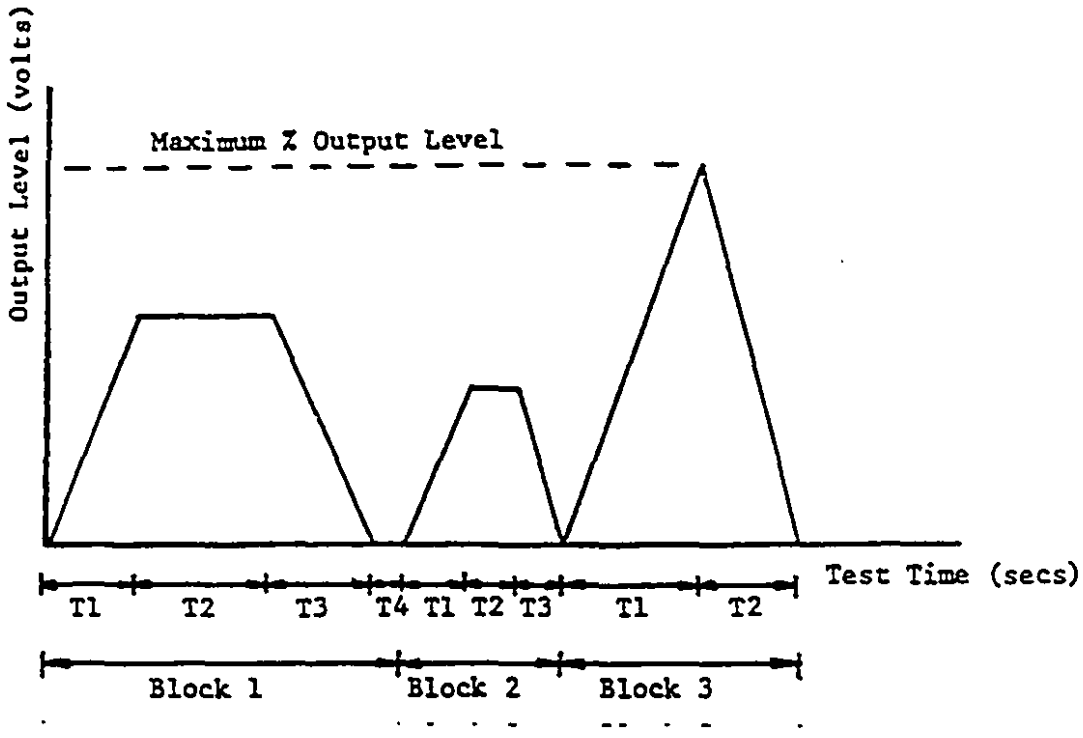

Figure 6-6: Waveform Output of Cyclic Test Routine.

When the program is loaded into the computer, the following options are available to the operator:

Data Display: allows the operator to display all transducer readings on the monitor to aid in the setting up of the experiment.

Test Information & Parameters: allows the operator to input test information and the test variables. The system can then be run from this options.

Zero Ramp Generator: allows the operator to reset the generated ramp condition to zero at the end of a test run.

Parameters Print out: prints the test information and test variables on the system printer.

Recordings Print out: prints the retrieved data from a selected test file on the system printer.

Recordings Transfer: transfers the retrieved data from a selected test file to another computer over an RS-232 port.

File Test on Disk: allows the operator to file on floppy disk a completed test format for future access and use.

Enter Test from Disk: allows the operator to recall from disk any filed test routine.

During a test run, the operator is able to key in various command signals which will either hold the test at an interrupted static level or abort the test in case of an emergency. At a hold condition, the program allows the operator to file on disk the data obtained to that point. This allows for a test to be prematurely halted but still obtain an output of the measured test variables. After a hold condition, the operator is able to either key in a command to continue the test or abort and rezero the generated ramp.

6.3) Acoustic Emission Monitoring System

In order to acquire acoustic emission (AE) events, two major manufacturers of AE equipment in North America, namely the Hartford Steam Boiler Inspection Technologies (previously Acoustic Emission Technologies) and Physical Acoustics Corporation, were contacted to inquire about the design and capabilities of their respective systems. After evaluating various equipment, an order was placed with the Hartford Steam Boiler Inspection Technologies for the purchase of the AET 5500 Acoustic Emission Properties Analyzer System.

The AET 5500 is a computer-based general-purpose acoustic emission monitoring system which consists of the following major sub-assemblies:
a) AET 5500 mainframe, incorporating up to 8 channels of AE input.
b) Intelligent Graphics Terminal (IGT).
c) Front end accessories.

This system has a high degree of flexibility because the emphasis has been put on the software rather than hardware. The principle feature of the system is its capacity to acquire data from all eight channels simultaneously, yet independently from each other. The system is also capable of locating the sources of acoustic emission signals by programming up to four 2-channel arrays. In addition, per-sensor AE data may be obtained from any sensors assigned to a running test [86].

6.3.1) Acoustic Emission Transducers

Standard piezoelectric resonant and broad-band sensors may be used to record signals. Resonant frequency transducers in the range 30 kHz up to 500 kHz are available. These sensors are omni-directional, differential and have a sensitivity of better than -70 dB referred to 1 volt per micro-bar. Broad-band sensors have lower sensitivity with the spectrum spanning from 100 kHz up to 2 MHz range.

6.3.2) Pre-amplifiers

Fixed gain 40/60 dB pre-amplifiers are available to amplify the input signal to the AET 5500 mainframe. They have a flat frequency response between 1 kHz and 2 MHz. The wide-band noise level is lower than 3.9 micro-volts r.m.s. referred to the input. The bandwidth can be restricted by replaceable plug-in filters.

6.3.3) Cables

Standard six-foot sensor cable interconnects the sensor and the pre-amplifier via 2-pin Lemo size 0 or BNC connectors. 25-foot power/signal cables carry the power for the pre-amplifiers, signals and ground lines. 4-pin Lemo size 1

or BNC connectors can be used to plug one end of the power/signal cables to the back of the AET 5500 mainframe unit. Theses cables normally hold up well in severe environments [86].

6.3.4) Signal Processor Unit

The AET 208 signal processor unit is a post-amplifier and signal conditioner that provides continuously adjustable gain for every two channels from 0 to 40 dB. In addition, the fully amplified and buffered signal is available at a front-panel BNC connector and a buffered signal level (quasi r.m.s.) at the rear panel.

The threshold level for the system is set in software and may be selected to be fixed or the patented automatic (floating) threshold which provides maximum discrimination between background noise and actual acoustic emission signals. The threshold voltage may be set in increments of 0.01 volt between 0.00 and 10.00 volts for any individual sensor or for all channels simultaneously.

The signal processor unit signals the digital AE function modules that the input signal has crossed the positive threshold. The LED on the front panel flashes at every threshold crossing. It also supplies a buffered ±24 Vdc to power the pre-amplifiers.

6.3.5) Ring-Down Counter/Event Duration Module

The ring-down counter / event duration module (REM) counts the number of threshold crossings, which has become one of the more standard data processing methods in the field of acoustic emission testing. In addition, it provides information about the duration of the event(s) that triggered the system.

The REM measures event duration by counting the pulses of a time base signal (the event duration clock) which oscillates at the basic rate of 8 MHz. Both the ring-down and event duration counters are 12 bits long, allowing a maximum of 4095 counts per event. The AE time bases are user-selectable through keyboard commands.

6.3.6) Amplitude/Rise Time Module

The amplitude/rise time module (ARM) is responsible for measuring the peak amplitude of an event in volts (the software records this value in decibels) and computes the rise time to peak amplitude. Thus, a picture of the positive changing AE signal envelope is obtained. Furthermore, the processor operates on the peak amplitude/rise time data, in order to determine the positive AE signal slope. The input to the ARM is the output of the pre-amplifier. That is, the signal is unaffected by SPU gain adjustments. This implies that amplitude measurements are always made with the same amount of gain. The results can therefore be easily interpreted through convenient references to sensor output levels.

6.3.7) Time Difference Module

In source location experiments, one requires to know the exact time of arrival of an event at different sensors. The time difference module (TDM) is designed to measure the difference in the time of arrival of an acoustic wavefront at two different sensors. For example, linear location of AE sources requires one TDM. Two TDMs are needed for planar location. Sensor location assignment is carried out through the keyboard entry.

6.3.8) Parametric Input Module

The analysis capabilities of the system are further increased by the addition of this optional module. User-defined analog inputs such as load, displacement, temperature and pressure can be sampled and recorded using eleven parametric channels provided at the back and front panels of the mainframe unit. The three rear end channels are configured to accept from -10 volts to +10 volts allowing it to monitor and record data from the R.D.P. Howden stiff testing machine.

6.3.9) Intelligent Graphics Terminal (IGT)

The intelligent graphics terminal is a separate micro-computer system. It utilizes the 80286 or 80386 micro-processor, and runs under the MS/DOS operating

system. The computer communicates with the AET 5500 mainframe through a high speed 8 bit parallel interface. It is also used for keyboard entries, data storage and graphics display. All data processing takes place in the mainframe unit.

Located at the end of the main computer bus, the time base module (TBM) provides the eight frequencies of the base clock that time the AE signals. The TBM outputs can be programmed for clock periods of 125, 250, 500, 1000, 2000, 4000, 8000 and 16000 nanoseconds per clock pulse, representing frequencies from 8 MHz down to 62.5 kHz. Each one of the digital AE function modules described in the preceding sections, selects one of these time bases for timing event duration, rise time or the time interval between sensors hit during source location studies.

6.3.10) Software

The AET 5500 system employs a general-purpose program for single sensor or multi-channel AE testing. The software records the following information for every event processed by the AET 5500 mainframe unit: (a) event time, (b) ring-down count, (c) event duration, (d) peak amplitude, (e) rise time, (f) slope, (g) energy, and (h) analog parameters.

Acoustic emission discriminations based on one or all signal parameters mentioned above, may be programmed at the keyboard. Plots are generated by invoking various menus built into the software. Distribution, cumulative distribution, linear and semi-logarithmic displays can be set up for each system sensor and every multi-sensor test (including source location), for any acoustic emission parameter versus time or any one of the user-defined analog inputs.

The software program supports linear as well as planar source location. The linear program allows the user to specify up to seven linear regions within a single test, thus providing spatial discrimination, event rejection and displays by specifying regions. The planar location routine utilizes the zone calibration technique, which enables the user to locate the source of acoustic emissions in a specimen of virtually any shape. This is done by defining up to two hundred zones of interest during the calibration phase. When the test is actually carried out, the computer compares the unknown emissions with the values specified during the calibration

procedure. The program allows any zone to be assigned to any region (up to seven) with no restrictions on the zone boundary.

6.4) Sample Preparation

Rock samples were stored at room temperature and humidity before and after they were cored and/or cut. For the laboratory testing programme, blocks of 36" x 36" x 12" granite, gneiss, gabbro, limestone were obtained from a local quarry. These blocks were cut on the site instead of blasted, to avoid introducing undesirable fractures and micro-fractures. The drilling machine shown in Figure 6-7 was used to core each block. Diamond impregnated core bits of various sizes can be easily fixed on the travelling piston. A hose connected to the adapter joining the core bit and piston provides tap water to cool down the core bits tip. After different diameter cores were recovered from the block they were cut with ratios of 1:1, 2:1, 3:1 and 4:1 depending on the requirements of every experiment. Both sample ends were then ground so that they deviated from parallelism by 0.001 mm according to ISRM Standards. A picture of the grinding machine used in this work is shown in Figure 6-8.

6.5) Reduction of Spurious Noise

Careful specimen preparation and testing is of vital importance in acoustic emission studies. To increase the signal to noise ratio from a rock sample, the noise generated by the testing equipment and the end-effects caused by friction between the ends of the specimen and the upper and lower platens of the testing machine must be diminished.

To reduce the level of noise, a large number of materials and procedures were tried. The best solution was obtained when a shield pad made of 100 thin layers of pre-stressed tightly bound straw paper was used between the upper platen and the travelling piston. This eliminated the machine noise to a large extend, however, the end-effects from the friction between the platens and the specimen remained. To remedy this situation, sample ends were lapped using sand paper until the surfaces became as smooth as possible. Then a piece of very thin plastic

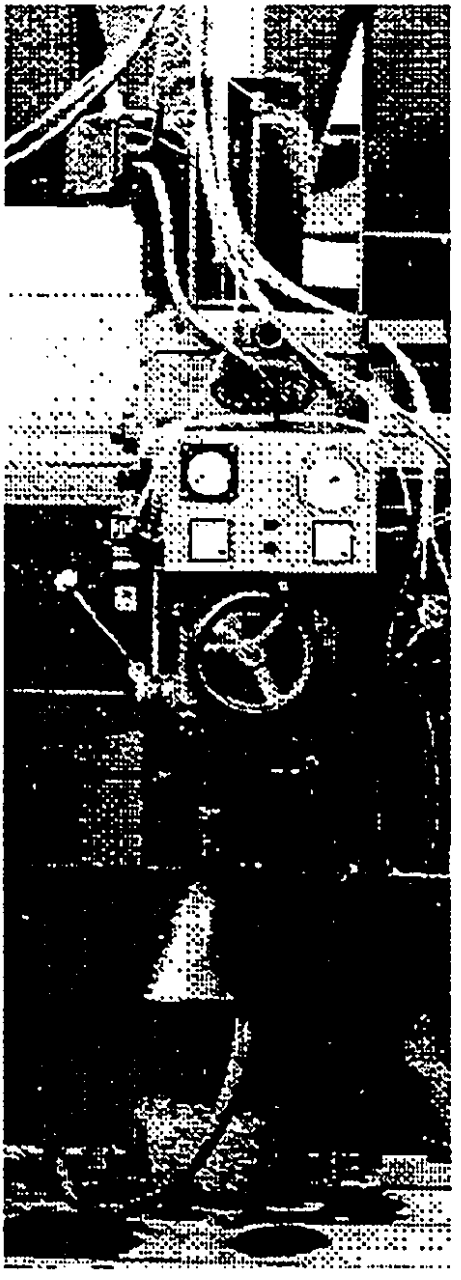

Figure 6-7: Coring Machine.

Figure 6-8: Grinding Machine

membrane used to cover soil samples for triaxial tests was cut to the same diameter as the sample and placed between the specimen end and the platen.

To evaluate the combined effect of these measures on the amount noise recorded by the AE equipment, tests were carried out on a hardened steel platen with a diameter of 5.430 cm. The philosophy was that steel generates very little or no acoustic emissions within the range of stresses imposed on the rock specimens in this work. It is further assumed that the events recorded by the AE equipment must be the noise from the press or the friction between the specimen and the platens.

Tests revealed that for a typical loading cycle of up to 60 MPa pressure, using a total system gain of 54 dB, a floating threshold of 5 mV and a stress rate of 0.336 MPa/sec, the total number of events detected by the AE equipment was 26440 events when the pad was not present. However, for the same stress level, AE system settings and stress rate, the equipment recorded only 35 events when the pad was used. The threshold and amplifier gain mentioned above are the uptimum values found for the given setup. The gain and threshold values were systematically raised and lowered respectively while the load on the hardened piece of platen was held at the 60 MPa. The values for the gain and threshold are those which allow the least number of events associated with the spurious noise to be detected. Any increase or deacrease in the amount of gain or threshold compared with the assigned values would results in tripling or quadrupling the number of recorded events over the same stress cycle. Based on this series of experiments, it was decided that the noise shield was performing satisfactorily in reducing the level of spurious noise generated by the testing equipment.

For the sake of consistency, all experiments were carried out using a total amplifier gain of 54 dB and threshold setting of 5 mV throughout this investigation.

CHAPTER 7

Maximum Curvature Method

7.1) Introduction

For many years, the only method of determining the Kaiser Effect load from acoustic emission (AE) data was to plot time or load versus cumulative acoustic emission (CAE) counts and visually estimate the deflection point in the curve. Although this method produces good results if high resolution data is available, it requires some experience in detecting the exact point where the change in the slope occurs. More recently, objective techniques such as the Method of Tangents [55, 88] have been proposed. These methods call for some level of judgment in the analysis of data and the results may not be particularly consistent or accurate.

This chapter discusses the details of a new technique that estimates the curvature at each point along the Kaiser Effect curve and provides the exact location of the deflection point which can then be used to determine the previous load level. The method can be implemented easily as an algorithm on a computer, allowing a large amount of data to be processed automatically. It is shown that if the number of data points are large enough, the Maximum Curvature Method provides consistent and precise estimate of the Kaiser Effect load. It is also shown that this technique is more efficient than the other objective method, the Method of Tangents, in terms of accuracy and speed of execution.

7.2) Method of Tangents

The Method of Tangents was first applied by Boyce [55] to estimate the previous stress level. Here, tangents were drawn by hand to the quiet as well as the more active portions of the stress versus AE data. The intersection of these tangents were then used to determine the previous stress value. Hardy et al. [88] applied statistical methods to compute the best fit lines to the reload stress versus incremental and total count data, in order to estimate the applied load. These

authors [88] were able to determine the previous uniaxial stress as well as confining pressure in samples that were loaded triaxially.

Based on Hardy's idea, a computer program was developed to estimate the Kaiser Effect from acoustic emission data. Here, a series of straight lines are fitted iteratively to the quiet and active portions of the cumulative acoustic emission counts versus time data. The chi-square test is performed to find out the goodness of fit between the cumulative acoustic emission curve and the two straight lines. The intersection of the two lines that provide the best fit to the cumulative acoustic emission curve is used to find the stress.

The method attempts to find the two straight lines that best approximate the cumulative acoustic emission curve using the search algorithm shown in Figure 7-1. The variable NPSRCHAL holds the number of points in the search algorithm and is incremented after each iteration. A value of NPSRCHAL=1 starts the search at the next point in every iteration, while a value of NPSRCHAL=5 begins the next search by jumping five data points. A high value for NPSRCHAL increases the execution speed of the program but reduces its accuracy because a large number of points are skipped during the search process.

It is found that the Kaiser Effect curve displays a much sharper deflection point when time values are used instead of load or stress on the x-axis. This sharpness reflects in the estimation of previous stress by producing estimates that are closer to the actual stress value by as much as 5 to 10 percent. The reason for the increased sharpness is that the time-based data is sampled at a constant rate, that is the independent series (x-axis) increases evenly. For this reason, time values are used instead of load or stress, when the regression lines are computed.

All the methods utilized to determine the Kaiser Effect load are based to various degree on the judgment of the person performing the analysis. The statistical approach proposed by Hardy et al. [88] is the first attempt at automating the process of analyzing AE data in the search for the previous stress level. The problem with this technique is that if one takes the best fit tangents (using linear regression) to the stress or time versus cumulative AE counts, it is not guaranteed that the intersection of the two lines will produce acceptable values for the Kaiser Effect load. In such cases, some degree of personal judgment must be exerted to

```
read CAE data;
read LOAD data;
N = number of points in CAE curve;
NPSRCHAL= number of points to skip;
i = 2;
j = N-1;

while i < j;
   {a,b,fit} = regression_line(t[1:i],CAE[1:i]);
   {c,d,fit} = regression_line(t[j:N],CAE[j:N]);
   intersection = (d - b) / (a - c);
   curve [1:intersection]= a * t[1:intersection] + b;
   curve [intersection:N]= c * t[intersection:N] +d;
   fit = chi-square_test(curve,CAE);
   if fit > best_fit;
      Kaiser_Effect_load = LOAD[intersection];
   endif;
   i = i +NPSRCHAL;
   j = j - NPSRCHAL;
endwhile;
```

where 'a' and 'c' are the slope
'b' and 'd' are the intercept
of each regression line.

Figure 7-1: Simplified Algorithm Implementing the Method of Tangents.

adjust the slope of either or both tangent lines in order to get more accurate values. Figure 7-2 is an example showing the CAE curve for sample GE501 and the best fit lines used to estimate the Kaiser Effect. The estimated stress taken at the intersection point is 37.212 kN. The sample was loaded up to 30 kN and the second cycle was applied only one hour later. If one visually estimates the change in slope of the CAE curve, a more accurate measure of the previous load level can be obtained.

A totally objective method for determining the Kaiser Effect point is valuable in the sense that it could be implemented as an algorithm, therefore accelerating the process of data analysis and allowing stress values to be estimated using the same set of rules. In addition, in cases where the change in the slope of the stress or time versus cumulative acoustic emission data is not sufficiently sharp to guarantee the correct detection of the Kaiser Effect point, an objective method would provide the most accurate estimate of the previous load using the same set of rules.

7.3) Maximum Curvature Method

Consider a typical Kaiser Effect curve such as the one shown previously in Figure 7-2. The change of slope is indicative of the effect of the previous load applied to the specimen. This manifestation of the effect of past load may occur at a slightly higher or lower load level than the one applied previously, depending on the specimen state and test conditions.

The Maximum Curvature Method (MCM) implements the idea of detecting the change in the slope of the cumulative acoustic emission data by calculating the amount of curvature along this curve. The maximum value for the curvature corresponds to the deflection point (i.e. the plot of time versus CAE is most "curved" around the Kaiser Effect point) which is used to obtain the Kaiser Effect load or stress.

According to Pang [89], there are different approaches available to calculate the curvature. The method that provides the best results with the data obtained from a Kaiser Effect experiment was found to be the one that computes the rate of

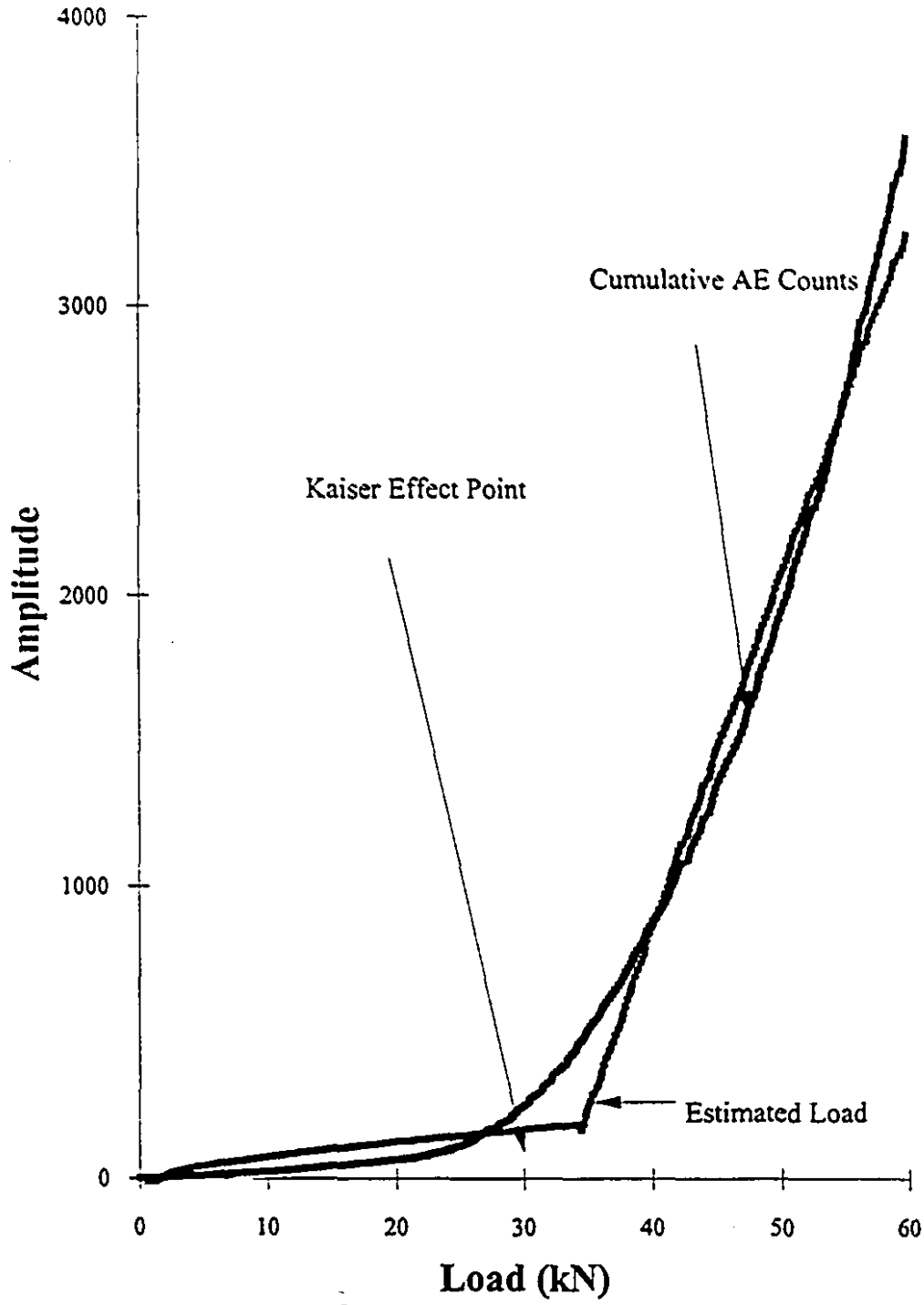

Figure 7-2: Estimation of Kaiser Effect Using the Method of Tangents for Sample GE501.

change of the angle. This idea can be most simply described as follows: the time or load versus CAE curve has an "exponential" shape, that is, it has the greatest curvature where the change in slope occurs, while the remaining portions can be approximated by straight lines. If one calculates the angle θ between this curve and the horizontal axis and differentiates the resulting series, a measure of the curvature along the entire length of the curve may be obtained. Denoting the curvature by K and the angle by θ we have:

$$\theta = \arctan(\text{CAE} / \text{Time}) \tag{7-1}$$

$$K = d\theta / dt \tag{7-2}$$

Assuming that the acoustic emission data is sampled at a rate of one second and the angle θ is expressed in degrees, then the curvature K wili be in degrees per second.

7.3.1) Measuring the Maximum Curvature of the Exponential Function.

According to Pang [89] and referring to Figure 7-3, the curvature at point P is formally defined as the derivative of the polar angle θ of the unit tangent vector T with respect to the arc length at that point. One can also interpret intuitively that the curvature is the rate of change of arc length per unit change in inclination θ, but it is preferable to consider its reciprocal, that is, the rate of change of inclination per unit change in arc length along this curve. The curvature K at point P can then be represented by:

$$K = \frac{d\theta}{dS} = \lim_{\Delta S \to 0} \frac{\Delta\theta}{\Delta S} \tag{7.3a}$$

If we denote the slope tan θ as y' = dy/dt or θ = arctan y' then:

$$\frac{d\theta}{dt} = \frac{y''}{1+(y')^2} \tag{7.3b}$$

using:

$$\frac{d\theta}{ds} = \frac{d\theta}{dt} \cdot \frac{dt}{ds} \tag{7.3c}$$

where:

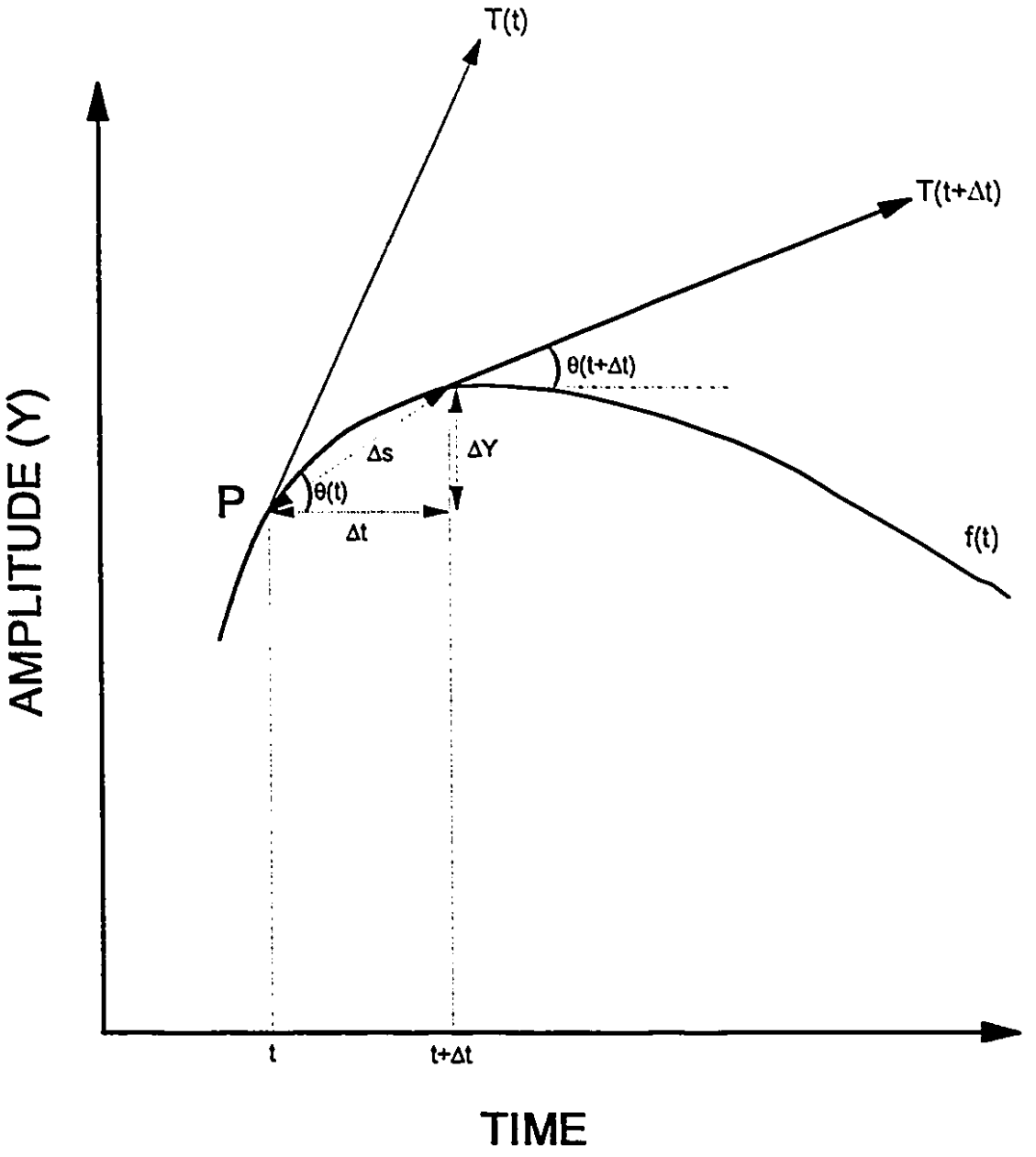

Figure 7-3: Parameters Used in Calculating the Curvature of Function f(t).

$$\frac{dt}{ds} = \sqrt{1+\left(\frac{dy}{dt}\right)^2} = \sqrt{1-\left(y'\right)^2} \tag{7.3d}$$

Equation (7.3b) is the reciprocal of the rate of change of arc length per unit change in time t so the expression for the curvature becomes:

$$K = \frac{y''}{\sqrt{1+(y')^2}} \tag{7-4}$$

where y' and y" are the first and second derivatives of the function $f(t)$at point P. Curvature measures the rate at which the tangent line rotates per unit distance moved along the curve, that is, the rate of change of direction of the curve.

Let us now calculate the maximum curvature of the exponential function $f(x) = e^x$. Because $f(x) = f'(x) = f''(x)$, the formula for the curvature becomes:

$$K = \frac{e^x}{\left(1+e^{2x}\right)^{3/2}} \tag{7-5}$$

Differentiating K with respect to x we obtain:

$$\frac{dK}{dx} = \frac{e^x(1-2e^{2x})}{(1+e^{2x})^{5/2}} \tag{7-6}$$

By setting $dK / dx = 0$ we have:

$$1-2e^{2x} = 0 \tag{7-7}$$

Solving for x we obtain the critical value:

$$x = -\ln\sqrt{2} = -0.347 \tag{7-8}$$

Therefore, the exponential function has its maximum curvature at x=-0.347. Figure 7-4 shows a graph of the exponential function over the interval [-5,4] as well as its calculated curvatures using the analytical formula (equation 7-4) and the Maximum Curvature Method. In addition, the plot of the exponential function shows a curvature around the point x=2 which can be seen by the eye. The analytical formula for the curvature cannot distinguish this fact and therefore it does not show up in the graph.

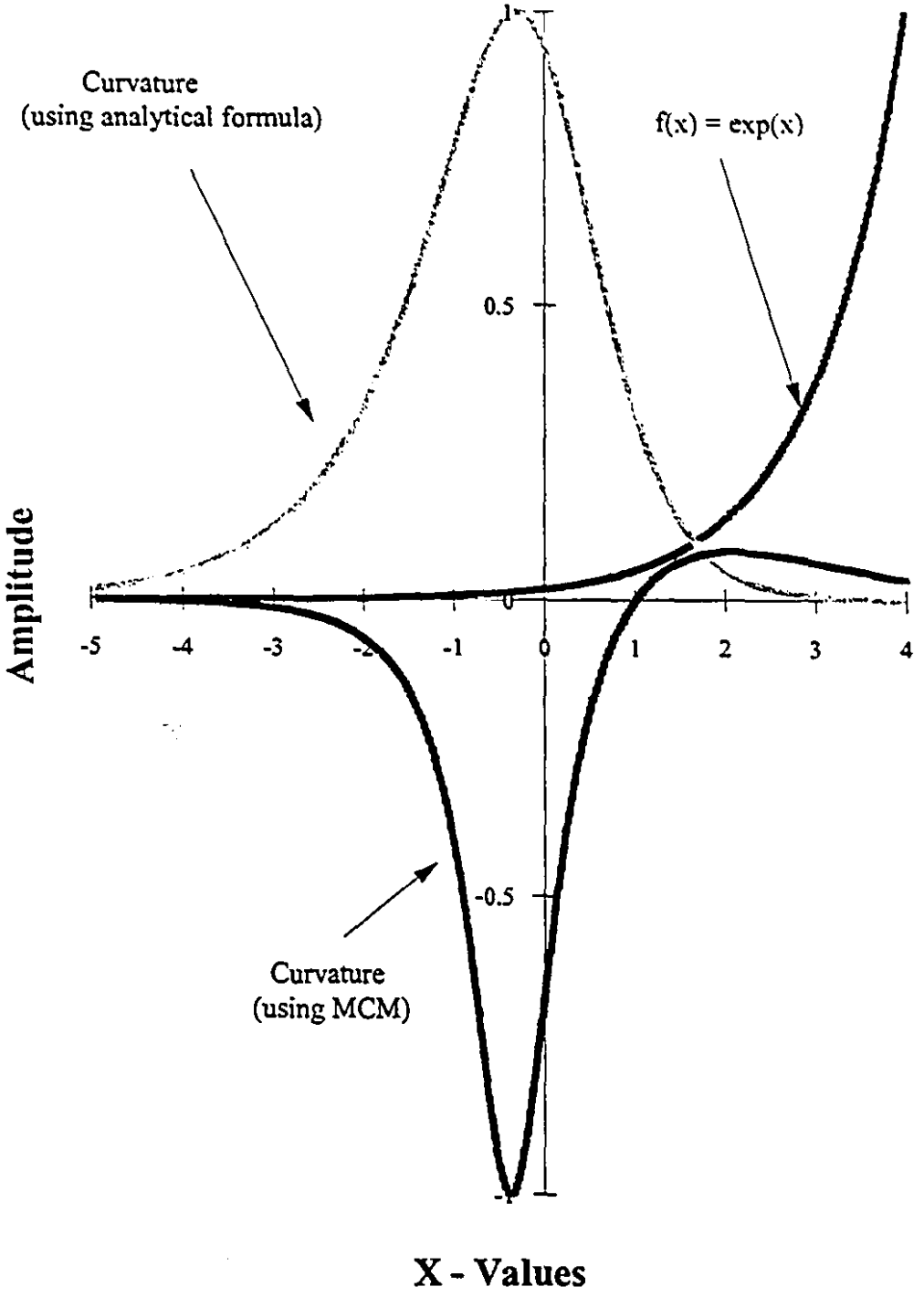

Figure 7-4: Exponential Function and Associated Curvatures.

However, the estimated curvature using the Maximum Curvature Method described above has its minimum and maximum value at x=-0.343 and x=2.074 respectively. These values correspond to the maximum curvature determined analytically (x=-0.347) and the one that appears in the graph of the exponential function around the point x=2.

7.3.2) Application of the Maximum Curvature Method to Long Length Acoustic Emission Data

To test the Maximum Curvature Method on experimental data, 4-cm diameter Stanstead Granite cores were loaded to a maximum level of 30 kN under displacement control and held there for 5 minutes. The second load cycle was applied a few hours later and the maximum level was allowed to reach 60 kN. For the second loading stage, acoustic emission data was collected at a sampling rate of one second. A 150 kHz resonant frequency transducer was used, while the monitoring system amplification and threshold were set at 54 dB and 5 mV, respectively.

In order to compute the curvature of the cumulative acoustic emission data, the Kaiser Effect curve must be smoothed before the MCM technique is applied. Although the cumulative acoustic emission curve increases exponentially, it has in almost all cases a "bumpy" shape. This implies that when the angle curve (equation 7-1) is differentiated, it will have a noisy shape similar to that of the acoustic emission rate because the cumulative acoustic emission counts is related to acoustic emission rate by the following expression:

$$CAE(t) = \int_{-\infty}^{t} r(t)dt \tag{7-9}$$

Figure 7-5 is an example of measuring the curvature of the CAE curve using unprocessed acoustic emission data. Sample GE501 was loaded up to 30 kN and was tested after a few hours. It can be seen that the calculated curvature has a very noisy response, however, the largest peak in the middle of the graph estimates the Kaiser Effect point at 33.856 kN. Therefore it is necessary to apply smoothing to give the curvature a continuous look with one peak representing the point of maximum curvature.

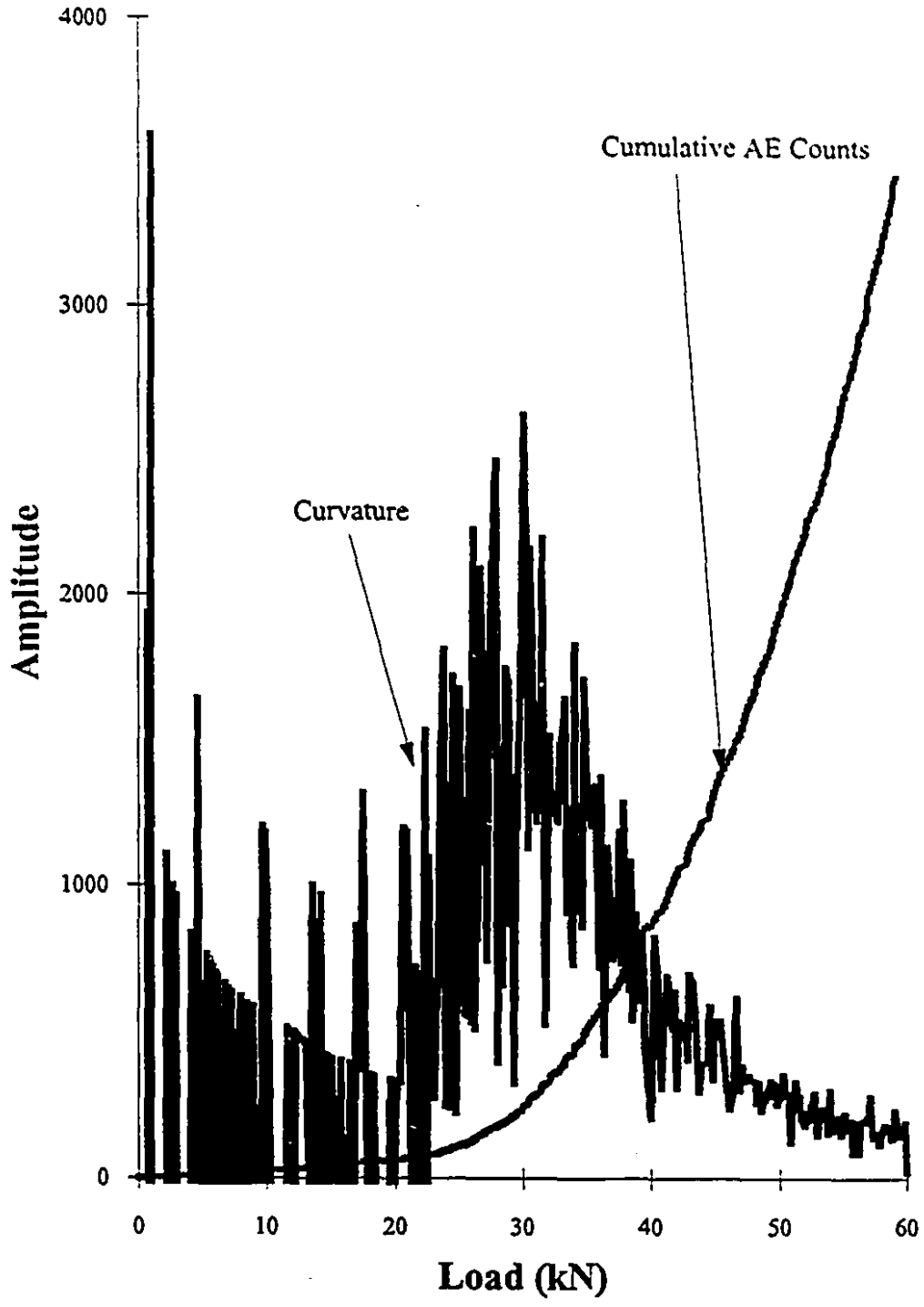

Figure 7-5: Kaiser Effect Curve and Related Curvature using Raw Data for Sample GE501.

The amount of smoothing that one applies directly affects the position of the deflection point in the time or load versus CAE curve. Depending on the quality and quantity of acoustic emission data, a number of criteria can be developed to stop the smoothing process. For example, the chi-square test can be run to find out the degree of departure from the original CAE data. A maximum deviation of 0.3% is usually sufficient to produce the desired results. In general, the smoothing process may be stopped as soon as a degree of departure equal to 0.1% to 0.3% with respect to the original series is achieved.

Smoothing acoustic emission data is performed using an averaging filter. The filter may have any length, however, for filter lengths greater than 7 points it was found that the amount of smoothing applied to the data may shift the Kaiser Effect point too much. This would be equivalent to allowing the degree of departure in the smoothed series to become greater than 0.3%. The main reason for using an averaging filter is that it smoothes out the acoustic emission data while keeping the shape of the processed curve around the Kaiser Effect point as close to the original CAE curve as possible. Other smoothing filters or approximation methods such as the 5-point triangle filter and polynomial curve fitting method were applied. The main disadvantage with these techniques is that they cannot fit accurately the critical portion of the CAE curve that is the area around the Kaiser Effect point. The 3 and 5-point averaging filter was found to produce the most accurate results when smoothing and calculating the curvature.

Figure 7-6 shows the curvature for processed CAE data using a 5-point averaging filter. It can be seen that smoothing CAE data affects greatly the shape of the curvature graph and the previous load using smoothed data was calculated to be 29.634 kN. The Table below presents the results for 8 Stanstead Granite samples by applying the Maximum Curvature Method and the Method of Tangents. The goodness of fit for all the samples analyzed with the Method of Tangents was better than 99%. As shown in Table 7-1, the Maximum Gurvature Method processes the data in a much shorter time and more accurately than the Method of Tangents. The reported execution time (in seconds) is the time it took to analyze all eight data files on a 25-MHz 386 computer using the GAUSS Mathematical and Statistical System and the Time Series Analysis package. Figure 7-7 shows the curvature for sample GE501 using both methods.

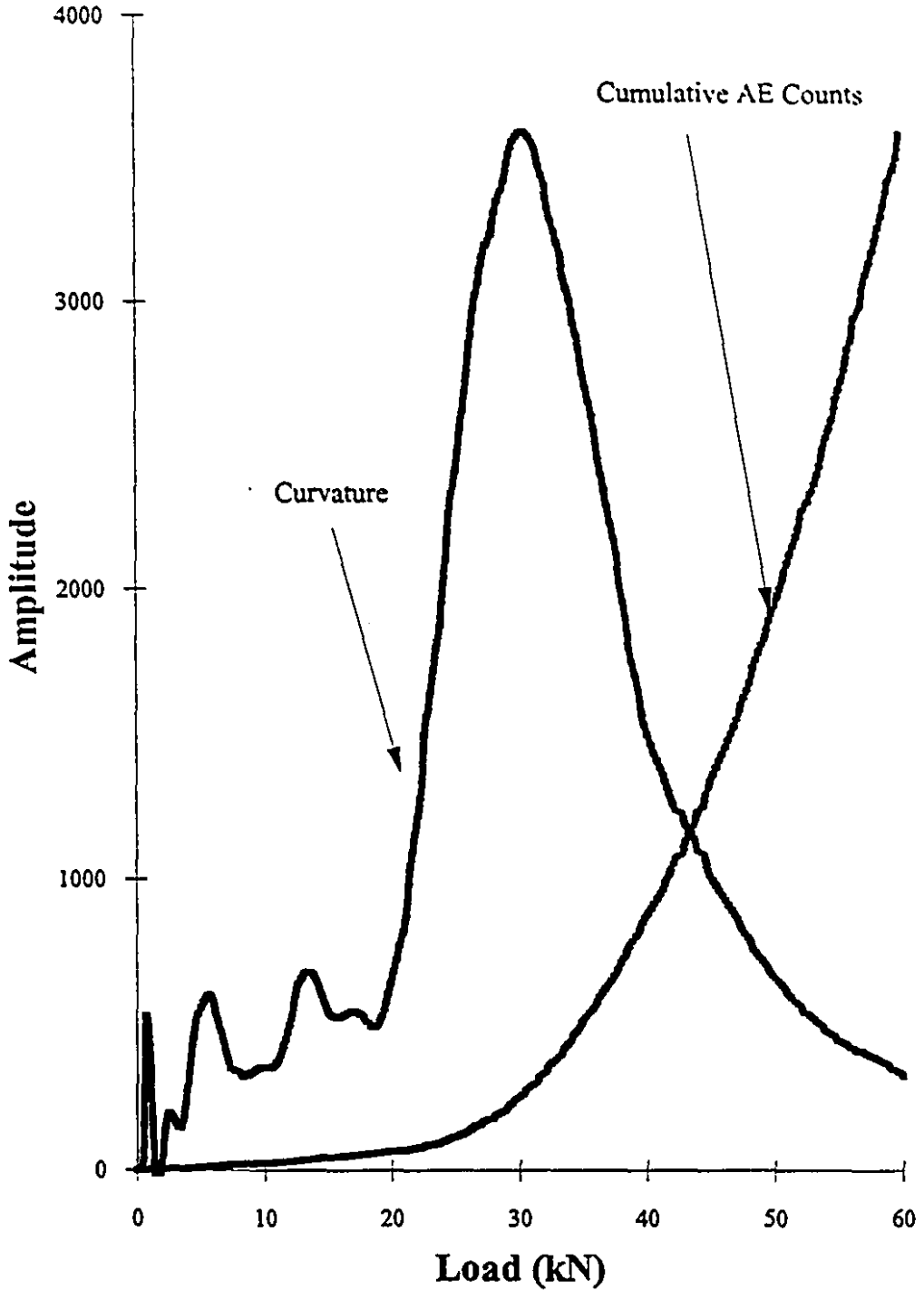

Figure 7-6: Kaiser Effect Curve and Related Curvature using Smoothed Data for Sample GE501.

Table 7-1: Results of Estimating Kaiser Effect using MCM and the Method of Tangents.

Sample (number)	First Level (kN)	Estimated Load MCM (kN)	Estimated Load Method of Tangents (kN)
GE501	30.4	29.634	34.249
GE502	30.6	29.391	34.735
GE503	30.5	33.763	39.107
GE504	30.2	30.848	35.463
GE505	30.8	30.484	37.407
GE506	30.3	31.091	36.799
GE507	30.2	32.063	39.471
GE508	30.6	30.848	39.107
		average = 30.818	average = 37.042
		variance = 1.250	variance = 4.320
		run time = 190. 370 sec	run time = 2715.63 sec

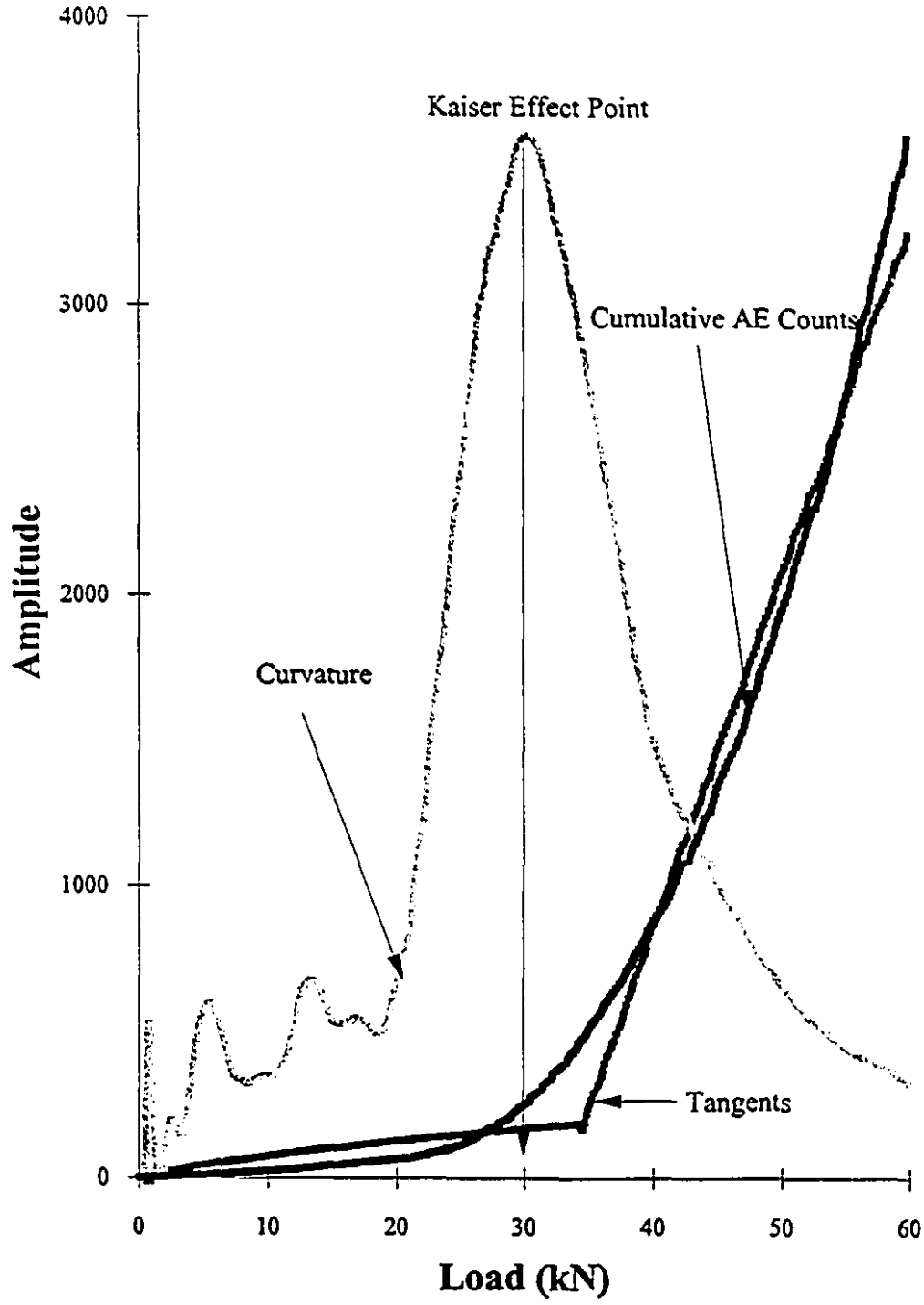

Figure 7-7: Previous Load Estimates using MCM and Method of Tangents.

Although Figures 7-5 and 7-6 show the Kaiser Effect curve and its calculated curvature as a function of load, it was found that plotting the data as a function of time produces much sharper and smoother curves. Figure 7-8 shows the same data as in Figure 7-6 plotted as a function of time. The reason for the increased sharpness is that the time-based data is sampled at a constant rate, that is the independent series (x-axis) increases evenly. For the same reason, when the curvature is computed, the CAE data is differentiated with respect to time instead of load or stress.

7.3.3) Application of Maximum Curvature Method to Short Length Acoustic Emission Data

In addition to the results presented above, the Maximum Curvature Method was used to analyze a large amount of acoustic emission data. It was found that the accuracy of values produced by using this technique depends on two important factors. The first is data quality, that is the CAE data must clearly show a deflection point in the vicinity of the Kaiser Effect load. The second concerns the number of data points collected during the experiment. When more data is available for a given test, the CAE curve will have better resolution and the Maximum Curvature Method will provide more accurate values.

Let us consider the situation where few data points (less than 100) are available. The amount of smoothing applied (using a 5-point averaging filter) to the data will affect to a great extent the shape of the Kaiser Effect curve. For example, when the 5-point averaging filter was applied 7 times to 66 data points sampled at a rate of 10 seconds from a limestone specimen, the difference between the two curves was found by applying the chi-square test to be about 1.783%. However, the 444 data points from specimen GE501 sampled every one second produced a degree of departure equal to 0.214% of the raw data when the averaging filter was applied 51 times. Figure 7-9 shows the curvature along with the raw and smoothed CAE curves for the limestone sample. The original CAE curve displays a very sharp Kaiser Effect point at 34.750 MPa while the maximum curvature calculated using the smoothed CAE curve provides a stress value of 33.074 MPa. The agreement between these two estimates can be attributed to the

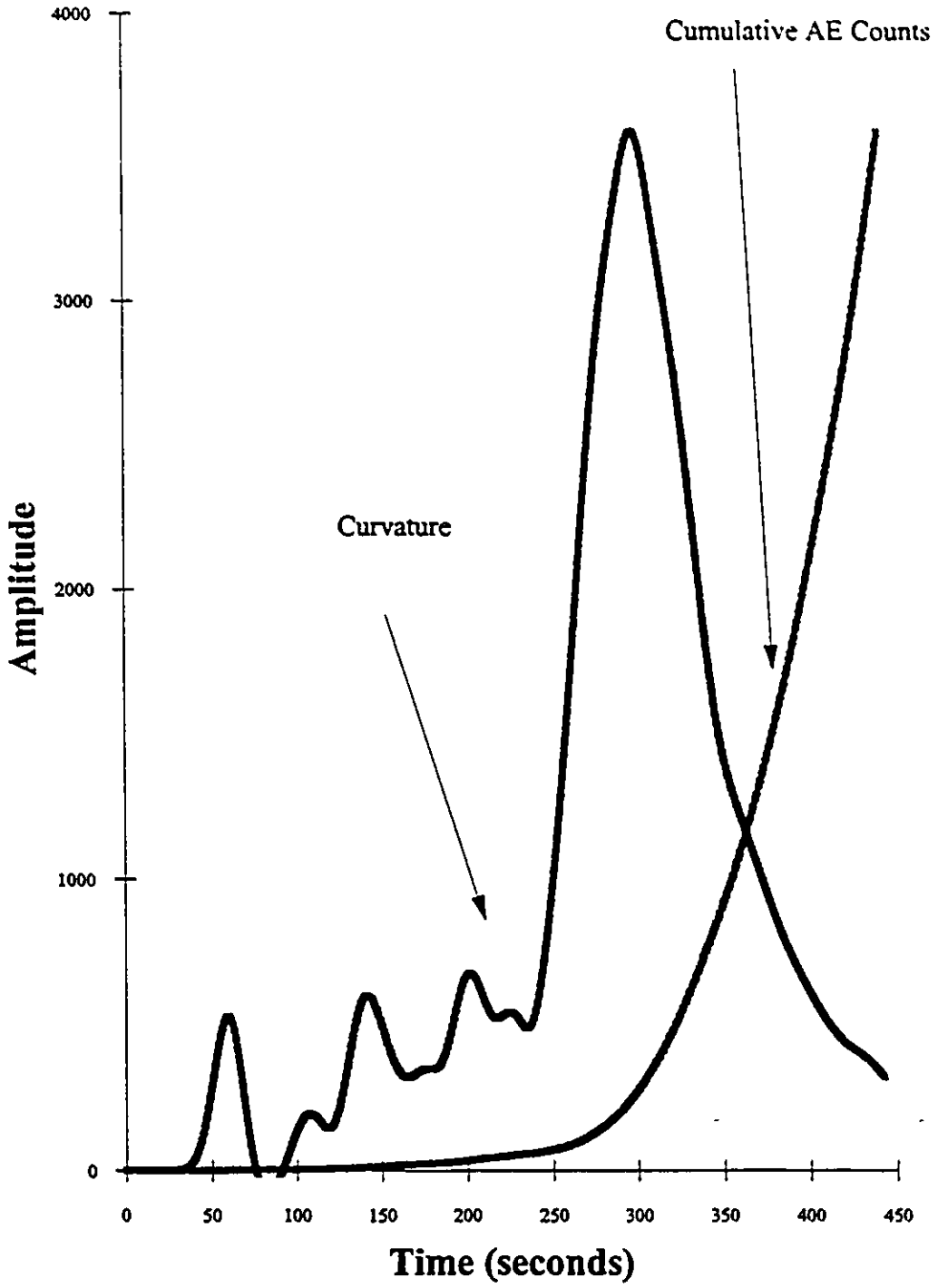

Figure 7-8: Kaiser Effect Curve and Related Curvature using Smoothed Data as a Function of Time.

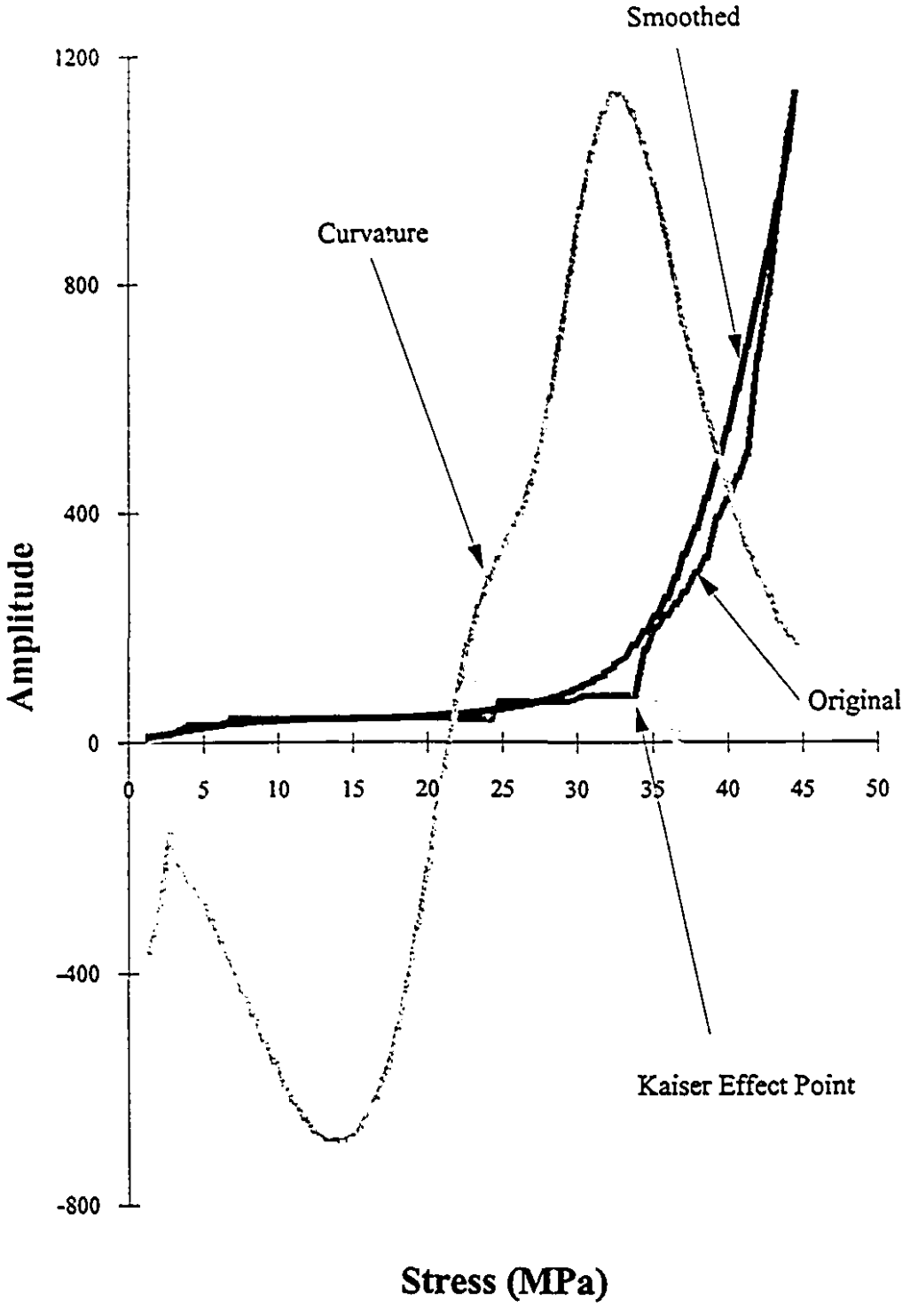

Figure 7-9: Application of MCM to Short but Well-Defined Data from a Limestone Sample.

quality of AE data, i.e. the Kaiser Effect curve possesses a very sharp deflection point at the previous stress level.

In general, short length series do not produce accurate estimates of the Kaiser Effect load if the Maximum Curvature Method is applied as described above. For instance, a typical case is represented in Figure 7-10 where the 37-point series for sample GC21 is used to calculate the curvature. The sample was loaded to 30 kN and then tested again with a fast loading rate. The series was smoothed as outlined previously and then the curvature was calculated by applying equations 7-1 and 7-2. This type of behavior is commonly encountered where the loading rate used to stress the sample is fast and therefore the duration of the experiment is less than few hundred seconds.

By comparing the data from long and short length series, the following observations were made possible. Where the experiment lasted between 300 to 500 seconds, the acoustic emission data sampled at a rate of 1 second produced very accurate estimates of the Kaiser Effect load when the Maximum Curvature Method was applied as described in previous sections. In addition, the ratio of the cumulative acoustic emission counts to the test duration or in other words the angle θ in equation 7-2 never exceeded 1.48 or 85 degrees. However, for short length series the ratio was always greater 1.48.

The limiting ratio above was determined empirically by scaling down the cumulative acoustic emission counts for short length series until an acceptable estimate for the previous stress level was obtained by applying the Maximum Curvature Method. By analyzing more than 45 different cases where the sample was reloaded at a fast rate (total test duration less than 300 seconds) it was found that at the point where the maximum angle value becomes equal or slightly less than 85 degrees, the Maximum Curvature Method produces an estimate that is very close to the true value for the Kaiser Effect load. Figure 7-11 illustrates this transformation for sample GC21 where the calculated curvature provides an acceptable estimate for the previous level equal to 27.205 kN. Figure 7-12 depicts the change in the shape of the curvature for sample GC21 as more and more scaling is applied. The graph is plotted in reverse order, that is, the curvature closest to the viewer was obtained from the data that was scaled down the most.

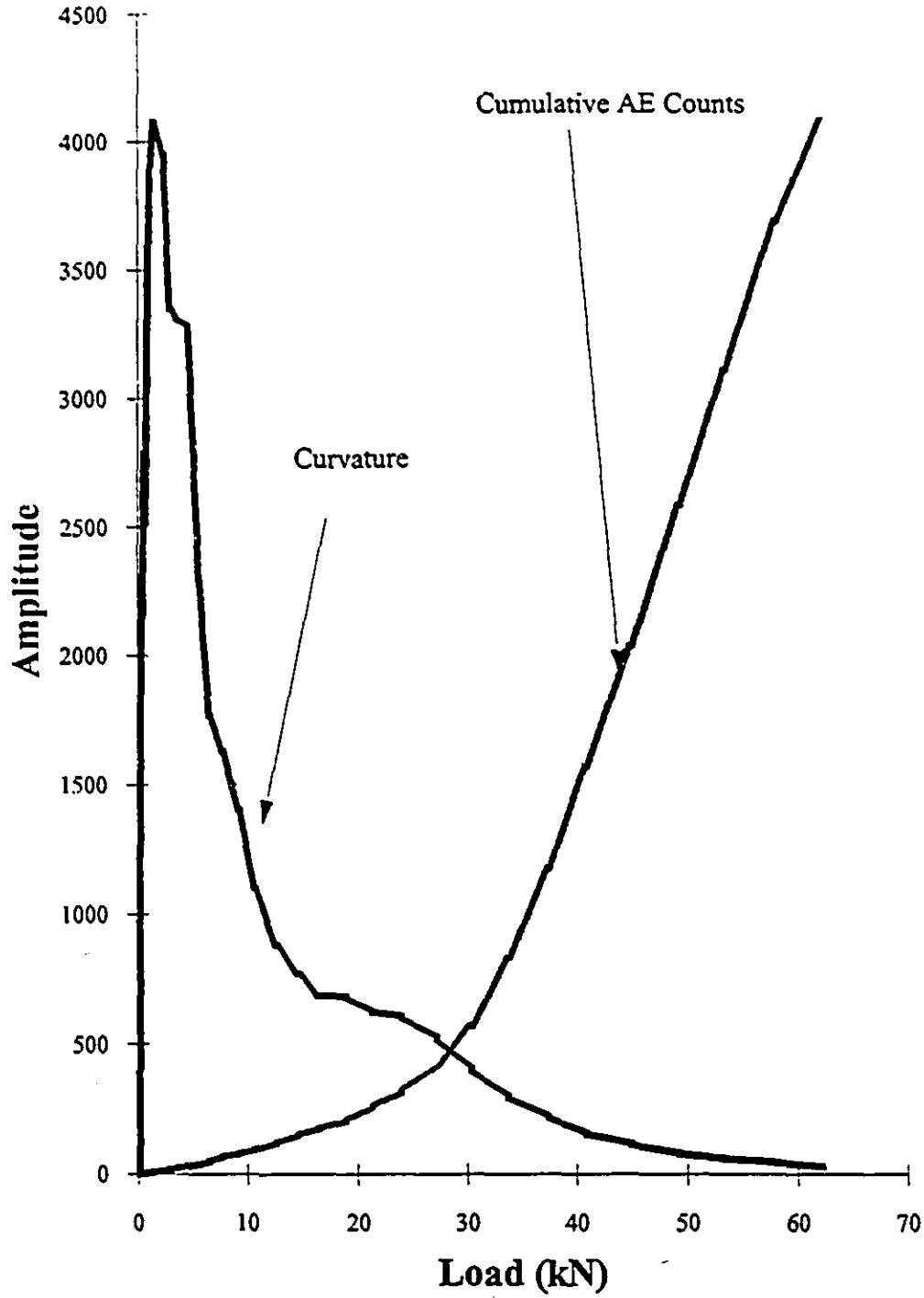

Figure 7-10: Kaiser Effect Curve and Related Curvature for Short Length Series Before Scaling.

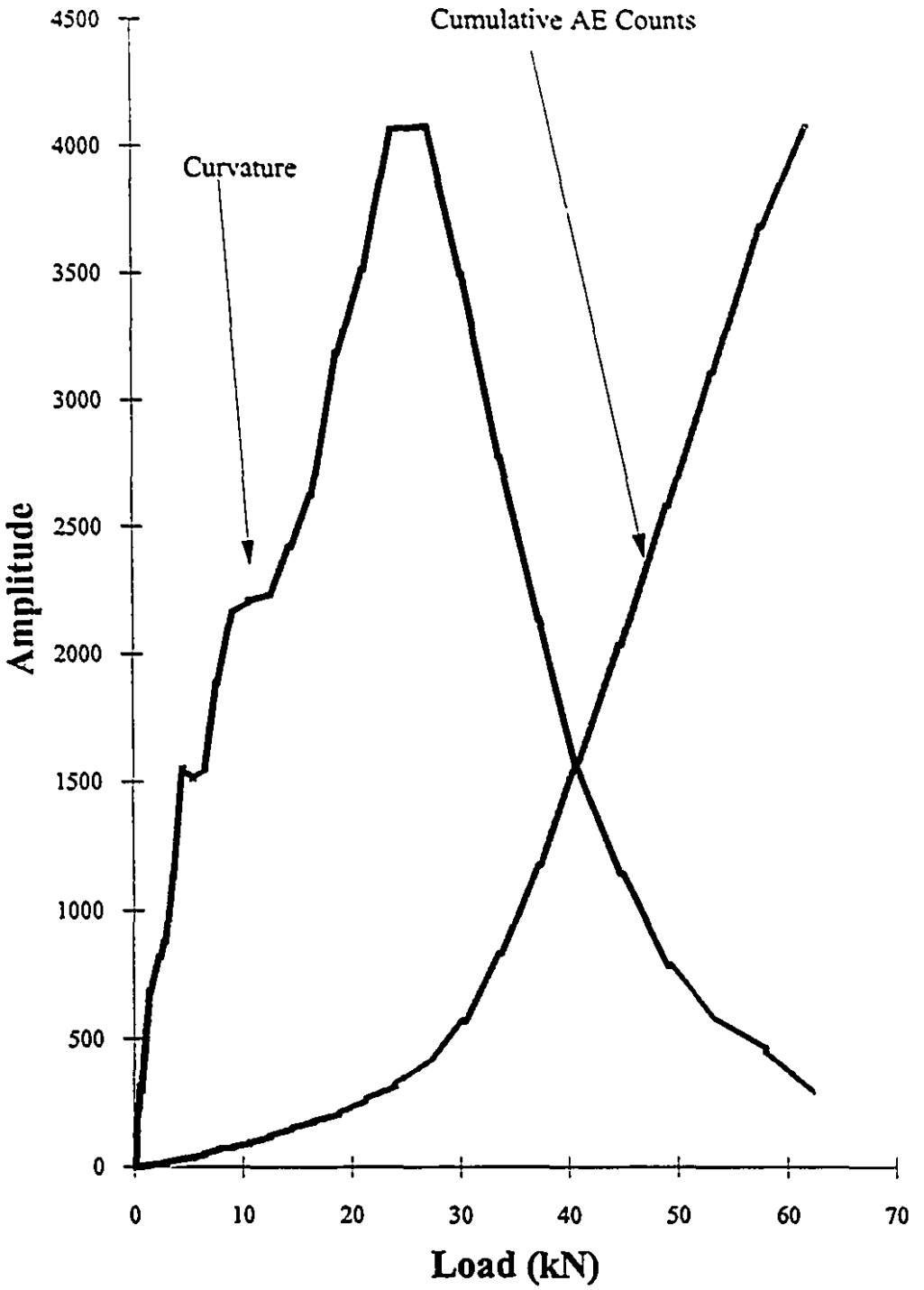

Figure 7-11: Kaiser Effect Curve and Related Curvature for Short Length Series After Scaling.

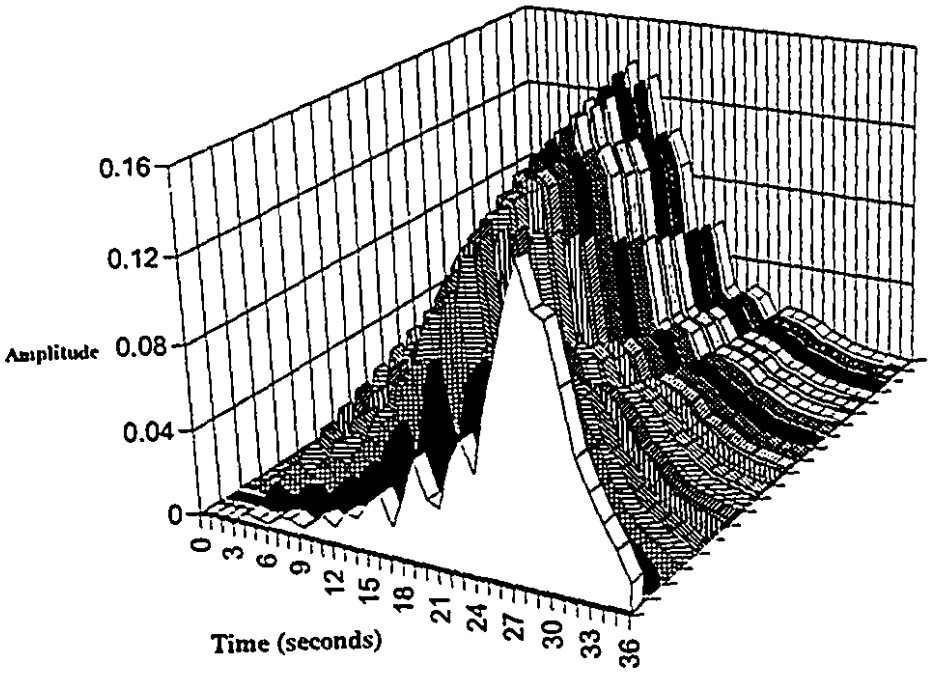

Figure 7-12: Effect of Scaling on Curvature for Short Length Series.

7.3.4) Maximum Curvature Method Algorithm

Figure 7-13 illustrates the algorithm developed to analyze the acoustic emission data recorded from the experiments conducted during the course of this research project. It is based on the concepts described in the previous sections and is composed of the following three modules: scaling CAE data (if necessary), smoothing CAE data, and measuring the curvature of the CAE data. This section discusses in more detail the stoppage criteria included in the algorithm in order to determine the amount of smoothing applied to the data.

The first criterion is called convergence rate and monitors how the smoothing process performs from one iteration to the next. As the number of iterations increases, the smoothing applied will have a smaller effect on the shape of the cumulative acoustic emission counts curve. The convergence rate criterion will therefore measure the amount of change in the shape of CAE data by taking the difference between the goodness of fits calculated from two previous iterations using the chi-square test. This difference is then compared with a preset constant determined empirically. Smoothing is stopped as soon as the convergence rate reaches the preset value. Because the difference between the goodness of fits from one iteration to the next is very small, it is multiplied by a large number (10^{10}) first to facilitate the monitoring process. The calculated rate drops very quickly after a few iterations and decreases thereafter at a slow pace. Here, smoothing is stopped when the convergence rate becomes equal to 100.

The second criterion is departure index. It was described in the previous sections as the difference between the smoothed series and the original series in terms of the value obtained by applying the chi-square test. This value is updated at each iteration after the CAE series is smoothed using the averaging filter. The analysis of a large number of test data showed that smoothing can be stopped if the smoothed data deviates from the original series by as much as 0.1 to 0.3 percent. Here, smoothing is stopped when this parameter reaches 0.1%.

The third and last stoppage criterion is the number of iterations performed during the smoothing process. The limit is set at 200 iterations, however, in all cases smoothing was stopped after no more than 85 iterations were carried out, implying that criterion number one or two were satisfied earlier.

```
ni is the number of iterations
cr is the convergence rate
di is the  departure index;

readCAE data;
read LOAD data;
N = number of points in CAE curve;

while ni< 200 or cr > 100 or dt < 0.1;
      newscae =smooth(oldscae);
      gfnew  = chi_test(oldscae,newscae);
      di = 100 - chi_test(cae,newscae);
      dgfnew  = gfnew - gfold;
      cr   =  abs((dgfnew - dgfold) * (10^10));
      gfold  = gfnew;
      dgfold  = dgfnew;
      oldscae = newscae;
      ni = n i + 1;
endwhile;

index = maximum(curvature(newscae));
Kaiser_Effect_load = LOAD(index);
```

Figure 7-13: Simplified Algorithm Implementing the Maximum Curvature Method.

7.4) Conclusions

To obtain the most reliable results when applying the Maximum Curvature Method it would be more appropriate to sample the data at a high rate for the whole duration of the experiment. It was found that smoothing should be stopped when the smoothed CAE data starts to deviate by more than 0.1 to 0.3% with respect to the original series depending on its quality and quantity, in order to keep the location of the deflection point within the correct range. If the acoustic emission data has a relatively well defined Kaiser Effect point but the series length is too short, then the scaling test discussed in section 7.3.3 must be applied before smoothing is attempted.

Studies have shown that a computer-based Maximum Curvature Method can be used to analyze the Kaiser Effect data obtained from various rock samples. The method produces accurate results if conditions such as (1) the quality of data, in terms of the presence of a well defined deflection point at the previous maximum and (2) the amount of data, in terms of a relatively high sampling rate are met. Another point to take into account when using this method is the degree of smoothing applied to the original data. Studies have shown that if smoothing is applied indiscriminately, the location of the deflection point will change and the correct Kaiser Effect load may not be obtained.

CHAPTER 8

Mechanical & Petrographic Study of Stanstead Granite

8.1) Introduction

The purpose of this study is to investigate the relationship between the acoustic emission and mechanical behavior of Stanstead granite (from Bebee region of the province of Quebec) under uniaxial compression and their correlation with the Kaiser Effect. To establish a relationship between AE behavior and the Kaiser Effect under compressional load, the porosity and microfractography of the Stanstead granite and their evolution at specific points along the loading cycle was monitored.

8.2) Mechanical Properties of Stanstead Granite

The physical and mechanical properties of Stanstead granite that are pertinent to this research programme were investigated. These included the density, porosity, uniaxial compressive strength, modulus of elasticity and Poisson's ratio. These parameters were obtained by testing 20 right circular granite specimens having a diameter of 3.92 cm and a height to diameter ratio of 2:1. The tests were conducted according to ISRM standards [90] on suggested method for determining the uniaxial compressive strength of rock.

To estimate the Poisson's ratio two vertical and two horizontal strain gauges were installed on every sample. The strain was monitored and recorded using a computer based strain measuring equipment. The ultimate strength and modulus of elasticity were determined by analyzing the data collected by the computer controlling the stiff testing machine. Figure 8-1 presents a typical stress-strain graph for the Stanstead granite and Table 8-1 summarizes the mechanical properties of this rock type.

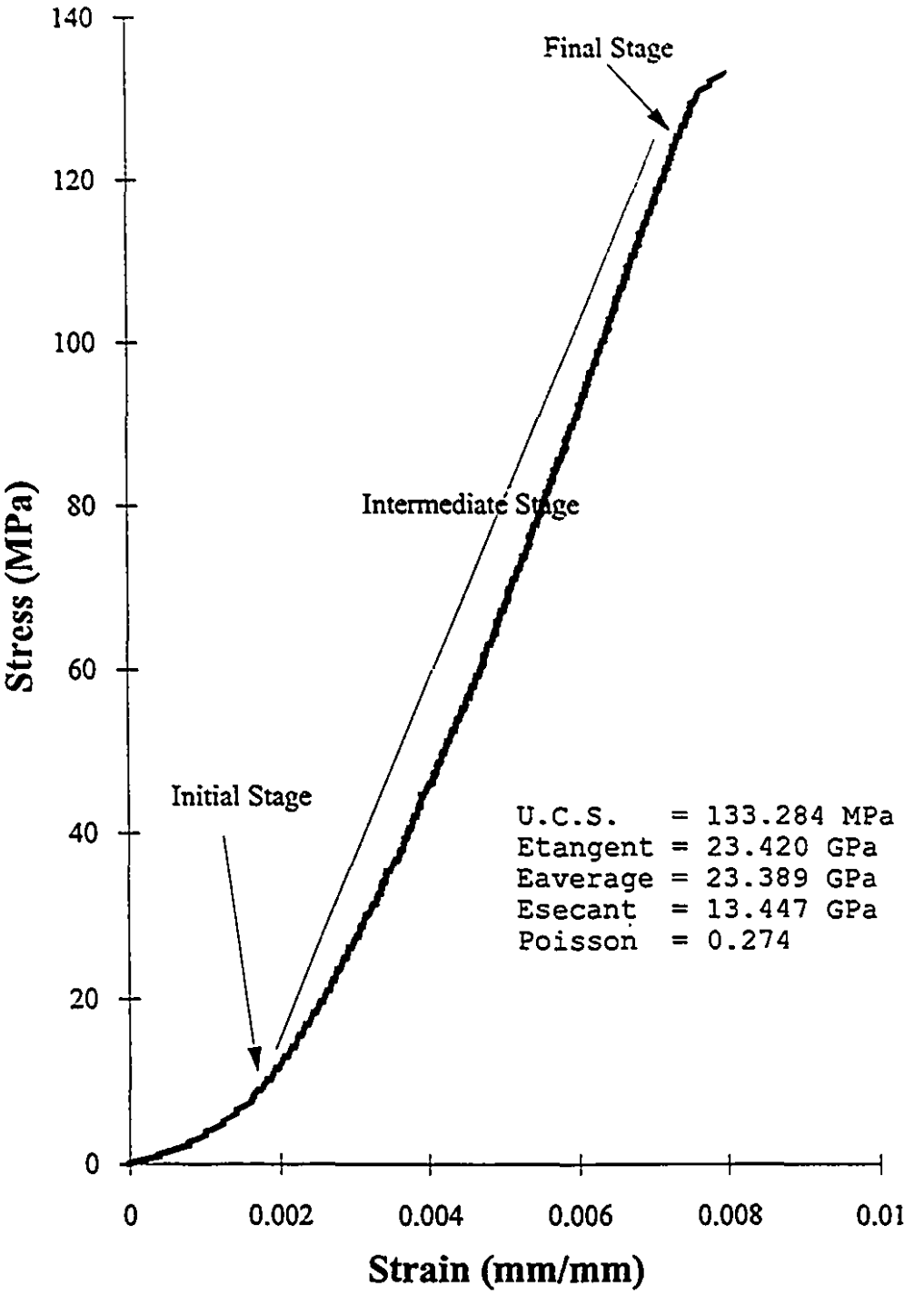

Figure 8-1: Stress-Strain Relationship for Stanstead Granite.

Table 8-1: Mechanical and Physical Properties of Stanstead Granite.

Properties	Average	Standard Deviation
Density	2.686 g/cm³	0.03
Porosity	2%	-
Strength	132.411 MPa	3.854
Young Modulus	23.895 GPa	2.183
Poisson's Ratio	0.264	0.05

8.3) Fracture Study in Relation to Acoustic Emission

In general, acoustic emissions (AE) in rocks are originated from three main classes according to Montoto et al. [82]:

1) Micro-level where AE is initiated by dislocations.
2) Macro-level where AE is caused by twinning, grain boundary re-arrangements and fracture initiation or/and propagation between or/and through the rock's mineral constituents.
3) Mega-level where AE is caused by the fracturing and structural failure of a section of the rock.

The acoustic emission is believed to be initiated due to the sudden release of the stored elastic strain caused by one of the three above cases. This abrupt release of energy is converted to elastic waves, originating at the source and traveling through the material until it is detected by a sensor located on the sample and identified as AE.

In rocks the mechanism responsible for the generation of acoustic emissions can also be explained as the result of intergranular, intragranular and transgranular activities which are initiated in response to the applied stress on the samples. Intergranular activities are related to dislocations, re-arrangements and fracturing in-between grain boundaries. Intragranular activities are related to the fracturing, re-arrangement and twining within the minerals. Transgranular activities are refereed to events such as fractures, where they traverse through a number of minerals and their boundaries.

8.3.1) Testing Programme

Physical properties of the granite were examined prior to application of stress and during the testing at various points along the stress path. The quantity and quality of the fractures were studied using thin section cut parallel and perpendicular to the axis of the cylindrical samples. Because porosity is considered to be a significant rock forming component, sample porosity was calculated in relation to the uniaxial loading. Light-transmitted polarizing petrographic microscope was used to evaluate the character of microcavities and microfractures

as a function of load. In addition, specimen porosity was calculated at every stress level. The samples were dyed with special solution (epo-tek blue dye) in order to enhance the resolution of the microfractures and cavities.

The test procedure requires that cylindrical specimen be loaded at different stress levels up to the maximum compressive strength. Stress was applied in steps of 10% with respect to the maximum compressive strength. This means that samples were subjected to load at 0%, 10%, 20%, 30% and so on until failure at 100%. Later, thin sections were cut and prepared from the loaded samples, parallel and perpendicular to the direction of stress. Microfractures were counted in each thin section. The method of counting required three selected circles with equal dimensions to be marked on each thin section. Circles were marked randomly on the samples in order to cover different areas. Later, fractures were counted and added for all three circles on each thin section with the aid of the light-transmitting petrographic microscope. Porosity values for each loaded sample was calculated prior to the thin section preparations. ISRM standard test procedure [90] was used for porosity calculations.

Right circular Stanstead granite samples having a diameter of 3.92 cm and a length of 7.90 cm were prepared. The testing procedure discussed in Chapter 9 was used to load the specimens and record the acoustic emission events along the stress path. A displacement rate of 0.002 mm/sec was used and a 150 kHz resonant frequency transducer was placed on each sample to detect and count AE signals.

8.3.2) Petrographic Analysis

Stanstead granite is considered to be isotropic, that is, the mechanical properties of the samples are uniform in all directions. In general, this granite has little to no alteration. Table 8-2 summarizes the petrographic properties of Stanstead granite.

8.3.3) Porosity

For an accurate interpretation of the AE activity, porosity variations in relation to the level of load was monitored. Figure 8-2 illustrates the changes in

Table 8-2: Petrographic Analysis of Stanstead Granite.

Name	A close petrography of the samples and percent rock forming minerals concludes the rock name being GRANODIORITE (UGIS).
37%	Plagioclase; 1.0 mm to 6.5 mm; subhedral to euhedral; slightly to moderately saussuritized (4% and even more in some cases). Alteration along the twinning planes and crystal boundaries; some of the crystals show oscillatory zoning; vermicular texture as a result of intergrowth of plagioclase and quartz (myrmekite).
35%	Quartz; 1.0 mm to 6.0 mm; anhedral; undulatory extinction.
12%	K-feldspar; 1.0 mm to 3.0 mm; subhedral to euhedral; little to no alteration; vermicular texture (myrmekite); mainly microcline.
12%	Biotite; 1.0 mm to 2.5 mm; subhedral.
1%	Hornblende; 0.5 mm to 1 mm; subhedral.
1%	Apatite; <0.1 mm to 1.5 mm; subhedral.
1%	Zircon; <0.1 mm to 0.8 mm; subhedral.
<1%	opaques; in thin section few sparse, finely disseminated minerals are evident.
Fabric	This rock is holocrystalline, hypidiomorphic, medium grained and essentially equigranular.

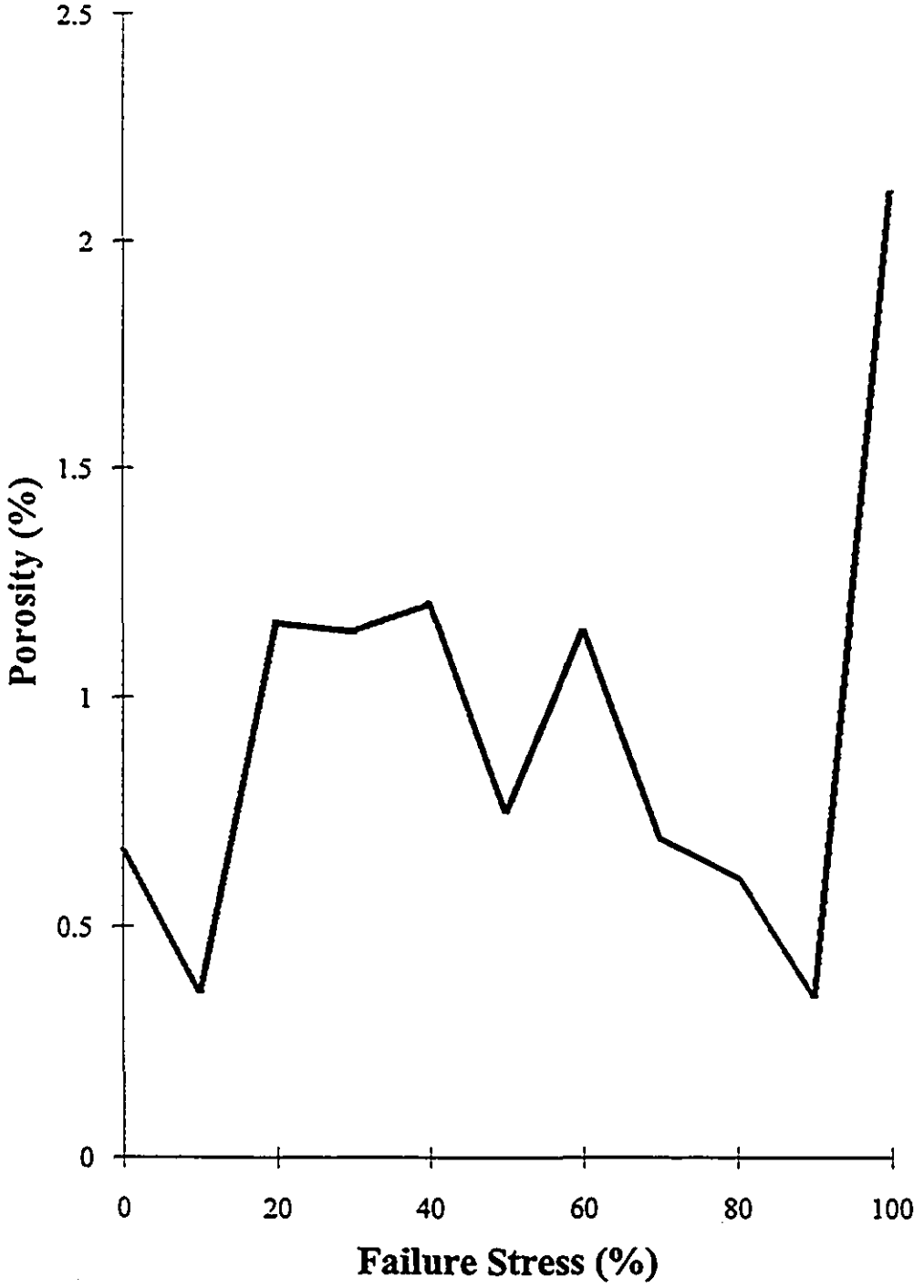

Figure 8-2: Changes in Porosity as a Function of Load.

percent porosity versus the percent maximum compressive strength of the granite. At the initial stages of the loading cycle the porosity decreases. Later at 20% of the uniaxial compressive strength the porosity increases. After 20%, porosity decreases slowly until 90% of the failure point. From this point on, there is a large increase in the porosity of the samples until failure occurs. This porosity variation could be the result of the closure of initial micro-cavities followed by the generation of new micro-fissures and their later closure due load increase. Finally, a large increase in the porosity content occurs prior to the failure.

8.3.4) Fractography

Acoustic emission activities were detected in the initial stage, as the load was applied on the samples. There is an increase in the number of AE events as the stress level increases. The relationship between load and the number of AE events is linear as shown in Figure 8-3. However, there are variations in the rate of AE events. According to Montoto et al. [82] there are three significant stages of AE behavior in various granites. A high AE rate at early stage of loading followed by a relatively low but accelerating AE rate, and finally a rapid increase in AE rate. The altered and porous rocks illustrate a continuous and steady increase in the AE rate as the load increases. On the other hand, rocks with low porosity and alteration content do not illustrate the intermediate stage. The initial stage is followed by the final stage. Stanstead granite demonstrates all three stages. During the initial stage, micro-level and macro-level activities are the source of acoustic emissions. In terms of petrographic analysis, the inner modification, friction between the grain boundaries, closure of the fractures and micro-cavities are responsible for the AE. A picture of Stanstead granite at this stage of loading is shown in Figure 8-4. The initial stage continues until 30-35% of the maximum compressive strength. Both micro-level and macro-level activities are progressing in the samples during the intermediate stage. Formation of the new cracks and fissures, local failures and volumetric changes are responsible for the increase in the AE activity in the intermediate stage as illustrated in Figure 8-5. In Stanstead granite the intermediate stage is responsible for the generation of acoustic emissions until 60-70% of the maximum compressive strength. Porosity values increase during the early portions of the intermediate stage and then decrease at a low but progressive rate. Intermediate stage illustrates a low but progressive

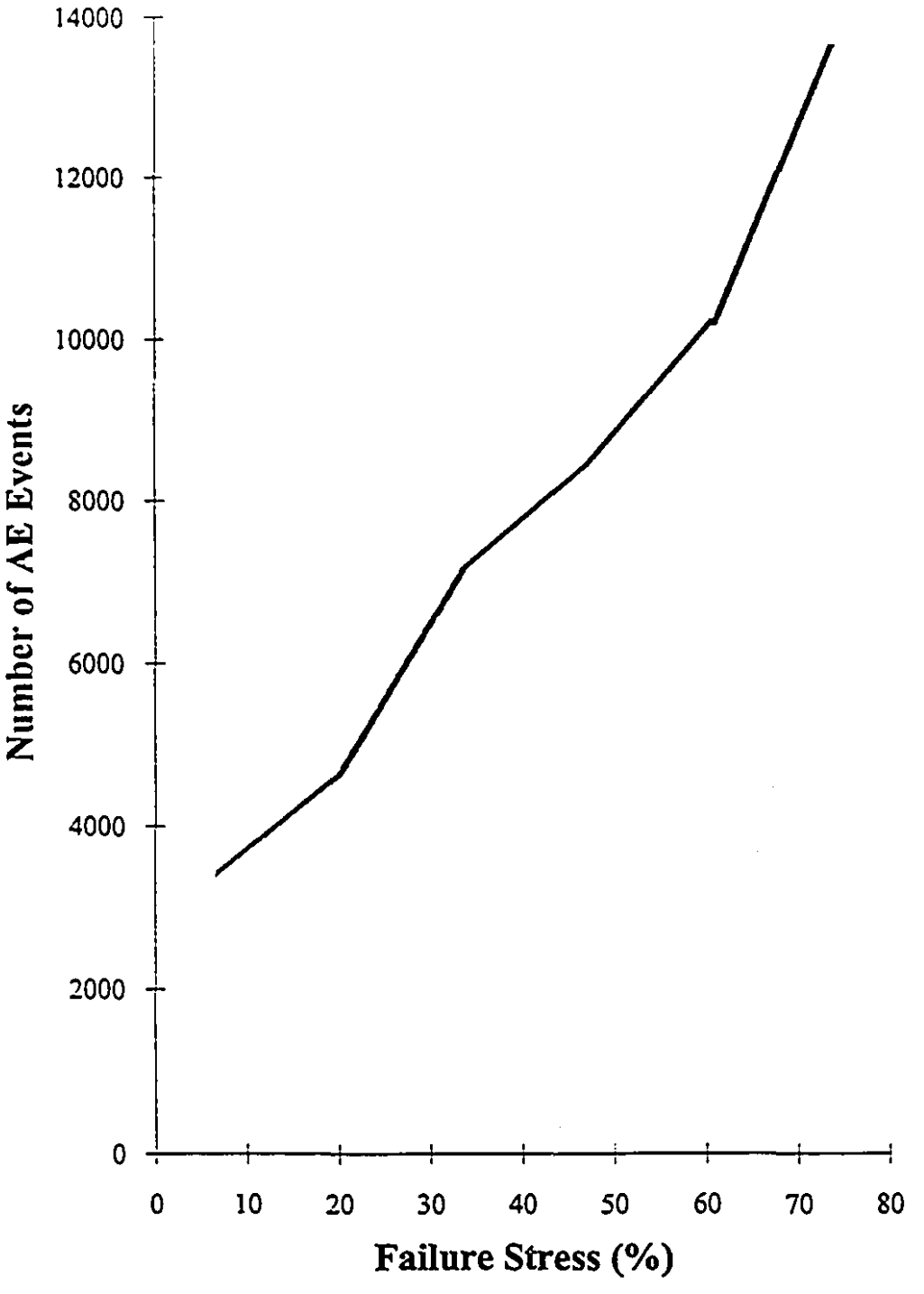

Figure 8-3: Increase in Total Number of Events as a Function of Stress.

Figure 8-4: State of Fractures in Stanstead Granite During Initial Stages of Loading.

Figure 8-5: State of Fractures in Stanstead Granite During Intermediate Stages of Loading.

increase in the rate of AE. In the final stage, mega-level activities are mainly responsible for the AE activity. The dilation, sub-granular activities, formation of the new fractures, friction between the grains and utmost failure of the sample are the main sources of AE. Figure 8-6 is shows the state of the rock at this stage where the porosity content increases. In Stanstead granite, the final stage of activities start, after 70% of the maximum compressive strength.

In order to evaluate the acoustic emission data with respect to petrographic results, thin sections were studied under a light-transmitting petrographic microscope. The sections were cut from the central part of the cylindrical samples. For observation purposes samples were cut in two directions: parallel to the direction of load or the maximum strain axis (Y-axis of the cylinder) and perpendicular to the direction of load or the minimum strain axis (X-axis of the cylinder).

The fractures form simultaneously as the load increases at a right angle to the greatest strain axis. In both X and Y direction the number of fractures increases with increasing load until 20% of the maximum compressive strength. In the X-axis the number of the fractures increases steadily until 90% of the maximum compressive strength where there is a jump in the number of fractures. However, in the Y-axis the number of fractures decreases continuously between 20% to 70% of the maximum compressive strength. Later, the number of fractures increases rapidly until failure. In the Y-axis direction, that is, the direction of maximum strain, fractures tend to open wider as they multiply in length. Figures 8-7 and 8-8 illustrate the relationship between the number of fractures parallel and perpendicular to the direction of stress as function of stress level. In case that twining planes, particularly in plagioclase, are located in the same direction as the Y-axis, more planes tend to open wider as the load increases (see Figures 8-9 and 8-10). In general, the number of fractures generated in both directions is equal.

8.4) Discussion

The source of acoustic emissions in Stanstead granite could be explained to be the result of intergranular, intragranular and transgranular activities that are

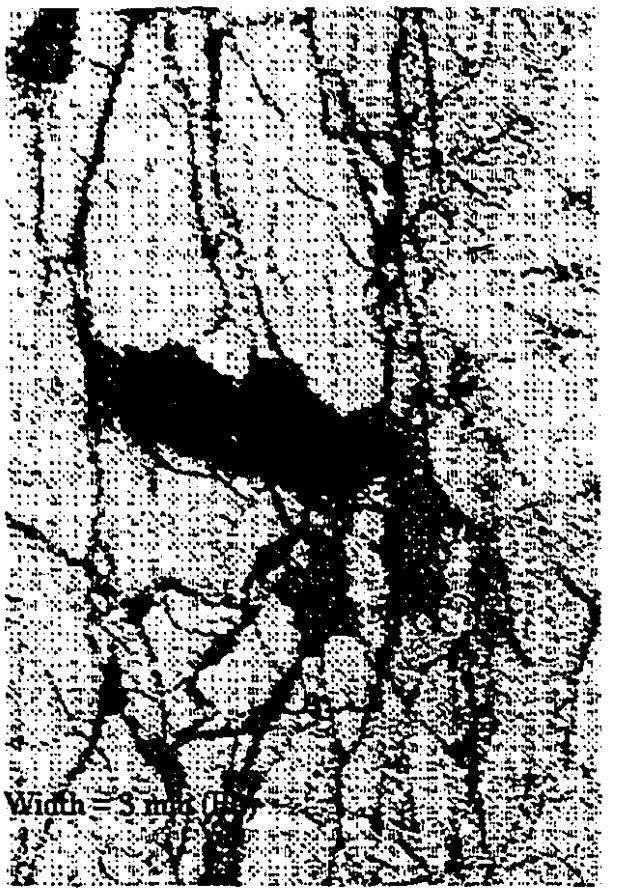

Figure 8-6: State of Fractures in Stanstead Granite During Final Stages of Loading.

initiated in the rock by the application of stress. These activities evolve from micro-scale to macro-scale as the level of load increases.

With respect to the sources responsible for triggering stress memory in rock materials Kurita and Fuji [40] have stated: "in the elastic stage, a crack, pre-existing or newly formed, grows to an equilibrium configuration corresponding to the applied stress and this stress would be memorized in the rock through the crack configuration. The opened crack would be closed after unloading, but not healed in an atomistic sense until the next loading." According to the experimental results obtained in this work, Kaiser Effect in Stanstead granite occurred only up to 75% of the maximum compressive strength of the samples (see Chapter 9). The petrographic analysis of tested samples indicates that 75% of the maximum compressive strength marks the end of the intermediate stage for the evolution of the AE source. This indicates that the imprinted stress memory in the samples are not retrievable as the samples leave the elastic stage toward their final failure stage.

A fractographic analysis of the samples both parallel and perpendicular to the direction of load indicated that the number of fractures are more or less equal. In the case of Stanstead granite this might be due to the fact that the rock is isotropic. In anisotropic rocks the formation of new fractures and their quantity might very much depend on the direction of the applied load. Therefore, in isotropic rocks, the stress memory could be preserved regardless of the direction(s) of the applied load.

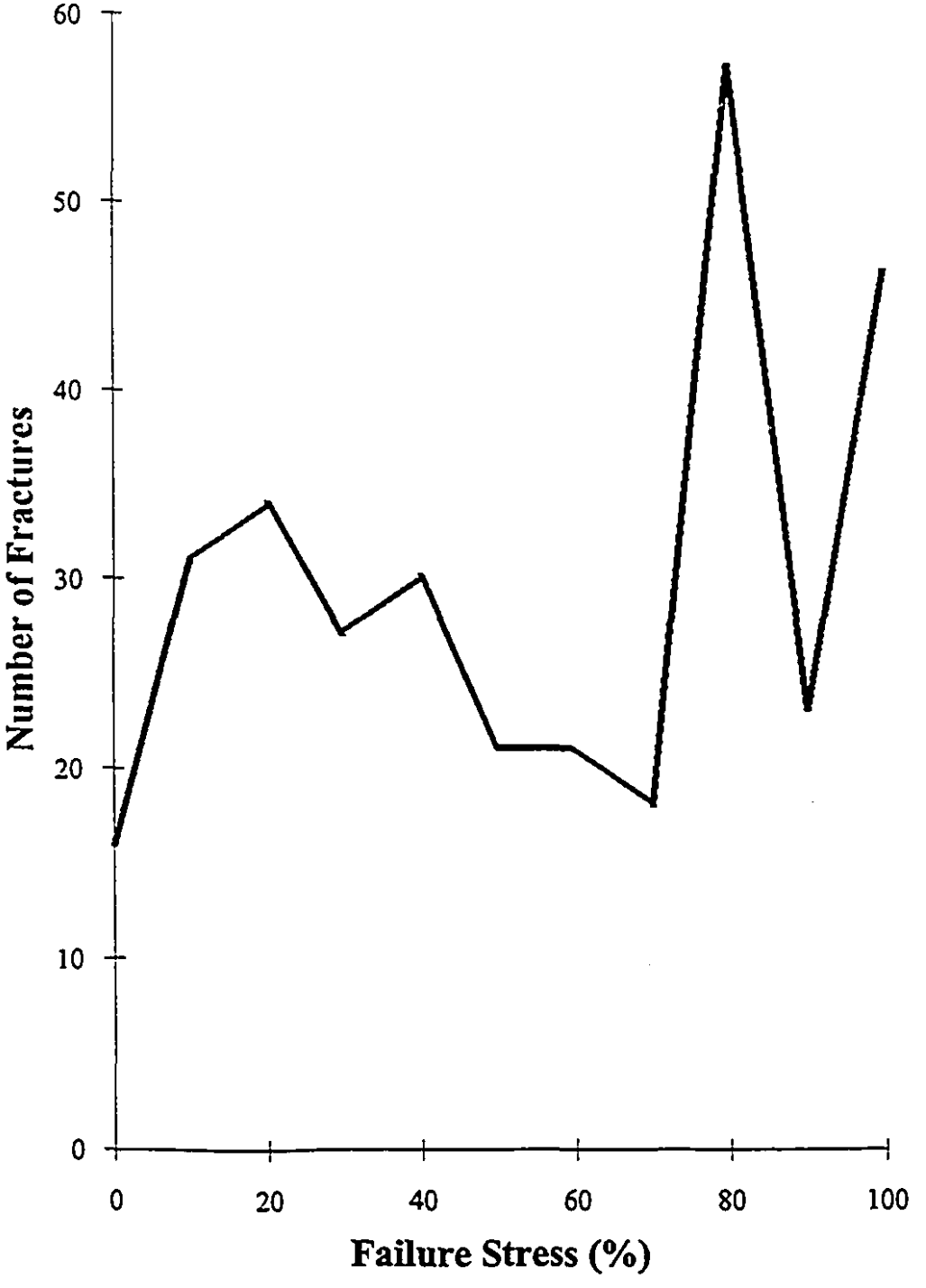

Figure 8-7: Number of Fractures Parallel to Stress Direction vs Stress Level.

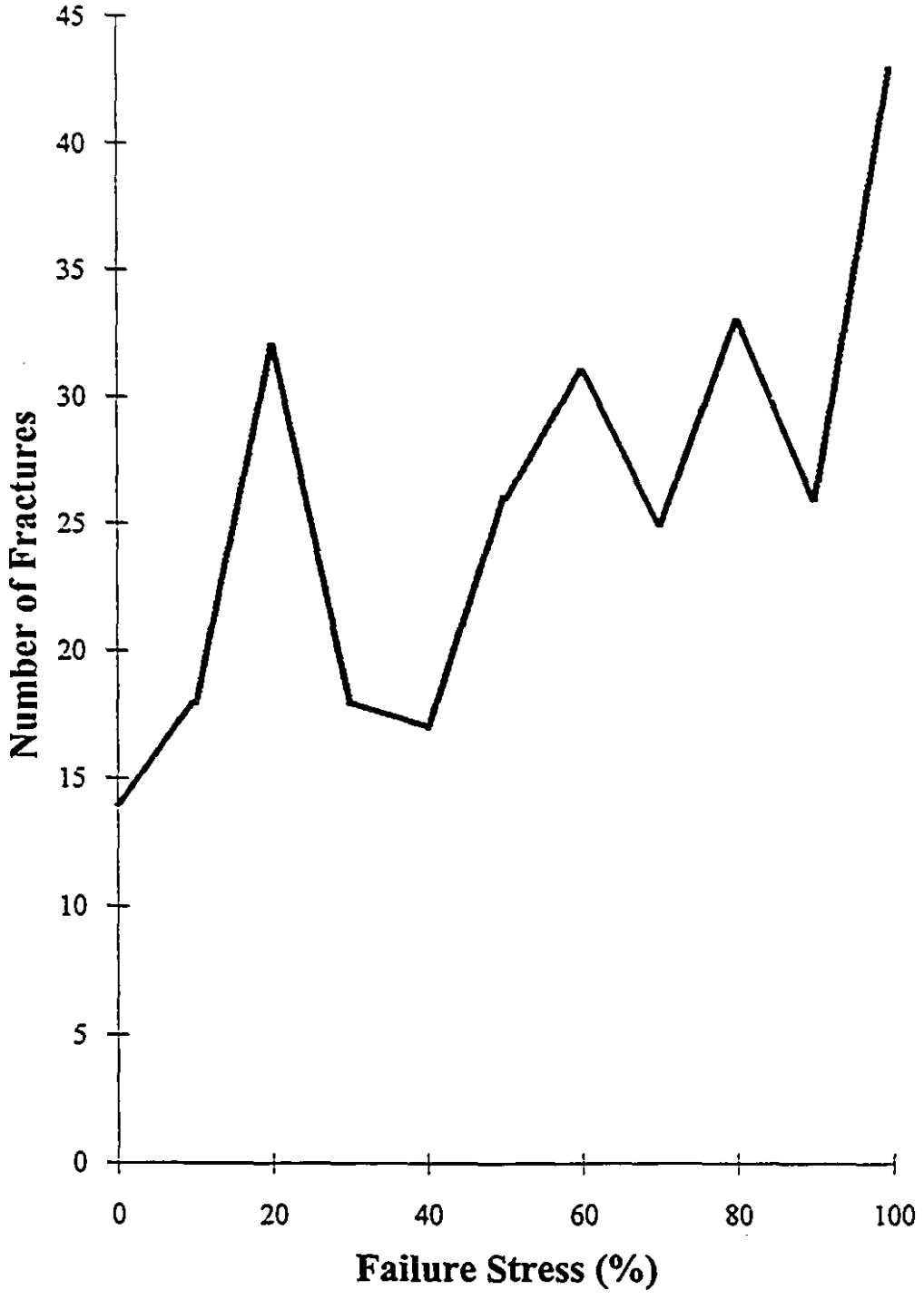

Figure 8-8: Number of Fractures Perpendicular to Stress Direction vs Stress Level.

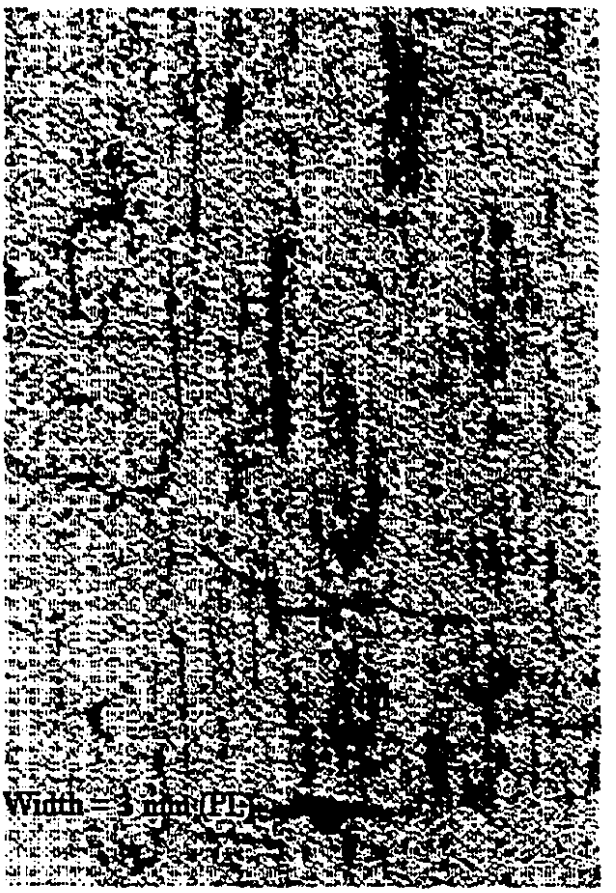

Figure 8-9: Opening of Twinings at 30% of Failure.

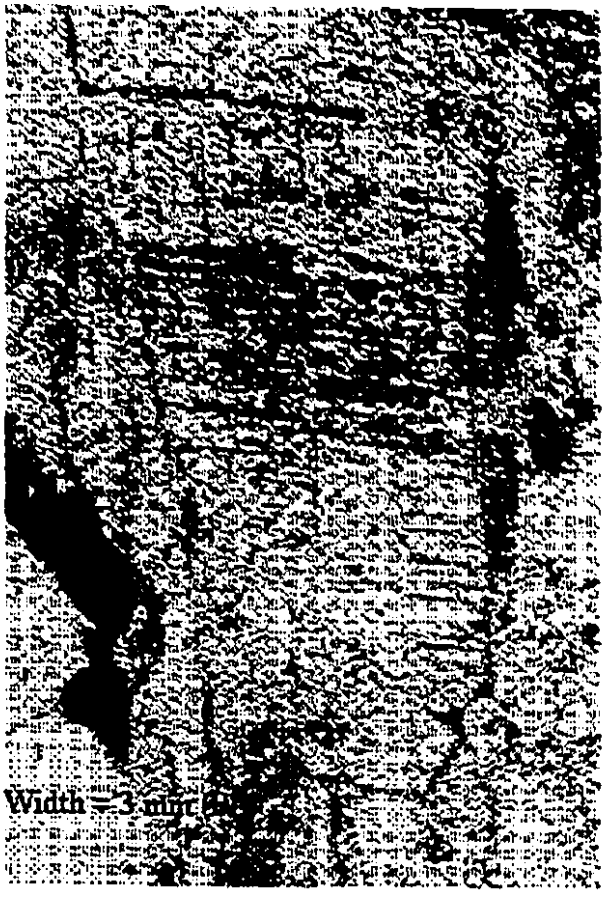

Figure 8-10: Opening of Twinings at 80% of Failure.

CHAPTER 9

Laboratory Programme: Factors Affecting Stress Memory

9.1) Introduction

A comprehensive research programme was undertaken to study the effect of various factors affecting stress memory determination in rocks. In order to evaluate the relative importance of factors such as transducer/amplifier frequency response, signal definition parameter, stress rate, strain rate, specimen size, stress level, delay time, temperature, water content, confining pressure, and directional loading over 700 samples were tested using one rock type, namely the Stanstead Granite for its homogeneous composition and its high level of acoustic emission noise.

Detailed petrographic and mechanical properties of this rock type were described in Chapter 8. This chapter discusses the results of the experiments conducted on the factors listed above. This is the first comprehensive study of its kind in the sense that (a) it takes into account factors that are likely to affect stress memory in rocks, (b) it is carried out on the same rock type throughout the testing programme using the same set of standards.

9.2) Selection of Transducer/Amplifier Frequency Response

To select the appropriate transducer and amplifier for the Kaiser Effect experiments different sensor/amplifier combinations were tried out. An attempt was made to cover as wide a range of frequencies as possible. Tables 9-1 and 9-2 show the type of transducers and amplifiers used in this investigation.

Test results from different rock types (granite, limestone and sandstone) showed that the broad-band transducer did not perform as expected due to its lower sensitivity. To compensate for the lack of sensitivity, the gain on the post-amplifier was increased until events were detected by the equipment. Tests on a hardened piece of steel cylinder determined that by increasing the level of gain, a

Table 9-1: List of Transducers Utilized.

Transducer	Manufacturer	Frequency (kHz)	Sensitivity (dB)	Diameter (mm)	Weight (g)
AC30L	AET	30	-70	29	35
AC75L	AET	75	-80	29	26
R15-2360	PAC	150	-66	17.5	19
FAC500	AET	100-2000	-90	25.4	170

Table 9-2: List of Amplifiers Utilized.

Amplifier	Manufacturer	Gain (dB)	Band-Pass Filter (kHz)
140B	AET	40	15-45 60-90 125-2000
1220A	PAC	40/60	100-300

large number of events were spurious noise related to the hydraulic press. After reducing the gain until no machine noise was detected, tests on various rock types showed that no considerable amount of acoustic emissions could be recorded to conduct a Kaiser Effect experiment. It was decided not to use flat frequency response transducers because the appropriate acoustic emission to machine noise ratio could not be obtained.

AET's AC75L type transducer having a resonant frequency of 75 kHz detected no acoustic emissions from any one of the different rock types tested. The sensor and the pre-amplifier were checked twice by the manufacturer for possible defects or malfunctions but none were found. This transducer, however, recorded the noise generated by the hydraulic machine, although the total number of events were lower by 55% compared to the most sensitive sensor described below.

The performance of the AET's 30 kHz resonant frequency transducer was satisfactory compared with the two sensors used earlier. Large numbers of acoustic emissions were detected and different Kaiser Effect experiments produced good results when the samples were loaded for a second time. These findings are not surprising if one considers the sensitivity of the transducer shown in Table 9-1 above.

PAC's 150 kHz resonant frequency transducer is the most sensitive among the four sensors available for this investigation. It also provided the best acoustic emissions to noise ratio, that is, for the lowest threshold setting and highest amplifier gain where the spurious noise from various sources was cut off, the number of acoustic emission events from any one of the rock types was the largest. As described in Chapter 6, this transducer was used to determine the most efficient threshold setting and level of amplification given the amount of noise generated by the testing equipment. Consequently, this sensor was used for the remainder of the investigation.

9.3) Signal Definition Parameters

Chapter 3 discussed all the parameters that define an acoustic emission event. The most important are signal amplitude, signal duration, energy and the

ring-down count. These parameters carry information about the type of mechanisms that generates the acoustic emission events. In Kaiser Effect studies, we are primarily interested to determine the point where the rate of emissions start to increase rapidly. Chapter 8 defined various sources of acoustic emissions at different stress level in relation with Kaiser Effect. A study was carried out to find whether parameters such as signal amplitude and energy could be used to "sharpen" the deflection point in the Kaiser Effect point.

Specifically, energy was selected as the parameter to study because it is derived from two more basic acoustic emission parameters, namely peak amplitude and event duration. The AET 5500 system uses the following expression to calculate the value for energy:

$$Energy = 10 * \log_{10}(event\ duration) + peak\ amplitude \tag{9-1}$$

Event duration is defined in micro-seconds as recorded and *peak amplitude* is in decibels. Figure 9-1 shows the graph of energy distribution for five different granite samples loaded up to a level of 30 kN during a Kaiser Effect experiment. Two characteristic peaks are present in the ranges 42 to 48 and 53 to 85.

The cumulative acoustic emission counts was calculated for each of two ranges and for the entire range of recorded events. For example, sample GE501 generated a total of 858 events with a signal energy between 42 to 48 and a total of 2460 events having a signal energy between 53 and 85. The total number of events recorded during the experiment was 3590. MCM produced the following estimates of the previous load level for the three different data sets.

Energy Range	Estimated Load (kN)
42 - 48	36.784
53 - 85	34.211
42 - 116	30.173

Similar results were obtained with other test samples and rock types. It was concluded that discriminating acoustic emission parameters does not improve the "sharpness" of the cumulative AE curve. Therefore, as many events as possible

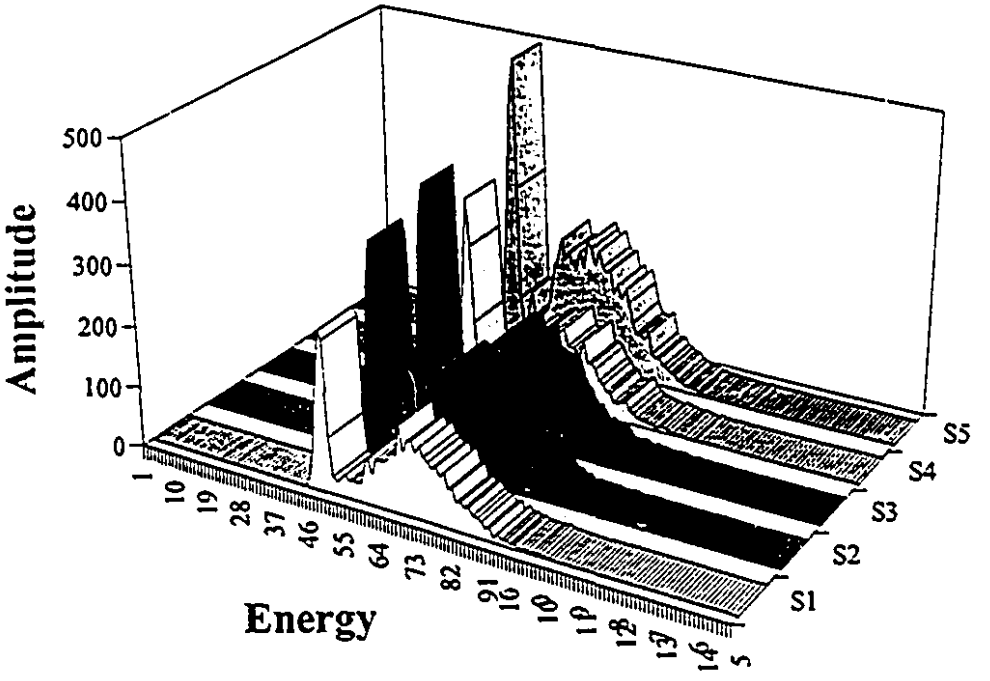

Figure 9-1: Energy Distribution for 5 Different Samples During the Second Load Cycle.

should be recorded for the analysis of Kaiser Effect data in order to get more accurate load estimates.

9.4) Effect of Loading Mode

An important issue in a Kaiser Effect experiment is the choice of loading mode, that is, should the specimen be stressed under load or displacement control. Because this study attempts to address the question of loading mode for the first time, a large number of samples were tested at different rates. The objective was to find out which loading mode and what loading rate gives the most accurate Kaiser Effect values. Based on the outcome of this investigation, the remaining Kaiser Effect experiments would be carried out under either load or displacement control.

9.4.1) Effect of Load Rate

To evaluate the effect of load rate on determining the stress memory of rocks a large number of samples were tested using different rates. In particular, samples with a diameter of 3.9 cm were loaded up to a level of 30 kN during the first cycle using three different load rates and held at that level for about 30 seconds. Load rates selected can be categorized as Very Fast, Intermediate, and Very Slow. An extra set of samples loaded using the intermediate rate was held at the 30 kN level for a period of 5 minutes to see the effect of strain saturation on the sharpness of Kaiser Effect curve. For the second cycle, the five load rates used were Very Fast, Fast, Intermediate, Slow and Very Slow. Table 9-3 provides the rates used in this investigation.

A total of 5 specimens were tested in each category. The complete set of results is shown in Figure 9-2. It can be seen that stressing samples immediately after the first load cycle using Very Fast and Fast rates produces lower estimates. Intermediate to Very Slow rates give more accurate values for the previous load level. Figure 9-3 displays the standard deviation for the averaged values in Figure 9-2. Here, the full effect of loading rate on the Kaiser Effect can be seen clearly.

Table 9-3: Load Rates for the First and Second Load Cycles under Load Control Mode.

First Load Cycle (kN/sec)	Second Load Cycle (kN/sec)
	1.5000 VF
	0.7500 F
1.5 VF	0.3750 I
	0.1875 S
	0.0938 VS
	1.5000 VF
	0.7500 F
0.3750 I	0.3750 I
	0.1875 S
	0.0938 VS
	1.5000 VF
	0.7500 F
0.0938 VS	0.3750 I
	0.1875 S
	0.0938 VS

VF: Very Fast
F: Fast
I: Intermediate
S: Slow
VS: Very Slow

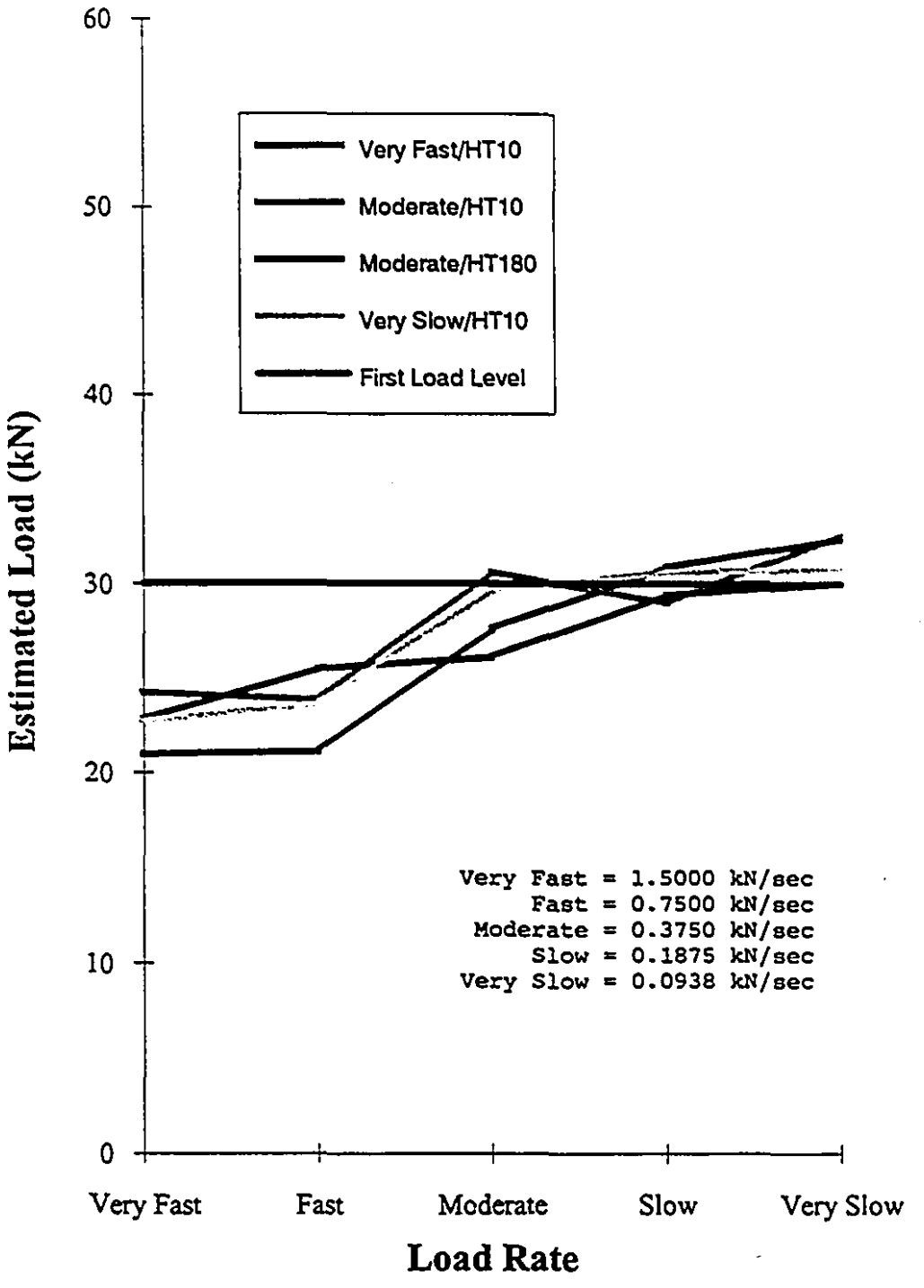

Figure 9-2: Effect of Loading Rate on Kaiser Effect for Samples Tested under Load Control.

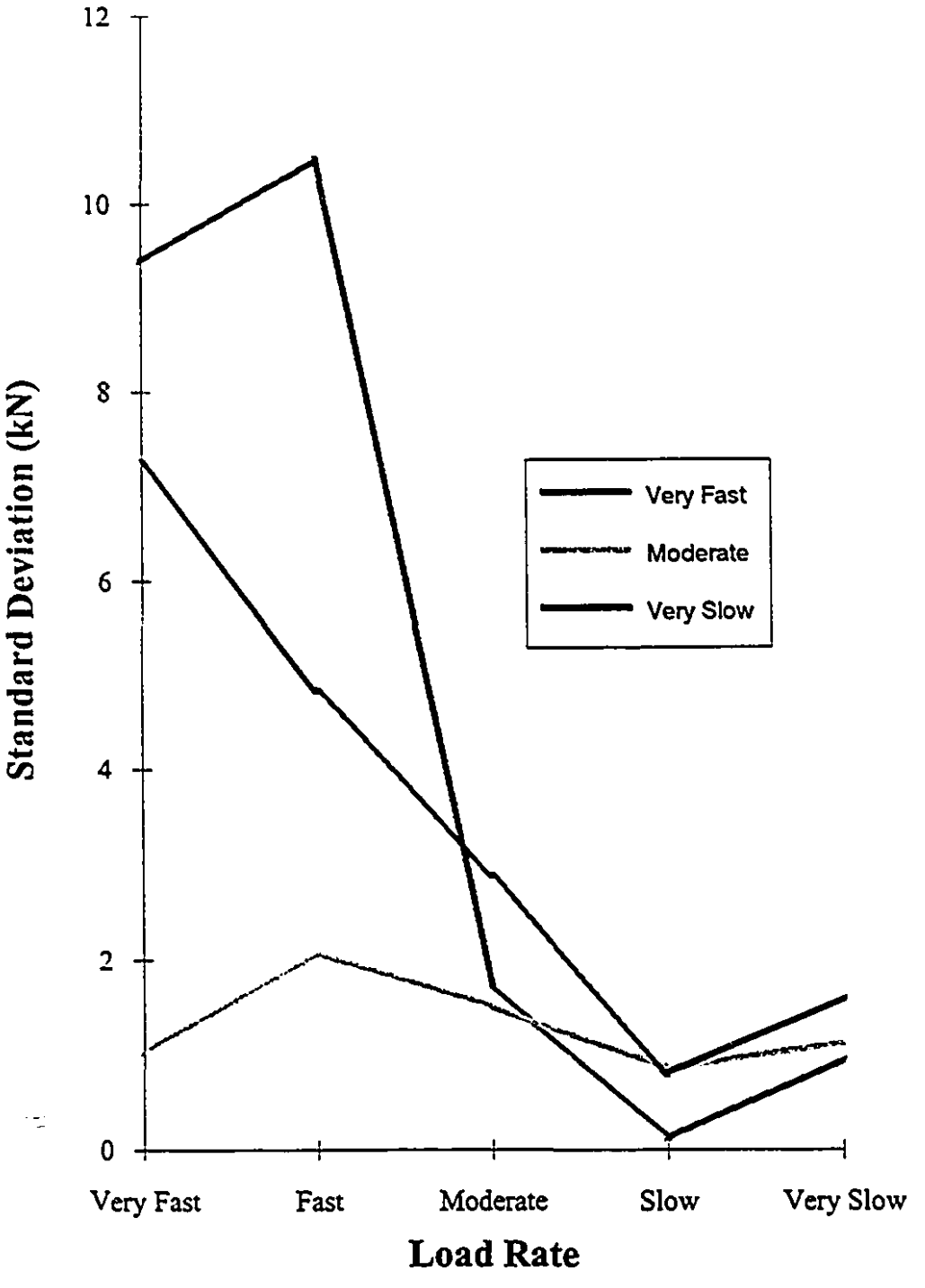

Figure 9-3: Standard Deviation for Estimated Loads Shown in Figure 9-2.

Fast rates cause a very high standard deviations while Intermediate to Very Slow rates show standard deviations about 2 to 3 MPa.

The shape of the curvature is distinctively different for fast and slow ranges. Although a fast loading rate produces less accurate estimates, the curvature is very smooth. A typical curve is shown in Figure 9-4 where sample GB11 was tested using the Very Fast rate for the second cycle. As far as slow loading rates are concerned, the curvature presents a sharp peak at the Kaiser Effect point, however, its shape is very noisy. Figure 9-5 shows the results for sample GB45 loaded using the Very Slow rate.

9.4.2) Effect of Displacement Rate

The effect of displacement rate on stress memory of rocks was tested in the same way as for the load rate. Specimens were loaded using Very Fast, Intermediate and Very Slow rates for the first cycle up to 30 kN and held at that level for 30 seconds. The displacement rates selected for the second cycle were Very Fast, Fast, Intermediate, Slow and Very Slow. Table 9-4 gives the actual displacement rates used in the investigation.

A total of 5 specimens were tested in each category. The complete set of results is shown in Figure 9-6. The load estimates follow the same general pattern as in the previous case. Specimens loaded using Very Fast and Fast rates exhibit a lower Kaiser Effect point. Intermediate to Very Slow rates give more accurate values for the previous load level. Figure 9-7 displays the standard deviation for the averaged values in Figure 9-6. Standard deviations for the averaged loads are lower than the values obtained from the load rate experiment.

The shape of the curvature and Kaiser Effect curve are characteristically different for fast and slow ranges. Here, a slow loading rate produces much sharper curvature around the Kaiser Effect point hence a more accurate load estimate. This situation is shown in Figure 9-8. In contrast, Figure 9-9 is the plot of the cumulative acoustic emission counts and its associated curvature for sample GC44 using the Very Fast rate for the second cycle. Fast to Very Fast loading rates

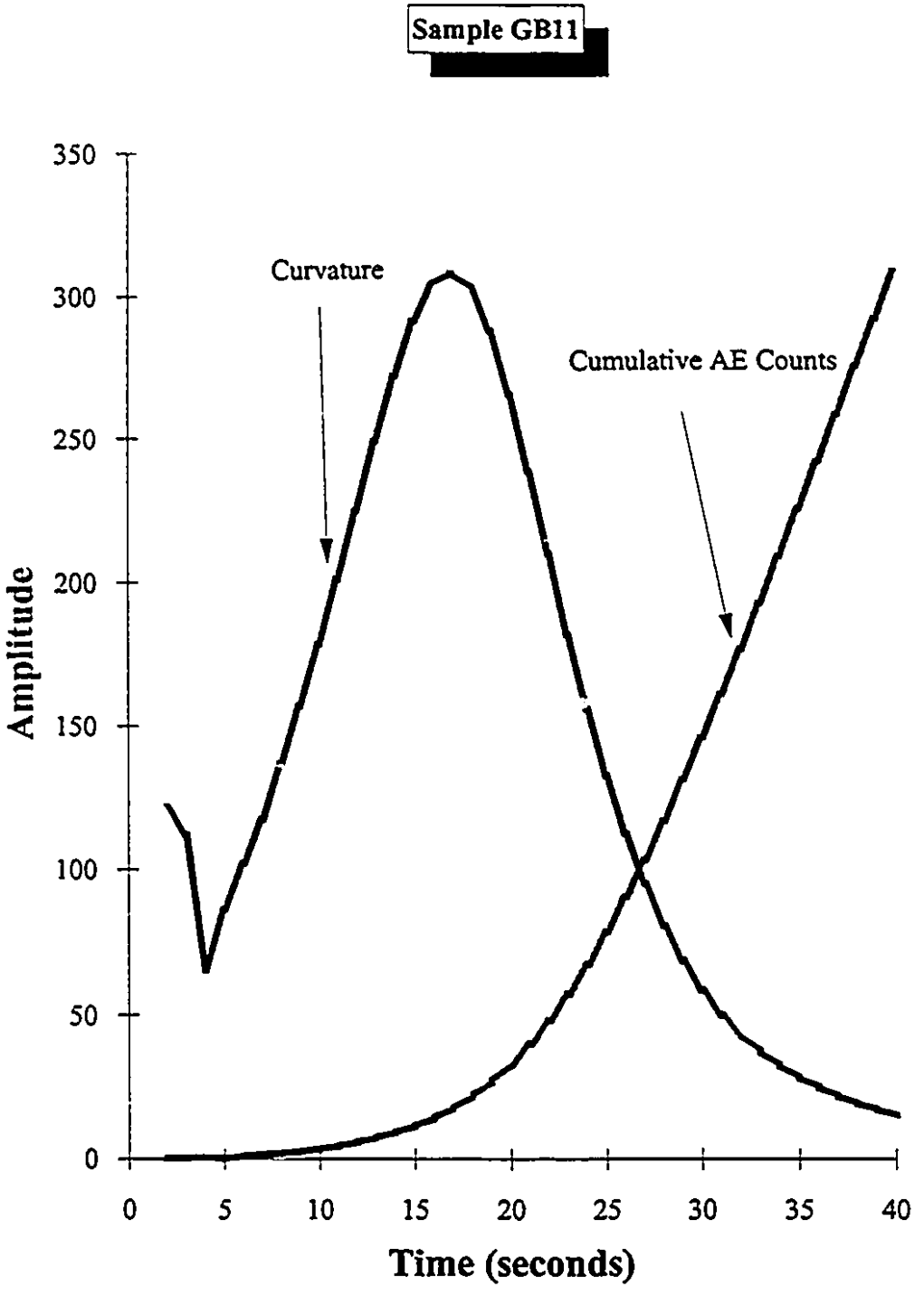

Figure 9-4: Result of Kaiser Effect Test under Load Control Using the Very Fast Rate.

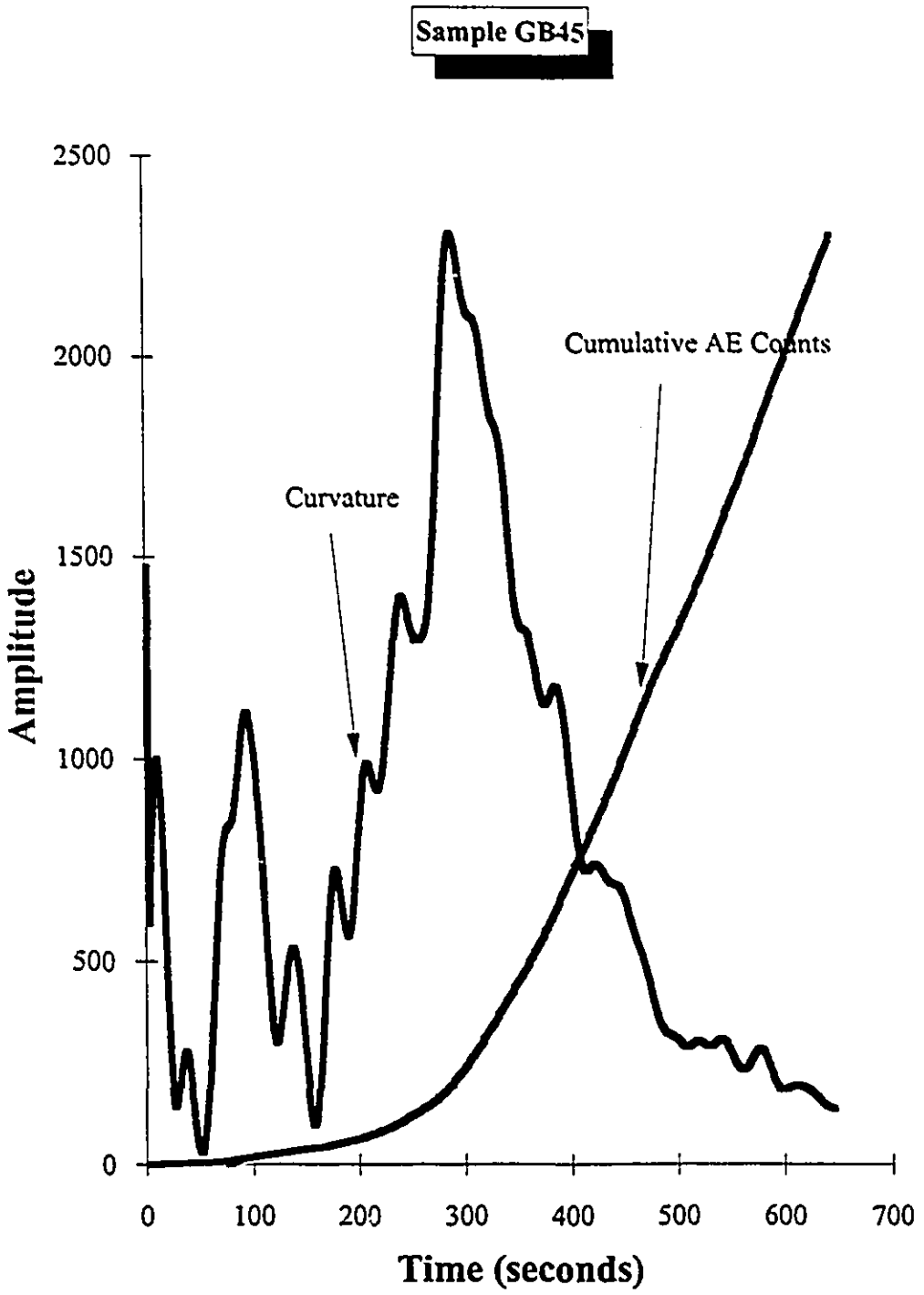

Figure 9-5: Result of Kaiser Effect Test under Load Control Using the Very Slow Rate.

Table 9-4: Load Rates for the First and Second Load Cycles under Displacement Control Mode.

First Load Cycle (mm/sec)	Second Load Cycle (mm/sec)
	0.02 VF
	0.01 F
0.02 VF	0.005 I
	0.0025 S
	0.00125 VS
	0.02 VF
	0.01 F
0.005 I	0.005 I
	0.0025 S
	0.00125 VS
	0.02 VF
	0.01 F
0.00125 VS	0.005 I
	0.0025 S
	0.00125 VS

VF: Very Fast
F: Fast
I: Intermediate
S: Slow
VS: Very Slow

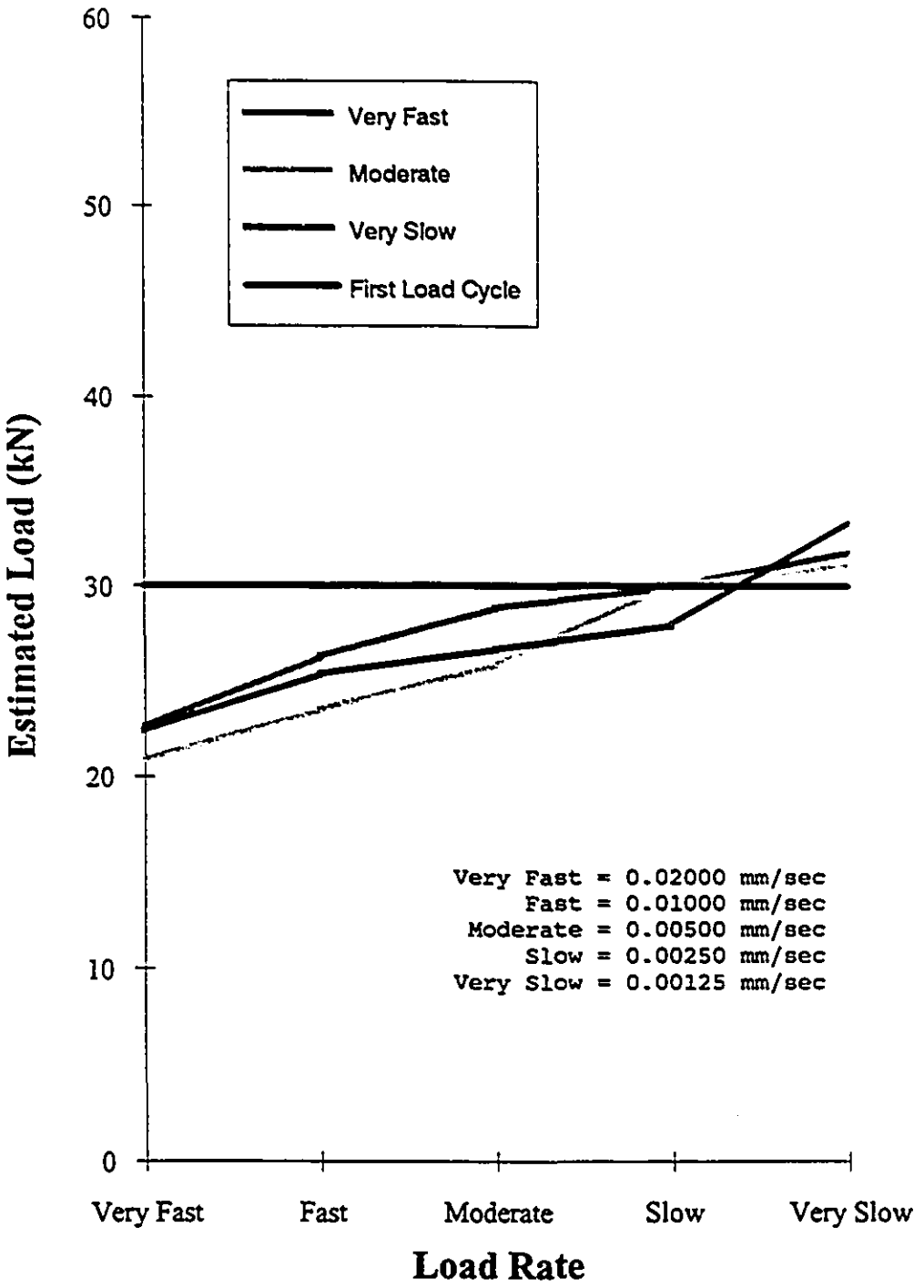

Figure 9-6: Effect of Loading Rate for Samples Tested under Displacement Control.

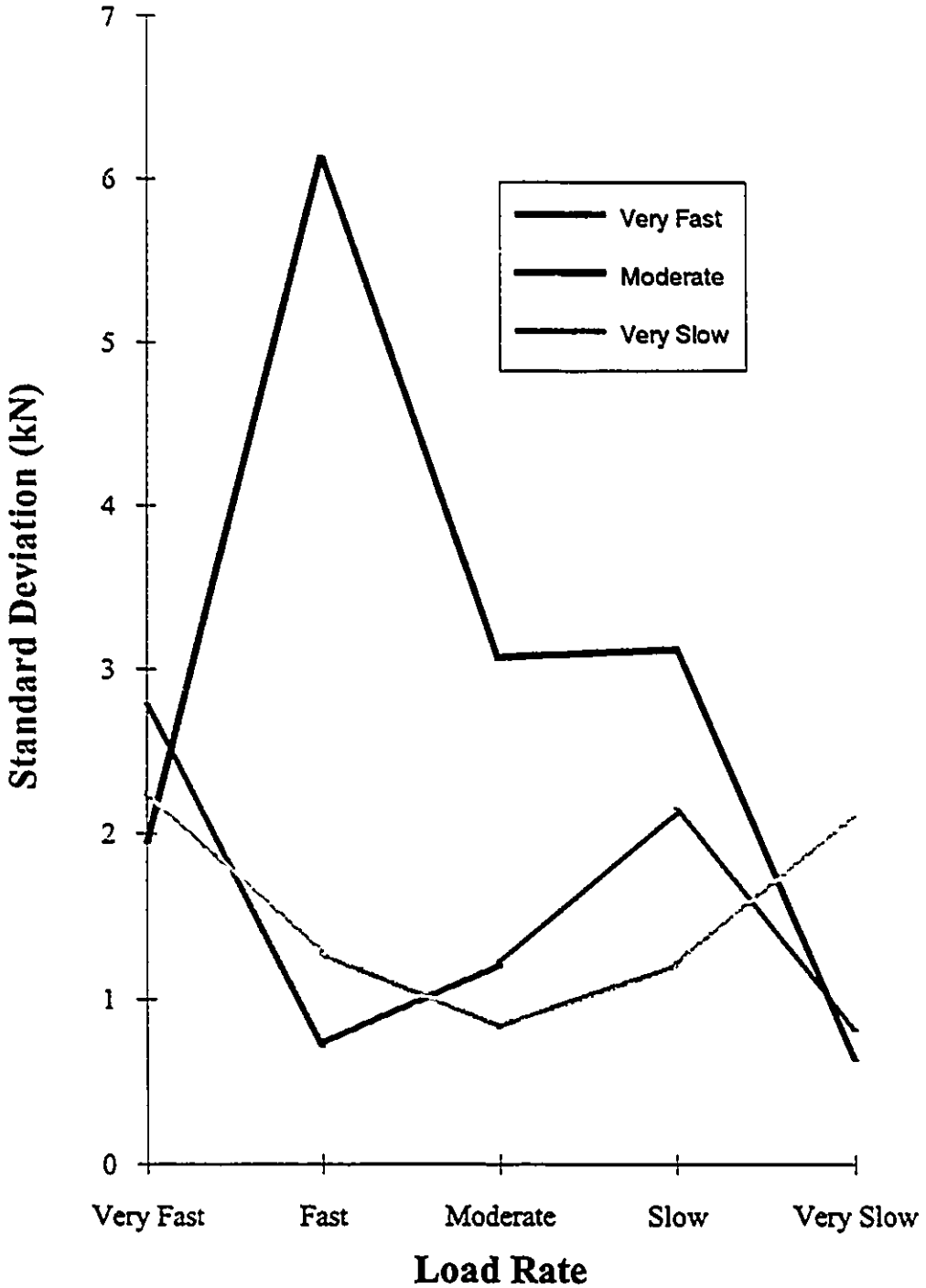

Figure 9-7: Standard Deviation for Estimated Loads Shown in Figure 9-6.

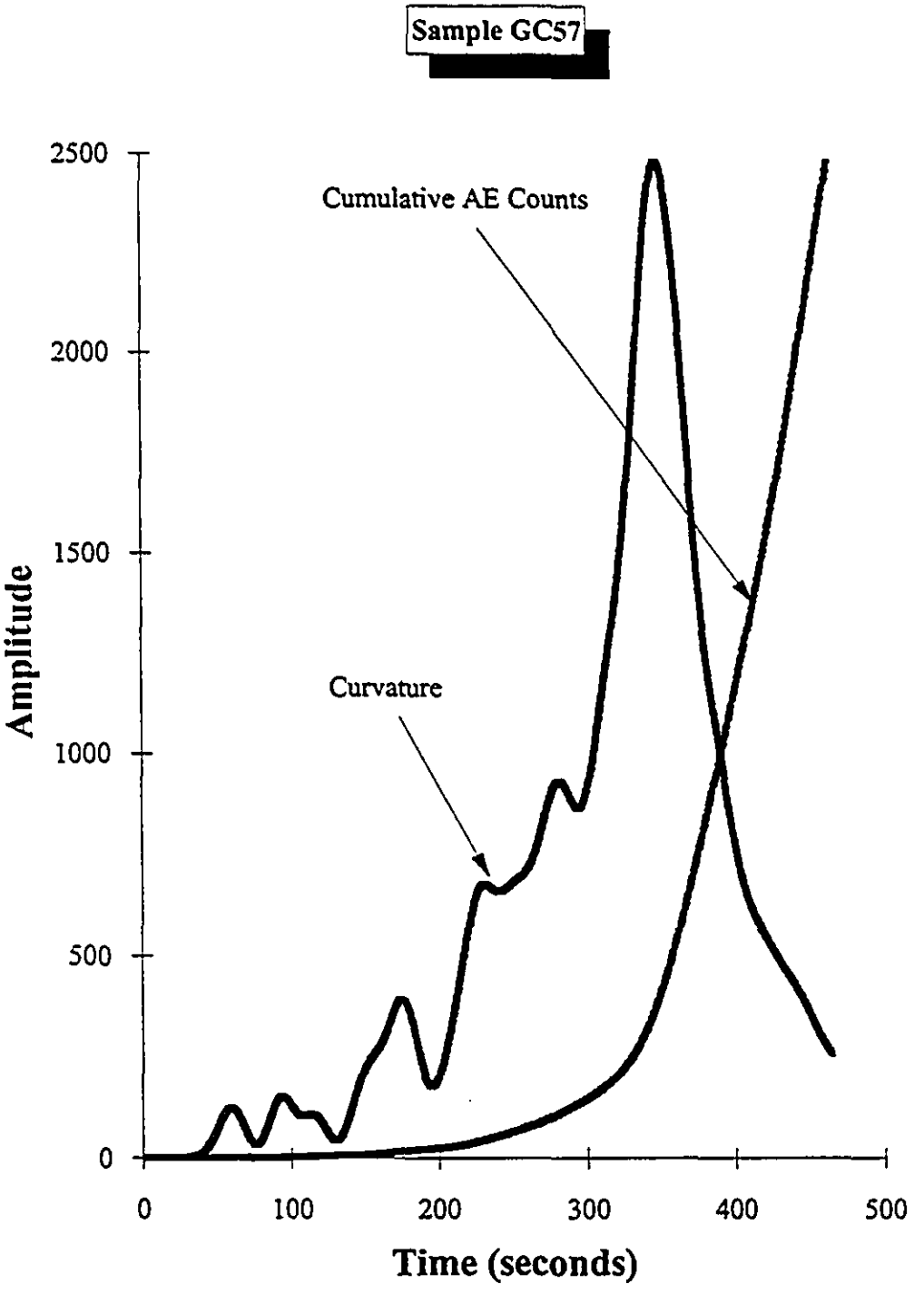

Figure 9-8: Result of Kaiser Effect Test under Displacement Control Using the Very Slow Rate.

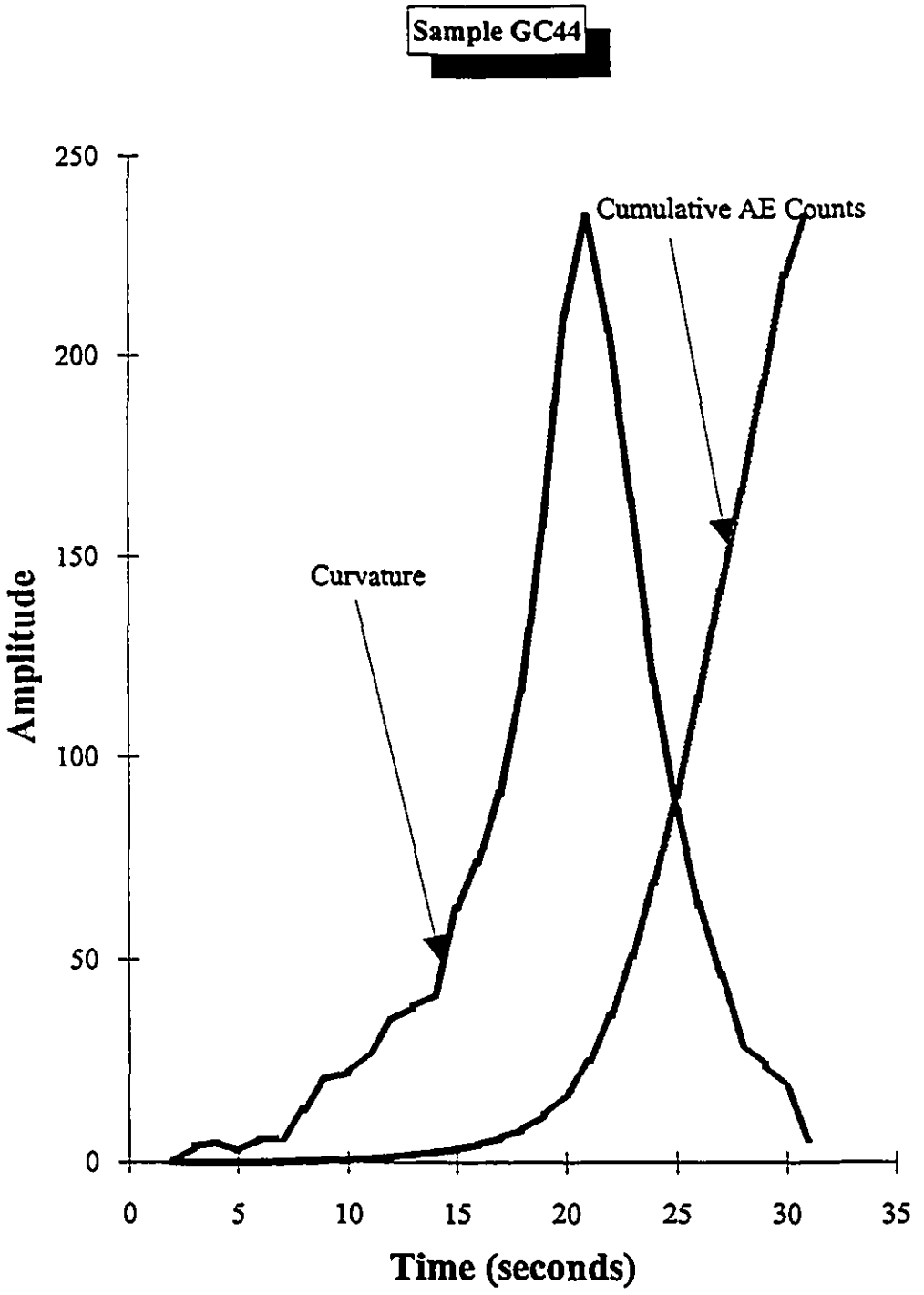

Figure 9-9: Result of Kaiser Effect Test under Displacement Control Using the Very Fast Rate.

typically exhibit broader curvature around the Kaiser Effect point which makes it more difficult to get an accurate estimate for the previous load level.

9.4.3) Discussion

Comparing the results of stress memory estimation using different load and displacement rates (see Figures 9-2 and 9-6) reveals that in general Intermediate to Very Slow rates give estimates that are much closer to the previously applied load level. The reason for this behavior may due to the adjustments constantly made by the rock specimen under pressure. Slower rates allow the sample to make more adjustments at a slower pace which is reflected in the lower number of acoustic emission events recorded before the previous stress level is reached. This fact allows the large burst in acoustic emissions, indicative of the Kaiser Effect, to display itself much more distinctly resulting in a sharper curvature and more accurate load estimate.

The same type of argument can be put forth when comparing the results of stress estimation from load and displacement control modes. It can be seen from Figure 9-8 for example that the Kaiser Effect curve shows a much sharper curvature when the test is carried out under displacement control mode. The appearance of the calculated curvature for samples loaded under displacement control is also much smoother and displays a sharper peak than the specimens tested under load control mode. This observation can be made for every specimen used during this investigation. Based on this fact, the remaining Kaiser Effect experiments were performed using the displacement control mode and an appropriately slow loading rate such as 0.002 mm/sec.

9.5) Effect of Specimen Size

To investigate the effect of specimen size on stress memory, three different diameter core sizes were prepared. Cores were cut with varying length to diameter ratios ranging from 1:1 to 1:4. Tests were conducted under load and displacement control modes using slow loading rates such as 0.1875 kN/sec and 0.0023 mm/sec.

The 3, 4 and 5 cm cores were loaded to 18.5, 35 and 60 kN respectively and held at that level for one minute. Specimens were then reloaded up to 37, 70 and 120 kN.

Tables 9-5 and 9-6 present the results of the Kaiser Effect experiments. Estimated load values are given here as percentages of the initial load for convenience because different load levels were used for different diameters. Therefore, the actual estimated load may have been higher or lower than the applied load.

The test results show that for length to diameter ratios of 2:1 and 3:1, core samples with a diameter of 4 cm retain a more accurate memory of the previous stress level. There is no marked difference in estimated load between each category of specimens in terms of diameter. The same conclusions can be drawn about the effect of length to diameter ratio. Referring to Table 9-6, it can be observed that for specimens having an L/D ratio of 1:1 to 4:1 the stress memory remains almost constant throughout the whole range whether the specimens are tested under load or displacement control mode. However, close examination of each individual value shows that the previous stress level was estimated more accurately for a length to diameter ratio of 2:1.

Although this study revealed that specimen size does not have a major effect on stress memory, it was deemed sensible to use a length to diameter ratio of 2:1 and a sample diameter of 4 cm for the remainder of this investigation.

9.6) Effect of Stress Level

The objective of this study was to find out for the first time whether Kaiser Effect exists at different points along the stress-strain curve. This information is useful because it would tell where the Kaiser Effect technique may be applied. Specimens were prepared and tested at 10, 30, 50, 70, 90 and 110 kN levels. Five samples were stressed at every level using both load and displacement control modes. The results are given in Figures 9-10 and 9-11.

The graphs in Figure 9-10 show estimated loads at 10, 30, 50, 70 and 90 kN load levels. The Kaiser Effect experiments at the 110 kN level were not successful

Table 9-5: Effect of Diameter on Stress Memory Determination.

Diameter (cm)	L/D Ratio	Error (%) Displacement	Error (%) Load
3	2:1	1.535135	6.917527
4	2:1	3.257143	3.783207
5	2:1	4.750417	6.054058
3	3:1	8.482432	7.943581
4	3:1	1.931429	7.349614
5	3:1	5.257083	7.676129

Table 9-6: Effect of Length to Diameter Ratio on Stress Memory Determination.

Diameter (cm)	L/D Ratio	Error (%) Displacement	Error (%) Load
3	2:1	1.535135	6.917527
3	3:1	8.482432	7.943581
3	4:1	9.486486	8.887595
5	1:1	4.447222	7.534187
5	2:1	4.750417	6.054058
5	3:1	5.257083	7.676129
5	4:1	5.658333	6.681963

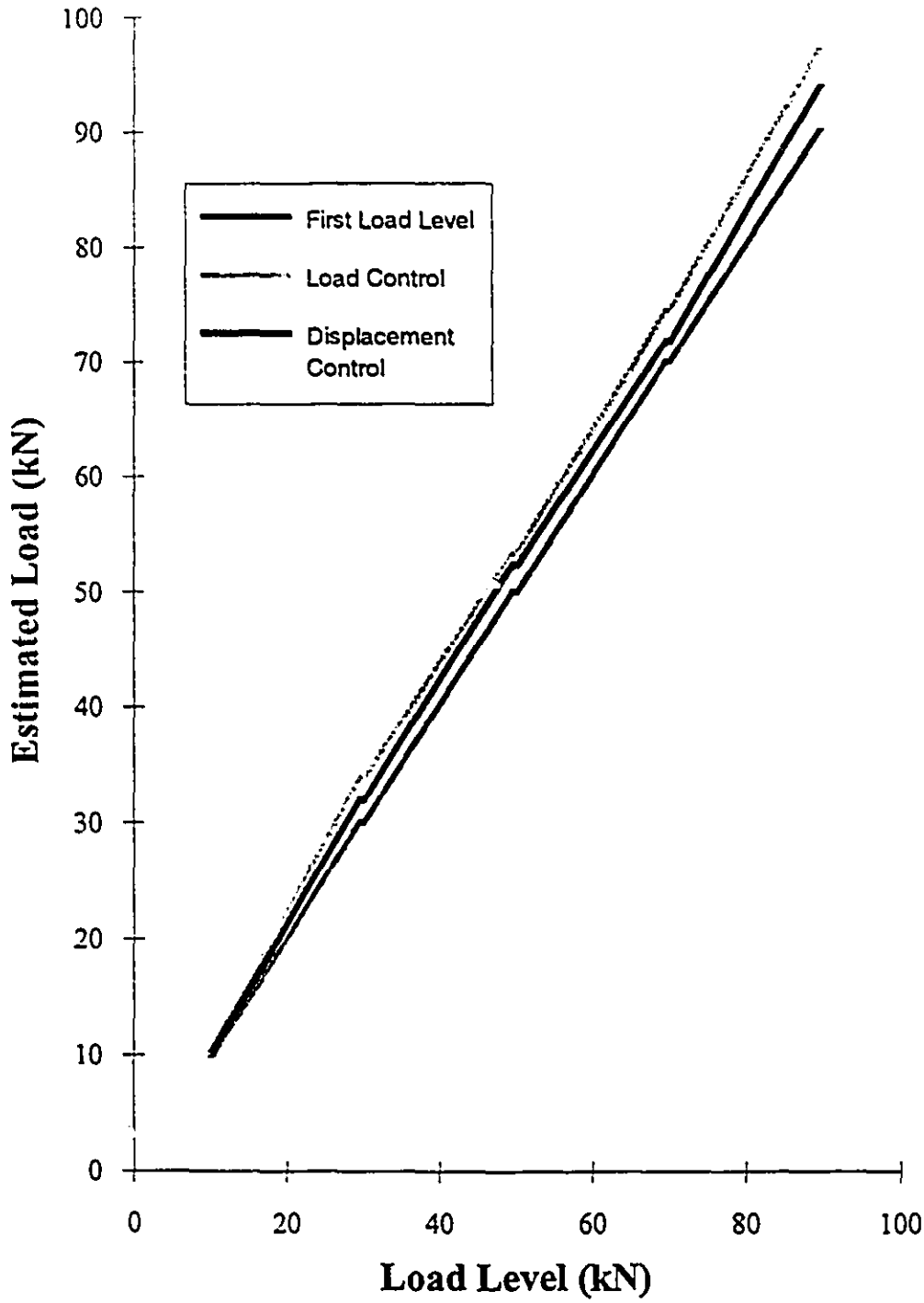

Figure 9-10: Effect of Load Level on Stress Memory.

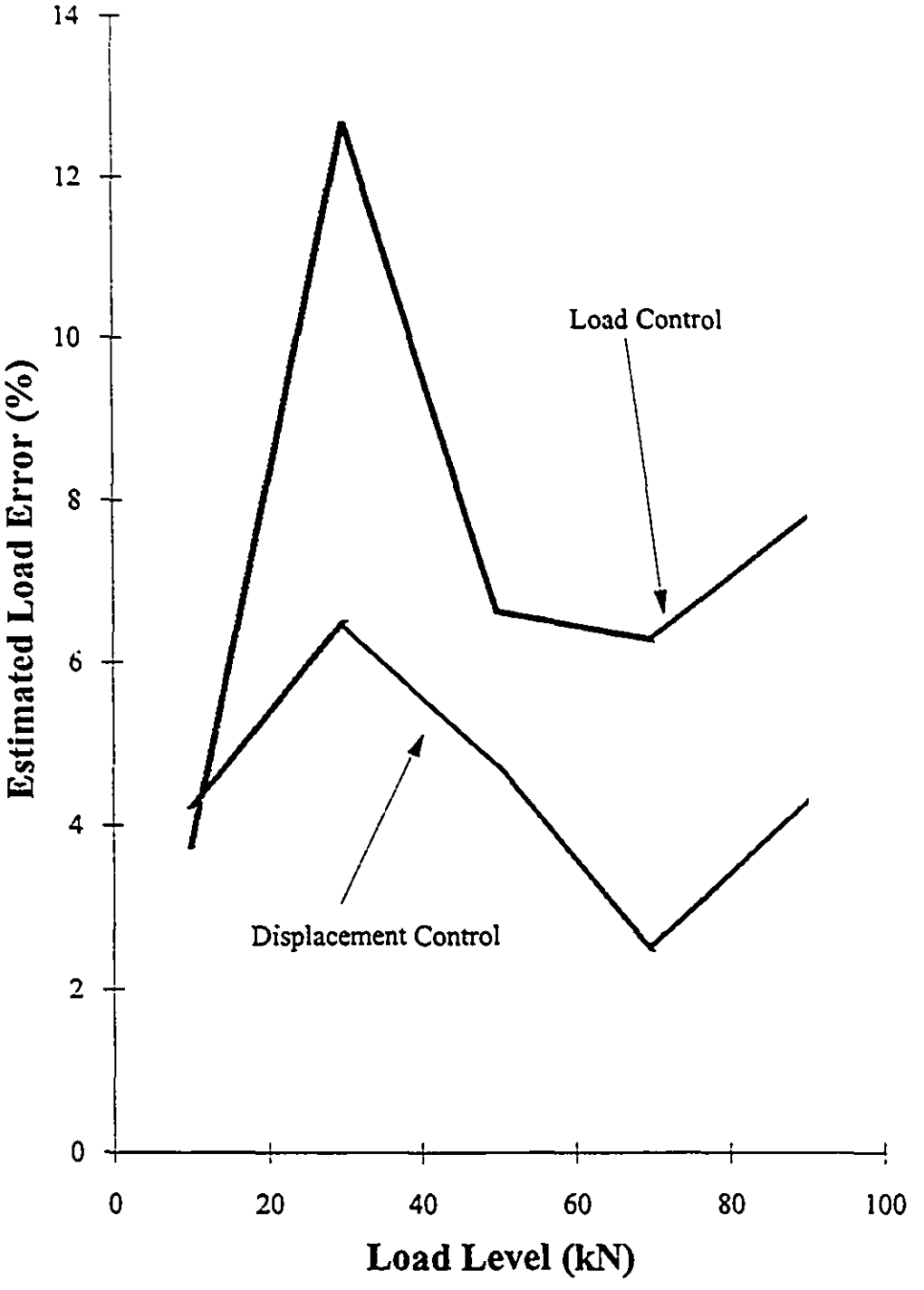

Figure 9-11: Errors in Estimated Load as a Function of Load Level.

because (1) too much noise was generated by the specimens after the applied load exceeded the 100 kN level and (2) some samples reached their ultimate strength between 140 to 156 kN.

It can be concluded from the results of Figure 9-10 that Kaiser Effect displays itself at every point in the pre-linear, linear and post-linear elastic region of the stress-strain curve for the Stanstead granite. Although the load estimated under load and displacement control modes show a small sign of divergence as the load level increases, the difference is within the experimental errors associated with this type of experiment. Specifically, the largest error in estimating the previous load level occurred by as much as 7.5 kN for samples tested under load control mode at the 90 kN load level.

The graphs of errors for estimated loads under different loading conditions confirm earlier findings. Tests carried out under displacement control tend to provide estimates that are closer to the applied load. It can be seen from Figure 9-11 that the curves for load and displacement control modes follow the same pattern. The largest error in estimating the previous load level occurs at 30 kN (25 MPa) level for both loading modes. These experiments suggest that the 25 MPa stress level, the beginning of the elastic range, has the poorest memory of previous stress level. The best values are obtained well inside the linear elastic region where the main source acoustic emission generation is crack growth.

Based on the presumption that for Stanstead granite, the stress memory is weakest when the rock enters the elastic region, it was decided that laboratory Kaiser Effect experiments would be conducted at the 25 MPa level equivalent to 30 kN load using the standard 3,93 cm diameter samples. Fortunately, all the tests carried out to this point and presented in the previous sections are conform to this standard.

9.7) Effect of Delay Time

In order to investigate the effect of delay time on memory recollection of Stanstead Granite, test samples were loaded up to a level of 30 kN at a displacement rate of 0.002 mm/sec. The load level was typically maintained for

about 5 to 10 minutes until a state of saturated strain was reached. The effect of delay time was monitored continuously for the first 24 hours on a two-hour basis and every day thereafter for a period of 1 month.

For every experiment a total of 5 specimens were loaded to a maximum level of 60 kN or 53 MPa while the same displacement rate was used as in the first load cycle. In order to compare the effect of delay time, the results obtained from the five samples tested every day were averaged. Figure 9-12 and 9-13 present the estimated loads using the Maximum Curvature Method and the Method of Tangents for a period of 24 hours and 30 days respectively. The standard deviation expressed in kN for the estimated loads varies on average between 2 and 4 kN with the largest value of 12 kN occurring on the 10th day as shown in Figure 9-14.

Analysis of these data indicate that reloading samples after one month produces accurate load values. Based on these data, it is very likely that Stanstead Granite will exhibit the Kaiser Effect at the known previous maximum even after many months. In addition, load estimates provided by the Method of Tangents are consistently greater than those calculated using the Maximum Curvature Method.

9.8) Effect of Physical Changes

In this section, the effect of water content and temperature disturbances imposed on Stanstead granite will be presented. The results are significant because they have been obtained under extreme conditions. Compared to these conditions, the effect of physical changes in the field on the memory recollection would be less severe.

9.8.1) Effect of Water Disturbance

Stanstead granite samples were loaded under identical conditions to a level of 30 kN. Then, the samples were subjected to three different disturbance regimes and tested at the end of every treatment:

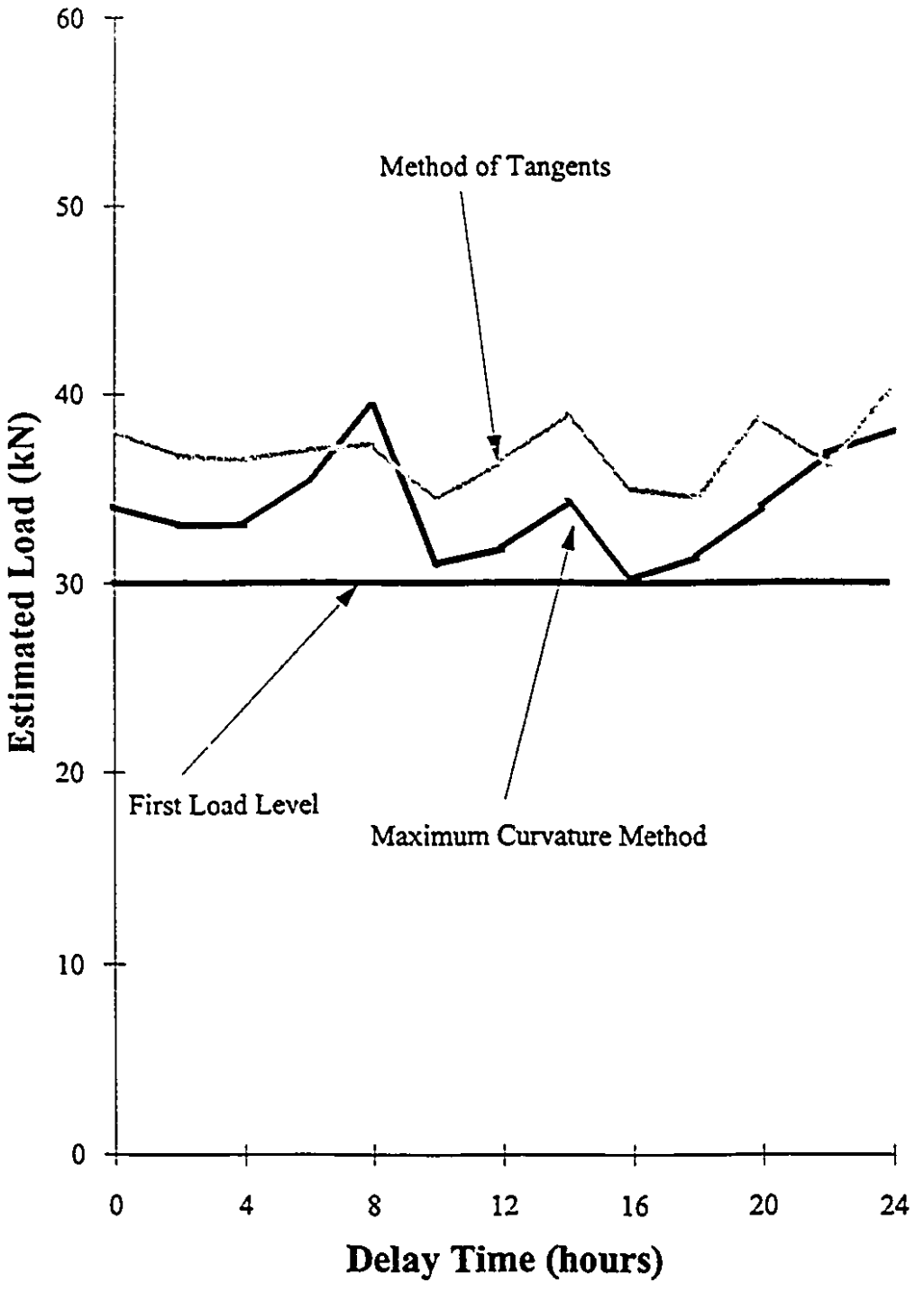

Figure 9-12: Estimated Loads as a Function of Elapsed Hours.

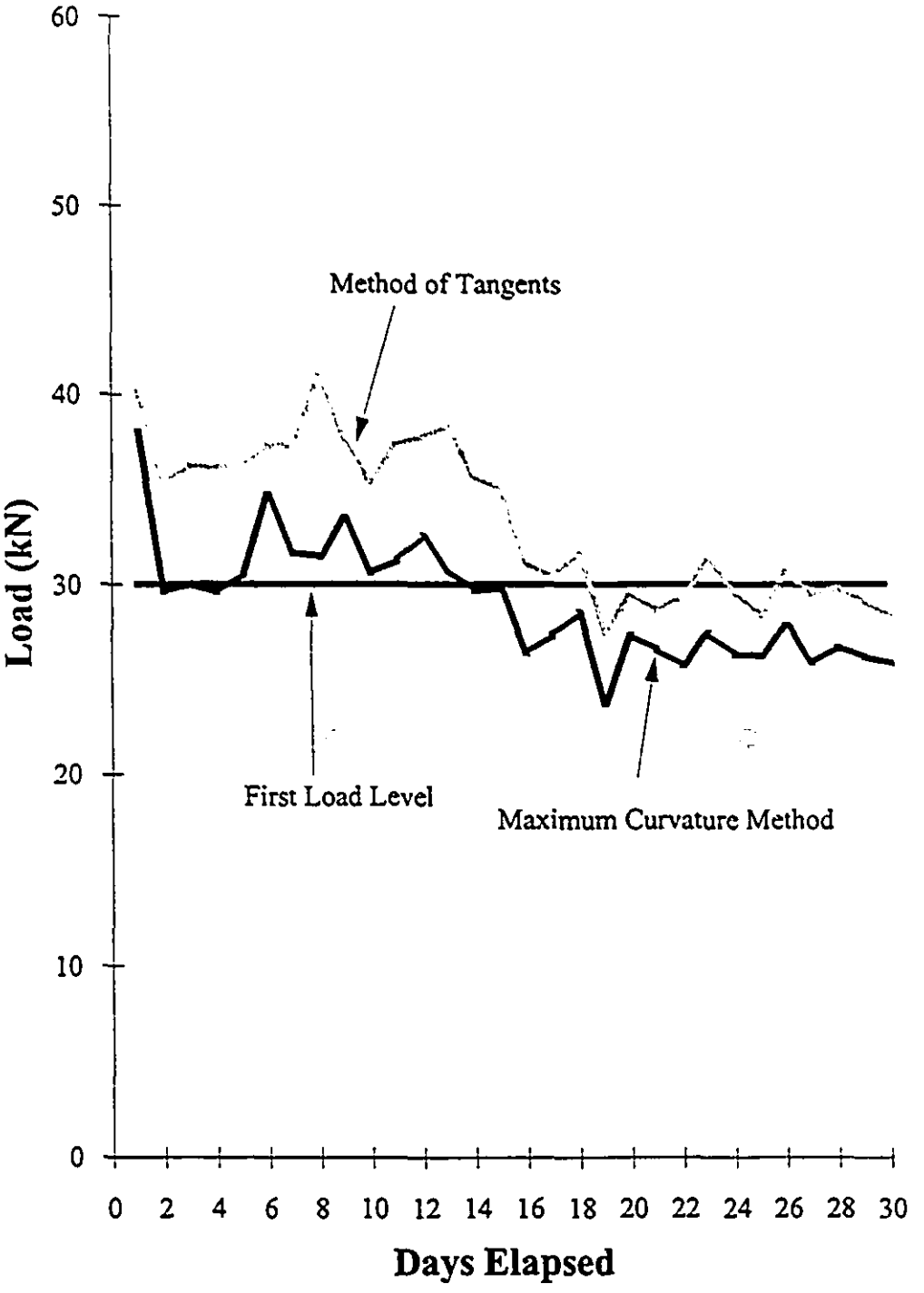

Figure 9-13: Estimated Loads as a Function of Elapsed Days.

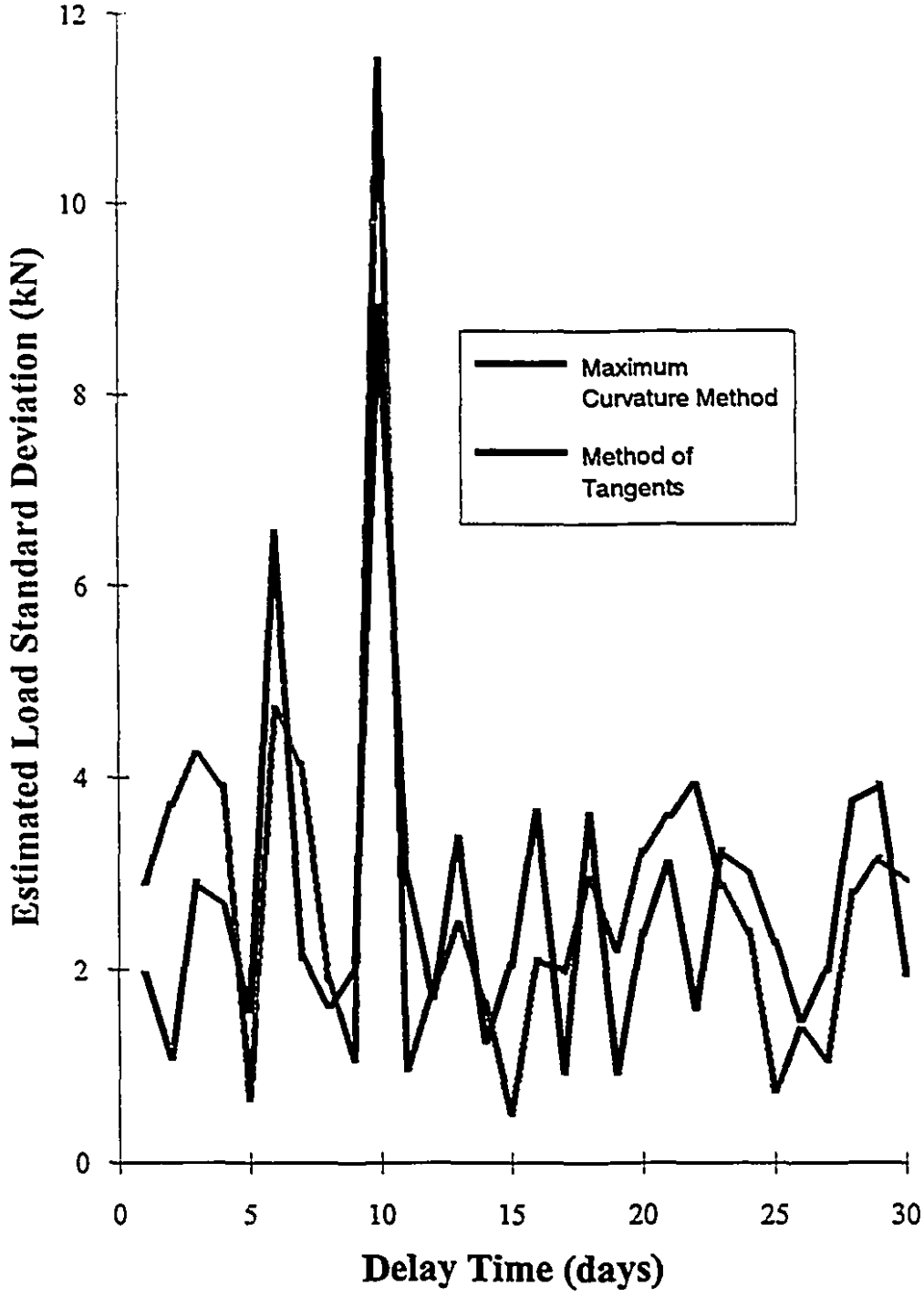

Figure 9-14: Standard Deviation for Estimated Loads in Figure 9-13.

1) soak samples in water for 24 hours and connect the water container to a vacuum pump to fully impregnate the samples.
2) soak samples in water for 24 hours and connect the water container to a vacuum pump. Then dry the samples in an oven for few hours to constant weight.
3) soak samples in water for 24 hours and connect the water container to a vacuum pump. Then dry the samples in an oven for few hours to constant weight followed by a second 24-hour water saturation.

The 24-hour soaking period was selected because it produced porosity values that were off by less than 0.1% compared to the values given in Chapter 8. Considering significant variations in Kaiser Effect determination was expected, a large number of samples were tested in each category. Specifically, a total of 35 samples were tested with the first five specimens subjected to no disturbance. The treated samples did not loose the memory of previous load level very much given the extreme conditions. Table 9-7 presents the averaged estimated load for 10 specimens treated under the above-mentioned conditions.

9.8.2) Effect of Temperature Disturbance

As in the previous case, Stanstead granite samples were loaded under identical conditions to a level of 30 kN. Then, the samples were subjected to similar disturbance cycles and tested at the end of every treatment using the following scheme:

1) dry samples in oven until constant weight is reached.
2) dry samples in oven until constant weight is reached followed by a soaking period of 24 hours. Samples were placed in a water container connected to a vacuum pump.
3) dry samples in oven until constant weight is reached followed by a soaking period of 24 hours followed again by a drying cycle to constant weight.

Testing conditions were similar to the previous case only the order of water/temperature treatment was reversed. Because significant variations in Kaiser Effect determination was expected for these tests as well a total of 35 samples were tested with the first five specimens subjected to no disturbance. The treated

samples lost no more memory than the specimens tested for the effect of water disturbance. Table 9-8 presents the averaged estimated load for 10 specimens treated under the above-mentioned conditions.

9.8.3) Discussion

Examining Tables 9-7 and 9-8 reveals that the estimated loads for treated and untreated samples are within the range of experimental errors and in acceptable agreement with the previously applied load. Excepting the results for the dry/wet condition in Table 9-8, the standard deviations for all the tests are also within acceptable limits. These results are in contradiction with the conclusions presented by Kurita and Fujii [40] regarding the effect of water treatment on stress memory. As discussed in Chapter 4, these authors showed that their granite did not keep an accurate memory of previous stress level after the specimens were soaked in water. Because Kurita and Fujii's reported values are the only instance in the literature where the previous stress memory is lost after samples have been subjected to water content disturbance, the findings from this investigation can be accepted with confidence.

In addition, the study by Yoshikawa and Mogi [43] and Boyce [55] regarding the influence of water and temperature disturbances on various rock types concluded that changing the water content or exposing stressed rocks to high temperatures for prolonged periods of time alters the memory by a small amount.

It is therefore important to conclude that based on this and past studies the water content or temperature differences imposed on the rock cores during drilling will not affect the stress memory of low porosity rocks. For medium to high porosity samples, the effect of water content may be important and must be thoroughly investigated.

9.9) Effect of Confining Pressure

A small scale experiment was set up to carry out a study on the effect of confining pressure on the Kaiser Effect of Stanstead granite. The experiment was

Table 9-7: Effect of Water Disturbance on Estimated Load from Stanstead Granite Samples.

Condition	Estimated Load (kN)	Standard Deviation (kN)	Error (%)
no treatment	29.118	5.979	3
wet	37.255	5.529	24
wet/dry	32.943	5.757	10
wet/dry/wet	34.462	5.571	15

Table 9-8: Effect of Temperature Treatment on Estimated Load from Stanstead Granite Samples.

Condition	Estimated Load (kN)	Standard Deviation (kN)	Error (%)
no treat.	34.583	2.307	15
dry	33.459	1.375	12
dry/wet	37.821	11.961	26
dry/wet/dry	31.394	4.515	5

not designed to be a comprehensive investigation because confining pressure was not included in the original objectives of this research program. To gain a feel for this parameter, samples were loaded for the first cycle to 30 kN axially using 0, 7, 10, 14, 17 and 21 MPa confining pressures. The applied load for the second cycle was 60 kN for all the samples. As with other experiments, a total of 5 specimens were tested in each category.

The Kaiser Effect point was determined using the Maximum Curvature Method. It is interesting to note that for these tests, the shape of the curvature was very different compared to all the data obtained previously. Specifically, the curvature from these specimens show multiple peaks instead of one peak at the Kaiser Effect point. For these data, the largest peak in the curvature does not always correspond to the expected Kaiser Effect load. However, there is always a peak at the previous maximum load.

For instance, Figure 9-15 presents the graph of the cumulative acoustic emission counts and its associated curvature for sample GM02 subjected to 7 MPa confining pressure. It can be seen that the largest peak occurs at a load of 25 kN while the peak corresponding to the applied load is at 32 kN. In Figure 9-16, the situation is similar to the previous case. Here, the data for sample GM11 loaded under a confining pressure of 14 MPa has the largest peak showing at 21 MPa and the peak corresponding to Kaiser Effect at 32.5 MPa.

Figure 9-17 is the graphs of applied confining pressures versus estimated axial stress. It should be noted that here pressure is expressed in MPa instead of kN because the applied confining pressure was in MPa. Two different approaches were used to determine the previous stress level. In the first case, the largest peak in the curvature was used to estimate the Kaiser Effect point. In the second case, the peak closest to known previous maximum was used to obtain an estimate of the applied load. It can be seen that both curves follow the same pattern for confining pressures between 0 and 10 MPa, while for confining pressures between 14 and 21 MPa the load estimates using the largest peak show no variation but are lower than those obtained from the closest peak.

It is important to note that these results differ from the data published in the literature (Holcomb [45], Hughson and Crawford [52] and Hardy [88]) in terms of

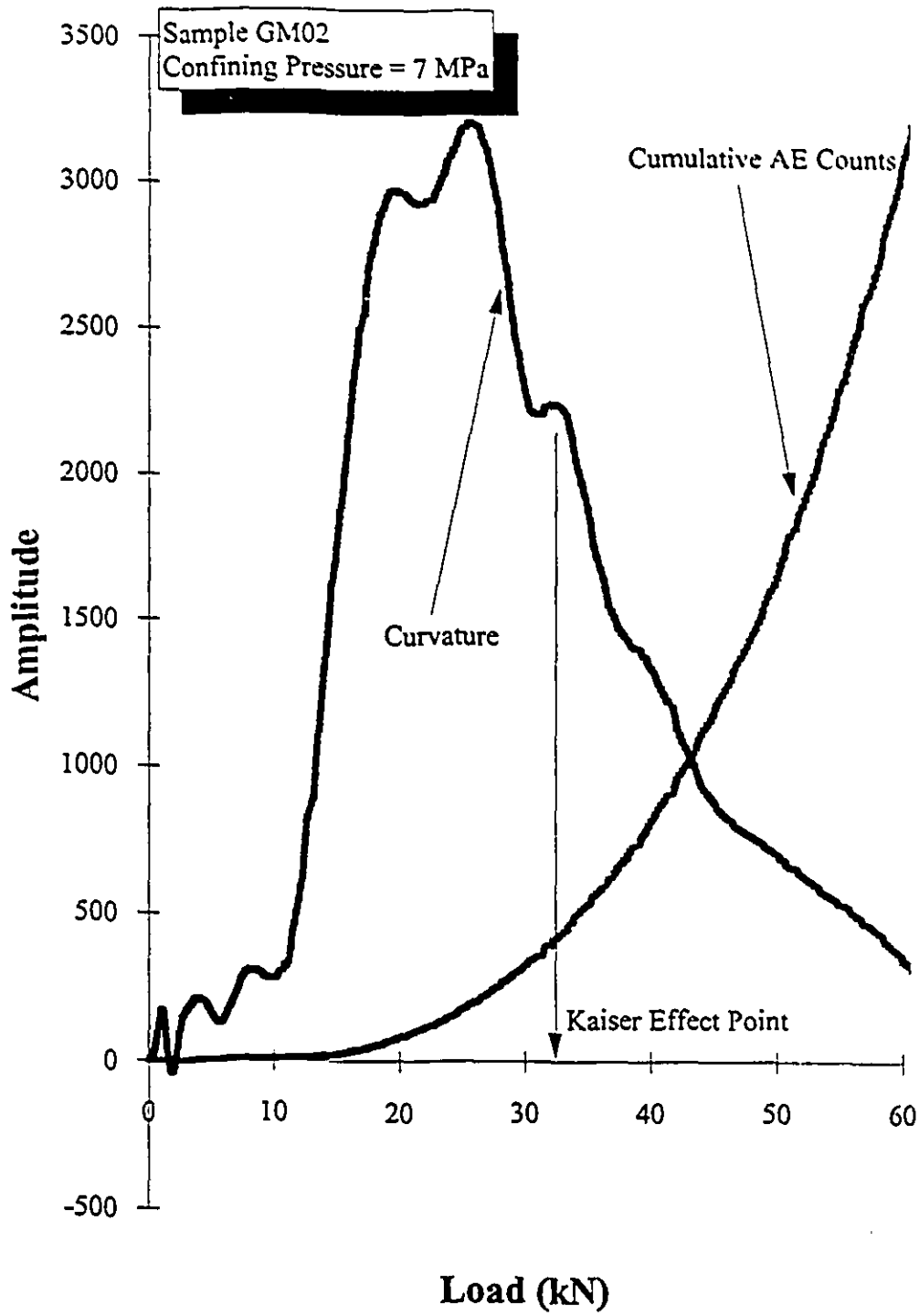

Figure 9-15: Kaiser Effect Curve and its Associated Curvature for a Confining Pressure of 7 MPa.

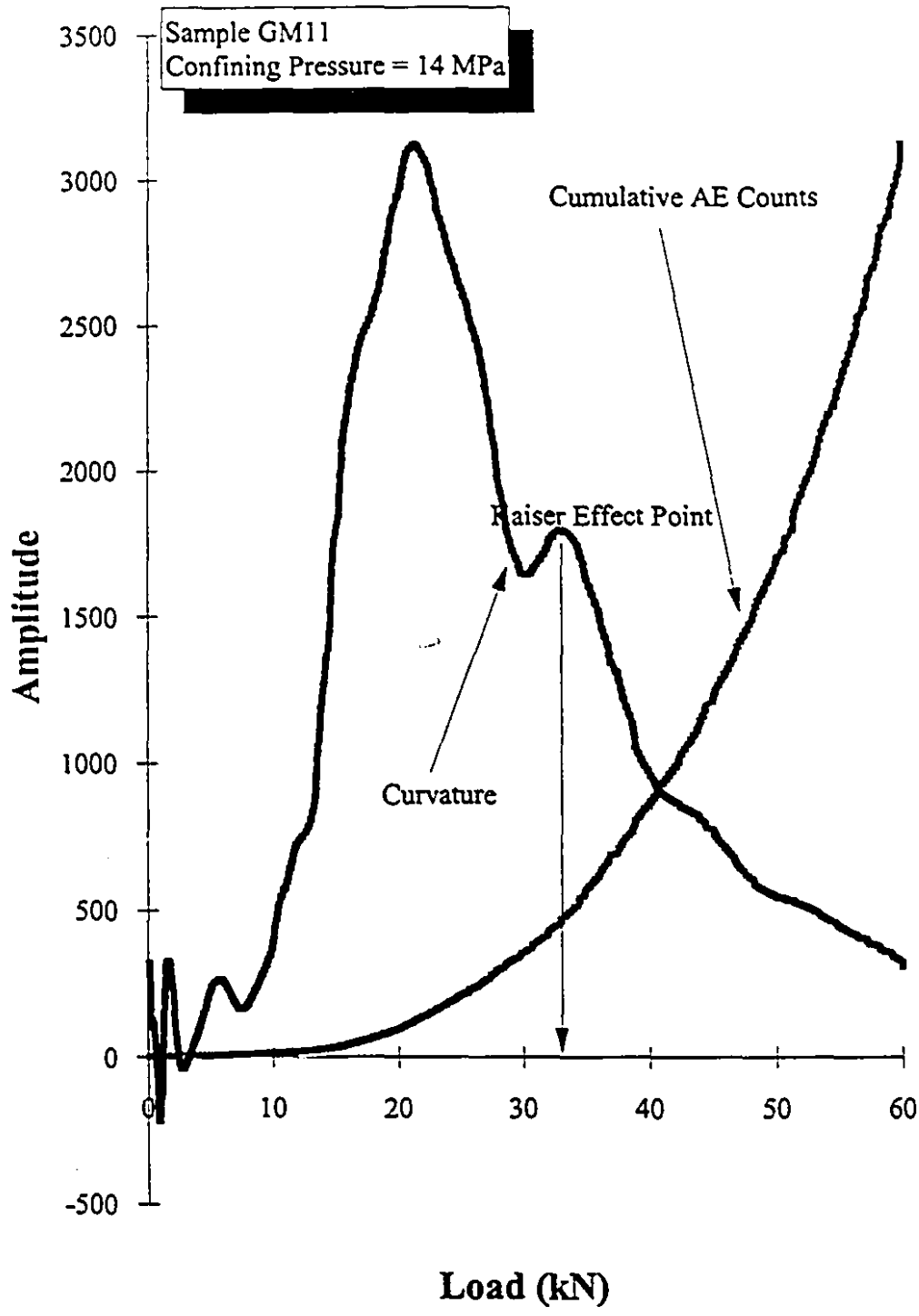

Figure 9-16: Kaiser Effect Curve and its Associated Curvature for a Confining Pressure of 14 MPa.

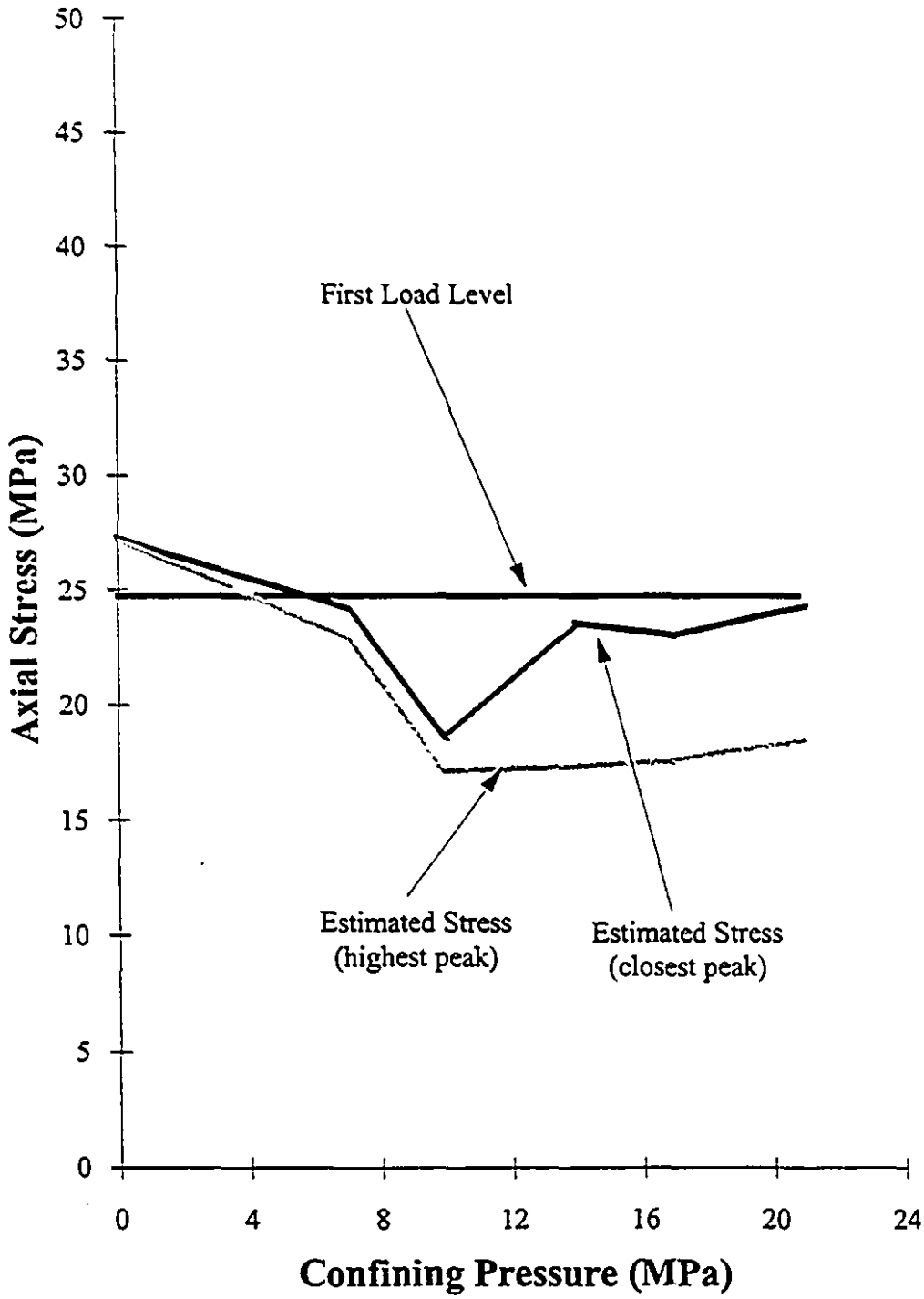

Figure 9-17: Relationship Between Confining Pressure and Estimated Axial Stress.

the relationship between the confining pressure and applied axial stress. For example, Holcomb reports a 1:3.4 relationship for the Westerly granite while Hughson and Crawford [52] obtained a 1:1 for Berea sandstone. In this investigation, excepting the axial stress estimate at 10 MPa confining pressure, all other stresses are very close to the previously applied stress if one uses the closest peak in the stress estimation. More specifically, for confining pressures of 0, 7, 10, 14, 17 and 21 MPa the errors in determining the previous stress level using the closest peak approach was 10%, 2%, 25%, 5%, 7% and 2% respectively.

The accurate stresses determined in this study may be attributed in great part to the analysis method. Referring to Figures 9-15 and 9-16, it becomes clear that without applying the Maximum Curvature Method, it would be very difficult to pick the Kaiser Effect stress at the points shown on the respective graphs. This study has shown that the effect of confining pressures below the applied axial stress is not significant and the previous maximum stress can be determined uniaxially. More tests are required to confirm this conclusion since it goes against the findings of researchers such as Holcomb [45], Hughson and Crawford [52].

The results of this study on the effect of confining pressure have important implications as far as in-situ stress determination is concerned. It suggests that when the rock is disturbed from its state of hydrostatic equilibrium, it recalls the applied stress in the direction of drilling. In contrast to Holcomb's statements that "the stress state that produces acoustic emissions is a strong function of the three principal stresses" and "the initial state of stress cannot be uniquely identified from uniaxial experiments" these tests show that the initial state of stress in the direction of drilling may be determined reliably using the Maximum Curvature Method.

9.10) Effect of Directional Loading

Similar to the effect of confining pressure, the study of the effect of directional loading is concerned with the influence of the overall state of stress in a rock mass on the stress in a particular direction. Here, the rock is subjected to a known stress from a few directions only and then specimens are sub-cored parallel to the applied stress directions and tested uniaxially.

Two sets of experiments were performed: (1) a block of granite measuring 15 x 15 x 15 cm was loaded in three different directions as shown in Figure 9-18 to a level of 370 kN (16.444 MPa) in all directions. (2) a granite block of dimensions 15 x 15 x 15 cm was loaded in directions B and C (see Figure 9-18) to a level of 370 kN (16.444 MPa) and to a level of 550 kN (24.444 MPa) in the A direction. The cores extracted from the block were 3.78 cm in diameter and between 5 and 10 samples were tested from each side. The reload specimens were stressed up to 1.5 to twice their previous maximum and the results were analyzed using the Maximum Curvature Method.

The test results for the first case are in agreement with the data published by Michihiro et al. [50], that is the effect of directional loading is minimal on the Kaiser Effect recollection of Stanstead granite. For the block stressed equally in all directions, the estimated stress was 16.679, 17.0125 and 17.121 MPa in the A, B and C directions respectively or an average error of %1, %3 and %4. Given the discrepancy in each measurement, the results can be regarded to be excellent.

For the second set of experiments, the stress estimates were somewhat less accurate compared with the first case. Here, the stress in the B and C directions were kept constant at 16.444 MPa while the applied pressure in the A direction was as high as 24.444 MPa. The differential stress had some effect on the estimated stress in other directions. In particular, the acoustic emission data in from the A, B and C directions gave an average stress of 25.311, 17.498, and 17.616 MPa respectively. These stress values correspond to an error of %4, %6 and %7.

Although the error in estimated stress is larger in the case where the applied differential stress is higher, the results are within an acceptable range. These findings are in agreement with the data published by Michihiro et al. [50]. In their investigation, the applied stress magnitude for the first cycle differed in all directions and the estimated stress was obtained within %2 of the previous level.

9.11) Remarks

As mentioned earlier, one rock type was used in the laboratory programme to provide a common denominator for all the experiments. Stanstead granite was

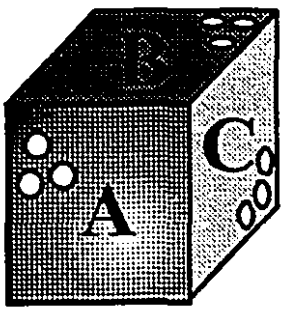

Figure 9-18: Schematic of Granite Block Stressed and Cored in Three Different Directions.

selected for its isotropic and homogeneous composition as well as its ability to produce large amounts of acoustic emissions. Although conclusive results were obtained with regard to the influence of the factors tested, these findings may not be directly applicable to other rock types. For example, many Phyllites are susceptible to pore water pressure and there is a major difference in their strength under dry and wet conditions. Water content may have a great influence on the recollection of previous stress in this rock type. The results of this study can be more easily related to rocks with composition and properties similar to those of the Stanstead granite.

The existence of micro-fractures in unstressed specimens is an important consideration. As discussed in section 6.4, the granite blocks obtained for this study were cut at the quarry site to avoid introducing undesirable micro-fractures. In some quarries, rock pieces are recovered by blasting. This practice can and often does damage the rock making it difficult to obtain reliable results as the mechanism responsible for triggering stress memory depends on the extent of micro-fracturing in the rock sample. In the event a rock sample was recovered by blasting, the Kaiser Effect does not manifests itself at stress levels that cannot propagate the existing cracks or develop new ones. Similarly, micro-cracks initiated by other mechanisms such as sudden changes in the temperature over a large scale could in effect mask any recollection of the previous stress, although the conditions required for thermal fracturing to take place are not commonly encountered in the mining industry.

Based on the above discussion, it is clear that the rock should remember the memory of the maximum stress and not necessarily the last stress. However, because stress memory fades away as shown by the results of the delay time experiments, given enough time it is possible that the memory of the maximum stress be totally erased and the stress level determined by the Kaiser Effect phenomenon would be the manifestation of some other stress. This is an important point to remember when in-situ stresses are measured using this technique, especially in virgin rock masses.

9.12) Suggested Testing Method

Based on the results of the laboratory programme, the following testing procedure was devised to guarantee that the data from a Kaiser Effect experiment under uniaxial compression conditions have the highest resolution and quality. The proposed method was used for all the experiments carried out in this work.

1) **Noise Reduction:** independent measures must be taken to reduce or eliminate the noise because this problem is equipment and test specific. The best suggestions that can be made concerns a minimum signal to noise ratio to respect in every test. If one compares the number of events generated by the testing equipment and the Stanstead granite in this investigation, the noise is about 10% of the total acoustic emission events or less. Because accurate results were obtained by achieving a signal to noise ratio of 10:1 or better, it is therefore proposed that all acoustic emission experiments be conducted under similar conditions.

2) **Sample Preparation:** specimens should be right circular with a height to diameter ratio of 2:1. It was found that the diameter size and height to diameter ratio do not have an important effect on stress memory, however, Kaiser Effect was estimated more accurately (by 2-3%) in specimens having a ratio of 2:1. The specimen ends should be parallel to ISRM standard, i.e., they should not deviate from parallelism by more than 0.001 mm. In addition, the surfaces should be smooth to reduce the amount of friction between the sample ends and platens. Water content and temperature changes have an insignificant effect on stress memory and therefore the usual equipment and procedures can be used in preparing rock specimens. Samples may be kept at room temperature and humidity before testing.

3) **Loading Mode and Rate:** this is one of the important parameters in Kaiser Effect experiments. Displacement control mode should be used for testing because laboratory investigations showed that stressing specimens under displacement control produces in general sharper deflection points in the CAE curves and smoother curvatures compared with load control mode. In addition, better estimates of stress memory may be obtained if rock samples are loaded

using slow rates such 0.001 to 0.003 mm/sec. Experiments should therefore be carried out at a displacement rate of 0.0015 to 0.002 mm/sec.

4) **Data Analysis:** the results of acoustic emission data analyzed using the Maximum Curvature Method (MCM) were more accurate compared to the Method of Tangents or other subjective techniques. It is suggested that an objective technique such as MCM be used for data processing.

CHAPTER 10

Laboratory Programme: Stress Memory of Various Rocks

10.1) Introduction

Based on the test procedure described in the previous chapter, a series of experiments on the stress memory of various rock types was set up. The main objective was to find out to what degree the Kaiser Effect technique may be effective in determining the previous stress level in rocks other than Stanstead granite. The effect of delay time on uniaxially stressed samples was investigated over long periods of time. A total of five rock types were selected for their composition and acoustic emission response. The following sections provide a description of the rock types tested and their respective stress memory.

10.2) Description of Rock Types

10.2.1) Gabbro

This inequigranular, hollocrystaline pyroxene hornblende gabbronorite is made of 72% hornblende crystals of 0.5 to 1.5 cm in size, 20% pyroxene (3-5 mm), 3% muscovite, 2% opaques and 3% alterations, mainly clay minerals.

10.2.2) Charnokite

Is an inequigranular and hollocrystaline rock made of 40% K-feldspar (0.5-2 cm), 25% quartz (2-9 mm), 30% pyroxene (0.5-cm) and 5% biotite (2-5 mm).

10.2.3) Gneiss

This is an equigranular, hollocrystaline pink granite with gneissosity having 35% quartz, 35% K-feldspar, 25% plagioclase and 5% biotite. The grains are 2-5 mm in diameter and the rock exhibits a sugary texture.

10.2.4) Limestone

Fine laminations less than 1 mm in thickness cut the core specimens at 85 degrees. The laminations compose about 5% of rock.

10.2.5) Darlye Dale Sandstone

This fine to medium grained quartz aranite exhibits very fine silt and clay lamellies cutting the core specimens at 60 to 70 degrees angle. They are less than 1 mm thick and less than 2% silt and clay are present.

10.3) Test Results

Gabbro, charnokite, gneiss and limestone specimens were cored with a diameter of 3.92 cm and a height to diameter ratio of approximately 2:1. The sandstone samples had a diameter of 3.77 cm and a height too diameter ratio of 2:1. Because the uniaxial compressive strength of the limestone and sandstone were lower compared to other rock types, 79.234 and 64.142 MPa respectively, the first level load was allowed to reach 25 kN for the limestone and 20 kN for the sandstone specimens. Gabbro, charnokite and gneiss were all loaded to 30 kN, the same level as for the Stanstead granite.

Each sample was subjected to a state of saturated strain during the first cycle and kept at room temperature before testing. During the second stage of loading, four or five specimens were tested each week and the level of load was doubled compared to the first cycle. The acoustic emission equipment was set up with the same level of sensitivity as for all the experiments carried out in this work, that is a threshold level of 5 mV and total system gain of 54 dB. The Kaiser Effect point was estimated using the Maximum Curvature Method.

The following figures show the effect of time on stress memory of gabbro, charnokite, gneiss, limestone and sandstone over a period of 1 to 21 weeks. Each figure is immediately followed by a sample graph of load versus cumulative acoustic emission counts curve. In the case of gabbro, charnokite and gneiss samples, the data between 4 and 10 weeks were lost and therefore a straight line is used to

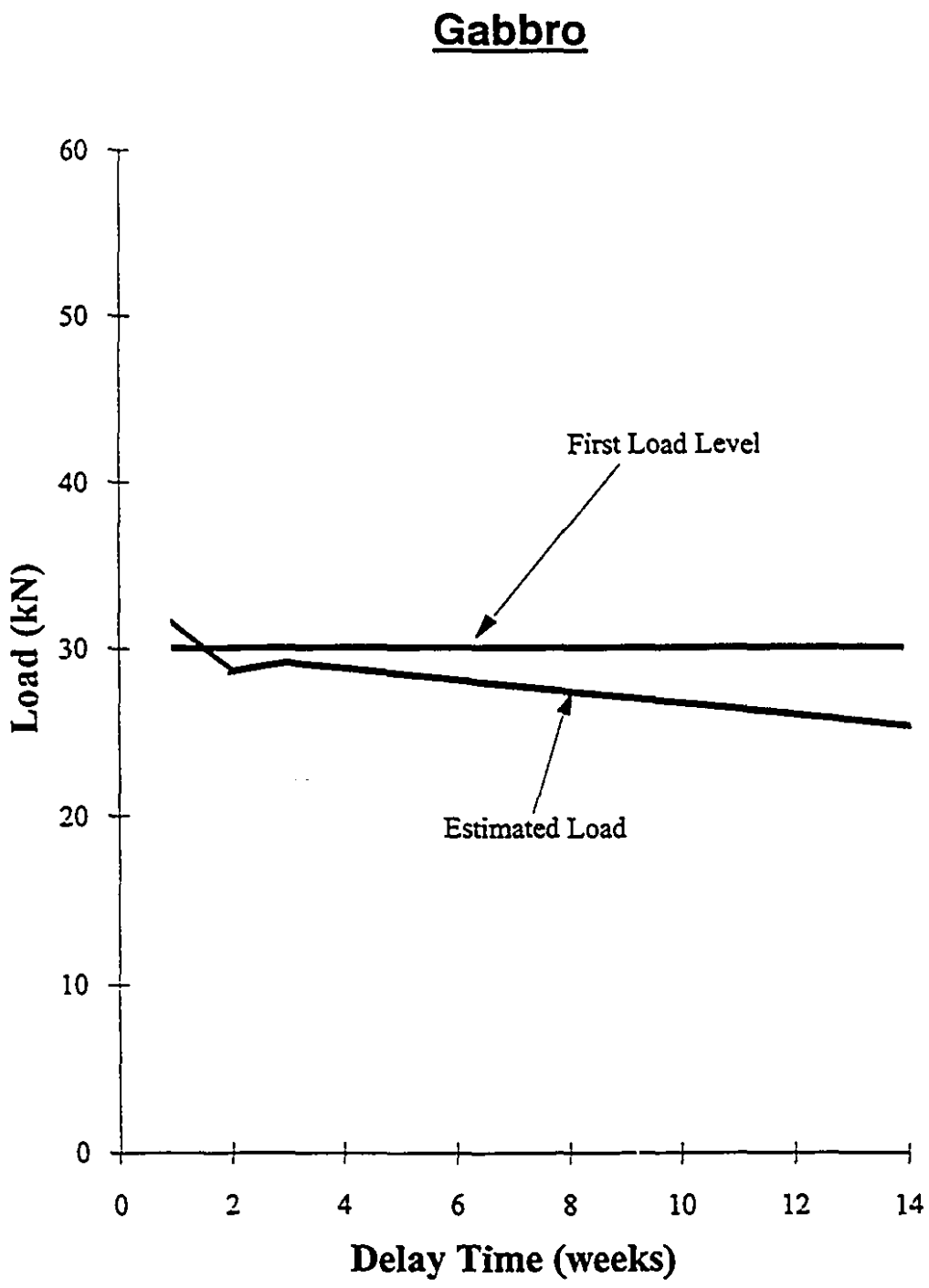

Figure 10-1: Effect of Time on Stress Memory of Gabbro.

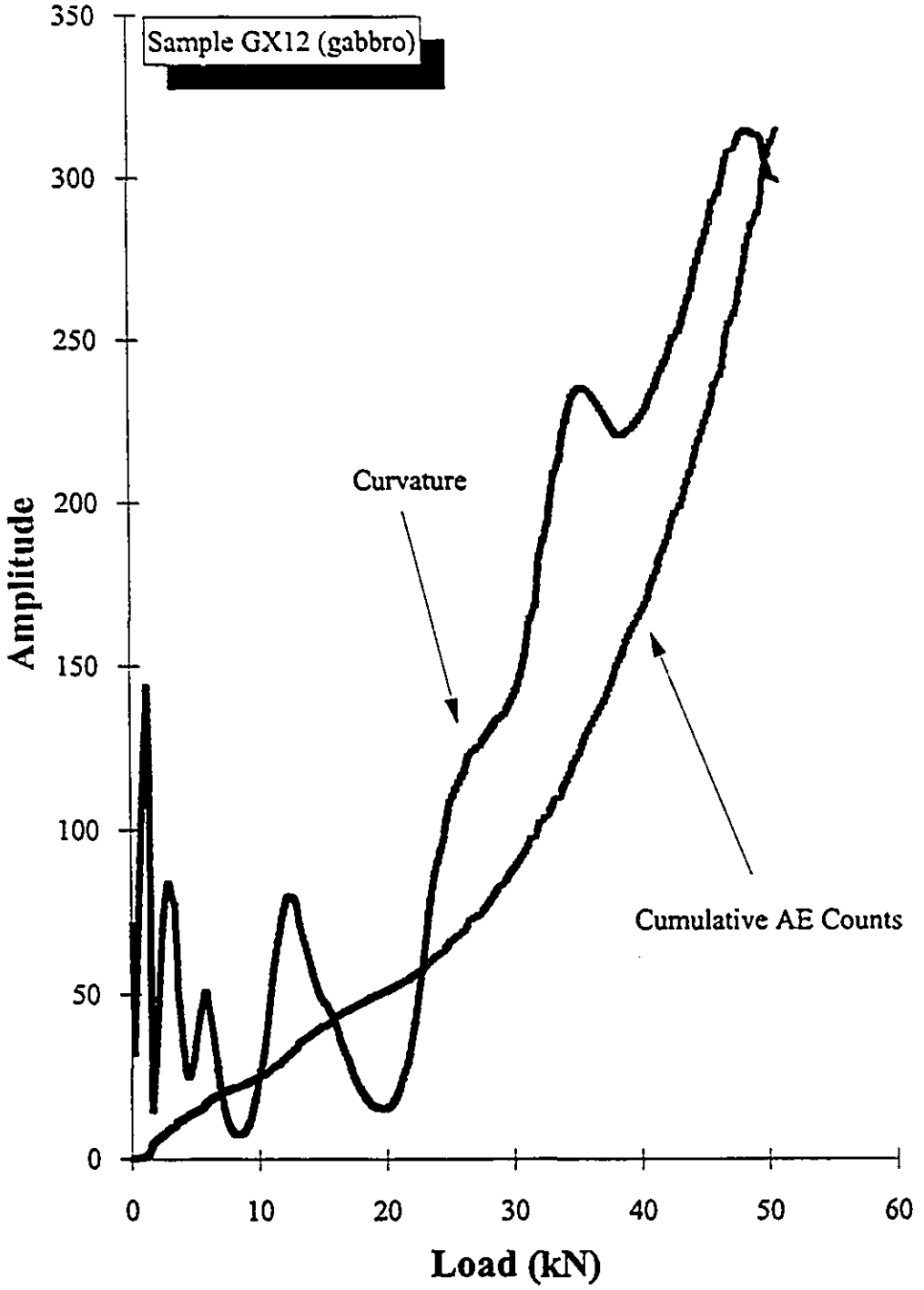

Figure 10-2: Kaiser Effect and Associated Curvature for Gabbro.

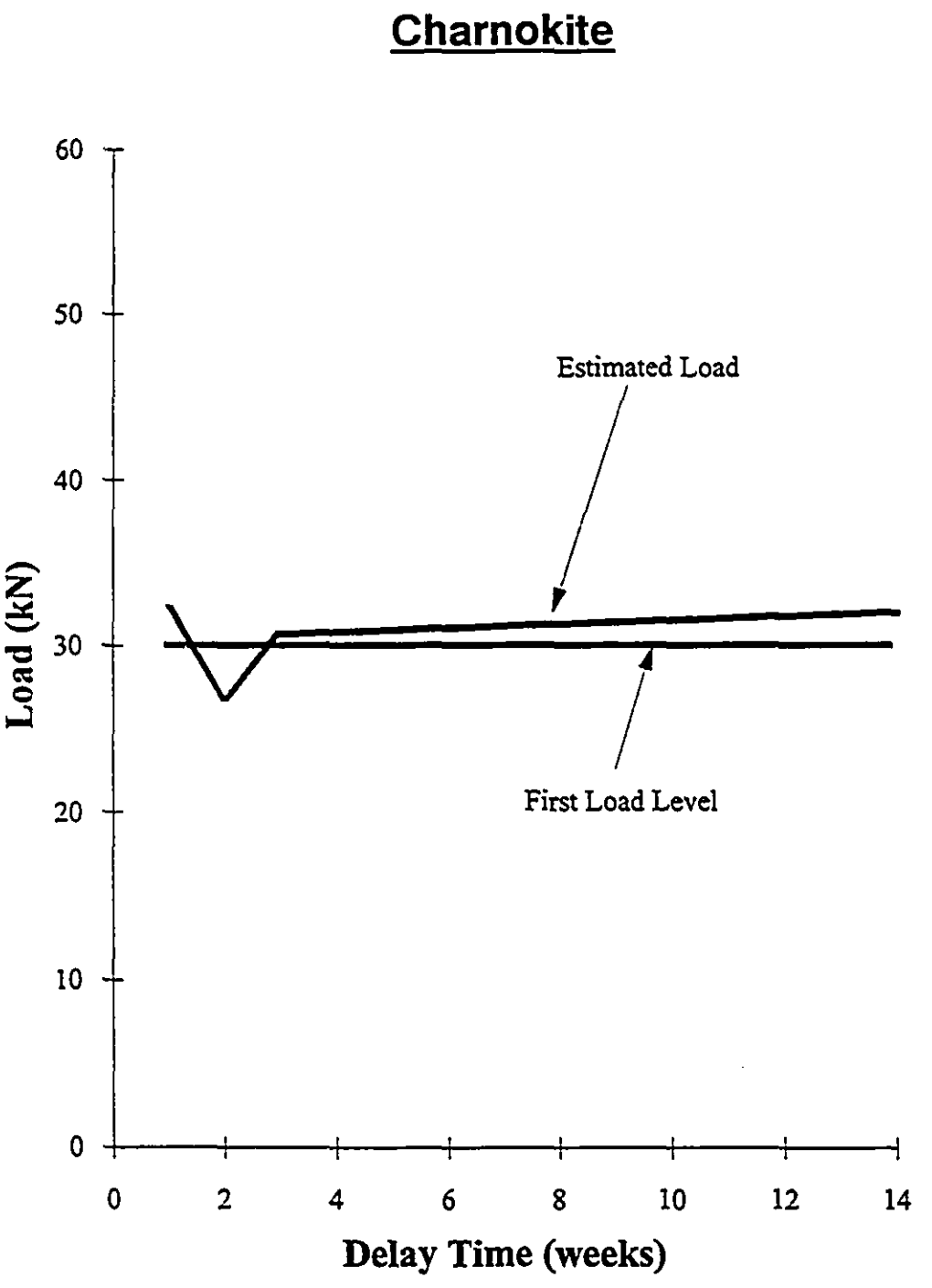

Figure 10-3: Effect of Time on Stress Memory of Charnokite.

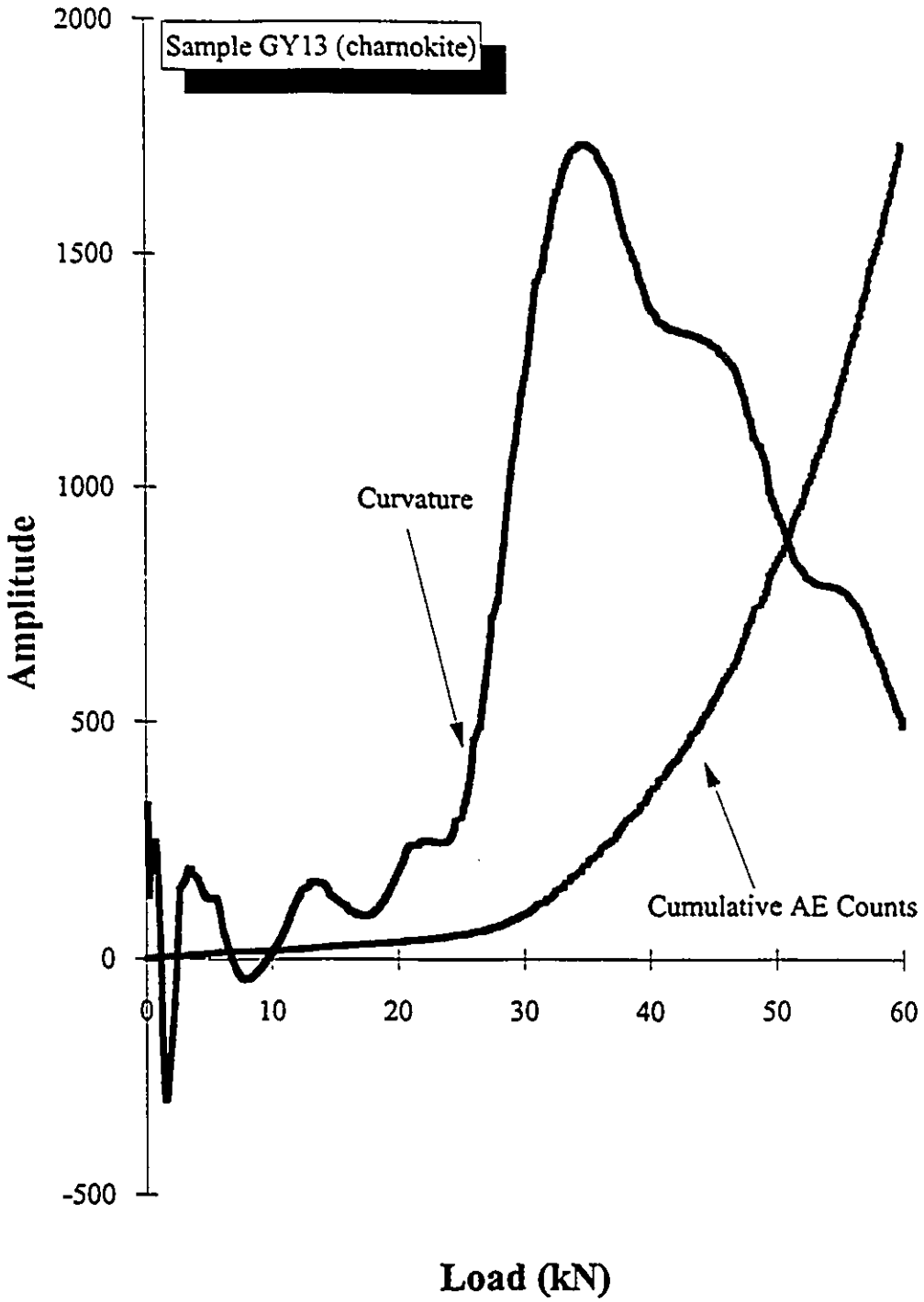

Figure 10-4: Kaiser Effect and Associated Curvature for Charnokite.

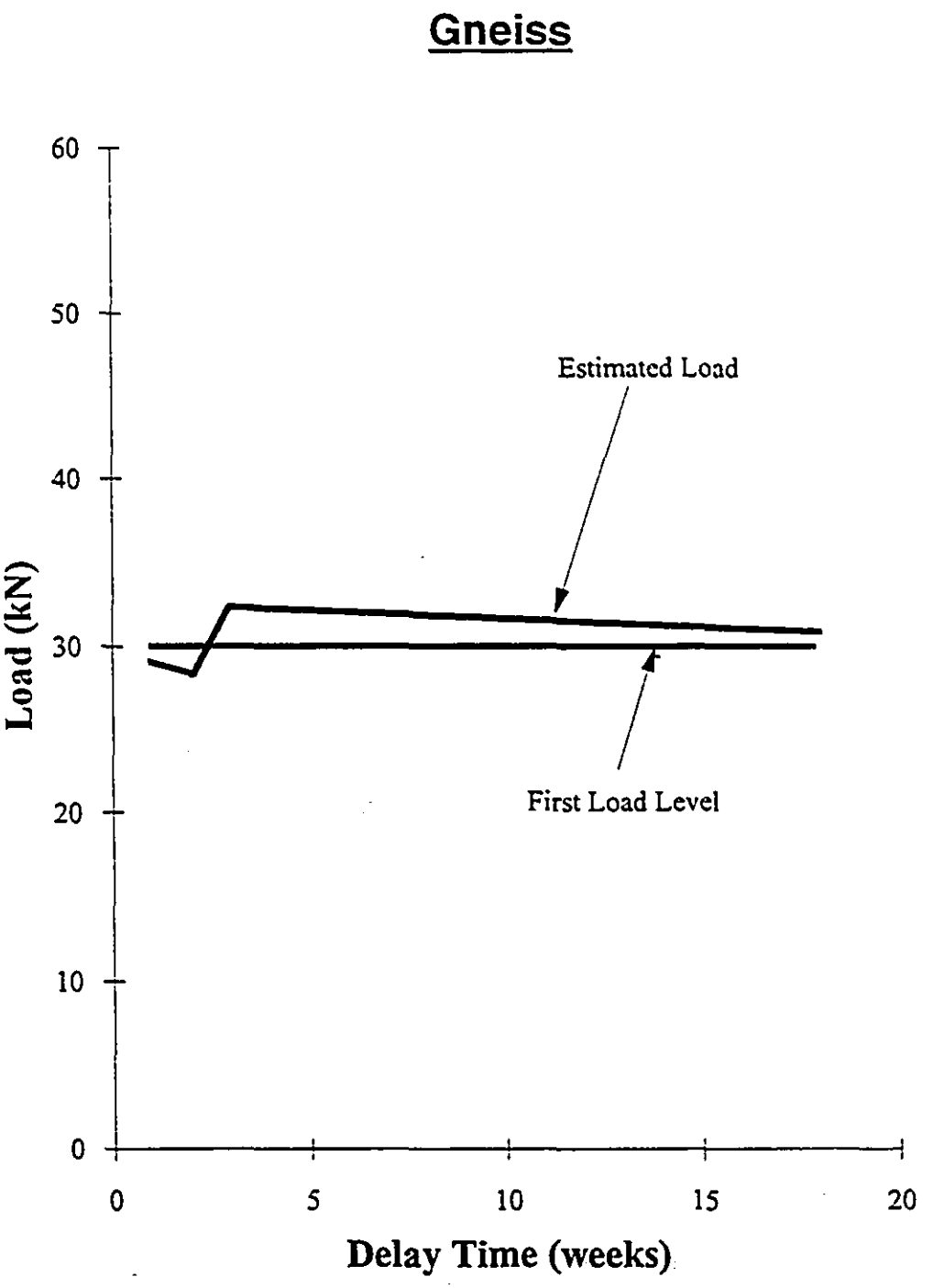

Figure 10-5: Effect of Time on Stress Memory of Gneiss.

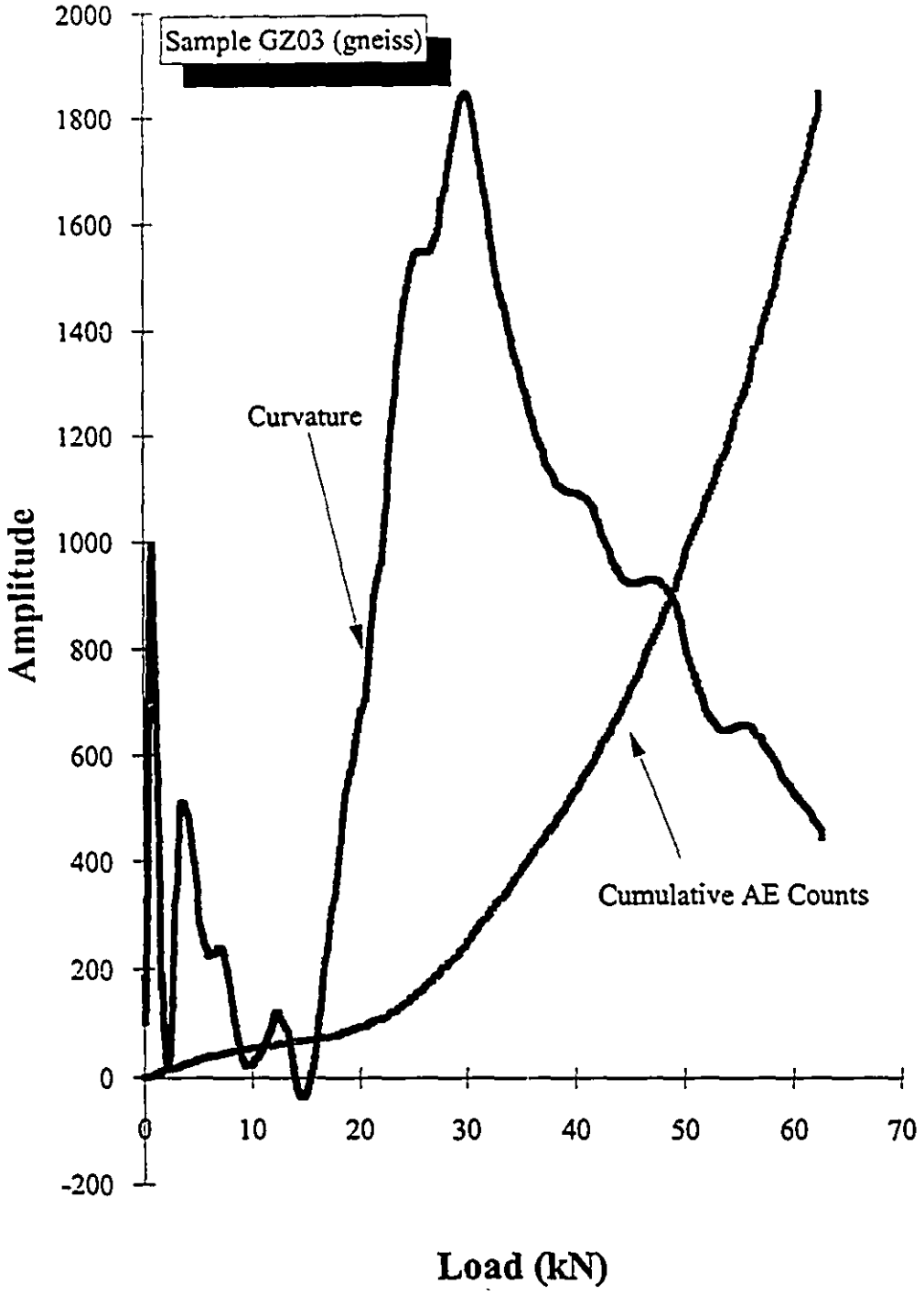

Figure 10-6: Kaiser Effect and Associated Curvature for Gneiss.

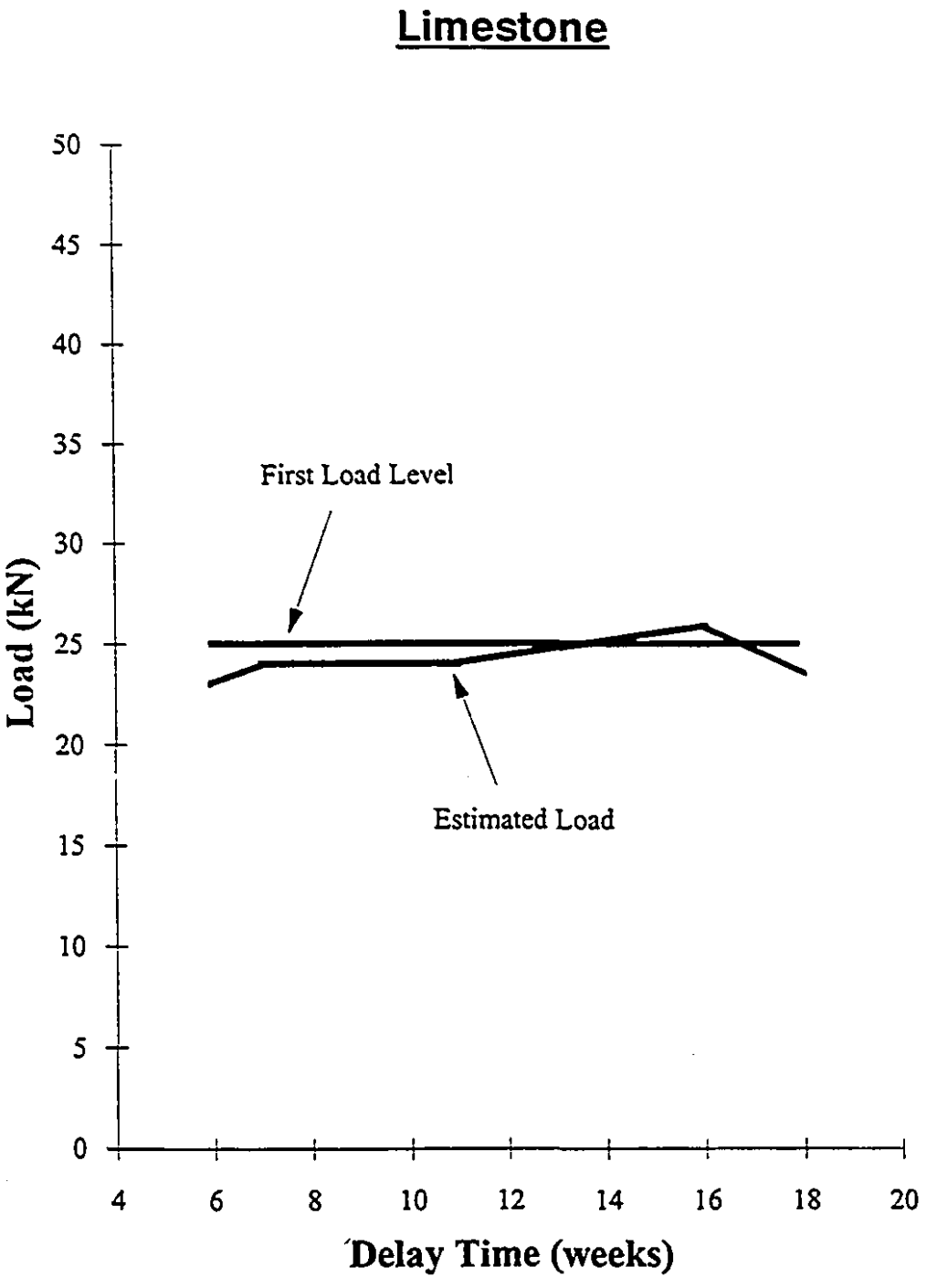

Figure 10-7: Effect of Time on Stress Memory of Limestone.

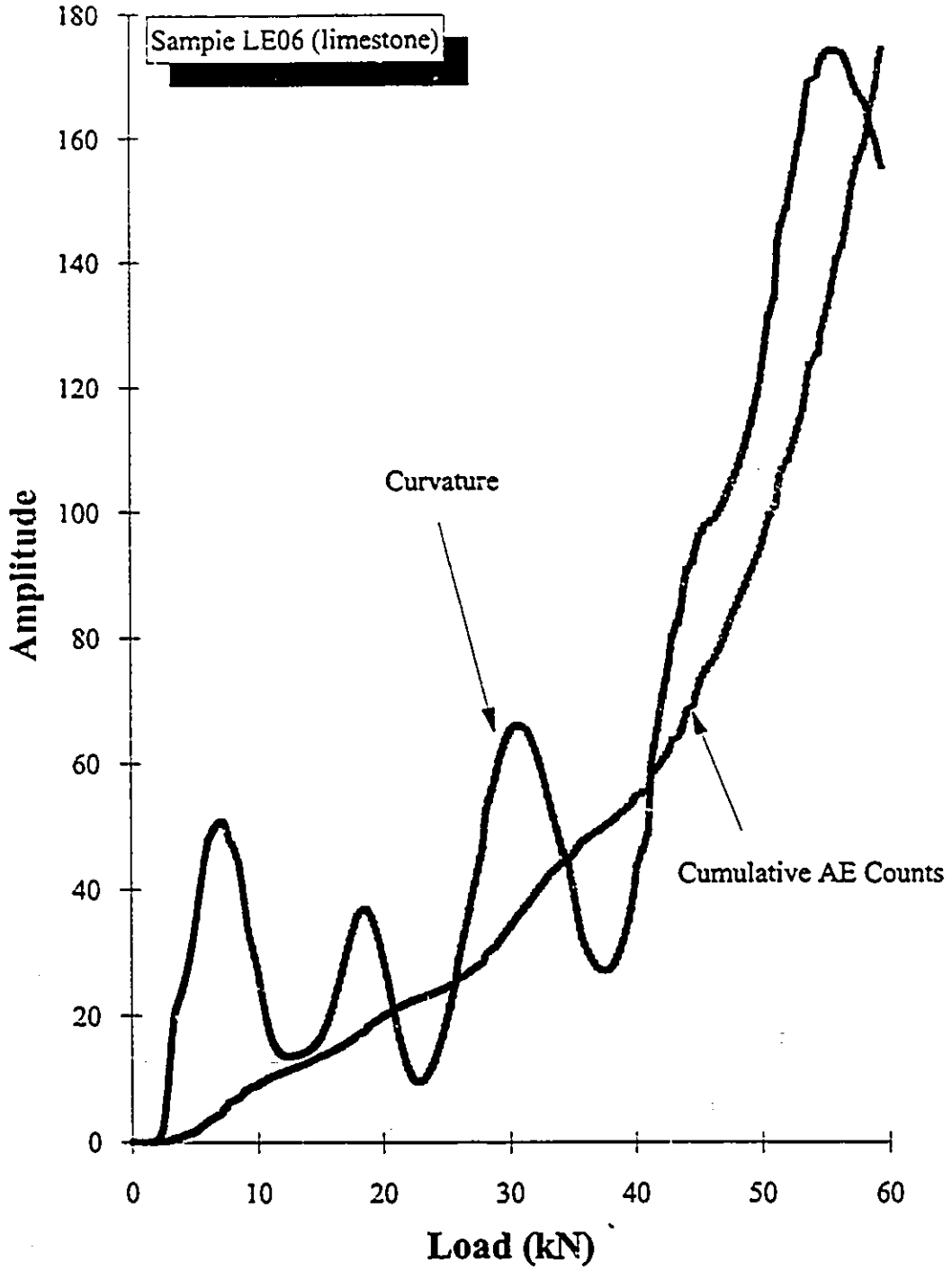

Figure 10-8: Kaiser Effect and Associated Curvature for Limestone.

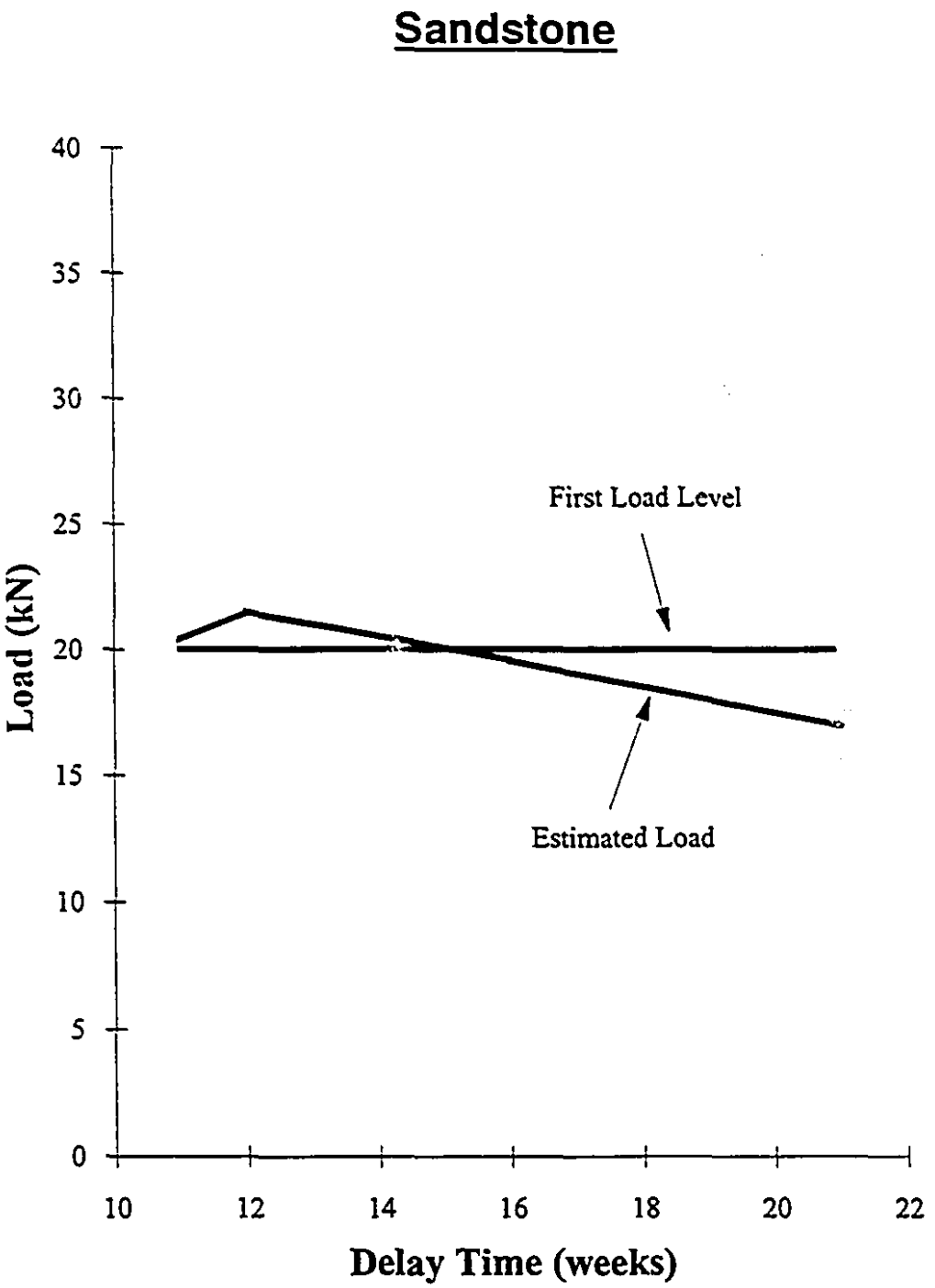

Figure 10-9: Effect of Time on Stress Memory of Sandstone.

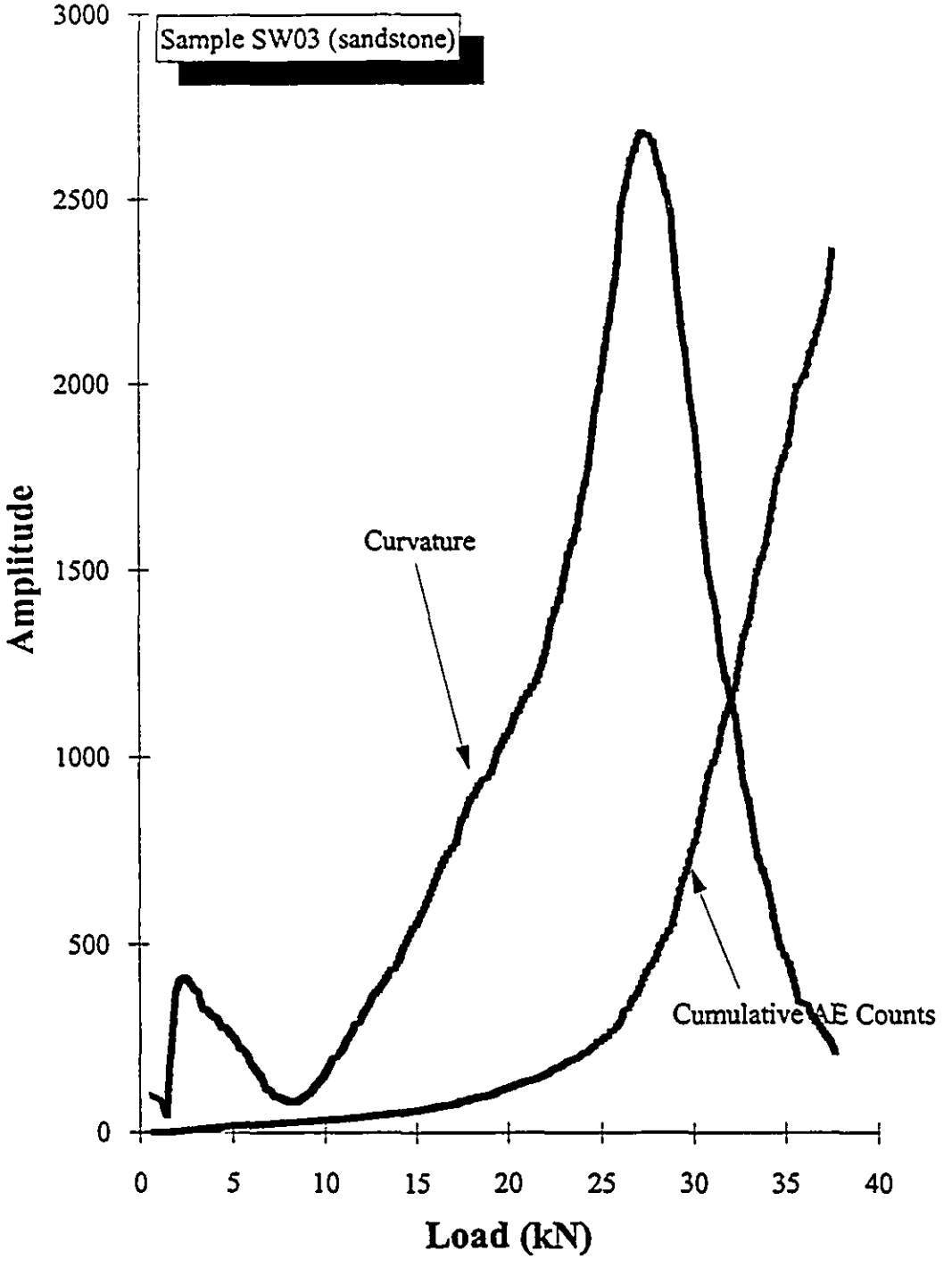

Figure 10-10: Kaiser Effect and Associated Curvature for Sandstone.

interpolate the missing points for those weeks. The memory loss was estimated at 16%, 7%, 3%, 6% and 15% for gabbro, charnokite, gneiss, limestone and sandstone respectively.

10.4) Discussion

The previous graphs show that stress recollection of gabbro, charnokite, gneiss, limestone and sandstone is very sharp even after a long period of time. In light of the findings of Chapter 8, the stress memory of these rocks, excepting limestone may be explained in terms of their isotropic nature. It was said in Chapter 8 that the Kaiser Effect may be most suitable for application in isotropic rocks because of the ability of the material to produce the same number and type of fractures when stressed in different directions. The stress memory estimates for rock types such as gabbro and limestone were subjectively after applying the Maximum Curvature Method due to the poor quality of acoustic emission data.

Examining the load versus CAE graphs for specimens with low numbers of acoustic emissions namely gabbro and limestone, one can see that the curvature possesses multiple peaks making the selection of the Kaiser Effect point very difficult. It is equally difficult to estimate the previous stress level by the eye because there are numerous breaks in the CAE curve that could qualify them as a Kaiser Effect point. The difficulty in getting an accurate stress estimate using poor quality AE data was discussed in Chapter 7 when the Maximum Curvature Method was presented.

To estimate the previous load for gabbro and limestone, the peak in the curvature closest to the known level was used. In the case of chanokite, gneiss and sandstone, the largest peak in the curvature provided the stress estimate.

In conclusion, to improve the resolution of acoustic emission data the sensitivity of the recording instrument must be raised. Given the type of testing equipment used here, doing so is tantamount to lowering the signal to noise ratio which is not desirable. Until a more sensitive testing environment is created, stress estimation in low activity rock types by the Kaiser Effect method will be a difficult task.

CHAPTER 11

Field Programme: In-situ Stress Determination

11.1) Introduction

To evaluate the feasibility of estimating stresses in a rock mass by the Kaiser Effect method, different mining companies were contacted to provide cores from their stress measurement program. Although there is no single independent and accurate way of determining the state of stress (many assumptions must be made about the nature of the rock mass), this component of the research programme provides the opportunity to find out how the results from the Kaiser Effect technique compare with conventional methods of stress determination.

Three case studies were conducted from three different underground environments in Canada and South Africa. In this chapter, two field studies, one carried out at the AECL's Underground Research Laboratory in Manitoba, Canada and another at the President gold and uranium mine in South Africa will presented. The third study will be discussed in Chapter 12 because the rock specimens from Noranda's copper mine in Gaspé, Québec did not display the characteristic Kaiser Effect curve, so no stress values could be obtained from these samples.

11.2) AECL Underground Research Laboratory

The Underground Research Laboratory is located in southeastern Manitoba, in the Lac du Bonnet granite batholith of the Canadian shield. It was constructed by the Atomic Energy of Canada Limited (AECL) to conduct geotechnical research for the Canadian Nuclear Fuel Waste Management Program, assessing the concept of permanent disposal of nuclear fuel waste deep in plutonic rock.

The design and monitoring of underground excavations requires an accurate knowledge of the state of stress in the rock mass. URL has set up a comprehensive in-situ stress measurement program for this purpose and uses techniques such as

overcoring, hydrofracturing and strain rosette to determine the stress magnitude and direction. The comparative study program between traditional stress measurement methods and the Kaiser Effect was specifically initiated to assess the feasibility of using acoustic emission as a tool to measure in-situ stresses.

11.2.1) Geology

The Underground Research Laboratory (URL) is situated within the boundaries of the Lac du Bonnet granite batholith, an elongated pluton with the long axis running approximately eat-northeast and a surface area of roughly 75 by 25 km (see Figure 11-1). The batholith is considered to be representative of the granite intrusives found on the Canadian Precambrian Shield.

The geology of the URL site has been determined by core logging and detailed surface and sub-surface mapping. From these observations, five work units have been identified in the batholith at the URL site: the pink (altered) or gray (unaltered) granitic rock mass of the batholith, xenolithic inclusions, leucocratic granitic segregations, granodiorite dikes and pegmatitic and aplitic dikes and related vein fillings. This classification scheme is primarily based on the relative ages between the rock units.

Two major fracture zones (Fracture Zones 3 and 2) and their associated splays (Fracture Zones 2.5 and 1.9) were intersected during the excavation of the URL shaft (see Figure 11-2). Other fracture zones (Fracture Zones 1.8, 1.5, and 1) were intersected only in exploratory boreholes. The fracture zones generally dip between 20° to 30° to the southeast and typically contain low-dipping fractures.

Above Fracture Zone 2.5, the rock is primarily composed of pink granite. In this region two sub-vertical joint sets are present: a prominent set striking about 20 to 40 degrees, and a less prominent, intermittent set striking about 150 to 180 degrees. Below Fracture Zone 2.5 the rock is essentially unfractured gray granite except for the fracture zones mentioned, their associated pink discoloration and a sub-vertical joint zone terminating near the 240 Level.

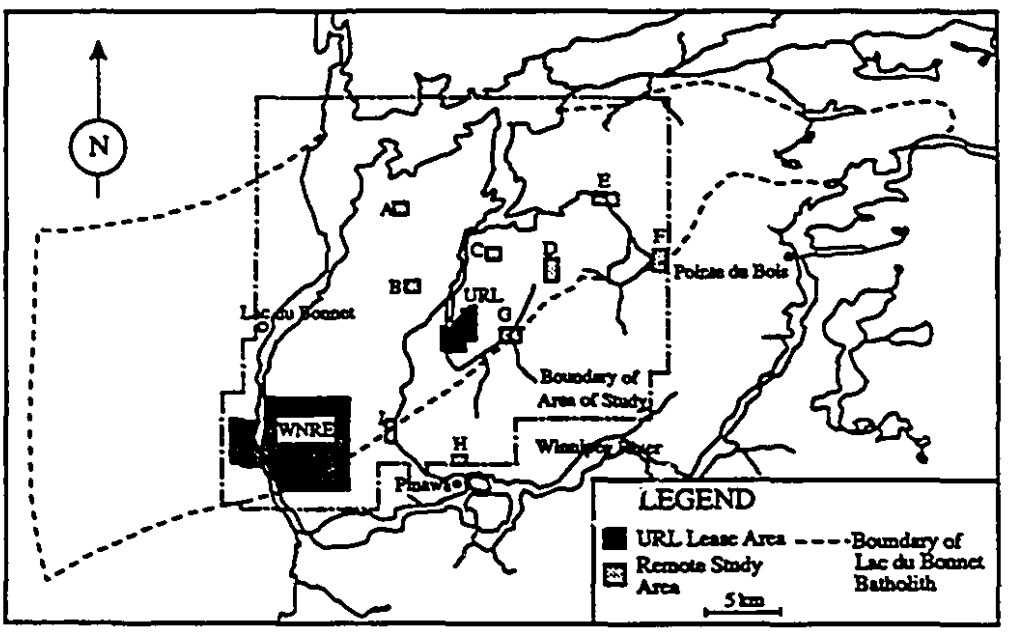

Figure 11-1: Location of the Underground Research Laboratory.

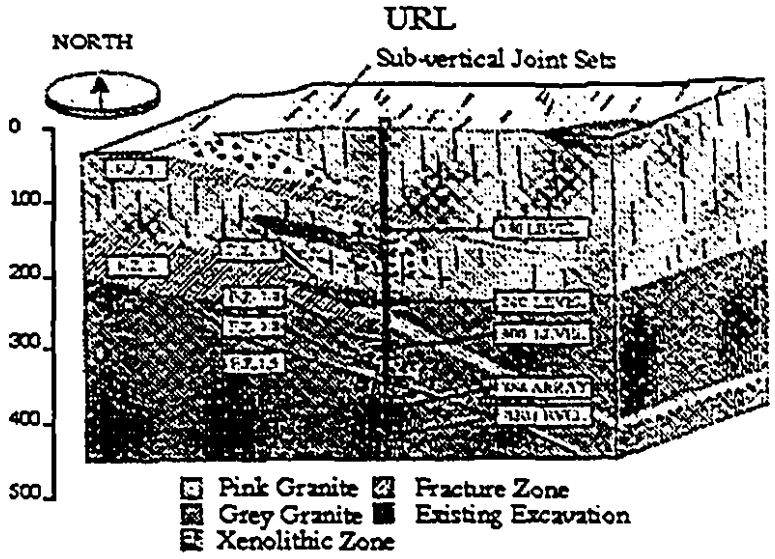

Figure 11-2: Simplified Block Diagram of the URL Site Geology.

11.2.2) Mechanical Properties

Core samples obtained from URL were of the gray granite rock type. The mechanical properties of this rock based on uniaxial compressive tests carried out on 20 specimens are [92]:

	Mean	Standard Deviation	Range
Density (g/cm^3)	2.63	0.04	
U.C.S. (MPa)	167	13	149-198
$E_{tangent}$ (GPa)	55.7	4.9	46.6-64.4
Poisson's Ratio	0.30	0.07	0.13-0.43

Petrographical tests carried out on the AECL gray granite showed that this rock has a composition similar to that of Stanstead granite. The rock itself is a white equigranular granite composed of 5% biotite, 43% quartz, 30% plagioclase, 20% feldspar and 2% opaques (pyrite).

11.2.3) Testing Program

The in-situ stress measurement program is an on-going part of the batholith characterization program. In some cases, the data from the overcoring stress determinations and biaxial pressure tests are used to learn about the stresses in the rock mass as well as the modulus and the Poisson's ratio. In general, two types of monitoring devices were used in overcore testing at different levels including the 420 Level: the United States Bureau of Mines Borehole Deformation Gauge and the AECL Continuously Monitored Council for Scientific and Industrial Research Triaxial Strain Cell. Standard biaxial pressure testing using the ISRM standards and some hydrofracturing tests are also carried out.

11.2.4) Test Site

The 420 Level where the granite samples were obtained is shown in Figure 11-3. Boreholes are drilled into the granitic rock mass at a depth of 420 m below the ground surface. Figure 11-4 shows the relative locations of only two of the

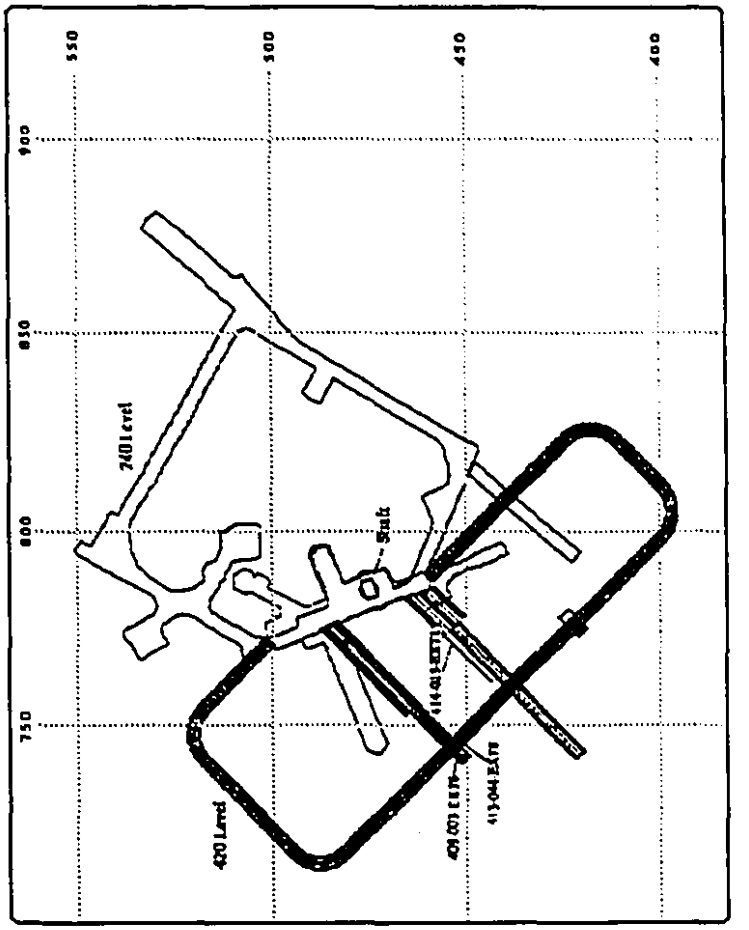

Figure 11-3: Plan View of the 240 and 420 Levels Showing Sample Borehole Locations.

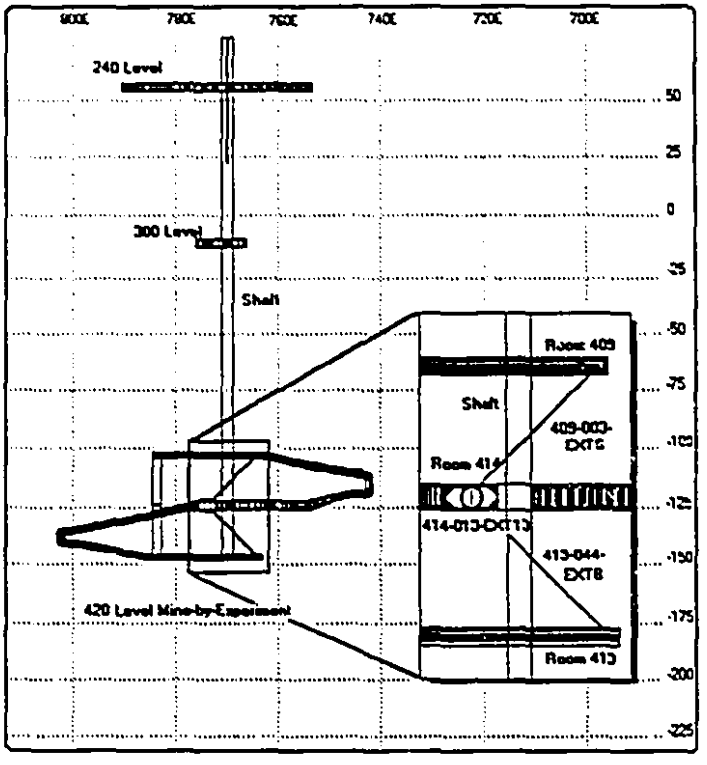

Figure 11-4: Section Showing the Relative Locations of the Sampled Boreholes.

three sampled boreholes. The three boreholes 404-016-SM4, 409-003-EXT6, and 413-044-EXT8 dip at -86, +45, and -45 degrees respectively.

11.2.5) URL Test Results

The work at the 420 m Level produced the following in-situ stress state [93]:

Stress Components	σ1	σ2	σ3
Magnitude (MPa)	55 ± 5	48 ± 5	14 ± 1
Trend (degrees)	135 ± 10	44 ± 10	290 ± 25
Plunge (degrees)	10 ± 5	5 ± 5	79 ± 5
Stress Ratios	**σ1/σ2**	**σ1/σ3**	**σ2/σ3**
	1.15 ± 0.1	3.93 ± 0.5	3.43 ± 0.5

11.2.6) Kaiser Effect Testing Program

A minimum of 10 specimens were sub-cored from the original cores in the direction of drilling to a diameter of 2.867 cm. The recovered cores were cut with a height to diameter ratio of slightly greater than 2:1. The samples were tested and analyzed using the procedure described in Chapter 9. Figure 11-5 presents a typical CAE data and curvature obtained by loading sample AE07 obtained from borehole 404-016-SM4. Gray granite specimens were loaded for the Kaiser Effect experiment sometime between three to six weeks (cores were received in 3 separate shipments) after they were extracted from the Underground Research Laboratory test site. Based on the test results from the effect of delay time on the stress memory of Stanstead granite, it is believed that the Kaiser Effect tests would produce accurate estimates of the in-situ stress in the direction of drilling. The Table below presents the results of the Kaiser Effect experiments.

Borehole (number)	Dip Angle (degrees)	Samples Tested	Estimated Stress (MPa)	Standard Deviation (MPa)
404-016-SM4	+90	10	10.968	±3.345
409-003-EXT6	+45	12	33.879	±6.431
413-044-EXT8	-45	12	38.327	±4.673

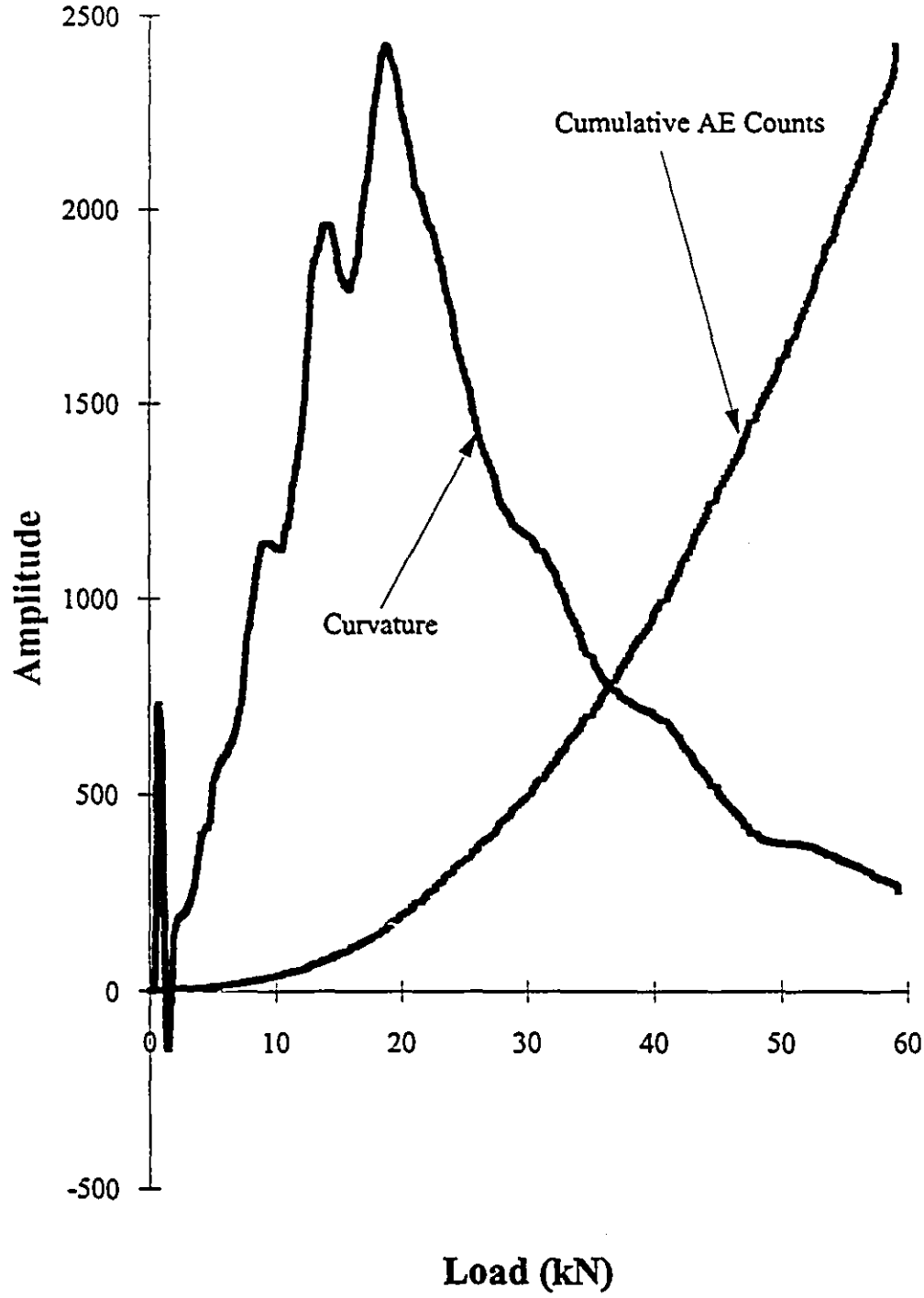

Figure 11-5: Cumulative AE and its Associated Curvature from Borehole 404-016-SM4.

11.2.7) Data Analysis

Stress values obtained from the in-situ testing program were used for two different purposes. In the first place the stress estimation from borehole 404-016-SM4 was compared with the theoretical estimate of the pressure exerted by the weight of the rock mass overlying the measurement point i.e.:

$$P = \rho \times g \times h = 2.65 \times 9.81 \times 420 = 10.918 \text{ MPa} \qquad (11\text{-}1)$$

where ρ is the average density of the granite measured from the core specimens, g the gravitational acceleration and h the depth of measurement. Equation (11-1) can be applied in this case because of the orientation of the borehole. The agreement between the theoretical and experimental values leads us to believe that the data obtained from the other boreholes are equally accurate.

Given the magnitude of stress in the direction of drilling and the dip angle of the borehole, it is possible to calculate the magnitude of the major and minor principal stresses using the data from three boreholes. A system of three equations in three unknowns can be set up as discussed by Popov [94] using the following formulas:

$$\sigma_{x1} = \sigma_x \cos^2\theta_1 + \sigma_y \sin^2\theta_1 + \tau_{xy}\sin 2\theta_1 \qquad (11\text{-}2)$$
$$\sigma_{x2} = \sigma_x \cos^2\theta_2 + \sigma_y \sin^2\theta_2 + \tau_{xy}\sin 2\theta_2 \qquad (11\text{-}3)$$
$$\sigma_{x3} = \sigma_x \cos^2\theta_3 + \sigma_y \sin^2\theta_3 + \tau_{xy}\sin 2\theta_3 \qquad (11\text{-}4)$$

where σ_{x1}, σ_{x2}, and σ_{x3} are the stress magnitudes in the direction of drilling and θ_1, θ_2, and θ_3 are the boreholes dip angle. Solving this system of equations yields σ_x, σ_y, and τ_{xy} which can be used in the following equation to find the major and minor principal stresses:

$$\sigma_{1,3} = \frac{\sigma_x + \sigma_y}{2} \pm \sqrt{[(\sigma_x + \sigma_y)/2]^2 + (\tau_{xy})^2} \qquad (11\text{-}5)$$

Using σ_{x1} = 38 MPa, θ_1 = 0 degree for borehole 413-044-EXT8, σ_{x2} = 34 MPa, θ_2 = 90 degrees for borehole 409-003-EXT6, and σ_{x3} = 11 MPa, θ_3 = 135 degrees for borehole 404-016-SM4, the major and minor principal stresses were

calculated to be equal to 61 MPa and 11 MPa respectively. There is an acceptable agreement between the values for principal stresses obtained from the Kaiser Effect tests and those measured in-situ from the URL program. The data provided by Atomic Energy of Canada (AECL) represent the overall state of stress in the rock mass under study using a number of different stress measurement methods such as overcoring and strain rosette. The table below shows the magnitudes for the major and minor principle stresses at the 420 Level:

Stress Axis	Major (σ_1)	Minor (σ_3)
Kaiser Effect Program	61 ± 6 MPa	11 ± 4 MPa
URL Stress Program	55 ± 5 MPa	14 ± 1 MPa

11.3) President Gold Mine

A joint program with the assistance of the Anglo-American Corporation of South Africa was initiated to measure in-situ stresses in the President gold and uranium mine. Cores from two boreholes were recovered and sent within 12 days for testing. The first borehole was drilled vertically upward at a depth of 1705 m below the ground surface into a quartzite body. The second borehole was drilled at an angle of 55 degrees upward into a dike at a depth of 2.7 km below the surface. Figure 11-6 shows the plan view of the area where the first borehole was drilled while Figure 11-7 is the section map for the second borehole.

The 3.196 cm diameter cores were cut to a ratio of 2:1 and lapped in order to obtain a smooth end surface. They were loaded uniaxially and the acoustic emissions were recorded using the test procedure described in Chapter 9. In general, the level of noise from both set of samples was low compared to the number of events obtained from the Stanstead granite. However, out of every five or six specimens tested only two samples generated sufficiently large numbers of acoustic emissions for the Kaiser Effect to be seen. This favorable condition can be attributed to the presence of a considerable amount of disseminated sulfides in the rock matrix.

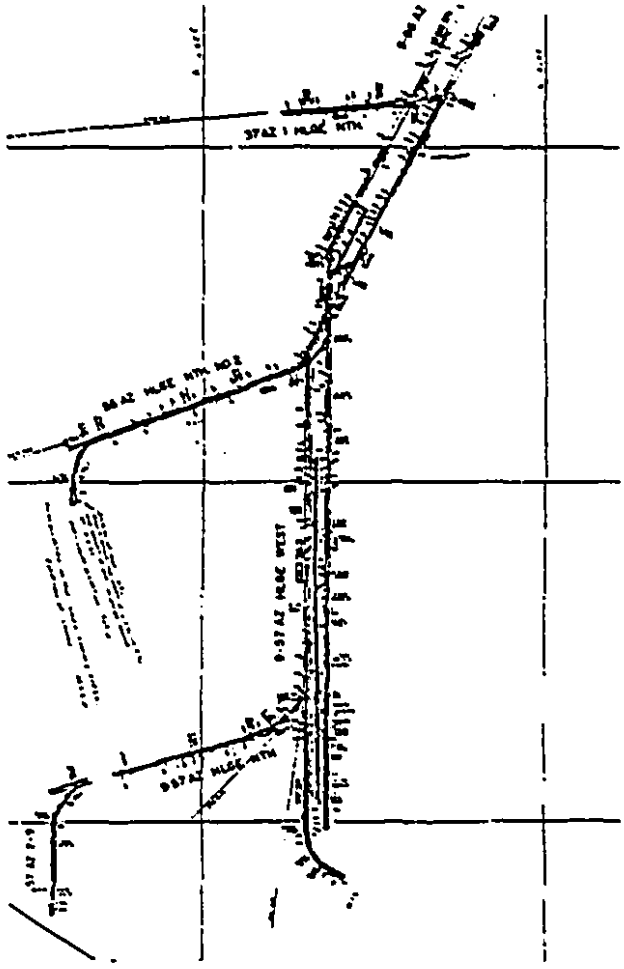

Figure 11-6: Plan View of Vertical Borehole Location.

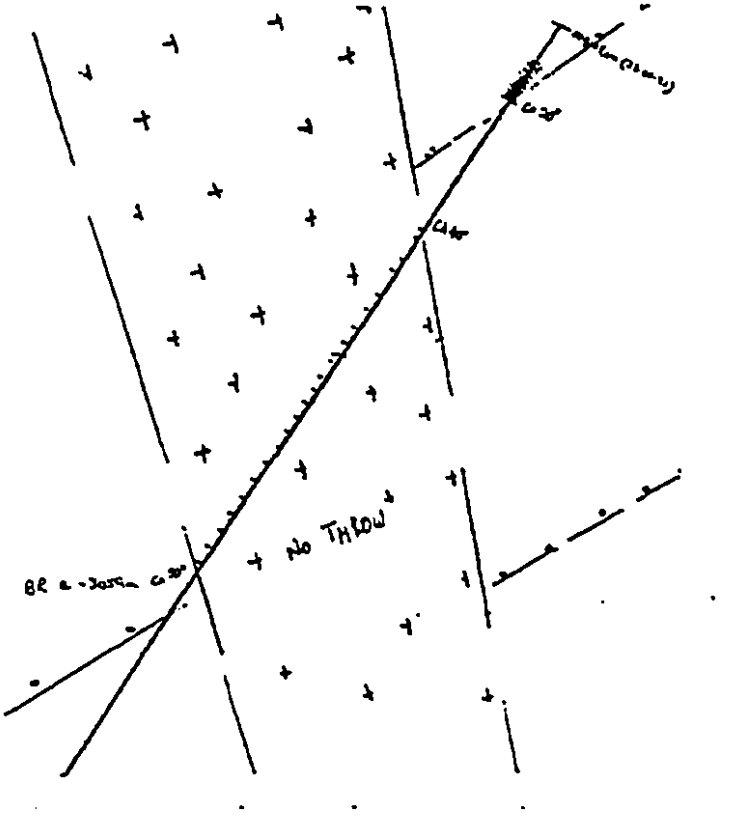

Figure 11-7: Section Showing the Dike and Borehole Location.

Estimated stresses for the samples recovered from the vertical borehole match with the theoretical value obtained by calculating the weight of overlying rock. That is, for an average density of 2.65 g/cm^3 for the quartzite, a sample depth of 1653 m and a value of 9.81 m/s2 for the gravitational acceleration, the pressure exerted by the overlying rock is approximately 43 MPa. The Kaiser Effect method using a total of 10 specimens produced a value of 44.93 ± 7 MPa.

The estimated stress for the second borehole came out to be equal to 51 ± 11 MPa. The standard deviation is high in this case considering the total number of samples used. Here, the results from all 12 re-stressed specimens, regardless of the number of events generated, were averaged to get the stress value. Because no in-situ stress values were provided by the Anglo-American Corporation, a general assessment about the quality of the Kaiser Effect values will be made using available data from the literature.

Figure 11-8 shows the variation of the ratio of average horizontal stress to vertical stress with depth [95]. It can be seen that in South Africa, for depths greater than 500 m, σ_h/σ_v becomes less than one. The samples recovered from the second borehole were subjected to a vertical stress equal to 70.2 MPa corresponding to a depth of 2700 m, a density of 2.65 g/cm^3 and a gravitational acceleration equal to 9.81 m/sec^2. At this depth the horizontal stress should be much smaller than 70.2 MPa. The average horizontal stress at a depth of 2700 m below the surface can be more accurately calculated using the data shown in Figures 11-9a and 11-9b. Here, the variation in vertical and horizontal stress as a function of depth for different locations in the world is plotted. Using the slope of the vertical and horizontal stress curves, one can obtain the desired ratio for South Africa.

According to Figure 11-9a, the increase in vertical stress with depth is 0.025 MPa/m while Figure 11-9b shows an increase of 0.015 MPa/m for the horizontal stress as a function of depth with a horizontal stress value equal to 6.5 MPa near the ground surface. Using these data one obtains the following stresses:

$\sigma_v = 2700 \times 0.025 = 67.5$ MPa.
$\sigma_h = 2700 \times 0.015 + 6.5 = 47$ MPa.
$\sigma_h/\sigma_v = 47 / 67.5 = 0.6963$

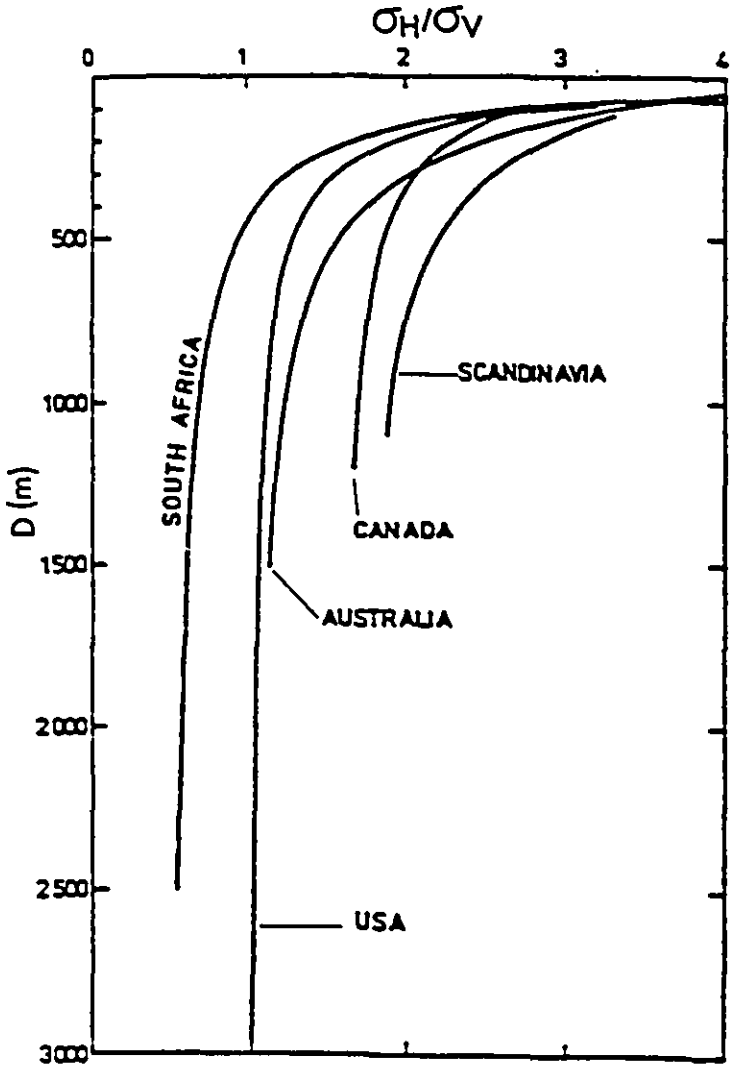

Figure 11-8: Variation of the Ratio of Average Horizontal to Vertical Stress with Depth.

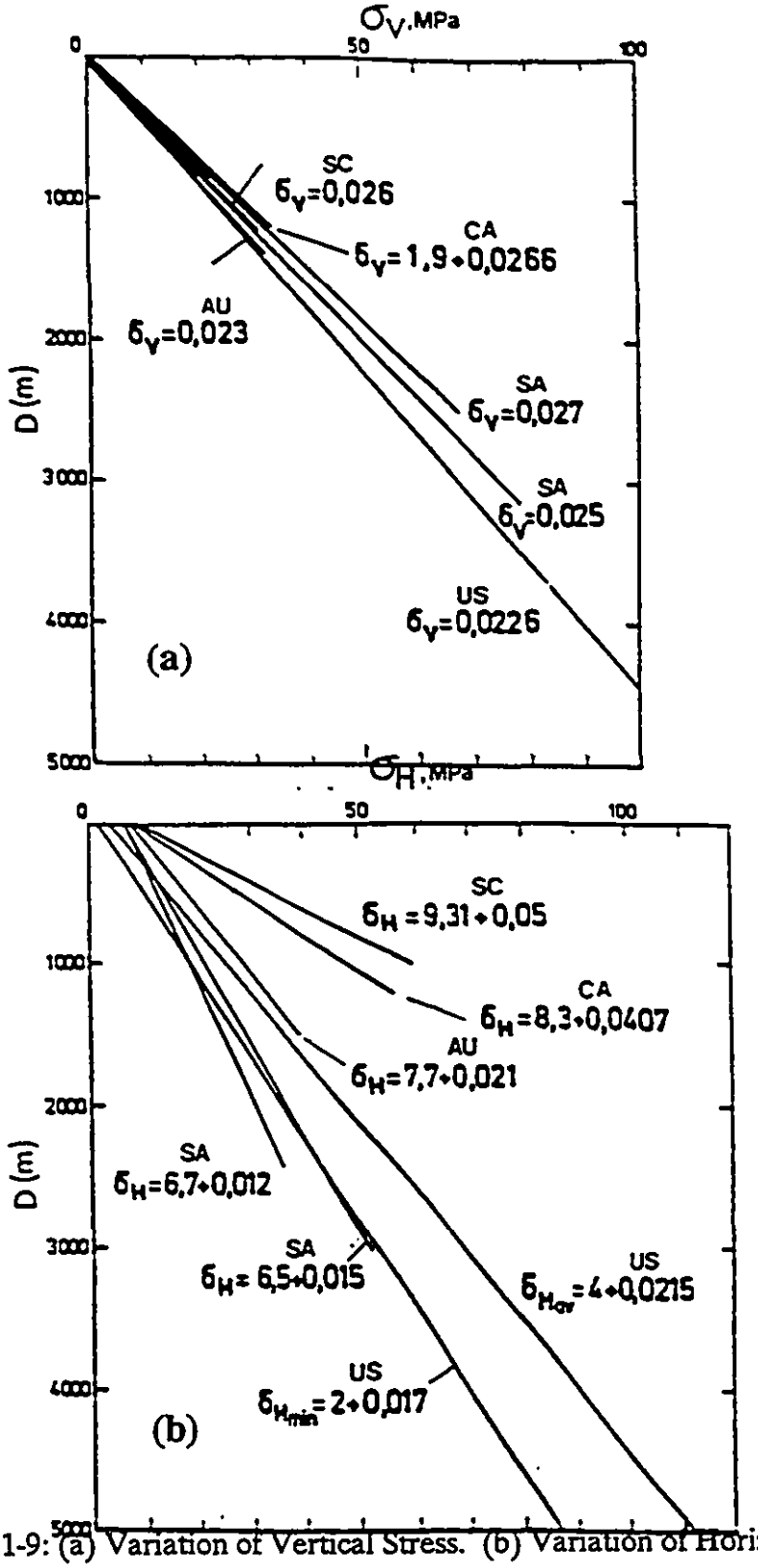

Figure 11-9: (a) Variation of Vertical Stress. (b) Variation of Horizontal Stress with Depth.

If a value of 70.2 MPa is used for the vertical stress instead of 67.5 MPa then the horizontal stress in the President mine at a depth of 2700 m would be 48.88 MPa. In this case, the average stress of 51 ± 11 MPa obtained from the Kaiser Effect experiments is therefore quite reasonable compared with the calculated value.

11.4) Conclusions

The conclusions that can be drawn from the results of the field studies carried out in this investigation are that the Kaiser Effect method can be a reliable means of stress determination if applied in a "suitable" environment. This means that the rock type sampled for stress determination must have the potential in terms of its composition and structure to (1) generate acoustic emission events in sufficient numbers, (2) exhibit the Kaiser Effect over a wide range of stress magnitudes and (3) be preferably isotropic.

The above-mentioned requirements are best illustrated by the two case studies presented in this chapter. Specifically, in the first study, the granite rock from the Canadian shield satisfied all three conditions and therefore a high degree of correlation was achieved between the major and minor principle stresses obtained by the Kaiser Effect method and traditional techniques.

It is important to note that the success of the Kaiser Effect method in determining in-situ stresses can be regarded to be site specific. That is, if the rock type in the target area meets the conditions stated above, then the Kaiser Effect can be used to estimate stresses in the direction of drilling.

CHAPTER 12

General Conclusions & Recommendations

12.1) Introduction

The work described in this thesis has been a comprehensive laboratory and field investigation into various aspects of stress memory in hard rocks under uniaxial compressive testing conditions. The laboratory programme consists of three components: (1) an investigation into different types of fracture mechanisms responsible for the generation of acoustic emissions in relation with the Kaiser Effect, (2) a detailed study of factors affecting stress memory using one rock type namely, the Stanstead granite for its homogeneous composition and structure and (3) a study of the effect of delay time in five different rock types based on a proposed testing procedure. The field programme was carried out with the assistance of mining companies and Canadian government agencies to compare stress values from traditional stress measurement techniques with estimates using the Kaiser Effect method. In addition, a new technique called Maximum Curvature Method was developed to determine the Kaiser Effect point automatically and used in estimating the previous maximum stress for all the experiments performed in this research project. The conclusions reached from these investigations and the recommendations for future research in this area are summarized in this chapter.

12.2) Maximum Curvature Method

The Maximum Curvature Method was developed to improve the accuracy of stress estimation and reduce the time required in computing the Kaiser Effect load compared with the Method of Tangents proposed by Boyce [55] and improved by Hardy et.al. [88]. Excepting the statistical approach by Hardy et.al. [88], the determination of the Kaiser Effect point used in estimating the previous stress level has been carried out by subjective methods, that is the judgment of the person performing the analysis. The proposed technique calculates the curvature at every point along the time (or load) versus the cumulative acoustic emission counts curve

and sets the Kaiser Effect stress at the point where the curvature has the largest value. It is the mathematical implementation of the definition of the Kaiser Effect phenomenon given in Chapter 4.

It was shown through a series of trials in Chapter 7 that the performance of the Maximum Curvature Method is many times superior to that of the Method of Tangents in terms of execution speed on a computer. The stress values obtained by applying MCM are also more accurate when conditions such as the presence of a sharp deflection point and a large number of acoustic emission events generated by the specimen are satisfied. When the data length and/or the number of events are small (less than approximately 300 sec and 1000 events per loading cycle respectively), the accuracy of the Maximum Curvature Method in estimating the previous load level is reduced. The accuracy may be improved in such a case by scaling the data as discussed in Chapter 7.

12.3) Fracture Mechanics and Kaiser Effect

A detailed petrographic analysis of the Stanstead granite was carried out at different stress levels under uniaxial compressive testing conditions. The objective was to determine the type of fractures responsible for the generation of acoustic emissions in the rock in relation with the Kaiser Effect. The major findings were:

1) the acoustic emission activity depends on intergranular, intragranular and transgranular re-arrangements that are set into motion in the rock by the application of stress. These activities evolve from micro-scale to macro-scale as the level of load increases.

2) in the elastic region, stress memory is due to the evolution of existing or newly formed cracks into an equilibrium configuration corresponding to the level of applied stress. Once the load is removed, these cracks close but do not heal in an atomistic sense, which is why the previous maximum can be remembered during a subsequent loading stage.

3) a fractographic analysis of thin sections prepared parallel and perpendicular to the direction of loading revealed that the number of fractures are more or less

equal at different stress level. This was assumed to be related to the isotropic nature of the rock implying that stress memory in such rock types could be preserved regardless of the direction of the applied stress.

12.4) Factors Affecting Stress Memory

This component of the research programme is the most comprehensive investigation carried out so far into major factors affecting the Kaiser Effect in hard rocks. The results obtained from these experiments are unique compared to previous work because of the large number of factors and samples tested using the same rock type and testing procedure. Based on the findings from this part of the project, a testing method is proposed in Chapter 9 and used subsequently for the remaining laboratory investigations and comparative field studies. The major conclusions drawn at the end of this benchmark study are the following:

1) the range of frequencies selected to record data is very important because it affects directly the number and type of acoustic emission events detected during the course of an experiment. To identify the frequency range most suitable for the purposes this investigation different transducer/amplifier combinations were tested. The transducers were resonant and broad-band frequency response piezo-electric accelerometers. It was found that the 150 kHz resonant frequency transducer with a band-pass filter in the range of 100 to 300 kHz produced the best results in terms of the number of acoustic emission events detected by the equipment.

2) a study regarding the effect of signal definition parameters revealed that screening events in terms of their relative amplitude or energy reduces the accuracy of load estimates. Various cumulative acoustic emission counts curves constructed by grouping events based on ranges of amplitude and energy showed unfavorable effects on the sharpness of the Kaiser Effect curve. For the rest of this project, the previous stress level was estimated using all the events recorded during an experiment.

3) the specimen size in terms of its diameter and height to diameter ratio has no significant effect on the stress memory of the rock type tested. However,

different diameter samples having a length to diameter ratio of 2:1 gave on average more accurate estimates of the previous stress level by less than 2% or 3%. This fact can be overlooked in many Kaiser Effect experiments in general, however, for the sake of accuracy and consistency, all the samples tested in this work were prepared with a ratio of 2:1.

4) the effect of loading mode and rate was investigated in great detail. It was found that the results from samples loaded under displacement control are more accurate (by 5-10%) than using load control. This fact is best illustrated by examining the shape of the curvature and the cumulative acoustic emission counts curve for a given sample. Where the rock is stressed using displacement control, there is a much sharper change of slope around the Kaiser Effect point. Therefore, the curvature shows a smooth and narrow peak where the previous maximum stress was exceeded. In contrast, the curvature in the case of load control has an irregular and noisy shape reflecting the difference in the acoustic emission and mechanical response of the rock. In addition, the effect of rate was thoroughly studied by applying three and five different rates during the first and second loading cycles, respectively. The data showed that Slow (0.1875 MPa/sec or 0.0025 mm/sec) to Very Slow (0.0938 MPa/sec or 0.00125 mm/sec) rates produced the most accurate values for the estimated load. Kaiser Effect tests were then carried out using displacement rates between 0.001 to 0.003 mm/sec.

5) when studying the stress memory of rocks, one of the fundamental questions that needs to be answered is at what rate will the memory of the previous maximum fade away. The memory depends on many factors such as the rock's composition and structure and the length of time a given stress level was applied. A detailed and systematic study of this factor was carried out at fixed intervals. All specimens used were subjected to a stress level for 5 to 10 minutes until the state of saturated strain was reached. The data for the first month (based on five tests performed every day) revealed that the stress memory of Stanstead granite (and possibly most rock types) does not vanish according to a uniform pattern, however, the overall trend is downward. After 30 days, the memory was lost only by 5 kN compared to the original level of 30 kN suggesting that stress values estimated one month after core recovery are within the limits of experimental error using traditional techniques.

6) extreme physical changes such as high temperatures and water content imposed on the specimens in vacuum did not seem to affect the stress memory of Stanstead granite to a large degree. Here, the estimated values for the re-load samples turned out to be within 15% of the previous maximum. This suggests that the effect of temperature and water content change during drilling may be ignored.

7) a small scale experiment was carried out on specimens subjected to different confining pressures and identical axial stress. The Maximum Curvature Method was used to determine the previous load level. The curvature for these specimens showed two peaks, one large and one small, around the Kaiser Effect point. Stresses determined using the larger peaks were off on average by 22% in contrast to 8.5% for the smaller peaks (closer to the known stress level).

8) loading samples under uniaxial condition in different directions was found to have no significant effect on the stress memory of Stanstead granite. In almost all cases stresses were determined with an error of 2-5%. This confirmed the results of the fractography study carried out in Chapter 8 regarding the isotropic nature of this rock type.

12.5) Stress Memory of Hard Rocks

The effect of delay time was also studied in other rock types using the test procedure suggested in Chapter 9. The rock types tested were gabbro, gneiss, charnokite, limestone and Darlye Dale sandstone. It was found that the accuracy of stress determination has a direct relationship with the rock's composition and acoustic emission response.

In the case of charnokite, gneiss and sandstone the number of acoustic emission events was large (greater than 2000 events per test). This produced a well defined Kaiser Effect point and a sharp peak in the associated curvature for each specimen. In contrast, the acoustic emission response of gabbro and limestone was poor and on average only 200 to 500 events were recorded per sample for these rock types. The calculated curvature from the gabbro and limestone data showed

multiple peaks and the cumulative acoustic emission counts curve did not exhibit a sharp change of slope at the previous maximum.

The estimated memory loss using the MCM for the gabbro and charnokite after 14 weeks was in the order of 16% and 7%, respectively. Gneiss and limestone's recollection of previous stress level was estimated to be about 3% and 6% after 18 weeks while sandstone showed a 15% loss after 21 weeks.

12.6) In-situ Stress Determination

Two field studies were carried out with contributions from the Atomic Energy of Canada in Manitoba and the Anglo-American Corporation of South Africa. Stress measurements using the Kaiser Effect was performed along with in-situ testing programme using traditional techniques such as overcoring, borehole slotter and strain rosette. The results from both programmes were compared to assess the accuracy of stress values obtained using acoustic emissions.

The major and minor principal stress magnitudes were successfully determined from cores provided by the Atomic Energy of Canada's Underground Research Laboratory. Here, cores from three different directions were first tested and the stresses in the direction of drilling were estimated using the Maximum Curvature Method. Subsequently, using the known borehole orientation and estimated stresses, the major and minor principal stresses were calculated by applying the equations given in Chapter 11. These stress values are in good agreement with values obtained from in-situ stress measurement programmes using conventional techniques.

Samples from two boreholes in a gold mine in South Africa provided reasonable results compared with theoretical values. The estimated stress values from the vertical borehole in a quartzite rock was within 5% of the pressure exerted by the weight of the overlying rock. The stress value from the second borehole drilled at an angle of 55 degrees upward into a dike 2.7 km below the ground surface was estimated to be 51 ± 11 MPa.

12.7) Kaiser Effect Appraisal

Based on the findings of this research programme, in-situ stress determination using the Kaiser Effect method can provide accurate estimates in isotropic rock types capable of generating large numbers of acoustic emissions. Given the number of experiments that can be performed in one day, that is somewhere between 12 and 16 tests including sample preparation, stress measurement using this method can provide more data at the cost of one uniaxial compressive test per sample compared to other techniques. A typical overcoring test may provide three data points in one day from one borehole. The price tag for one such test would be in the thousands of dollars compared with a couple of hundred dollars for a uniaxial compressive test. Although more fundamental work remains to be done in this area, the economic merits of this method are attractive.

The point to emphasize again is that the Kaiser Effect technique works best in rock types that can generate large numbers of acoustic emission events under load. The isotropic and homogeneous nature of the rock become an important consideration if the stress magnitude must be measured in different drilling directions. Because the Kaiser Effect phenomenon depends on the propagation and/or initiation of cracks, it may be difficult to observe in all rock types. For example, the acoustic emissions in a sedimentary rock stressed parallel to its bedding, come largely from the friction and sliding of the layers rather than crack generation. Another rock type that does not exhibit the Kaiser Effect is marble. This fact was discovered when samples from the third field study were tested as discussed in the following section.

From the statistical point of view, the number of samples needed to obtain an accurate stress value depends on the conditions stated in the previous paragraphs. For example, in an active rock type such as granite, five samples from one borehole would provide a good estimate of stress. On the other hand, stress measurement in quiet rocks such as the quartzite from South Africa may produce a large standard deviation. It is important to point out that granite and quartzite tested during the field component of this project have a high compressive strength and therefore large variations in terms of the magnitude of the estimated stress using the Kaiser Effect method will not have a major impact on the design or safety of the excavation. It would be more valuable to determine whether the Kaiser

Effect technique can be applied with precision in soft (e.g. potash) and sedimentary rocks. Although this research project focused primarily on the feasibility of determining in-situ stresses in hard rocks, the data obtained in Chapter 10 using limestone and sandstone and the case studies reported in the literature all point to the fact that the Kaiser Effect can equally provide accurate results in other rock types. More field tests must be conducted to ascertain the previous statement.

Comparing the results of the Kaiser Effect technique with conventional methods such as overcoring, flatjack and hydraulic fracturing could be criticized on the basis that how much confidence one has in these methods ? This is a valid question because a number of assumptions are made when the data from these techniques are analysed. It is assumed that the rock is isotropic, homogeneous, elastic and intact which are not always true. Many techniques depend on the measurement of strain. The errors involved in measuring this quantity and the elastic properties of the rock type (needed in calculating the state of stress) make it difficult to acknowledge that the calculated stress values represent the exact stresses in the rock mass.

In applying the Kaiser Effect method, one should recognize the fact it will give the compressive stress which acted on the rock in the direction of drilling, when samples are compressed in the laboratory. Tensile forces should also leave their mark in the rock as shown by Boyce [55], however, due to the difficulties associated with pulling a rock apart, the tensile stress memory is not practical to measure. Another problem concerns the use of the Kaiser Effect method to determine tectonic stresses in a seismically active zone. Because of the relatively rapid changes in the stress combined with the effect of high temperatures (thermal fractures), the obtained values may not be representative of the current state of stress in and around a fault.

12.7.1) Noranda's Copper Mine

Rock cores from Noranda's Copper Mine in the Gaspé region of the province of Quebec were tested to compare the results of stress determination using the Kaiser Effect with the borehole slotter instrument. Three boreholes were drilled into a face in different directions with an identical dip angle at a depth of

800 m below the ground surface. The rock type is an extremely homogeneous, equi-granular white to greyish white calcareous marble with less than 3% disseminated sulfides (< 3 mm in diameter).

Specimens from a depth of 11 to 15 m were sub-cored in the direction of drilling to a diameter of 2.870 cm. They were then loaded using the procedure described in Chapter 9 to failure in many cases because the number of acoustic emissions recorded was extremely low until a few MPa before failure occurred. The total number of events recorded during the entire experiment for most samples did not exceed 800. A typical graph of the load in kN versus the cumulative acoustic emission counts and curvature would display a rapid increase in the rate of acoustic emissions from the onset of loading. One may speculate that (1) the stress in the direction of drilling was very small as evidenced by the peak in the curvature shown in Figure 12-1 or (2) this rock type does not exhibit the Kaiser Effect and therefore acoustic emissions recorded from these specimens do not carry any information about the stress memory.

Because marble behaves very much like glass in terms of its acoustic emission signature, that is very little or no events are generated until failure, it is very hard to determine the in-situ stress using the data obtained from this series of tests. To check for the existence of Kaiser Effect in this rock, twelve specimens were pre-loaded to various levels and tested during a second cycle to see if the Kaiser Effect manifests itself. From this total only 2 samples exhibited the Kaiser Effect. As far as the remaining specimens are concerned, because of the very low number of emissions, the previous level could not be determined reliably.

This case study showed that the successful usage of the Kaiser Effect method may be hindered by the rock material's inability to generate acoustic emissions in sufficient quantity. The number of generated events must be large enough to ensure an appropriate signal to noise ratio for the most sensitive system settings in terms of amplification and threshold. This particular application of the Kaiser Effect method was not successful because the required signal to noise ratio could not be achieved for the given experimental setup. It is however possible that if the sources of mechanical and electronic noise are further reduced, a more sensitive system setting can be selected which in turn may help in recording more low amplitude events generated by the specimens.

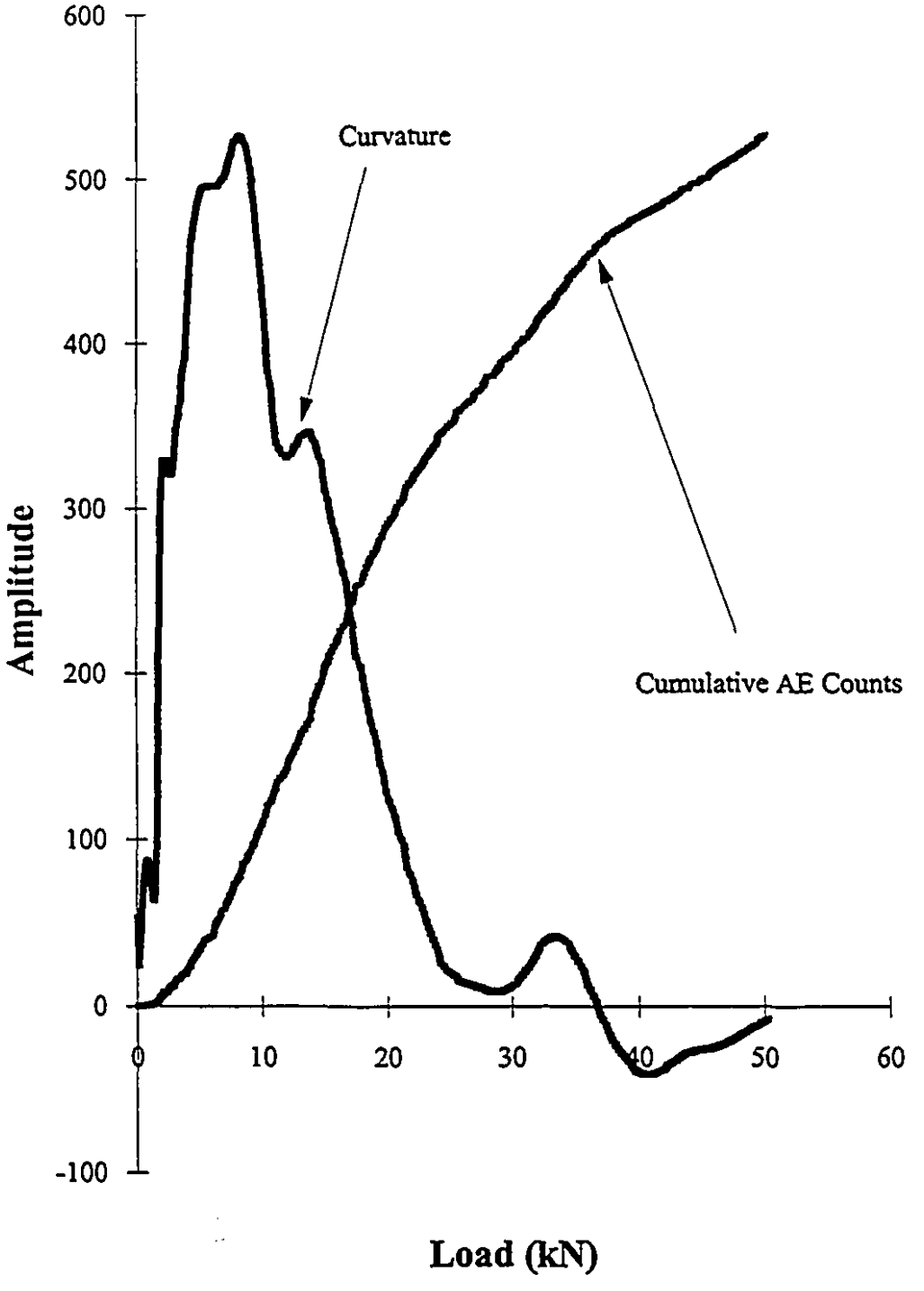

Figure 12-1: Cumulative AE and its Associated Curvature from Sample GP25.

In addition, one may note that because of the structural homogeneity and uniformity of this type of marble, no discernible grain movements, crack initiation and propagation, sliding or twining may occur in the rock's matrix and constituent minerals. This condition will generate no acoustic emission events (or with such low amplitudes that would make their detection difficult) in which case this type of rock materials can be regarded as being unable to retain any recollection of the previous stress level. A similar study by Michihiro et al. [91] on very fine grain marble showed that large numbers of acoustic emission events are produced from the onset of loading contrary to the results obtained in this investigation. However, their marble did not show any memory of previous maximum given the different stress levels and conditions imposed on the samples. Montoto et al. [82] explain the absence of AE activity during the initial and intermediate stages of loading of rock types such as marble to be due to their very low porosity and very high compactness that reduce the possible inner rearrangements of mineral constituents to a minimum.

12.7.2) Rock Types Exhibiting the Kaiser Effect

Various researchers have tested a variety of rock types. Many rocks have displayed the characteristic Kaiser Effect. Based on the results of this investigation and the data gathered from the literature, the following Table lists the rock types that are known to exhibit the Kaiser Effect phenomenon:

Amphibolite [51]	Marble (coarse grain) [55]
Andesite [38, 51]	Mica Gneiss [55]
Charnokite [+]	Mica Schist [55]
Felsic Gneiss [51]	Mudstone [39, 41]
Gabbro [+, 51]	Potash [+, 44]
Gneiss [+, 51]	Quartzite (Elliot Lake) [51]
Granite (Lac du Bonnet) [+, 51]	Rhyolite (Timmins) [51]
Granite [40, 45, 51]	Sandstone [+, 51, 55, 88]
Granodiorite [+]	Shale [55]
Limestone [+, 38, 51, 55, 88]	Tuff [37, 41]
+ *this author*	

The very fine grain marble tested in this project and by Michihiro et al. [91] is the only rock type that has failed to show the Kaiser Effect phenomenon so far. Until further experiments are carried out, the justification given by Montoto et al. [82] (low porosity and high compactness) can be used to explain the absence of the Kaiser Effect phenomenon in very fine grain rocks or those that are mainly composed of one constituent.

12.8) Recommendations for Future Work

The work carried out by the author was mainly concerned with a detailed study of the Kaiser Effect phenomenon under uniaxial compressive testing conditions. Although promising results were obtained from the application of this phenomenon to estimate in-situ stresses, the full effect of disturbing the state of hydrostatic equilibrium on stress memory of rocks in the direction of drilling must be thoroughly investigated. To carry out such an investigation, a cell fitted with a special casing to hold an acoustic emission transducer is needed to record AE events under triaxial testing conditions. In addition, the testing machine should be equipped with a system to control the rate at which the confining pressure is applied. A large triaxial cell is also needed to simulate field conditions, whereby large rock samples stressed triaxially would be later sub-cored in various directions and re-loaded under uniaxial and triaxial testing conditions.

As in all acoustic emission studies, the noise generated by the testing equipment, that is the mechanical noise from the hydraulic press and friction from the end platens or electronic noise from the recording instrument, must be reduced to an absolute minimum. More work is required in this area to eliminate the unwanted machine noise at the source such as placing the servo-valve responsible for most of the mechanical noise as far away from the test specimen as possible. This is a major investment in time and money but is necessary to increase the sensitivity of the acoustic emission instrument beyond its present settings.

Although it is extremely expensive to perform in-situ stress measurements using conventional methods, more comparative studies must be performed on different rock types using the knowledge and experience gained from laboratory experiments carried out under uniaxial and triaxial testing conditions.

Finally, a detailed study should be conducted to find out whether stresses imposed on the rock during blasting and rockbursting can be determined. This is interesting because currently, there is no way to measure the stresses that cause rockburst in underground mining operations.

References

01) Obert, L., 1967.
Determination of stress in rock - a state-of-the-art report.
ASTM STP 429.

02) Hooker, V.E. and Bickel, D.L., 1974.
Overcoring equipment and techniques used in rock stress determination.
United States Bureau of Mines Information Circular 8618.

03) Gilby, J.L., 1988.
Insitu stress measurements using the method of overcoring and hydrofracturing.
Internal Report, Dept. of Mining and Metallurgical Engineering.
McGill University, Montreal, Canada.

04) Habib, P. and Marchand, R., 1952.
Measurements of ground pressures by the flatjack experiment.
Annales de l'institut du Batiment et des Travaux Publiques, Serie Sols et Fondations.
Paris, France, No. 58, pp.905-940.

05) Panek, L.A. and Stock, J.A., 1964.
Development of rock stress monitoring station based on the flat slot method for measuring existing rock stress.
United States Bureau of Mines RI-6537.

06) Hubbert M.K. and Willis, D.G., 1957.
Mechanics of hydraulic fracturing.
American Institute of Mining Engineers, pp. 153-167.

07) Haimson, B.C. and Fairhurst, C., 1967.
Initiation and extension of hydraulic fractures in rock.
Society of Petroleum Engineer. No. 7, pp. 310-318.

08) Kehle, O.K., 1964.
The determination of tectonic stresses through analysis of hydraulic well fracturing.
Journal of Geophysical Research. Vol. 69, No. 2, pp. 259-273.

09) Grant, F.S. and West, G.F., 1965.
Interpretation theory in applied geophysics.
McGraw-Hill.

10) Obert, L. and Stephenson, D., 1965.
Stress conditions under which core discing occur.
Transactions AIME (mining) Vol. 232, No. 3, pp. 227-236.

11) Zandman, F. and Wood M.R., 1956.
Photostress.
Product Engineering, Sept., pp. 167-178.

12) Roberts, A., 1964.
Progress in the application of photoelastic techniques to rock mechanics.
Proceedings 6th Symposium on Rock Mechanics.
University of Missouri Rolla, pp. 606-648.

13) Barron, K., 1965.
Glass insert stressmeter.
Society of Mining Engineering, Dec., pp. 287-294.

14) Hult, J., 1963.
On the measurement of stresses in solids.
Transactions, Chalmers University of Technology.
Gothenburg, Sweden, No. 280.

15) Hult, J., Kvapil, R. and Sundkvist, H., 1966.
Function and scope of stress meters in rock mechanics.
Int. J. Rock Mechanics and Mineral Sciences, Vol. 3, No. 1, pp. 1-10.

16) ASTM E610-82.
Standard definitions of terms relating to acoustic emission.

17) Obert, L., 1939.
Measurement of pressures on rock pillars in underground mines.
United States Bureau of Mines RI 3444.

18) Obert, L., 1941.
Use of subaudible noises for prediction of rock bursts, part I.
United States Bureau of Mines RI-3555.

19) Obert, L. and Duvall, W.I., 1942.
Use of subaudible noises for prediction of rock bursts, part II.
United States Bureau of Mines RI-3654.

20) Hodgson, E.A. and Gibbs I.E., 1945.
Seismic research program, rock burst problem - lakeshore mine.
Dept. of Mines, Resources and Surveys, Eng. Branch Report No. 14, Ottawa, Canada.

21) Blake, W., 1982.
Microseismic applications for mining. a practical guide.
United States Bureau of Mines, Contract J0215002.

22) Cook, N.G.W., 1963.
The seismic location of rock bursts.
Proceedings 5th Symposium on Rock Mechanics, pp. 493-516.

23) Blake, W. and Duvall, W.I., 1969.
Some fundamental properties of rock noises.
Trans. AIME, Vol. 244, No. 3, pp. 288-290.

24) Blake, W. and Leighton, F.W., 1970.
Recent developments and applications of the microseismic method in deep mines.
Rock Mechanics - Theory and Practice, AIME, New York.

25) Leighton, F.W. and Blake, W., 1970.
Rock mechanics source location techniques.
United States Bureau of Mines RI-7432.

26) McCauley, M.S., 1965.
The use of subaudible noise (sarn) recordings to monitor slope stability.
Association of Engineering Geologists.

27) Krawiec, A., Tronbik, M. and Zuberek, W., 1975.
Use of electronic computer techniques for the determination of rock burst hazard.
Przegled Gornesy, No. 1, pp. 4-6.

28) Pocek, V., Rudajev, V. and Polach, V., 1975.
Problems of occurrence of rock bumps within the bituminous coal district of kladno.
Seminar on Mining Geophysics, Mining Inst. Czech. Academy Sci.
ACTA Monitor V, (32), pp. 185-195.

29) Will, W., 1979.
Seismoacoustic activity and mining operations.
Proceeding, Second Conference on AE/MS Activity in Geological Structures and Materials.
Trans Tech Publications, pp. 191-209.

30) Hardy, H.R., Mowrey, G.L. and Kimble, E.J., 1978.
Microseismic monitoring of a longwall coal mine: vol I - microseismic field studies.
Final Report, USBM Grant No. G0144013, Pennsylvania State University, pp. 318.

31) Koerner, R.M. and Lord, A.E., 1975.
Acoustic emission monitoring of the stability of earth dams.
International Water Power and Dam Construction, Vol. 27, No. 9.

32) Koerner, R.M. and Lord, A.E., 1978.
Predicting dam failure.
Research Directions, Vol. 1, No. 1, Drexel University.

33) Hardy, H.R. and Leighton, F.W., 1981.
Acoustic emission/microseismics activity in geological structures and materials.
Proceeding Third Conference, Trans Tech Publications.

34) Hardy, H.R. and Leighton, F.W., 1984.
Acoustic emission/microseismics activity in geological structures and materials.
Proceeding Fourth Conference, Trans Tech Publications.

35) Hardy, H.R., 1972.
Application of acoustic emission techniques to rock mechanics research.
Acoustic Emission, ASTM, STP 505, pp. 41-83.

36) Blake, W., Leighton, F.W. and Duvall, W.I., 1974.
Microseismic techniques for monitoring the behavior of rock structures.
United States Bureau of Mines Bull. 665.

37) Kanagawa, T., Hayashi, M. and Nakasa, H., 1976.
Estimation of spatial geostress components in rock samples using the kaiser effect of acoustic emission.
Proceedings of the 3rd Acoustic Emission Symposium, Tokyo, Japan.

38) Yoshikawa, S. and Mogi, K., 1978.
Kaiser effect of acoustic emission in rocks, influences of water and temperature disturbances.
Proceedings of the 4th Acoustic Emission Symposium, Tokyo, Japan.

39) Hayashi, M., 1979.
Acoustic emissions to detect the geostress.
Proceedings of the 4th International Rock Mechanics Symposium, Montreux, Switzerland.

40) Kurita, K. and Fujii, N., 1979.
Stress memory of crystalline rocks in acoustic emission.
Geophysical Research Letters, Vol. 6, No. 1, pp. 9-12.

41) Hayashi, M., Kanagawa, T., Hibino, S., Motozima, M. and Kitahara, Y., 1979.
Detection of anisotropic geo-stress trying by acoustic emission, and non-linear rock mechanics on large excavation caverns.
Proceedings of the 4th International Rock Mechanics Symposium, Montreux, Switzerland.

42) Sondergeld, C.H., and Estey, L.H., 1981.
Acoustic emission study of microfracturing during the cycling loading of westerly granite.
Journal of Geophysical Research, Vol. 86, No. B4, pp. 2915-2924.

43) Yoshikawa, S. and Mogi, K., 1981.
A new method for estimation of the crustal stress from cored rock samples: laboratory study in the case of uniaxial compression.
Tectonophysics, 74, pp. 323-339.

44) Vance, J.B., 1983.
Application of microseismic techniques in potash mines.
Potash Technology, pp. 179-184.

45) Holcomb, D.J., 1983.
Using acoustic emission to determine in-situ stress: problems and promise.
Geomechanics AMD, vol. 57, pp. 11-21.

46) Murayama, S., Michihiro, K, Saito, J., Fujiwara, T., Yoshioka, H and Hata, K., 1984.
The kaiser effect of a granite under various loadings.
Proceedings of the 7th Acoustic Emission Symposium, Tokyo, Japan.

47) McElroy, J.J., Koerner, R.M. and Lord, A.E., 1985.
An acoustic emission jack to assess in-situ rock behavior.
Internation Journal of Rock Mech. Min. Sci. & Geomech. Abstr., Vol. 22, No. 1, pp. 21-29.

48) Holcomb, D.J. and Martin III, R. J., 1985.
Determining peak stress history using acoustic emissions.
26th US Symposium on Rock Mechanics/Rapid City, SD/26-28 June, pp. 715-722.

49) Watters, R.J. and Soltani, A.M., 1985.
Directional acoustic emission activity in response to borehole deformation in rock masses.
26th US Symposium on rock Mechanics/Rapid City, SD/26-28, June, pp. 723-730.

50) Michihiro, K., Fujiwara, T. and Yoshioka, H., 1985.
Study on estimating geostress by the kaiser effect of AE.
26th US Symposium on Rock Mechanics/Rapid City, SD/26-28, June, pp. 557-564.

51) Hugson, D.R. and Crawford, A.M., 1986.
Kaiser effect gauging: a new method for determining the pre-existing in-situ stress from an extracted core by acoustic emissions.
International Symposium on Rock Stress & Rock Stress Measurements, Sept. 1-3, Sveden.

52) Hugson, D.R. and Crawford, A.M., 1987.
Kaiser effect gaugung: the influence of confining stress on its response.
Proceedings of the 6th International Congress on Rock Mechanics, Montreal, Canada.

53) Michihiro, K., Hata, K., Fujiwara, T. and Yoshioka, H., 1988.
Estimation of initial stress in various rocks by acoustic emission.
Zairyo, Vol. 37, No. 423.

54) Hugson, D.R. and Crawford, A.M., 1988.
Felicity ratio: a significant factor in the determination of previous stress through kaiser effect gauging.
Proceedings of the 15th Canadian Rock Mechanics Symposium, Toronto, Canada.

55) Boyce, G.L., 1981.
A study of the acoustic emission response of various rock types.
Master of Science, Drexel University.

56) Goodman, R.E., 1963.
Sub-audible noise during compression of rocks.
American Geological Society Bulletin 74, pp. 487-490.

57) Tanimito, K., Nakamura, J., Fudo, R., 1981.
Application of acoustic emission in in-situ test.
10th ICSMFE, Vol. 2, pp. 573-576.

58) Koerner, R.M., Lord, A.E. and Deutsch, M., 1984.
Determination of pre-stress in granular soils using AE.
Journal of Geotechnical Engineering, Vol. 110, No. 3, pp. 346-358.

59) Koerner, R.M., Lord, A.E. and Deutsch, M., 1984.
Determination of pre-stress in cohesive soils using AE.
Journal of Geotechnical Engineering, Vol. 110, No. 11, pp. 1537-1548.

60) Deutsch, M., Koerner, R.M. and Lord, A.E., 1989.
Determination of pre-stress of in-situ soils using acoustic emissions.
Journal of Geotechnical Engineering, Vol. 115, No. 2, pp. 228-244.

61) Mlakar, P.F., Walker, R.E. and Sullivan, B.R., 1980.
Acoustic emission from concrete specimens.
WES/MP/SL-81-26 Proj. 4A161101A91D.

62) Cheng, E., 1986.
Determining characteristic profiles of geological materials and concrete.
Thesis for the B.A.Sc. degree, University of Toronto.

63) Muravin, G.B. and Gur'ev, V.V., 1986.
Kaiser effect and structural state of concrete.
Soviet Journal of Non-Destructive Testing, october, pp. 660-664.

64) Bradley, C.C. and St.Lawrence, W., 1975.
Kaiser effect in snow.
Snow Mechanics, Proceedings of the Grindelwald Symposium, IAHS-AISH Publ. No. 114.

65) Mityaev, P.V. and Tokmagambetov, G.A., 1986.
A law observed in the generation of sound in ice samples subjected to loading.
Akust. Zh., March-April, 32, pp. 277-278.

66) Simmons, G. and Richter, D., 1976.
Microcracks in rock in the physics and chemistry of rocks and minerals.
R.G.J. Streus, Wiley, London, England.

67) Fonseka, G.M., Murell, S.A.F. and Barnes, P., 1985.
Scanning electron microscope & acoustic emissions studies of crack development in rocks.
International Journal of Rock Mechanics & Geochemical Abstracts, 22, No.5, pp. 273-289.

68) Lux, K.M. and Rokahr, R., 1984.
Laboratory investigations and theoretical statements as a basis for the design of caverns in rock salt formations.
1st Conference on the Mechanical Behavior of Salt, Pennsylvania State University.
TTP, Germany, pp. 275-309.

69) Brace, W.F., 1961.
Dependence of fracture strength of rocks on grain size.
Proceedings of the 4th US Symposium on Rock Mechanics, University Park, pp. 99-103.

70) Kranz, R.L., 1979.
Crack-crack and crack-pore interactions in stressed granite.
International Journal of Rock Mechanics & Geomehanical Abstracts, Vol. 16, pp. 37-47.

71) Sprunt, E.S. and Brace, W.F., 1974.
Direct observation of microcavities in crystalline rocks.
International Journal of Rock Mechanics & Geomechanical Abstract, Vol. 11, pp. 139-150.

72) Scholz, C.H., 1968.
Experimental study of the fracturing process in brittle rock.
Journal of Geophysical Research, 73, No. 4, pp.1447-1486.

73) Taponnier, P. and Brace, W.F., 1976.
Development of stress-induced microcracks in Westerly grnite.
International Journal of Rock Mechanics & Geomechanical Abstract, Vol. 13, pp. 103-112.

74) Peng, S. and Johnson, A.M., 1972.
Crack growth and faulting in cylindrical specimens of Chelmsford granite.
International Journal of Rock Mechanics & Geomechanical Abstract, Vol.9, pp. 37-86.

75) Bieniawski, Z.T., 1967.
Mechanisms of brittle fracture of rock. Part II - experimental studies.
International Journal of Rock Mechanics & Geomechanical Abstract, Vol. 4, pp. 407-423.

76) Brace, W.F., 1960.
An extension of the Griffith theory of fracture to rock.
Journal of Geophysical Research, Vol. 65, pp. 3477-3480.

77) Lawn, B.R. and Wilshaw, T.R., 1975.
Fracture of brittle solids.
Cambridge University Press.

78) Waversik, W.R. and Brace, W.F., 1971.
Post failure of a granite and diabase.
Rock Mechanics 3, pp. 61-85.

79) Sarfarazi, M. and Ghosh, S.K., 1987.
Microfracture in polycrystalline solids.
Engineering Fracture Mechanics, Vol. 27, pp. 257-267.

80) Bombolakis, E.G., 1973.
Study of the brittle fracture process under uniaxial compression.
Tectonophysics 18, pp. 231-248.

81) Kowallis, B.J., Raeleffs, E.A. and Wang, H.F., 1982.
U crack studies of basalts from the iceland research drilling project.
Journal of Geophysical Research, Vol. 87, No. 38, pp.6650-6656.

82) Montoto, M., Suarez del Rio, L.M., Khair, A.W. and Hardy, H.R. Jr., 1984.
AE in uniaxially loaded granitic rocks in relation to their petrographic character.
Proceedings 3rd Conference on Acoustic Emission / Microseismic Activity in Geological Structures and Materials, Pennsylvania State University, Trans Tech Publication, Clausthal, Gemany, pp. 83-100.

83) Olsson, W.A. and Peng, S.S., 1976.
Microcrack nucleation in marble.
International Journal of Rock Mechanics & Geomechanical Abstract, Vol. 13, pp. 53-59.

84) Sangha, C.M., Talbot, C.J. and Dhir, R.K., 1974.
Microfracturing of a sandstone in uniaxial compression.
International Journal of Rock Mechanics & Geomechanical Abstract, Vol. 11, pp.107-113.

85) White, M.J., 1983
Influence of post failure characteristics of coal measures rocks on the stability of mine tunnels.
Ph.D. Thesis, University of Nottingham.

86) Hartford Steam Boiler Inspection Technologies, 1989.
Operating instructions for the aet model 5500 acoustic emission monitoring system.

87) Herget, G., 1988.
Stresses in rock.
Balkema, Rotterdam, Netherlands.

88) Hardy, H.R. Jr., Zhang, D. and Zelanko, J.C., 1985.
Recent studies of the Kaiser Effect in geological materials.
Proceedings 4th Conference on Acoustic Emission / Microseismic Activity in Geological Structures and Materials, Pennsylvania State University, Trans Tech Publication, Clausthal, Gemany, pp. 27-55.

89) Pang, L.C.F., 1975.
A method for measuring the curvature of a boundary on a 2-dimensional quantized grid.
Master of Science, McGill University.

90) ISRM Commission on Standardization of Laboratory and Field Tests.
Suggested method for determining the uniaxial compressive strength and deformability of rock materials.
International Journal of Rock Mechanics & Geomechanics Abstract, 1977.

91) Michihiro, K., Yohioka, H., Hata, K. and Fujiwara, T., 1985.
Strain dependence of the Kaiser Effect for various rock types.
Proceedings 4th Conference on Acoustic Emission / Microseismic Activity in Geological Structures and Materials, Pennsylvania State University, Trans Tech Publication, Clausthal, Gemany, pp. 87-95.

92) *URL Report No. 456.*

93) Woodcok, D., 1992.
Personal Communication.
AECL, Manitoba, Canada.

94) Popov, E.P., 1978.
Mechanics of Materials.
Prentice-Hall, Inc., Englewood Cliffs, New Jersey.

95) Arjang, B., 1992
Personal Communication.
CANMET, Elliot Lake Laboratory, Ontario, Canada.

96) Montoto, M., Ruiz de Argandoña, V.G., Calleja, L. and Suarez del Rio, L.M., 1985.
Kaiser Effect in thermo-cycled rocks.
Proceedings 4th Conference on Acoustic Emission / Microseismic Activity in Geological Structures and Materials, Pennsylvania State University, Trans Tech Publication, Clausthal, Gemany, pp. 87-95.

97) Dunning, J.D., Leaird, J.D. and Miller M.E., 1985.
The Kaiser Effect and frictional deformation.
Proceedings 4th Conference on Acoustic Emission / Microseismic Activity in Geological Structures and Materials, Pennsylvania State University, Trans Tech Publication, Clausthal, Gemany, pp. 87-95.

98) Yoshikawa, S. and Mogi, K., 1989.
Experimental studies on the effect of stress history on acoustic emission activity - a possibility for estimation of rock stress.
Journal of Acoustic Emission, Vol. 8, No, 4, pp. 113-123.

99) Friedel, M.J. and Thill, R.E., 1990.
Stress determination in rock using the Kaiser Effect.
US Bureau of Mines, RI-9286.